Papers presented to the

THIRTEENTH SYMPOSIUM

ON ANTARCTIC METEORITES

7-9, June 1988

NATIONAL INSTITUTE OF POLAR RESEARCH, 国立極地研究所
TOKYO

Papers presented to the

THIRTEENTH SYMPOSIUM

ON ANTARCTIC METEORITES

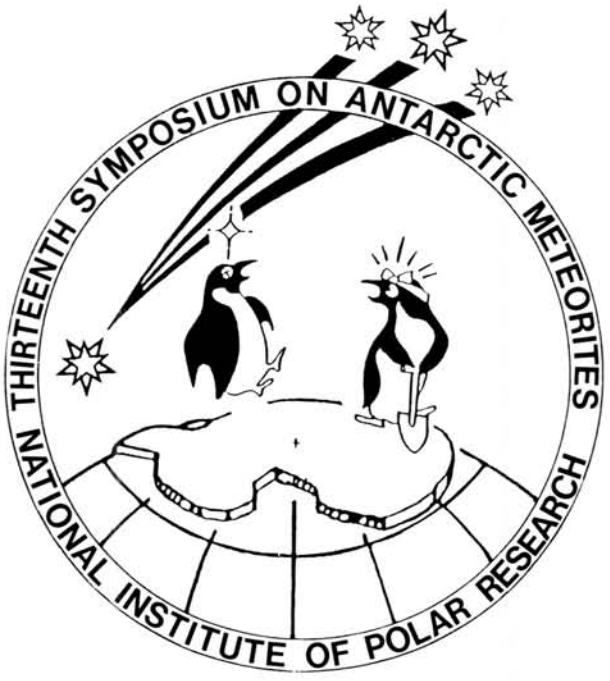

7–9, June 1988

NATIONAL INSTITUTE OF POLAR RESEARCH, 国立極地研究所
TOKYO

Tuesday, June 7, 1988

	0900 - 1200	Registration	Auditorium (6th Floor)
	0930 - 0935	Opening Address	Tatsuro Matsuda Director General National Institute of Polar Research

* Speaker

Chairmen: Takaaki Fukuoka and Akira Shimoyama

1	0935 - 0950	Nishio F. Comparison of meteorite concentration and age of ice in the Allan Hills and the Meteorite Ice Field near the Yamato Mountains
2	0950 - 1005	Higashi A.*, Fujii Y. and Takamatsu S. Microparticles in Antarctic deep ice core - Cosmic dusts observed? -
3	1005 - 1030	Fireman E. L. Uranium-series dating of tephra-banded ice at ablation sites
4	1030 - 1040	Meteorites team of the 29th JARE Search for Antarctic meteorites on the bare ice field around Sør Rondane Mountains by JARE-29 Asuka party in 1987-1988 field season
5	1040 - 1055	Kojima H.* and Yanai K. Classification of small meteorites in Yamato-79 collection
6	1055 - 1110	Yamato Lunar Meteorite Consortium Group (Takeda H.*) Preliminary consortium studies of the Yamato-86032 lunar meteorite
7	1110 - 1135	Warren P. H.* and Kallemeyn G. W. Geochemistry of lunar meteorite Yamato-86032
8	1135 - 1200	Sánchez-Rubio G.*, Nagasawa H. and Matsui T. New meteorite finds in the Allende area, Mexico
	1200 - 1300	Lunch Time

Chairmen: Yukio Ikeda and Hiroko Nagahara

9 1300 - 1315 Shimoyama A.*, Komiya M. and Harada K.
Thermal release of organic compounds from insoluble organic matter in the Yamato-791198 carbonaceous chondrite

10 1315 - 1330 Murae T.*, Masuda A. and Takahashi T.
Pyrolytic studies of HCl and HF residues from carbonaceous chondrites

11 1330 - 1345 Takano S.*, Hirahara Y., Masuda A., Suzuki H., Ohishi M., Ishikawa S. and Kaifu N.
Detection of five 13C isotopic species of HC5N in the Taurus dark cloud TMC1

12 1345 - 1410 Wang D.
Petrology and mineralogy of the Ningqiang carbonaceous chondrite

13 1410 - 1425 Ikeda Y.
Major element chemical compositions of the constituents in C3 chondrites and their formational environments

14 1425 - 1440 Nagahara H.* and Nagasawa H.
Formation of type B1 CAI

15 1440 - 1455 Noguchi T.*, Nagahara H. and Kushiro I.
Texture and chemical composition of pyroxenes in some carbonaceous chondrites and comparison with those in the unequilibrated ordinary chondrites

1455 - 1525 Tea Time

16 1525 - 1540 Matsunami S.
Origin of positive correlation of Mn with Fe in matrix Fe-rich olivine of primitive type 3 ordinary chondrites

17 1540 - 1605 Hewins R. H.
The evolution of chondrules

18 1605 - 1620 Noguchi T.
Lamellae-bearing "pigeonite" in "equilibrated" ordinary chondrites (H4-6) and other texture in pyroxenes in ordinary chondrites (type 3-4): implication to the thermal history

19	1620 - 1640	Sánchez-Rubio G. Chondrule-like objects in terrestrial volcanic rocks
20	1640 - 1655	Tazawa Y. and Sasaki T.* Chemical and mineral compositions of fusion crusts on Antarctic chondrites
21	1655 - 1710	Fukuoka T.* and Kimura M. Chemistry of Y-74025 chondrite
22	1710 - 1725	Misawa K.*, Nakamura N., Watanabe S. and Kitamura M. Chemical and petrological studies on a light-colored fragment in the Hedjaz chondritic breccia
23	1725 - 1740	Noda S.*, Nagamoto H., Nishikawa Y., Misawa K. and Nakamura N. Further studies of trace element distribution in chondrule cores and rims of the Tieschitz (H3.6) chondrite
24	1740 - 1755	Yabushita S.* and Wada K. Neutron activation measurement of iridium concentration in Yamato CV chondrite

1800 - 2000 Reception

Wednesday, June 8, 1988

Chairmen: Noboru Nakamura and Mitsuru Ebihara

25 0900 - 0915 Ebihara M.
Abundances and distribution of trace elements in enstatite chondrites

26 0915 - 0930 Uyeda C.* and Okano J.
The correlation of magnesium isotope abundance and chemical composition in type 3 chondrites

27 0930 - 0945 Takahashi K.*, Shimizu H. and Masuda A.
Isotopic studies on diogenites, based on the Rb-Sr systematics

28 0945 - 1030 Paul R. L., Lipschutz M. E.*, Kruse H. and Sack R. O.
Howardite, eucrite and diogenite (HED) meteorites from Antarctica and elsewhere: chemical clues to their origin

29 1030 - 1045 Yoneda S.*, Shimizu H. and Masuda A.
Rare earth and major element fractionations in evaporation of chondritic matter

30 1045 - 1100 Isobe H.*, Tsuchiyama A. and Kitamura M.
Fractionation experiments of chondritic material

31 1100 - 1115 Saito T.*, Shimizu H. and Masuda A.
Experimental studies on rare earth elements partitioning between olivine and silicate melt using chondrite as a starting material, in relation to pallasites

32 1115 - 1130 Shimaoka T.* and Nakamura N.
Volatilization studies of alkali metals on a chondritic material (Part I)

33 1130 - 1145 Nakamura N.* and Shimaoka T.
Volatilization studies of alkali metals on a chondritic material (Part II): Chemical compositions of residual melts

34 1145 - 1200 Nagahara H.* and Kushiro I.
Vaporization and condensation experiments in the system plagioclase-hydrogen

35 1200 - 1225 Hou W.*, Wang D., Xie H. and Wang M.
An experimental study on heating-melting of Zhaodong chondrite

1225 - 1330 Lunch Time

Chairmen: Jun-ichi Matsuda and Nobuo Takaoka

36 1330 - 1345 Sugiura N.* and Hashizume K.
A preliminary report on the nitrogen isotope measurements using a quadrupole mass spectrometer

37 1345 - 1400 Kaneoka I.
Noble gas degassing from meteorites inferred from 40Ar-39Ar analytical data

38 1400 - 1415 Sasaki S.
Penetration of solar energetic particles into the planetary region after dissipation of the solar nebula

39 1415 - 1430 Matsuda J.* and Nagao K.
Noble gases in shock-produced diamonds

40 1430 - 1445 Nagai H., Honda M.*, Imamura M., Kobayashi K., Yoshida K., Miyaki Y. and Chonan Y.
Some cosmogenic nuclides in chondrites and iron meteorites

41 1445 - 1500 Futagami T.*, Ozima M. and Nakamura Y.
4He+ ion implantation experiments into minerals and their implications for planetary sciences

1500 - 1530 Tea Time

42 1530 - 1545 Miura Y.*, Rucklidge J., Beukens R., Nagao K. and Koga H.
Comparative study in cosmic-ray and terrestrial ages of Antarctic meteorites

43 1545 - 1600 Miura Y.*, Beukens R. P. and Rucklidge J. C.
Discussion of C-14 "weathering ages" of some Yamato and Allan Hills meteorites

44 1600 - 1615 Takaoka N.* and Miura Y.
Noble gases in K-T boundary clay: Evidence for meteorite impact.

45 1615 - 1630 Miura Y.* and Imai M.
Anomalous data on the K-T boundary samples

Thursday, June 9, 1988

Chairmen: Naoji Sugiura and Akira Tsuchiyama

48 0900 - 0915 Fujii N.*, Horii Y. and Takeda H.
Mechanical and morphological characterization of shock effects in Antarctic meteorites (I)

49 0915 - 0930 Miyamoto M.*, Kojima H. and Yanai K.
Weathering of some Antarctic meteorites: Information from absorption bands near 3μm

50 0930 - 0945 Nagai H.*, Momose K. and Funaki M.
Magnetic properties of the mixtures of Fe-Ni alloys simulated to Y-74354, Y-74362 and Y-74190 chondrites

51 0945 - 1010 Funaki M., Danon J.* and Nagata T.
Studies on magnetic properties and Mössbauer spectroscopy of the Nova Petropolis iron meteorite

52 1010 - 1025 Funaki M.*, Danon J. and Nagata T.
Natural remanent magnetization of magnetic grains in St. Severin and Y-75097 ordinary chondrites

53 1025 - 1040 Nagata T.* and Funaki M.
Magnetic analysis of Antarctic chondrites and achondrites on the basis of a magnetic binary system model

54 1040 - 1055 Kitamura M.*, Tsuchiyama A., Watanabe S., Syono Y. and Fukuoka K.
Melting and deformation of a chondrite by shock-loading

55 1055 - 1110 Tsuchiyama A.
A new gas condensation furnace and its application to condensation in the system Mg_2SiO_4-H_2

56 1110 - 1125 Tomeoka K.*, Kojima H. and Yanai K.
Yamato-82162: A new kind of CI carbonaceous chondrite found in Antarctica

57 1125 - 1140 Watanabe S.*, Tsuchiyama A. and Kitamura M.
A preliminary report of mineralogy of Y-82162 (CI)

58 1140 - 1155 Tomeoka K.*, Kojima H. and Yanai K.
Yamato-86720: An extensively altered and thermally metamorphosed CM carbonaceous chondrite?

59 1155 - 1220 Kallemeyn G. W.
Compositional study of carbonaceous chondrites with CI-CM affinities

1220 - 1320 Lunch Time

Chairmen: Masao Kitamura and Yasunori Miura

60 1320 - 1345 El Goresy A.* and Ehlers K.
Critical analysis of the application of the sphalerite cosmobarometer to EH chondrites

61 1345 - 1410 Jakeš P.* and Ceplecha Z.
Carbonaceous chondrite or SNC composition for the phobos?

62 1410 - 1425 Ogata H.*, Mori H. and Takeda H.
Mineralogy of interstitial rim materials of ureilites and their origin

63 1425 - 1440 Takeda H.*, Tagai T. and Graham A. L.
Mineralogy of slowly cooled eucrites and thermal histories of the HED parent body

64 1440 - 1455 Saito J.*, Tachikawa O., Takeda H. and Tagai T.
Mineralogical study of the Yamato-791694 ataxite with reference to Santa Catharina

65 1455 - 1510 Miura Y.
Low-density plagioclases from meteoritic impact crator

1510 - 1530 Tea Time

-- Special Lecture --

66 1530 - 1630 Hutchison R. (Invited Speaker, Doctor, British Museum Natural History)

Title: Advances in our understanding of the ordinary chondrites

Abstract only

Tuesday, June 7, 1988

0900 - 1200	*Registration, 6th Floor*
0930 - 0935	*Opening adress, Auditorium*
0935 - 1755	*Symposium, Auditorium*
1800 - 2000	*Reception, Lecture Room, 2nd Floor*

Comparison of meteorite concentration and age of ice in the Allan Hills and the Meteorite Ice Field near the Yamato Mountains

FUMIHIKO NISHIO
National Institute of Polar Research

In order to compare and estimate the meteorite concentration and age of ice in the Meteorite Ice Field near the Yamato Mountains and the Allan Hills bare ice field, meteorite mass concentration and age of ice are computed based upon the model of meteorite mass concentration by Whillans's equqtion. Figure 1 shows the distribution of meteorite mass concentration, bedrock and surface topography of the bare ice in the area upstream of the Allan Hills Nunataks. In this area an enormous number of meteorites have been found on its blue ice surface and the total now exceeds 624 kg. Most of meteorite pieces were found on the bare ice surface downstream of the presence of the sub-ice ridge, that is, a steep ice thickness gradient. This situation means that ice arrives at the surface with slow downglacier movement and there is more time for concentration before the meteorites are delivered to the end of the glacier.

(1) Meteorite mass concentration.

The expected meteorite mass concentration in various parts of the Meteorite Ice Field and the Allan Hills bare ice fields can be calculated by Whillans's equqtion. In the results the meteorite mass concentration computed by the equation of the model are more than 10 times larger than that of the Meteorite Ice Field. The less meteorite mass concentration predicted by the equation of the model may be affected by the younger ice age in the Meteorite Ice Field and the meteorite infall rate on the earth's surface.

On the contrary, the meteorite mass concentration in the Allan Hills are nearly equal to the predicted concentration as shown in Figure 1.

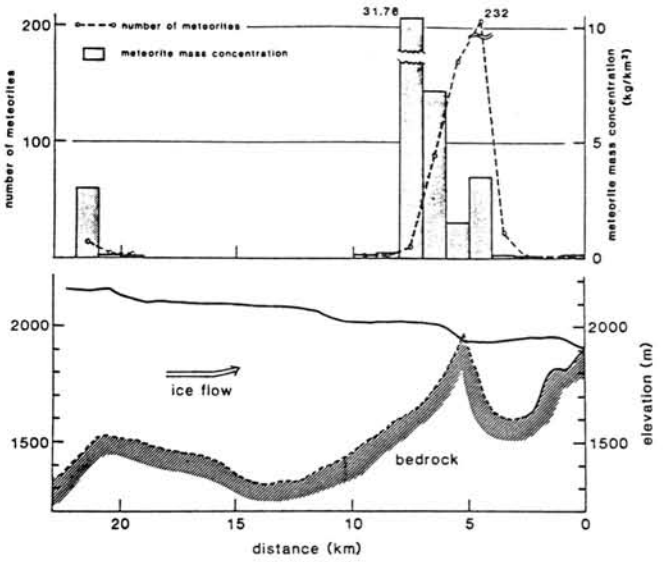

(2) Age s of ice.

Based upon the structural laboratory studies of ice collected at the surface near Massif A in the Yamato Meteorite Ice Field, the age of the bare ice, approximately 30 ka, are estimated by fabric characterristics and estimated stress condition of ice flow. The estimated ages of ice by ice core study are also about 10 times larger than the age of ice computed by the equation of the model.

Figure 1. Meteorite mass concentration, ice surface and bedrock elevation from the upstream area of the Allan Hills bare ice field to the Allan Hills Nunatak.

MICROPARTICLES IN ANTARCTIC DEEP ICE CORE —Cosmic dusts observed ?—

Higashi, A. Fujii, Y.* Takamatsu, S.

International Christian University, Osawa 3-10-2, Mitaka-shi, Tokyo 181
*National Institute of Polar Research, Kaga 1, Itabashi-ku, Tokyo 173

Scanning electron-microscope (SEM) observations were carried out for microparticles in the 700m deep ice core retrieved at Mizuho Station, Antarctica in 1983 and 84. Preliminary results of the analyses of the core is given elsewhere (Higashi et al, 1988). Ice samples used in this study were cut into 5 cm thickness from individual 50 cm length core samples of 336.53m and 600.68m depth. In addition of these 20 samples, a small sample from 401.70m was used.

These samples were melted from outside, rinsing gradually by their own melt water, in a clean room of class 1000. The final solid sample provided 150 ml water, which was divided into three; 15 ml for the microparticle counting by the Coulter counter, 30 ml for the electric conductivity measurement, and the remainder for the major chemical analysis. Samples of microparticles for the SEM observations were obtained by filtering the last part with a Nucleo filter which was transferred onto a sample holder of the SEM.

In almost all samples, microparticles which morphologically resemble the interplanatory dust particles were found among many particles of terrestrial origin. A particle shown in Fig.1 resembles a chondritic aggregate micrometeorite in a photograph of Fig.4 in a paper by Brownlee et al (1980). Rounded aggregates as shown in Fig.2a are often found in 600.58 and 401.70 ice, and they are like that in Fig.1 (W7029 H15) in a paper by Zolensky (1987). The EDS analysis result of this particle exhibits abundance of Al, S, K, Ca and Fe besides of Si (Fig.2b), which may indicate the particle is interplanetary.

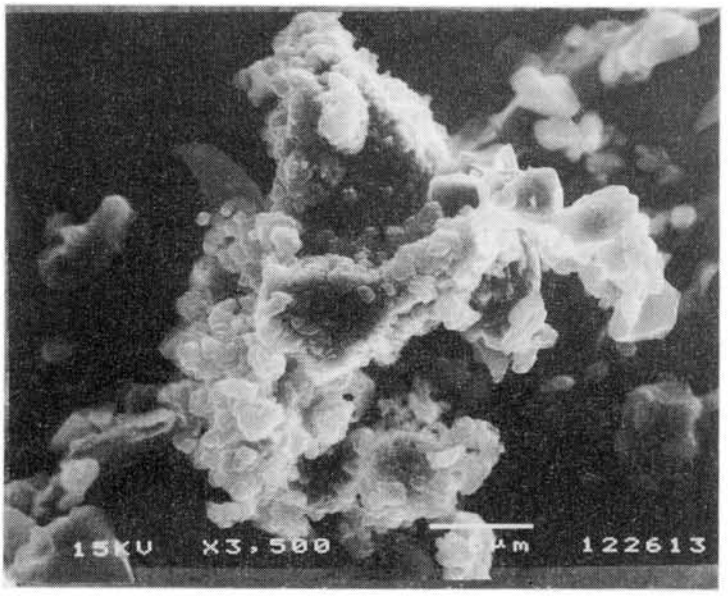

Fig. 1 Aggregate of submicron particles, which resembles Brownlee particle. From 336.53m core.

A spherical particle found in 401.70m core is shown in Fig.3a. Its diameter is in the order of 10 μm, the same as spherical particles found in the stratsphere collection (NASA cosmic dust catalog, 1982). It is difficult to distinguish whether they are cosmic origin or products of the solid-fuel rocket exhausts in the case of the stratsphere collection, but the one in Fig.3a is certainly a micrometeorite because ice in 401.70m core must be formed from snow fell on the Antarctic ice sheet before the industrial revolution.

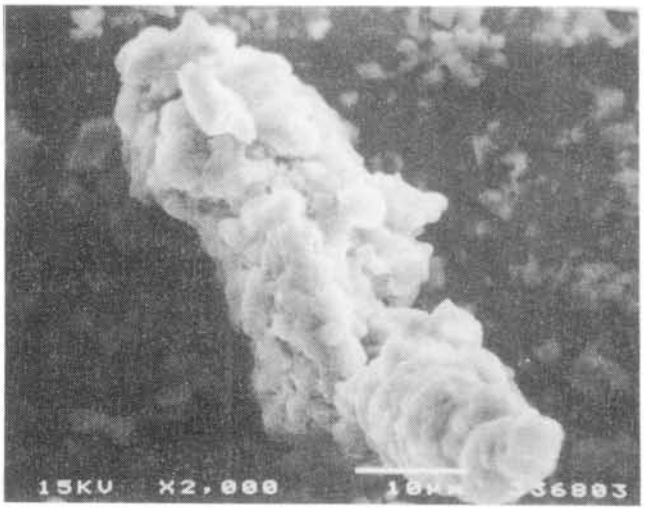

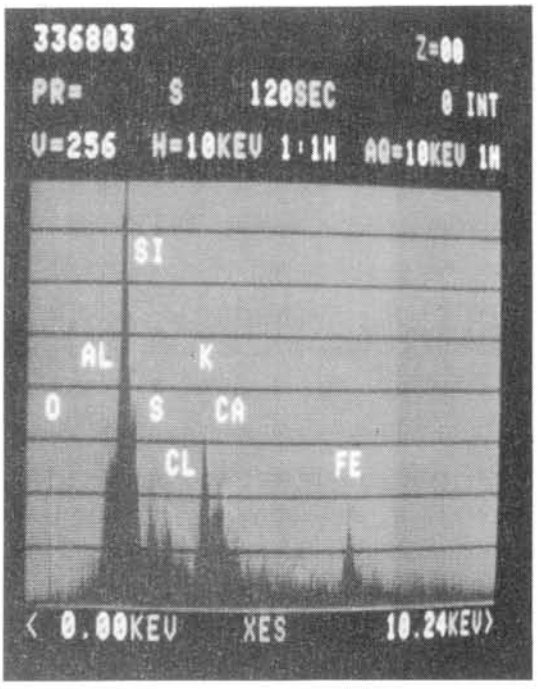

Fig. 2a (above) A particle from the 336.53m core, 2b (right) EDS record of the same particle

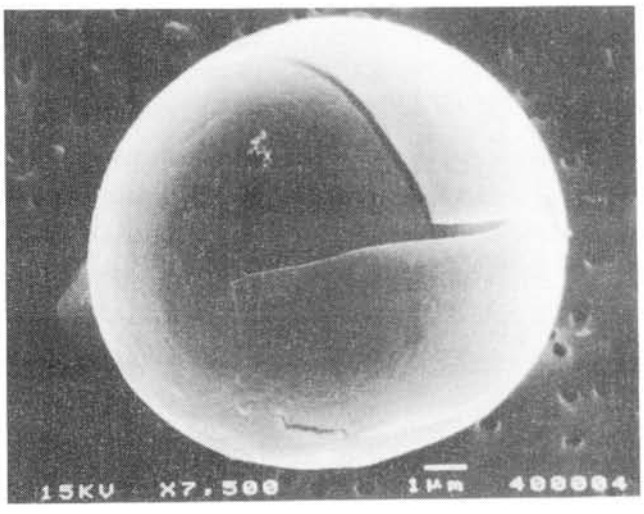

Fig. 3a A spherical particle from the 401.70m core. Note crustal crack.

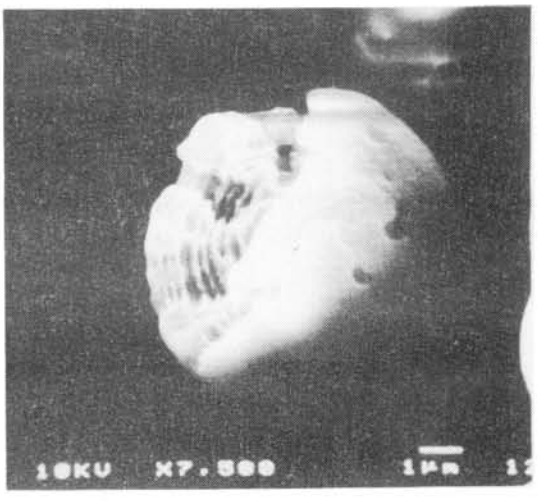

Fig. 3b A nearly spherical particle, which exhibits inner layer structure.

Surface crust of the sphere seems to be fragile, because there happened cracking on it. It was very smooth when the sphere was first observed 20 days before the photograph of Fig.3a was taken. Fig.3b shows another nearly spherical particle of which surface crust seems to have been partly peeled away. There appear layer structure of inner material under the crust, which might indicate that the layer growth took place on the formation process of spherical paticles.

Most commonly observed particles in the 401.70m core are rounded mineral particles as shown in Fig.4a. They look like clay particles ablated in ice during the transformation of snow into ice and also the deform-

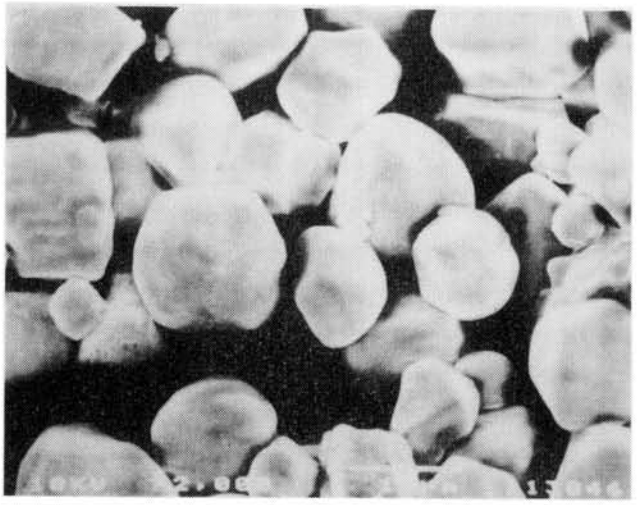

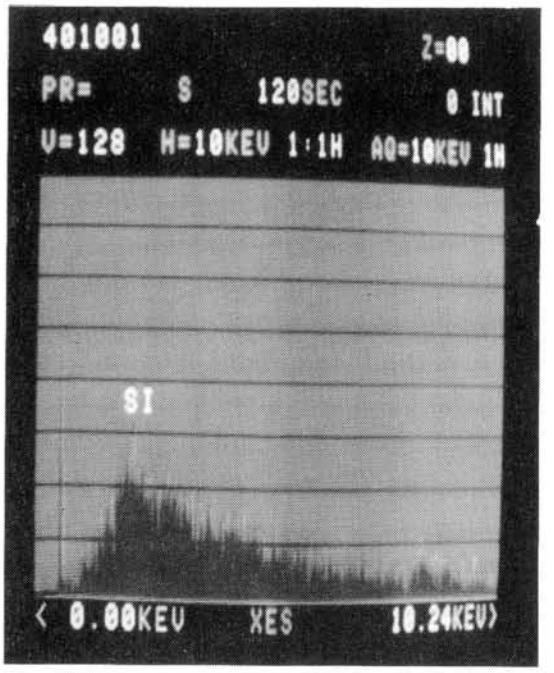

Fig. 4a (above) Commonly observed microparticles in 407.10m ice core, 4b (right) EDS record of a particle in 4a.

ation of ice. EDS record of a particle shown in Fig. 4b exhibits only a line of Si significantly. A reason why particles of aggregates as shown in Fig.1 and Fig.2a are not ablated in ice is that they are composed of refractory materials as was claimed by Zolensky (1987).

If we can distiguish microparticles of cosmic origin from others morphologically with some aids of EDS analyses as shown above, deep ice cores obtained by drilling ice sheets could be very good sources for collection of interplanetary dust particles. We may be able to find time variations of the dust fall on the earth, if the ages of ice are determined correctly. It is tentatively evaluated that the bottom 700m ice is approximately 10,000 years old.

References:

Brownlee, D.E. et al: Solid Particles in the Solar System, IAU Symp. No.90 (1980), 333-342.
Higashi, A. et al: Ann. Glaciology, 10 (1988), 52-56.
NASA: Cosmic Dust Catalog, Vol.1, No.1 (1982) and following several volumes.
Zolensky, M.E.: Science, 237 (18, Sept. 1987), 1466-68.

URANIUM-SERIES DATING OF TEPHRA-BANDED ICE AT ABLATION SITES

Fireman, E. L.

Harvard-Smithsonian Center for Astrophysics

Tephra-banded ice samples at Antarctic ablation sites are dated by a uranium-series method described by Fireman (1). The ages obtained for four locations at the main Allan Hills meteorite collection site are as follows: $(66\ ^{+7}_{-5}) \times 10^3$, $(98 \pm 7) \times 10^3$, $(195 \pm 20) \times 10^3$, and $(295\ ^{+60}_{-90}) \times 10^3$ years. The locations of the dated ice samples are consistent with the horizontal stratigraphy expected from the ice flow, with the older ice being closer to the western margin of the land barrier. The 98×10^3, 195×10^3, and 295×10^3 year old ice samples are within an approximately 50 km^2 area of exposed ice that is richly laden with meteorites. The meteorites with terrestrial ages less than 10^5 years and of sufficient weight to be unmoved by wind must have fallen directly in this area. The mass influx of these specimens averaged over the past 10^5 years is approximately 7×10^{-6} kg km^{-2} yr^{-1}. The mass influx is relatively independent of the meteorite fragmentation, which increases the number of specimens. Based on observed falls, Hawkins (2) and Brown (3) estimate the meteorite mass influx to be between 2×10^{-6} and 8×10^{-6} kg km^{-2} yr^{-1}. The agreement between the meteorite mass influx averaged over 10^5 years with the observed fall influx indicates a relatively constant influx on the earth during the past 10^5 years. The meteorites with terrestrial ages between 100×10^3 and 400×10^3 years in this area are overabundant relative to the constant fall expectation and indicate that approximately twice as many meteorites were transported into the 50 km^2 area during this time than fell at the site. The meteorites with terrestrial ages between 400×10^3 and 10^6 years are underabundant relative to the constant fall expectation. These older meteorites have been either partially transported away from the site by the ice movement or have been partially weathered away. The lack of meteorites with ages older than 10^6 years indicates that the ice overrode the Allan Hills land barrier at this time and flushed away the prior meteorite accumulation. The particles in the tephra bands consist mainly of fine volcanic glass shards. Their chemical composition was determined by instrumental neutron activation analysis (INAA) and by electron probe analysis.

References: (1) Fireman, E. L. (1986) J. Geophys. Res., 91, B4, D539 and 91, B8, 8393. (2) Hawkins, G. S. (1960) Astron. J., 65, 318. (3) Brown, H. (1960) J. Geophys. Res., 65, 1679.

Acknowledgment: This research is supported in part by NSF Grant DPP-8516601.

4

Search for Antarctic Meteorites on the Bare Ice Field around Sør Rondane Mountains by JARE-29 Asuka Party in 1987-1988 Field Season

Meteorites team of the 29th JARE*

Two parties of the 29th Japanese Antarctic Research Expedition (JARE) visited the bare ice field around Balchenfjella (Mt. Balchen), eastern part of the Sør Rondane Mountains in January and February 1988, and Nansenisen (Nansen Plateau), southern of the Sør Rondane Mountains in February and March 1988, respectively. The parties tried reconnoitering search for meteorites on the several bare ice fields around the Mountains, and collected total 338 specimens with some unique types of meteorites in the two major sites of the bare ice fields of the Balchen and Nansen area.

After preliminary processing in the field, the meteorites collected in this field season included as following kinds and types; one iron, a few carbonaceous chondrites (C2 and C3), several eucrites and howardites, ureilites, diogenite, mesosiderite and number of ordinary chondrites belong to several petrologic types. The largest specimen is L or LL type chondrite (almost complete stone) and weight about 46kg, however, most of the specimens are fragment under 10g.

Systematic search for meteorites will be tried on the bare ice fields around the Mountains in the coming field season; October 1988 and February 1989.

* Yanai K.[1], Naraoka H.[2], Fujita S.[1], Kami K.[3], Kawauchi M.[1], Shimoda Y.[1], Shirota T.[1] and Yonezawa Y.[1]

1. National Institute of Polar Research
2. University of Tsukuba
3. Maritime Safety Agency

Classification of small meteorites in Yamato-79 collection

Kojima H. and Yanai K.
National Institute of Polar Research
9-10, Kaga 1-chome, Itabashi-ku, Tokyo 173

189 pieces of relatively small meteorites from Yamato-791358 to Yamato-791794 are classified as follow. They include 1 CR, 1 CV3, 3 CO3, 1 E3, 1 E5, 4 H3, 1 L3 AND 4 L-LL3. Remains are equilibrated ordinary chondrites.

Meteorite Name	Weight(g)	Class	Meteorite Name	Weight(g)	Class
Yamato-791358	2.74	H4	Yamato-791502	131.02	H3
791359	2.05	H5withH6clast	791504	41.55	H4
791360	2.14	H4	791505	31.11	H4
791362	3.42	LL6	791506	16.62	H5
791363	6.83	H5	791507	12.77	H5
791366	23.04	L3	791508	12.81	H5
791367	15.20	H6	791509	9.90	H5
791368	20.55	L6	791510	9.77	E5
791369	11.05	LL6	791511	10.34	H5
791399	0.95	L orLL3	791512	4.69	H5
791420	18.91	H4	791517	17.12	L6
791437	28.20	H5	791518	6.42	L6
791443	11.32	L6	791519	26.89	H4
791446	17.60	H6	791520	2.85	L4
791447	1.99	H4	791521	2.82	L4
791454	8.40	H4	791522	2.48	L4
791455	54.83	L6	791523	0.82	L6
791456	37.05	L6	791524	0.68	H4
791457	41.39	H4	791525	0.71	L6
791458	8.04	H4	791526	6.47	H6
791459	23.65	L6	791527	4.14	H4
791460	10.59	L6	791528	1.40	L4
791461	11.44	L6	791529	0.77	L6
791463	10.28	L6	791531	77.92	L4-5
791464	18.02	H4	791535	15.52	H4
791465	3.23	H6	791537	66.18	H3
791468	11.29	H5	791544	1.58	H6
791469	5.09	H4	791547	2.92	H4
791470	6.96	H5	791548	2.10	H4
791472	7.00	H3	791549	1.90	H4
791473	6.81	H4	791550	1.17	H4
791474	67.05	H5	791555	1.06	H6
791475	14.38	H5	791556	129.25	H5
791476	23.47	H5	791557	90.65	L6
791487	13.95	L6	791558	101.64	L-LL3
791488	8.08	H5	791559	26.21	H6
791490	10.19	H6	791567	67.98	H4
791494	20.88	L6	791569	10.58	L6
791495	45.29	H5	791571	23.68	L6
791496	5.37	L4	791572	6.31	H4
791498	3.11	CR	791575	3.19	L6
791499	9.94	L6	791578	191.44	L6

Meteorite Name	Weight(g)	Class
Yamato-791579	108.06	L6
791580	114.60	L6
791581	9.61	L6
791584	2.52	L6
791589	3.91	H6
791590	20.57	H4
791595	5.84	H5
791596	1.92	L?4
791598	8.16	L4
791599	8.55	L4
791600	0.74	H4
791601	2.06	CV
791602	3.35	H6
791607	55.63	H5
791608	19.77	H5
791609	18.90	H5
791610	22.61	H5
791611	14.85	H5
791612	15.97	H5
791613	15.50	H5
791614	21.47	H5
791615	18.22	H5
791616	7.29	H5
791617	8.93	H5
791618	6.70	H5
791627	1.82	L6
791628	4.95	L6
791631	12.30	H5
791637	109.23	L4
791638	63.72	L4
791639	13.66	H5
791640	8.69	H3
791641	5.37	L4
791642	4.35	L4
791643	2.85	L4
791644	134.58	L4
791645	55.95	L4
791653	7.89	L4
791654	3.35	L4
791655	48.78	L4
791656	9.96	L-LL3
791657	1.53	L-LL3
791658	14.87	H4
791659	10.17	L4
791660	3.25	L4
791661	114.10	L4
791662	89.57	L4
791663	50.42	H4
791664	45.54	H4
791665	20.15	H4
791666	9.94	H4
791669	334.85	L4
791671	13.29	L4

Meteorite Name	Weight(g)	Class
Yamato-791673	2.64	H4
791674	50.10	L4
791675	27.85	L4
791678	259.10	L4
791680	284.98	L4
791681	71.07	L4
791682	123.73	L4
791683	96.60	L4
791684	33.01	H5
791685	27.02	H5
791686	19.03	H5
791696	0.81	LL6
791697	1.44	L4
791699	2.91	H4
791700	1.39	L6
791703	25.48	L4
791704	93.10	L4
791705	172.47	L4
791706	341.10	L4
791708	126.98	L4
791709	174.32	L4
791711	28.91	L4
791715	13.39	L5
791716	193.21	H4
791726	4.98	H4
791727	18.17	L4
791728	48.20	H4
791729	51.30	H4
791737	15.34	H4
791743	16.63	L6
791744	20.73	L5
791745	17.62	CO3
791746	8.59	CO3
791748	8.33	CO3
791749	2.01	H5
791750	83.53	L4
791771	156.43	L6
791772	7.18	L6
791773	4.14	L6
791774	37.50	H6
791777	43.81	H6
791779	6.08	H6
791784	44.07	H5
791786	64.47	L
791887	37.38	H4
791788	21.68	L shocked
791789	2.55	L6
791790	31.64	E3
791791	45.46	H4
791792	2.78	H5
791793	53.14	H4
791794	11.31	H4

PRELIMINARY CONSORTIUM STUDIES OF THE YAMATO 86032 LUNAR METEORITE.

Yamato Lunar Meteorite Consortium Group*.
Takeda, H.[1], Kojima, H.[2], Yanai, K.[2] (Compilers)
1 Mineralogical Inst., Faculty of Science, Univ. of Tokyo, Hongo, Tokyo 113.
2 National Inst. of Polar Research, Kaga, Itabashi-ku, Tokyo 173.

Yamato 86032 is the largest lunar meteorite ever recovered and weighs 648.43 g. A preliminary examination by Yanai et al. (1) showed that it is an anorthositic regolith breccia similar to the Yamato-82 lunar meteorites. Y-86032 is the fifth lunar meteorite identified in the Yamato meteorite collection. It was recovered from the area where Y-82192 and Y-82193 were recovered (2).

The purpose of the 3rd lunar meteorite consortium study is to continue our efforts to characterize lunar meteorite Y-86032 to find possible impact sites and pairing of several specimens recovered to date. The origin of lunar highlands especially of the far side and the formation processes of lunar crust from a magma ocean will then be investigated on the basis of the data obtained by our group. Because of the large size of the Y-86032 sample, new scopes of researches will be possible. To find variabililty of clast types and matrices within the large breccia and origin of the glass veins is another important subject of our consortium study. It is also hoped to confirm the proposed pairing with the Yamato-82 lunar meteorites.

Physical descriptions of each side of Y-86032 are given in Photographic Catalog (1). It has the typical appearance of lunar meteorites, but it is characterized by presence of numerous impact melt veins and deep narrow cavities. The S and T views show such features. Impact melts are seen at the upper right and low left corner of the T view. A part of the fusion crust is visible together with a number of large white clasts on the W and N view. The yellow-brown coating is visible in the N view. A typical fresh breccia matrix with white clasts has been observed on the E view. Adjacent to this area, a large grayish white (light) clast with fine-grained compact texture 1.0 X 0.5 cm is enbedded in a gray fine-grained compact impact melt. Samples for the first allocation were chipped off from this portion, including large part of the large light clast.

These first consortium samples consist of three large fragments, of which two fragments include a part of the large light clast and many small fragments containing small white clasts. The large light clast enclosed by matrix and one side are bordered by a dark glass vein. Small chips are almost entirely dark to medium gray matrix and occasionally contain small white clasts. Except for a few chips they have no visible glass veins. Three fragments (,71, 1.191g), one including a large light clast were allocated to the U.S. investigators.

Thin section Y-86032,83-1 is a PTS of a part of the large light clast, which is an anorthositic breccia similar to one found in Y-82192 (3). The breccia is fine-grained with some large plagioclase fragments set in light brown matrix of fine comminuted anorthosites and light colored glassy materials. One side is bounded by darker fragment-laden glass, which is a part of the impact glass vein seen on the E surface. The other side of the clast are sorrounded by dark clast-rich matrix, which represents the matrix portion of the entire breccia.

The compositions of the glassy matrix within the anorthositic breccia, the impact melt glasses, and bulk matrices, plotted in the silica-olivine

-anorthite diagram (Fig. 1), show that the composition of the matrix of the anorthositic breccia is more anorthitic than the bulk matrix, and is similar to those of the Y-82192 anorthositic breccia clast (3). The composition of the dark clast-laden glassy vein is rich in mafic components and silica. Such veins penetrate into the breccia matrices.

The PTS of the representative portion as is given in the Photographic Catalog (1) shows all characteristics of the Yamato-82 lunar meteorites. Granulitic clasts and clast-laden vitric (devitrified) breccias are dominant. The mineral fragments consist of plagioclases, pyroxenes, and olivines, and mafic components are richer than those of Y-791197 (4). The distribution of pyroxene compositions in the pyroxene quadrilateral(Fig. 2) is similar to those of Y-82192 and Y-82193 and to Apollo 16 anorthositic fragmental breccia 67016,111 (5). All kinds of pyroxenes from non-mare crustal rocks are represented in the fragments. One large fragment is an inverted pigeonite with blebby augite inclusions and another large fragment shows moderately coarse (100) exsolution in an orthopyroxene. One subophitic clast includes iron-rich pyroxenes, but they may be a mesostasis portion.

Among the research proposals of our consortium group, those accepted by NIPR for a preliminary examination are listed in a separate table. Some of the results of these members are included as separate abstracts in this volume. O. Eugster will report his noble gas study, which indicates that Y-86032 is noble gas poor and may be paired with Y-82192 and Y-82193.

We thank National Inst. of Polar Research for the samples, and Dr. M. M. Lindstrom and Miss Robie Score for their help on characterization and distribution.

References:

(1) Yanai K., Kojima H. (compiled) and Graham A. L. (1987) Photographic Catalog of the Antarctic Meteorites. 197-199, National Inst. of Polar Research, Tokyo.
(2) Nishio F., Ohmae H., Mori K., Osada K. and Urazuka S. (1987) Abstr. 12th Symp. Antarctic Meteorites. 1-2, NIPR, Tokyo.
(3) Takeda H., Mori H. and Tagai T. (1987) Mem. Natnl. Inst. Polar Res., Spec. Issue 46, 43-55.
(4) Ostertag R., Stöffler D., Bischoff A., Palme H., Schultz L., Spettel B., Weber H., Weckwerth G. and Wänke H. (1986) Mem. Natnl. Inst. Polar Res., Spec. Issue 41, 17-44.
(5) Takeda H. and Miyamoto M. (1988) Lunar and Planetary Science XIX, 1171-1172, Lunar and Planetary Institute, Houston.

*Lists of the Consortium Members

Nishio F., Kojima H. and Yanai K. (NIPR): Recovery, processing and characterization
Kushiro I. and Haramura H. (Univ. of Tokyo): Bulk chemistry and petrology.
Lindstrom M. M. et al. (NASA/JSC): Geochemistry, INAA.
McKay D. S. et al. (NASA/JSN): Regolith study.
Koeberl C. et al. (Univ. of Vienna): Halogens and other trace elements.
Eugster O. (Univ. of Bern): Exposure ages, terrestrial ages, noble gases.
Lipschutz M.E. (Purdue Univ.): Volatile trace elements by RNAA.
Warren P. H. et al. (UCLA): Compositional, petrographic studies by INAA.
Takeda H. et al. (Univ. of Tokyo): Mineralogy.

Clayton R. N. (Univ. of Chicago): Oxygen isotopes.
Masuda A. et al. (Univ. of Tokyo): Geochronology and REE.
Nishiizumi K. and Arnold J. R. (UCSD): Cosmic-ray exposure histories.
Fukuoka T. et al. (Gakushyuin Univ.): Trace element chemistry.
Takaoka N. (Yamagata Univ.): Noble gas analyses.
Tatsumoto M. et al. (USGS Denver): Pb chronology.
Kaneoka I. (Univ. of Tokyo): Ar-Ar chronology.
McFadden L. et al. (UCSD): Reflectance spectroscopy.
Nagata T. and Funaki M. (NIPR): Magnetic properties.
Stöffler D. et al. (Inst. of Planet., Univ. of Münster) and Wänke H. and Begemann F. (Max-Planck-Inst.): Shock metamorphism, multi-element chemistry.
Phillinger C. T. and Grady M. M. (Open Univ.): Carbon and Nitrogen.
Nagao I. (Okayama Univ.): Kr exposure age.
Tanaka T. (Japan Geol. Survey): Ce isotopes.
Nyquist L. E. et al. (NASA/JSC): Rb-Sr and Sm-Nd isotopic studies.
Xie Xiande et al. (Inst. Geochem., Academia Sinica).

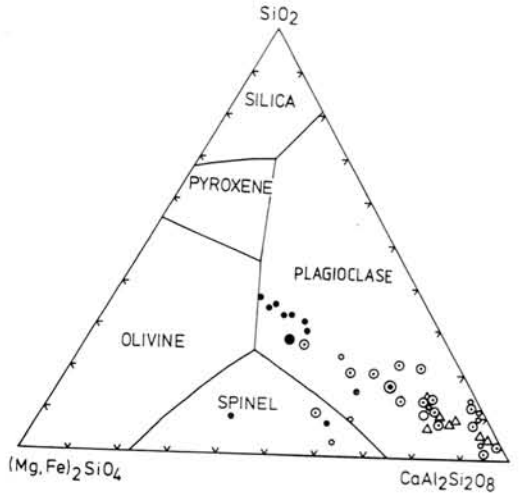

Fig. 1 Compositions of matrix glasses in the Y-82192 anorthositic breccia clast (triangles) and Y-86032 plotted in the silica-olivine-anorthite pseudo-ternary system. Open circles: Y-86032 anorthositic breccia clast; circles with dot: bulk matrix; and solid circles: clast-laden glass vein. Large symbols are average compositions.

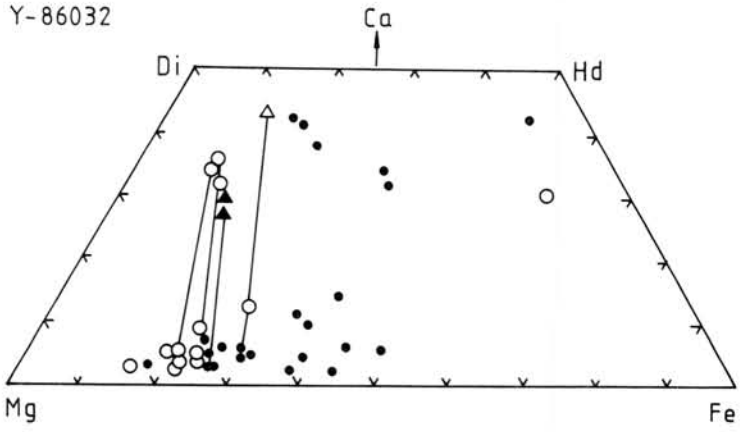

Fig. 2 Pyroxene quadrilateral of Y-86032. Solid circles are compositions of individual fragments of pyroxenes in the matrix. Open circles are those of lithic clasts. Tie lines connect between the host and exsolved lamella augite pairs.

GEOCHEMISTRY OF LUNAR METEORITE YAMATO-86032

PAUL H. WARREN AND GREGORY W. KALLEMEYN

Institute of Geophysics and Planetary Physics, University of California, Los Angeles, CA 90024, USA

Japanese petrologists (Yanai, Kojima, Takeda, and coworkers) have identified the 650 g Yamato-86032 achondrite as an apparent lunar meteorite. We have studied Y86032 using our standard INAA and fused bead - electron probe techniques [1]. Our INAA counting is still incomplete, and for most elements our current results (Table) are strictly preliminary. Nevertheless, the bulk-rock data clearly confirm that Y86032 is lunar. The answer to the second most fundamental question regarding Y86032, a possible pairing with the Y82192/Y82193 meteorites collected at the same area [2], is not so obvious.

Even though the four lunar meteorites that were thoroughly studied before now are remarkably similar in composition (Table), they probably were derived from three separate lunar cratering events. Obviously Y82192 and Y82193 are paired [3,4]. However, the time since lunar blast-off (i.e., the sum of the Moon-Earth transit time plus the terrestrial exposure age) is clearly far longer for Y82192/3 (11 ± 2 My [5]) than for ALHA81005 (0.17 ± 0.5 My [6,7]). The time since lunar blast-off is only marginally different for Y791197 (<0.12 My [6,8]) vs. ALHA81005. However, these two samples are so dissimilar in Mg/(Mg+Fe) ratio (hereafter abbreviated as *mg*), 0.629 vs. 0.728, that a single provenance seems unlikely. Both Y791197 and ALHA81005 are clearly regolith breccias [4,9]. If they were from a single lunar crater, their compositions would probably be highly similar, as they would represent the well-mixed regolith of a single small highlands region. The disparity in *mg* between Y791197 and ALHA81005 exceeds the total range among ~30 regolith breccias from Apollo 16, which sampled at sites as much as 8.5 km apart along a traverse over two distinct highlands formations (Cayley vs. Descartes) [10]. In contrast, the regolith maturity of Y82192/3 is extremely low [3,5,11]. Y82192/3 has been variously described as an immature regolith breccia [4] that may have lost part of its former contents of noble gases due to shock-metamorphism [11], or a well-mixed ordinary fragmental breccia "never exposed to solar wind" albeit "with a minor regolith component" [3]. Either way, and even if Y86032 and Y82192/3 are paired, they cannot be expected to be as compositionally uniform as pieces from a single *mature* regolith breccia.

Yanai and Kojima [2] and Takeda [pers. comm.] have noted a general textural similarity between Y86032 and Y82192/3. In crushing our Y86032 and Y82192/3 samples prior to INAA, we noted that they both are remarkably tough, tougher by far than any other regolith or fragmental breccia we have encountered. This toughness presumably developed by grain boundary melting during one or more extraordinarily severe shock events. Takaoka [11] infers that much of the original noble gas content of Y82192/3 was lost as a result of the shock of the impact that propelled this meteorite off the Moon. If Y86032 proves to be similar, early inferences that lunar meteorites are no more shocked than analogous Apollo rock samples [e.g., 12] may have to be revised, with attendant negative implications for the hypothesis that the massive, often lightly-shocked SNC achondrites are derived from Mars [13].

The general compositional similarity between Y86032 and Y82192/3 (Table) is consistent with the pair hypothesis. Both Y86032 and Y82192/3 have low Ni contents compared to the other lunar meteorites, and low contents of siderophile elements in general (and Au in particular) compared to Apollo and Luna highlands soils (Figure 1). Compared to the other "old" lunar meteorites (A81005 and Y791197), Y82192/3 has far higher Na/Ca, Na/Al, and Eu/Al (ratios that tend to increase as a melt evolves by crystallizing plagioclase) [1]. These ratios are even higher in Y86032 than in Y82192/3 (Figure 2). Both Y86032 and Y82192/3 have even lower contents of REE, Ba, Th, U, and other incompatible elements than the other lunar meteorites, which themselves are remarkably REE-poor compared to Apollo and Luna highlands soils (Table, Figure 3). The La/Lu ratio of Y86032,78 is higher than any La/Lu determination for Y82192/3 [1,3,14-17], but considering the "immaturity" of Y82192/3

this disparity is not necessarily significant. Judging from our single bulk-rock analysis of Y86032, the most potentially significant disparity between Y86032 and Y82192/3 appears in their Fe contents, which differ by a factor of 1.23. This disparity is not simply a manifestation of displacement of mafic silicates by plag in the Y86032 sample, because the Mg contents are nearly identical. The disparity in *mg* ratio between Y86032 and Y82192/3 (Figure 3) raises at least a glimmer of hope that these two meteorites are not paired, despite their similar overall composition, petrology, and terrestrial provenance.

No thin-section petrographic observations are yet available for the two Y86032 clasts that we analyzed. The Y86032,105 clast appears to be a nearly pure-plagioclase anorthosite.

Collectively, the three (or four, if Y86032 is unrelated to Y82192/3) lunar meteorites greatly augment the sample coverage for the lunar surface. In many respects these meteorites are consistently unlike the Apollo and Luna highlands samples, which are of known provenance but unfortunately all from a comparatively minuscule central nearside region of the Moon, around which a polygon could be drawn covering just 4.7% of the lunar surface [12]. The low K, Th, U, etc., contents of the lunar meteorites imply that many current models [e.g., 18,19] for the bulk-Moon composition give overestimates for Th, U, and other refractory lithophile elements. Orbital gamma-ray results for Ti in the highlands apart from the central nearside [e.g., 20-22] also appear spuriously high. Many models for lunar siderophile element geochemistry require revision, particularly the model of Ringwood et al. [23], who argued that lunar Mg-rich melts tend to have Ni contents comparable to terrestrial komatiites.

References: [1] Warren P. H. and Kallemmeyn G. W. (1987) *Proc. Sym. Ant. Met. (SAM) 11th*, 1-20. [2] Yanai K. and Kojima H. (1987) *Abs. SAM 12th*, 3. [3] Bischoff et al. (1987) *Proc. SAM 11th*, 21-42. [4] Takeda H. et al. (1987) *Proc. SAM 11th*, 43-55. [5] Eugster O. (1988) *Proc. SAM 12th*. [6] Nishiizumi K. et al. (1986) *Abs. SAM 11th*, 25-27. [7] Sutton S. R. and Crozaz G. (1983) *GRL* **10**, 809-812. [8] Sutton S. R. (1986) *Proc. SAM 10th*, 133-139. [9] Ostertag R. et al. (1986) *Proc. SAM 10th*, 17-44. [10] Warren P. H. et al. (1987) *LPS XVIII*, 1060-1061. [11] Takaoka N. (1987) *Proc. SAM 11th*, 96-104. [12] Warren P. H. et al. (1983) *GRL* **10**, 779-782. [13] Vickery A. M. and Melosh H. J. (1983) *Icarus* **56**, 299-318. [14] Fukuoka T. et al. (1986) *Abs. SAM 11th*, 40-42. [15] Nakamura N. et al. (1986) *Abs. SAM 11th*, 47-48. [16] Koeberl C. (1988) *Proc. SAM 12th*, in press. [17] Lindstrom M. et al. (1987) *Abs. SAM 12th*, 19-21. [18] Taylor S. R. (1986) In *Origin of the Moon* (W. K. Hartmann et al., eds.), 125-143. [19] Drake M. J. (1986) In *Origin of the Moon* (W. K. Hartmann et al., eds.), 105-124. [20] Haines E. L. and Metzger A. E. (1977) *PLSC* 11, 689-718. [21] Metzger A. E. and Parker R. E. (1979) *EPSL* **45**, 155-171. [22] Davis P. A., Jr. (1980) *JGR* **85**, 3209-3224. [23] Ringwood A. E. et al. (1987) *EPSL* **81**, 105-117.

Fig. 1

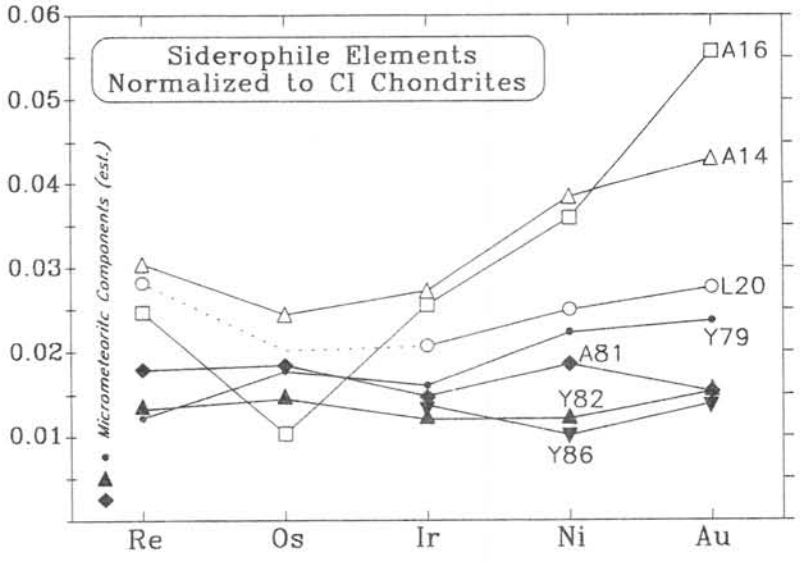

		Y791197 Wtd. Mean	ALHA81005 Wtd. Mean	Y82192-3 Wtd. Mean	Y86032,78 Bulk, 244 mg	Luna 20 Avg. Soil	Apollo 16 Avg. Soil	Y86032,104 Clast 2.5 mg	Y86032,105 Clast 2.4 mg
Na	mg/g	2.43	2.24	3.06	3.31	2.88	3.5	3.41	2.81
Mg	mg/g	36.7	49.3	33.0	33.5	56.3	35.0		
Al	mg/g	138	135	141	147	122	143		
Si	mg/g	203	214	211	211	212	210		
K	μg/g	220	194	182	209	622	920	161	149
Ca	mg/g	110	107	110	112	102	112	140	131
Ti	mg/g	2.01	1.51	1.62	1.2	2.81	3.40		
Fe	mg/g	49.77	42.32	40.26	32.8	56.21	41.0	26	3
Sc	μg/g	13.0	9.1	11.0	8.0	16.5	9.3	6.1	0.79
V	μg/g	31.2	24.6	34.3	30	45.1	21.1		
Cr	μg/g	892	885	879	666	1265	728	1520	197
Mn	μg/g	633	583	563	476	850	512	380	65
Co	μg/g	25.5	21.0	16.6	14.5	30.0	26.8	6.0	<2
Ni	μg/g	245	198	130	100	261	384		
Ga	μg/g	5.6	2.7	3.7	3.4	3.7	4.3	3.7	3.5
Br	μg/g	159	188	80	120	140	140		
Ba	μg/g	31.0	28.4	22.9	36	98	127		
La	μg/g	2.11	1.98	1.21	1.6	6.60	11.9	1.3	1.27
Nd	μg/g	3.46	3.22	1.91	1.9	11.3	19.0		
Sm	μg/g	1.05	0.95	0.58	0.66	3.24	5.7	0.3	0.22
Eu	μg/g	0.77	0.69	0.82	1.04	0.91	1.20	1.11	0.91
Tb	μg/g	0.247	0.214	0.155	0.14	0.59	1.13		
Dy	μg/g	1.53	1.33	0.94	1.21	4.17	7.4	0.59	0.16
Yb	μg/g	0.99	0.84	0.62	0.64	2.22	4	0.4	
Lu	μg/g	0.145	0.124	0.096	0.09	0.361	0.59	0.048	<0.12
Hf	μg/g	0.87	0.72	0.46	0.49	2.35	4.1	<2.5	
Ir	ng/g	7.33	6.76	5.51	6.2	9.51	11.7		
Au	ng/g	[3]	2.17	2.3	1.8	3.97	8.02		
Th	μg/g	0.321	0.291	0.178	0.23	1.06	1.90	<1.9	<1.9
U	μg/g	0.113	0.098	0.051	0.062	0.345	0.56		
Molar Mg/(Mg+Fe)		0.629	0.728	0.653	0.701	0.697	0.662		

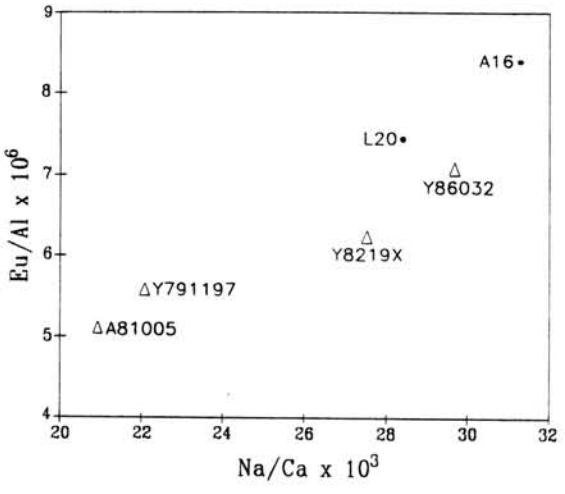

Fig. 2

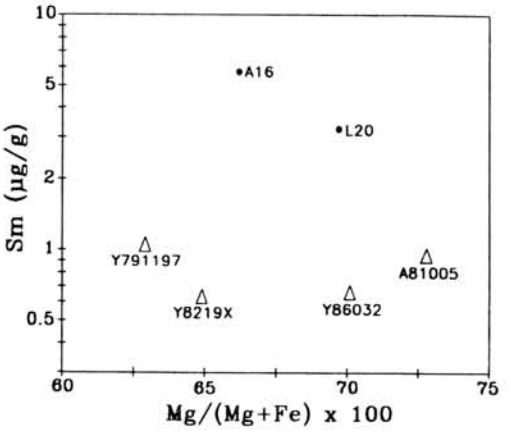

Fig. 3

NEW METEORITE FINDS IN THE ALLENDE AREA, MEXICO.

Sánchez-Rubio, G.*, Nagasawa, H.**, Matsui, T.***

*) Instituto de Geología (UNAM), México, D.F., MEXICO.
**) Gakushuin University, 1-5-1 Mejiro Toshima, TOKYO.
***) Geophysical Institute, Univ. Tokyo, TOKYO 113, JAPAN.

A research project aiming at studying the results of meteoritic impacts and recovery of meteorite material in northern México and southern USA, allowed us to reach the Allende area in August 1984. Following a suggestion of Sr. Evodio Arellanes we carried out a special search in the field near Pueblito de Allende, looking for remnants of a previously discovered meteorite. We found 3 small fragments (2.3, 1.7, and 1.6 grams) which we named provisionally Allende III. Another fragment (20.0 g) was provided by Sr. Arellanes afterwards. Also at Pueblito de Allende, Sr. Francisco Betances showed us another small stone (214.6 g) which we identified as a meteorite later on. It was given the provisional name "Allende II". According to Sr. Betances it was found 6 km east of Pueblito de Allende.

Allende II is an olivine-hypersthene chondrite, petrologic type L6. Olivine range in composition from Fa23.8 to Fa25.8 (average of 5 microprobe analyses: Fa24.5). Low-Ca pyroxene varies in composition from Fs20.4 to Fs20.5 (2 microprobe analyses).

Texture in Allende II is granoblastic with small patches of crypto-crystalline material (remnants of a former matrix?). Plagioclase amounts to less than 1% and appears in small xenomorphic crystals without twinning. Uneven extinction is common to all mineral grains. Chondrules are mainly barred and excentroradial with diffuse borders.

Allende III is also an ordinary chondrite with olivine and pyroxene as main components. Seen under the microscope it looks extremely inequigranular, breccia-like, and chondrules, more abundant than in Allende II, show sharp edges. Glass in chondrules is poorly devitrified and plagioclase shows its usual polysynthetic twinning.

Other meteorite finds formerly reported in the Allende area are:

Salaices, olivine-bronzite chondrite, H4.
Abajo, olivine-bronzite chondrite, H5.
Torreón de Mata, olivine-hypersthene chondrite, L6.
Villa Coronado, olivine-bronzite chondrite, H5.

Allende II may be the same as Torreón de Mata, but the latter was a fresh and completely crusted individual when found in 1983. Neither Allende II nor Allende III had fusion crust.

THERMAL RELEASE OF ORGANIC COMPOUNDS FROM INSOLUBLE ORGANIC MATTER IN THE YAMATO-791198 CARBONACEOUS CHONDRITE

Shimoyama, A., Komiya, M., and Harada, K.

Department of Chemistry, University of Tsukuba, Tsukuba, Ibaraki 305

A large portion of organic matter in carbonaceous chondrites are present in insoluble form. Some attempts have been reported to clarify the insoluble organic matter chemically by thermal treatment of the chondrite and analysis of the released organic compounds(or fragments). So far, in most of these studies, the sample was heated at a few to several different temperatures to release organic compounds.

We carried out a continuous heating experiment of a carbonaceous chondrite from room temperature to 1000 ^{o}C, in order to reveal released organic compounds(fragments) and their distributions over the heating temperature range.

The sample was placed in a platinum cell for the differential thermal analysis(DTA) and thermogravimetric analysis(TG). The two analyses were done simultaneously in the ordinary manner under a stream of He. The heating temperature was programed from room temperature to 80 ^{o}C by the temperature increasing rate of 20 ^{o}C/min, held for 15 min at 80 ^{o}C, and heated to 1000 ^{o}C by the rate of 10 ^{o}C/min.

The DTA/TG instrument was connected to a mass spectrometer(MS) for a further simultaneous detection of organic compounds. However, the amounts of compounds continuously released from the DTA/TG were too small to be detected by the MS. Therefore, we set a cold trap in between the DTA/TG and the MS. Starting at 100 ^{o}C of the sample heating temperature, volatiles from the sample were trapped by the cold trap at every 50 ^{o}C for 3 min (equivalent to 30 ^{o}C in the temperature increase during the sample heating). As soon as each trapping was over, the trap was heated at 280 ^{o}C for 2 min (eq. 20 ^{o}C), and the volatiles were transfered into the MS by the stream of He.

The sample we examined was a powder portion(41.2 mg) of Yamato-791198 pre-extracted with benzene and methanol(9:1 by vol).

The DTA and TG curves are shown in Fig. 1a. The first endothermic peak appeared under 100 ^{o}C accompaning weight loss. From the MS analysis, the released compounds could be largely H_2O(m/z 18) with some amounts of NH_3 (17), and CO_2(44). The second endothermic peak appeared between 100 - 200 ^{o}C with weight loss, indicating further increase of released H_2O and NH_3. The TG curve shows almost continuous release of compounds from 200 ^{o}C till 1000 ^{o}C, except around 600 ^{o}C. In the temperature range between 650 - 700 ^{o}C, the DTA curve shows an exothermic peak accompaning a rather notable weight loss. Figure 1b shows the percent of weight loss for 30 ^{o}C at every 50 ^{o}C interval starting at 100 ^{o}C. It is clear from the graph that the peaks of the weight loss appeared at 150 ^{o}C, 400 - 500 ^{o}C, and 650 - 700 ^{o}C.

Figure 2 shows relative intensities of the total ions and major ions at the 50 ^{o}C interval by the MS analysis. These major ions are tentatively assigned to H_2O, CO_2, NH_3, and SO_2. It seems that the major release of H_2O took place over the temperature range from 80 ^{o}C to 750 ^{o}C. A similar release pattern was observed with NH_3, although this release became decreasing around 650 ^{o}C. The release of CO_2 was delayed as compared with H_2O and NH_3, became intense at 250 ^{o}C and lasted till 850 ^{o}C. On the other hand, the release of SO_2 did not occur untill 200 ^{o}C and became intense around 300 ^{o}C, 500 ^{o}C, and 950 ^{o}C.

Figure 3 shows the release patterns of hydrocarbons. The aromatic compounds appeared in lower temperature range, less than 500 ^{o}C, while the aliphatics did in higher temperature range from 500 ^{o}C to 900 ^{o}C.

Figure 4 shows bimordial distributions of ions, m/z 27 and 41. On the basis of that appearance of the aliphatic hydrocarbons in Fig. 3, the two ions which became notable over 600 ^{o}C were assigned to unsaturated aliphatic hydrocarbons in Fig. 4. On the other hand, these two ions likely represented those for HCN and CH_3CN in the temperature range of less than 500 ^{o}C. The release pattern of NH_3 was similar to those for the two compounds.

Heterocyclic compounds, such as thiophene(S-containing), pyrrole(N-containing), and furan(O-containing) were released between 250 ^{o}C and 450 ^{o}C as seen in Fig. 5. These release patterns were basically similar to those of aromatic hydrocarbons.

Those compounds released were inorganic volatiles, aliphatic and aromatic hydrocarbons, nitriles, thiophenes, pyrroles, and furans. All of those compounds shown in Figs. 2 to 5 except SO_2 could be derived from insoluble organic matter. It is likely that the insoluble organic matter degradated and released organic compounds(fragments) in two major stages during the chondrite heating. The first stage maximized around 350 ^{o}C and the second around 750 ^{o}C, although benzene did not fall in this pattern. Data of the DTA and TG supported the two major stages for the degradation.

Characterization by those compounds and their distributional patterns along the heating temperature, together with the consideration of extractable organic compounds, such as amino acids, carboxylic acids, and hydrocarbons, would give useful information on the insoluble organic matter in a carbonaceous chondrite and on primordial organic chemistry in the early solar system.

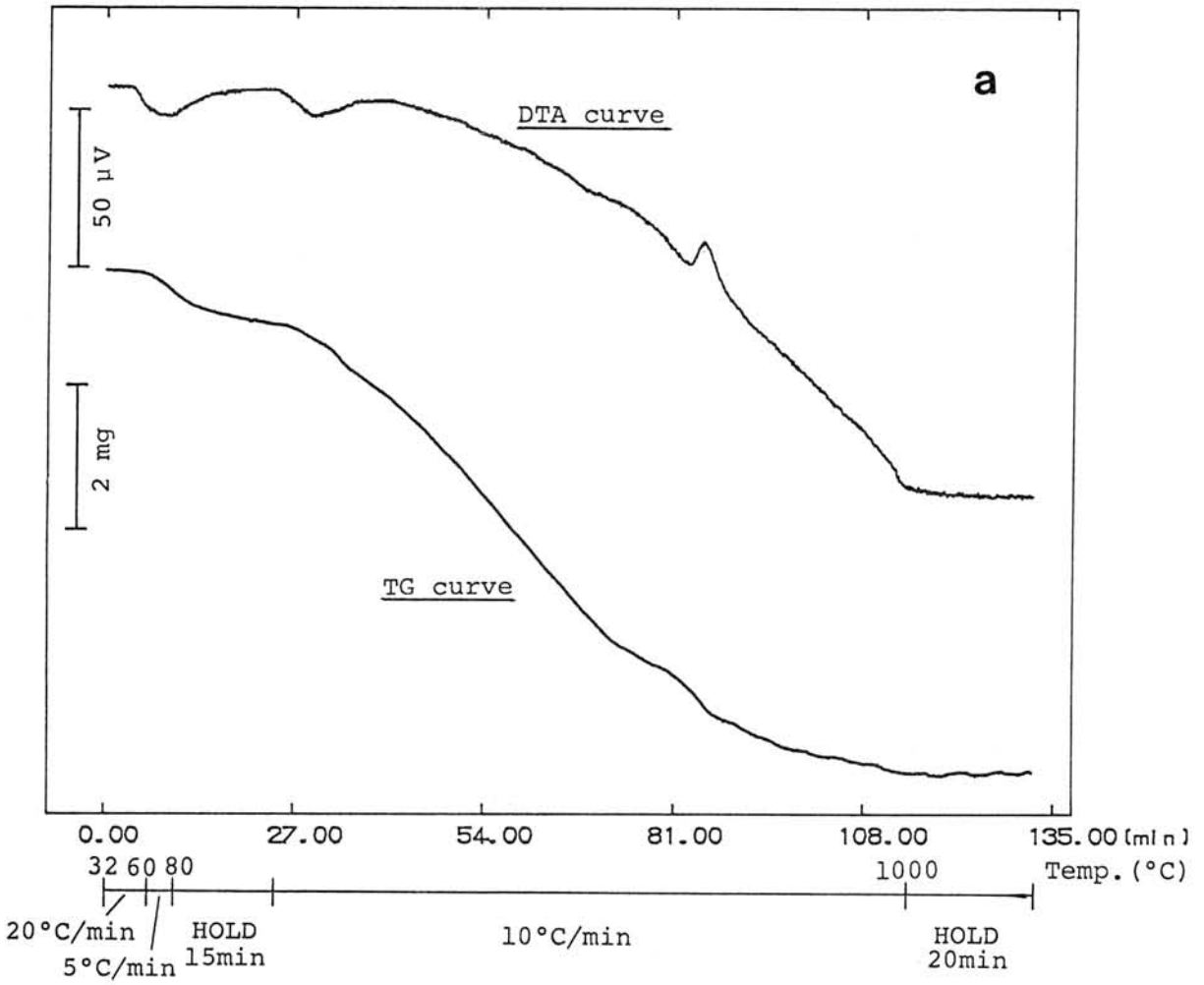

Sample : Yamato-791198.22(pre-extracted with benzene/methanol)
Sample size : 41.20mg, He flow 50ml/min

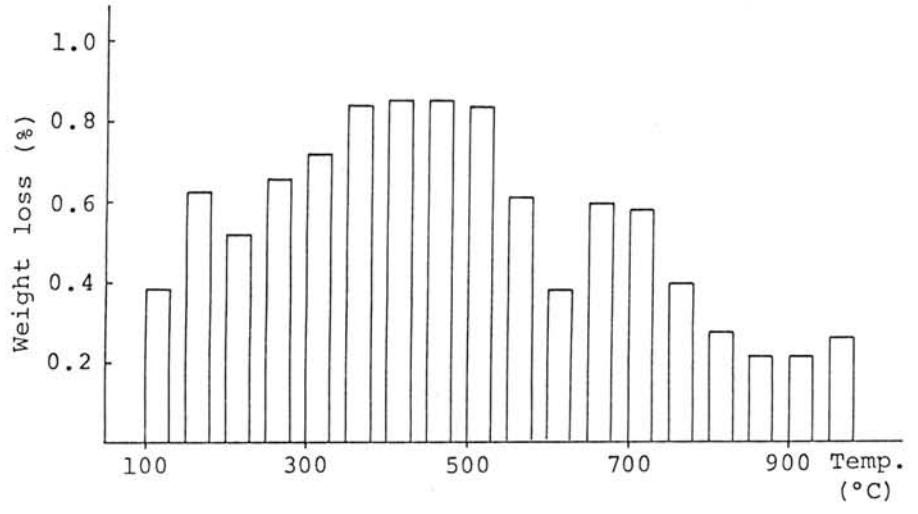

Fig. 1. a : Thermal analyses (DTA and TG) of Yamato-791198 and
b : the weight loss for 30°C at each 50°C interval.

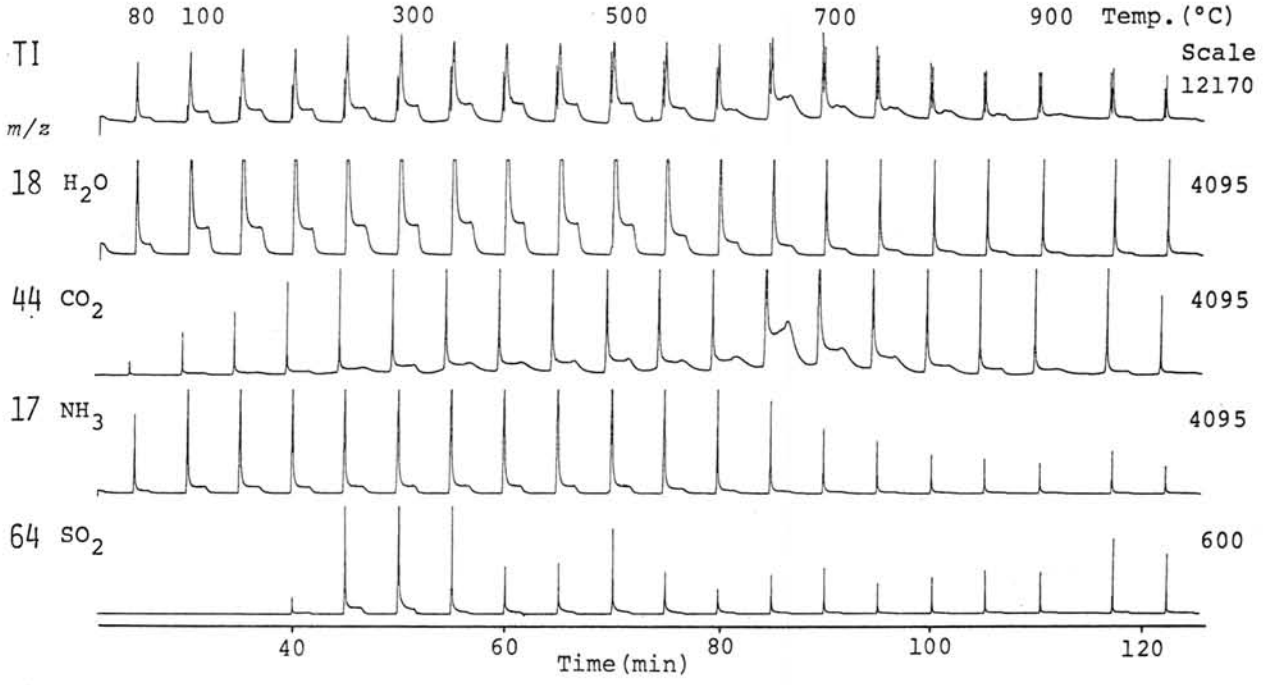

Fig.2. Distributions of major ions generated from components released from Yamato-791198 along the heating temperature. (TI:total ions)

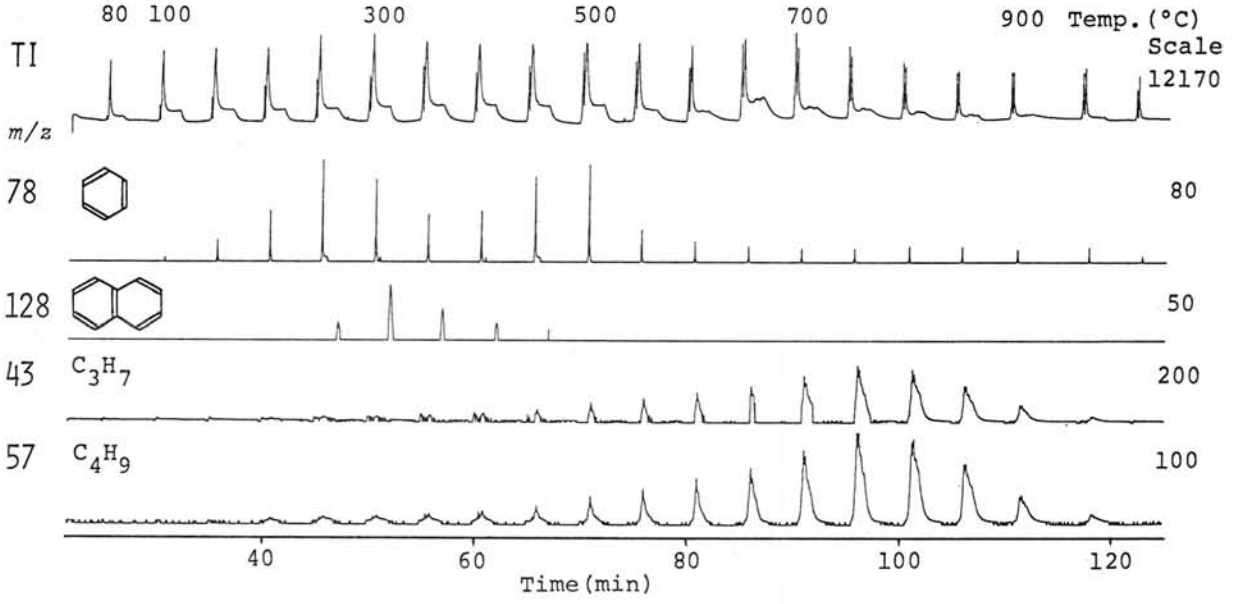

Fig.3. Distributions of ions for hydrocarbons generated from components released from Yamato-791198 along the heating temperature. (TI:total ions)

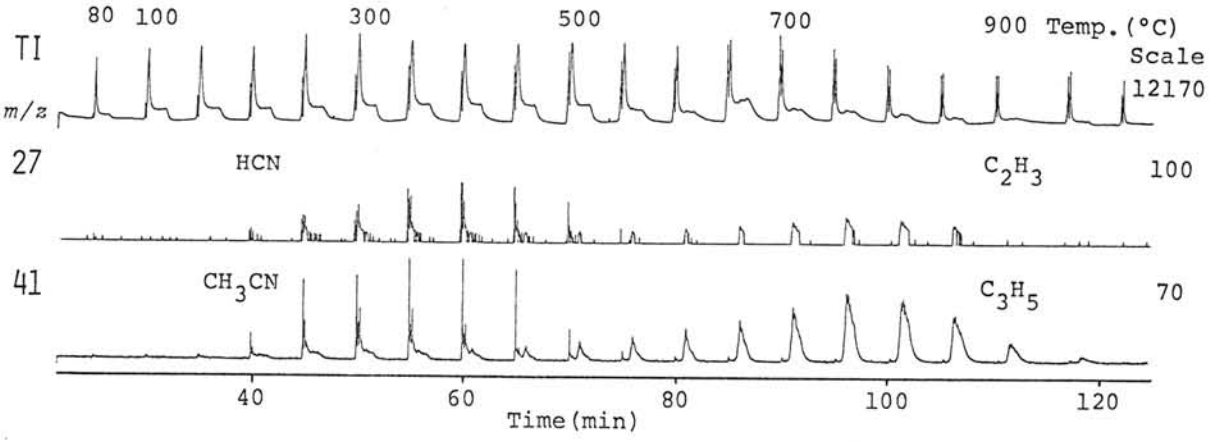

Fig.4. Distributions of ions containing two components generated from components released from Yamato-791198 along the heating temperature. (TI:total ions)

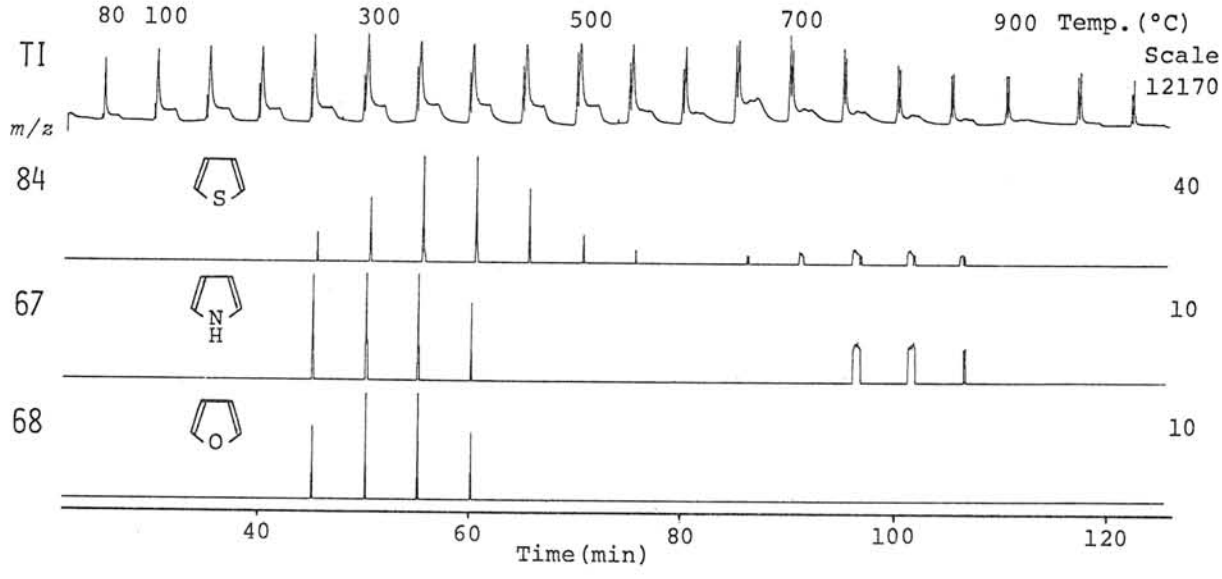

Fig.5. Distributions of ions for heterocyclic compounds generated from components released from Yamato-791198 along the heating temperature. (TI:total ions)

PYROLYTIC STUDIES OF HCl AND HF RESIDUES FROM CARBONACEOUS CHONDRITES

Murae, T., Masuda, A., and Takahashi, T

Department of Chemistry, Faculty of Science, University of Tokyo, Bunkyo-ku, Tokyo 113.

Organic polymers are major components of carbonaceous matter in carbonaceous chondrites. The polymers concentrate in the residues given by treatments with hydrochloric acid (HCl) and hydrofluoric acid (HF). Most of characterization of organic polymers in carbonaceous chondrites has been done on the HCl and HF residues. Alterations of the structure of the polymers may have occurred on the acid treatments. Pyrolytic studies on the HCl and HF residues give some informations on the alterations.

Carbonaceous chondrite Allende (C3V) and Antarctic carbonaceous chondrites ALH-77307 (C3) and Y-791717 (C3) were treated with hydrochloric acid (HCl) and hydrofluoric acid (HF) to give residues whose minerals were partially dissolved. Organic matter contained in the residues examined by pyrolysis-GC-FID and pyrolysis-GC-MS.

A number of organic sulfur compounds were observed with significant intensities in the pyrolysis products from the samples half whose minerals were dissolved. These sulfides (except thiophen and benzothiophen) did not give intense peaks in the pyrograms of acid-untreated samples (ex. Fig. 1). Relative intensities of the sulfides to aromatic hydrocarbons were increased on repetition of acid treatments.

Treatments in concd HCl at room temperature, collection of residues by centrifugation, and washing with water were carried out successively and the sequence was repeated three times. After similar treatments using 48% HF instead of HCl, the residues were treated with HCl and water again and washed with methanol to remove water. The residues obtained by the above treatments were extracted with a mixed solvent of benzene - methanol (2:1) using a Soxhlet extractor. By these procedures, 572 mg of Allende yielded 5.36 mg of black residues and 1.06 g of ALH-77307 gave 10 mg of residues containing 45.5% of carbon.

The residues obtained above were examined by pyrolysis-GC-FID (Fig. 2). The components given by pyrolysis of the residues were simple compared with those obtained by pyrolysis of the acid-untreated samples. The intensities of the peaks were much weaker than those expected on the basis of the carbon contents. We consider that the increase of the sulfides on the acid treatments are due to an increase of free sulfur generated from FeS on the treatments (crystals of free sulfur were obtained on evaporation of the solvent of the organic extracts) and the decrease of the products on pyrolysis of the final residues indicates possible occurrence of an alteration of the structure of the organic polymer in the chondrites on the acid treatments.

Fig. 1. Gas chromatograms of the products in pyrolysis at 740 °C for A: Y-791717 (9 mg) (after HCl treatment; C: 0.22%), B: Y-791717 (16 mg) (before acid treatment; C: 0.12%). Column: OV-1, 25m x 0.25mm i.d. Detector: FID, Attenuation: 1. Range: 8.

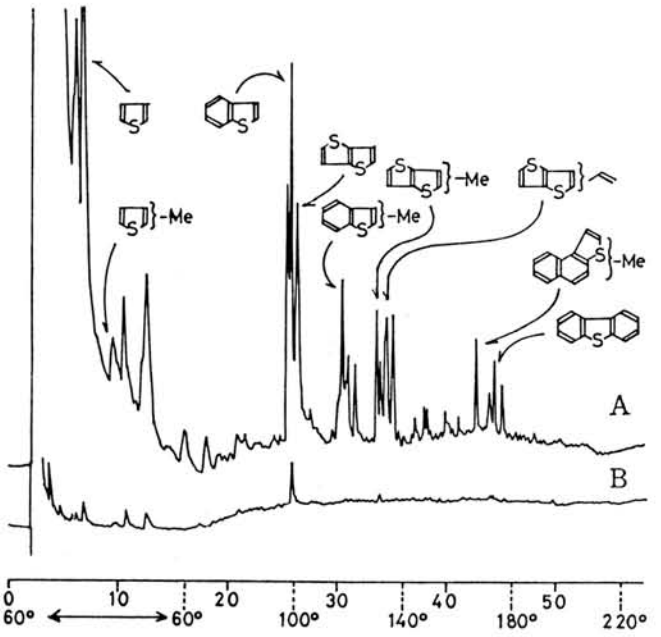

Fig. 2. Gas chromatograms of the products in pyrolysis at 740 °C for A: Allende treated with HCl, HF, and PhH - MeOH (1.074 mg), B: ALH-77307 treated with HCl, HF, and PhH - MeOH (0.356 mg, C: 45.5%). Conditions are the same as those in Fig. 1.

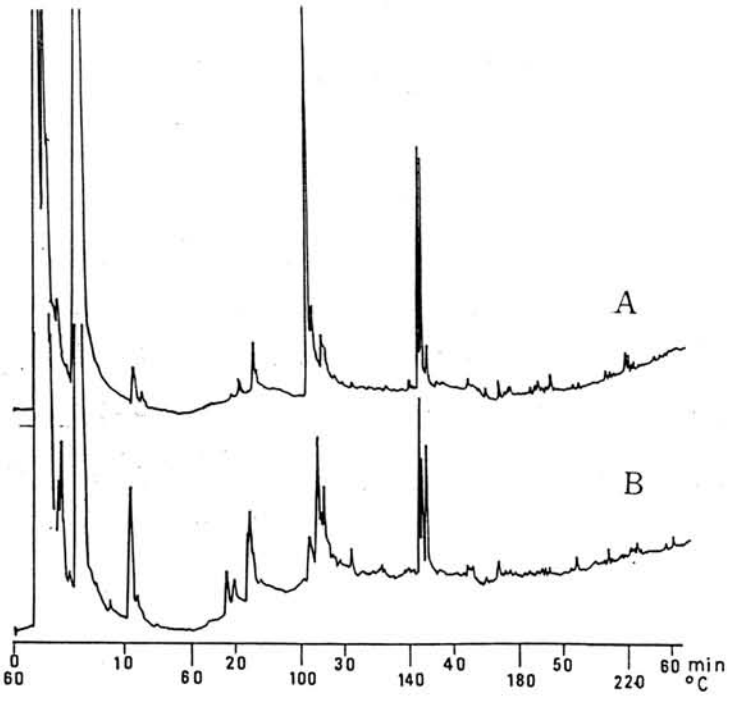

DETECTION OF FIVE ^{13}C ISOTOPIC SPECIES OF HC_5N IN THE TAURUS DARK CLOUD TMC1

Shuro Takano*, Yasuhiro Hirahara*, Akimasa Masuda*, Hiroko Suzuki**, Masatoshi Ohishi**, Shin-ichi Ishikawa**, and Norio Kaifu**

* Department of Chemistry, University of Tokyo, Hongo, Tokyo 113 Japan

** Nobeyama Radio Observatory, Minamimaki, Minamisaku, Nagano 384-12 Japan

Interstellar HC_5N (H-C≡C-C≡C-C≡N) was first detected in the Galactic center (Sgr B2) in 1976(1). Its deuterated species was already reported(2,3), but the attempts to detect the ^{13}C isotopic species have been unsuccesful(4,5). If the ^{13}C isotopic species (five mono-substituted species) could be detected by radiotelescope, the information on the chemical fractionation of ^{13}C isotope and, furthermore, on the reaction mechanisms for the production of interstellar HC_5N and related carbon chain molecules would be obtained.

A 45-meter radiotelescope with the low noise receiver using SIS (Superconductor-Insulator-Superconductor) mixer at Nobeyama Radio Observatory was used for our observation. The observation was carried out four times from June 1987 to March 1988 toward Taurus dark cloud TMC1 where strong emissions of carbon chain molecules including HC_5N are detected. The transitions in 37 GHz region for the rotational quantum number J=14-13 was searched for, and as a result all ^{13}C isotopic species were detected for the first time.

Some of the obtained spectra are shown in Figs. 1 and 2, and integrated intensities of these spectra are listed in Table 1. Since the molecular constants are nearly the same for each species, the integrated intensities can be used directly to estimate their abundances. The data presented in the Table seem to show that the integrated intensities are the same within their observational errors. This result suggests that the production of HC_5N is not affected by chemical fractionation, or that the effects of chemical fractionation for each ^{13}C isotopic species are similar since the speed of the carbon chain growing is constant. From the abundance of normal HC_5N species, we also calculated the carbon isotopic ratios ($^{12}C/^{13}C$) for each ^{13}C isotopic species (see Table 1). The values in parentheses represent the lower and upper limits taking into account the estimated errors. These isotopic ratios are rather near to the

solar value ($^{12}C/^{13}C$=89), and it seems certain that the effect of the chemical fractionation is small assuming that the solar value is near the value in TMC1.

References:
(1)L.W.Avery, N.W.Broten, J.M.Macleod and T.Oka Astrophys.J., **205**, L173 (1976)
(2)J.M.Macleod, L.W.Avery and N.W.Broten Astrophys.J., **251**, L33 (1981)
(3)F.P.Schloerb, R.L.Snell, W.D.Langer and J.S.Young Astrophys.J., **251**, L37 (1981)
(4)E.Churchwell, G.Winnewisser and C.M.Walmsley Astron.&Astrophys., **67**, 138 (1978)
(5)F.Tölle, H.Ungerechts, C.M.Walmsley, G.Winnewisser and E.Churchwell Astron.&Astrophys., **95**, 143 (1981)

Table 1 Integrated intensities and carbon isotopic ratios for each ^{13}C species

^{13}C SPECIES	INTEGRATED INTENSITY(K*km/s)	ISOTOPIC RATIO ($^{12}C/^{13}C$)
$H^{13}CCCCCN$	0.021±0.010	102(57,217)
$HC^{13}CCCCN$	0.021±0.008	106(61,210)
$HCC^{13}CCCN$	0.019±0.006	117(73,203)
$HCCC^{13}CCN$	0.023±0.006	98(63,158)
$HCCCC^{13}CN$	0.025±0.008	90(54,161)

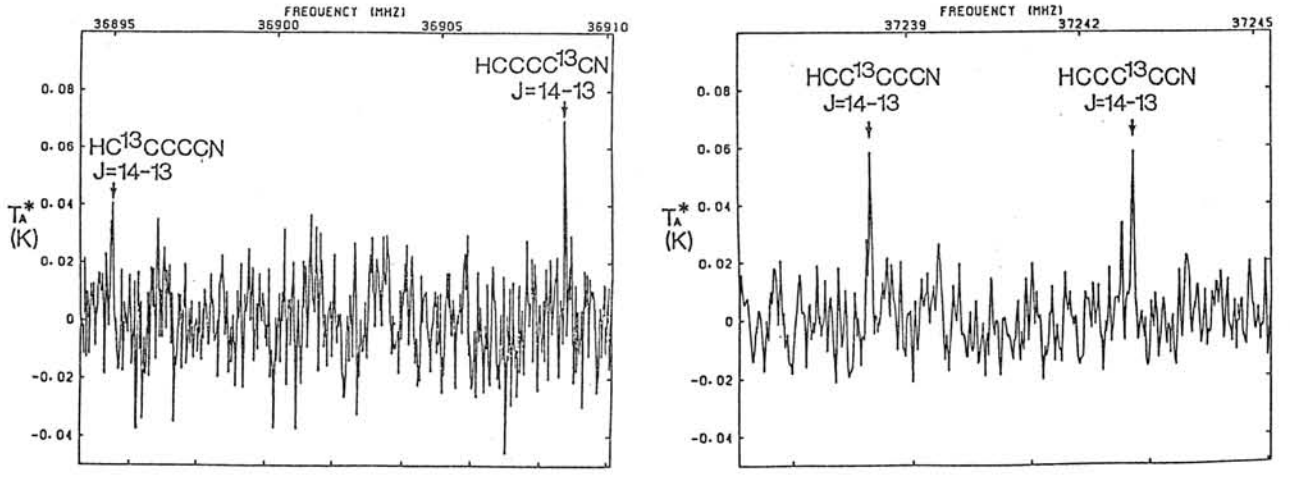

Figure 1 and 2 The spectra of ^{13}C isotopic species of HC_5N by the radiotelescope. The ordinate is shown by T_A^*, antenna temperature, which corresponds to the intensity of the radiowave.

PETROLOGY AND MINERALOGY OF THE NINGQIANG CARBONACEOUS CHONDRITE

Wang Daode

Institute of Geochemistry, Academia Sinica, Guiyang, China

The Ningqiang meteroite fell at 19:00 hours local time on June 25, 1983 in Ningqiang County, Shanxi Province in the People's Republic of China. Four stones with respective masses of 0.35, 0.38, 0.78 and 3.1 kg were recovered. The bulk chemical composition of Ningqiang is shown as fallows (wt.%): SiO_2 33.95, TiO_2 0.13, Al_2O_3 2.74, Cr_2O_3 0.53, FeO 26.11, MnO 0.19, MgO 24.51, CaO 2.25, Na_2O 0.54, K_2O 0.04, P_2O_5 0.25, Fe 0.31, Ni 0.95, FeS 5.74, NiS 0.94, Co 0.07, Cu 0.031, Zn 0.01, C 0.68. Modal analysis indicates that Ningqiang contains (in vol.%): 93.2% silicates, 3.3% magnetite, 3.0% sulfide and 0.5% metallic Fe-Ni. The high abundance of matrix (49.5 vol.%) and the occurrence of many chondrules$\geq$1.0 mm in diameter show that Ningqiang resembles CV3 chondrites. The high magnetite/metallic Fe-Ni ratio (6.6) and the occurrence of awaruite(roughly Ni_3Fe) as the principal metal phase indicate that Ningqiang is similar to the oxidized CV3 subgroup. Random analyses of$\geq$5 μm grains of olivine and low-Ca pyroxene show these minerals to be compositionally heterogeneous with olivine the more variable. The mean olivine composition is Fa 2.8; σFa=1.8 and the percent mean deviation (%MD) is 44. The low-Ca pyroxene compositional distribution at Fs 0.8; the mean composition is Fs 1.3 (σFs= 0.87, %MD=46). The predominant opaque minerals in Ningqiang are magnetite, metallic Fe-Ni (awaruite) and sulfide (troilite and pentlandite). A few pentlandite grains contain small patches of mackinawite that probably exsolved from Fe-rich regions in the pentlandite. We have found igneous chondrules (PO, BO and POP), microgranular chondrules, aggregational chondrules and granoblastic chondrules. Refractory inclusions are rare in Ningqiang. Most abundant are the fine-grained inclusions. One coarse-grained and two fine-grained inclusions were analyzed in thin sections. One coarse-grained inclusion is

round, 2.6 x 3.0 mm in size, and consists (in wt.%) of 71% anorthite, 25% spinel and 4% forsterite. The bulk composition of the inclusion, calculated from modal abundances and mineral composition is (in wt.%): 33% SiO_2, 42% Al_2O_3, 0.3% Cr_2O_3, 0.2% FeO, 9.5% MgO, 14% CaO, 0.5% Na_2O and 0.04 K_2O. This composition is very refractory: Mg-normalized Al and CV abundances are at 32 x CV, respectively. Another Ca-Al-rich inclusion is irregular (300 x 250 μm), and consists of 60% melilite, 25% spinel, 12% fassaite and 3% perovskite. The third Ca, Al-rich inclusion consists of 70% melilite, 30% spinel and minor perovskite. The mean composition of three melilite grains is (in wt.%): Na_2O 0.10, K_2O 0.02, MgO 1.49, CaO 42.64, FeO 0.20, Cr_2O_3 0.02, Al_2O_3 34.44, TiO_2 0.10, SiO_2 20.42. The mean composition of three pervskite grains is (in wt.%): Na_2O 0.10, K_2O 0.03, MgO 0.34, CaO 41.20, FeO 0.16, Cr_2O_3 1.21, TiO_2 56.12, SiO_2 0.22. Olivine aggregates include unrimmed olivine and rimmed olivine aggregates. The are some olivine aggrests that are intemediate between the rimmed and unrimmed varieties.

Relative to Mg and mean CV chondrites (kallemeyn and Wasson, 1981), Ningqiang is significantly depleted in refractory lithophiles (~0.82 x CV). Thus, Ningqiang has a very low abundance of refractory inclusions (2± vol.%). Ningqiang is an anomalous CV chondrite (oxidized subgroup), and shows a cosmic-ray exposure age of 43.2± 1.0 m.y., the highest of all CV3 chondrites found so far (Eugster et al, 1987).

We thank A.E. Rubin, G.W. Kallemeyn and J.T. Wasson for discussions and supports.

References: G.W. Kallemeyn and J.T. Wasson. The compositional classification of chondrites: I. the carbonaceous chondrite group. Geochim. Cosmichim. Acta 45, 1217-1230, 1981. O. Eugster et al, Exposure ages and radiogenic ages of two unusal chondrites: Guangnan (L6) and Ningqiang (CV), preprint.

MAJOR ELEMENT CHEMICAL COMPOSITIONS OF THE CONSTITUENTS IN C3 CHONDRITES AND THEIR FORMATIONAL ENVIRONMENTS

Ikeda, Y.

Department of Earth Sciences, Ibaraki University, Mito 310.

Carbonaceous chondrites of C3 type include various kinds of constituents. The main constituents are coarse-grained CAI's, fine-grained CAI's, amoeboid olivine inclusions(AOI's), chondrules, dark inclusions and matrix. The major element chemical compositions of these main constituents in Allende(CV3), ALH-77003(CO3) and Y-790992(CO3) except for coarse-grained CAI's were obtained using a broad beam of an electron-probe micro-analyser, and their compositional and genetical relationships are discussed.

There are two distinct compositional trends: inclusion-matrix trend and chondrule trend. The inclusion-matrix trend consists of type-A CAI's, fine-grained CAI's, AOI's, dark inclusions and matrix, showing a continuous compositional spectrum in an Al-Si-(Mg+Fe) diagram. On the other hand, the chondrule trend consists of various textural types of chondrules and deviates from the inclusion-matrix trend in the Al-Si-(Mg+Fe) diagram.

A remarkable mineralogical difference between the two trends is that the all constituents of the inclusion-matrix trend are lacking in low-Ca pyroxenes although most chondrules include low-Ca pyroxenes as a main phase.

Fig. 1 shows clearly the compositional difference between the two trends. The chondrule trend ranges mainly from a high Mg/Fe and Al/Na composition to low Mg/Fe and Al/Na composition via a high Mg/Fe and low Al/Na composition (Fig. 1-a). On the other hand, the inclusion-matrix trend ranges mainly from a high Mg/Fe and Al/Na composition to a low Mg/Fe and Al/Na composition via a low Mg/Fe and high Al/Na composition with some exceptions (Fig. 1-b). The exceptions are explained by the idea that fassaitic pyroxenes in fine-grained CAI's and AOI's reacted more or less with an oxidized gas to introduce alkalis and FeO into the fine-grained CAI's and AOI's in a low-temperature range.

The experiments for formation of alkali-zoned chondrules, which occur in C3 chondrites, indicate that the introduction of alkalis and FeO into chondrules and inclusions took place at the temperatures from 800°C to 600°C for a short duration. This temerature range suggests that the reacted gas was an extremely-oxidized one and the H/O atomic ratio may have been lower than about 10.

In conclusion, the inclusion-matrix trend was produced by condensates from oxidized gases which may have formed by evaporation of comets, and the chondrule trend was produced by condensates from relatively-reduced nebular gases. After the mixing of inclusions and chondrules in oxidized gases, alkali-zoned chondrules were produced from glassy chondrules and the matrix of C3 chondrites condensed to accrete on the parent body.

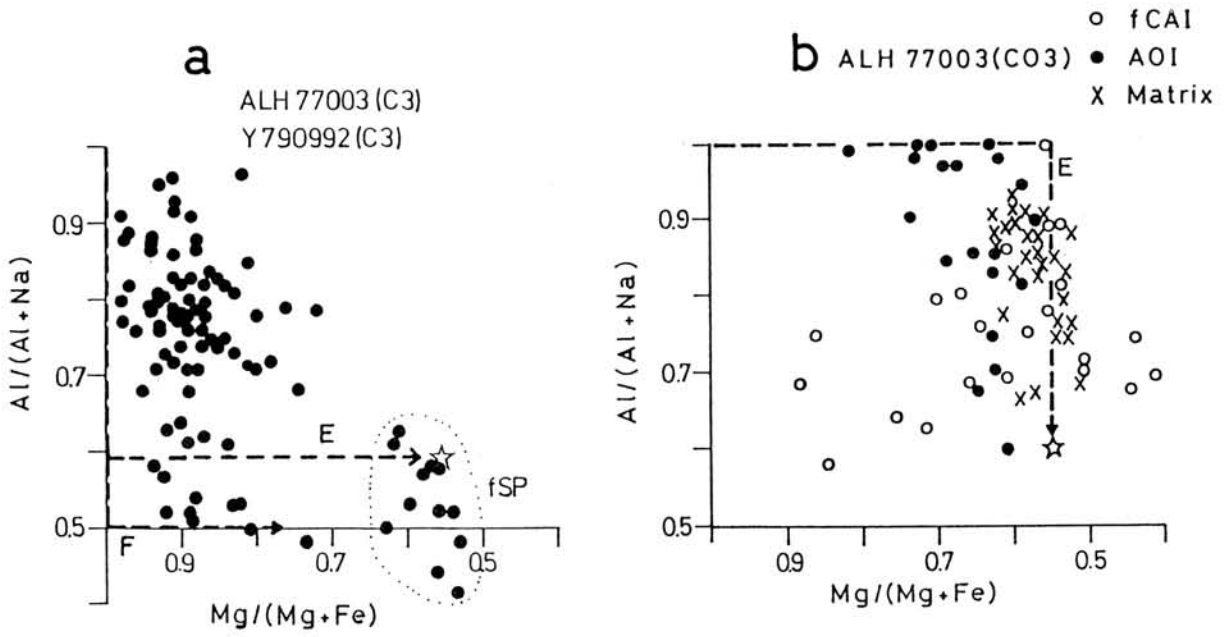

Fig. 1. Chemical compositions of (a) chondrules in ALH-77003 (CO3) and Y-790992(CO3) and (b) fine-grained CAI's, amoeboid olivine inclusions(AOI's) and matrix in ALH-77003(CO3). Open stars in (a) and (b) are solar system elementary abundances, and fSP is ferroan SP-type chondrules. Dash-lines E and F in (a) are trends of equilibrium- and fractionation-condensates from a reduced gas, respectively. A dash-line E in (b) is a trend of equilibrium-condensates from an oxidized gas.

FORMATION OF TYPE B1 CAI

Hiroko Nagahara[1] and Hiroshi Nagasawa[2]; [1]Geol. Inst., Univ. Tokyo, Hongo, Tokyo 113, Japan; [2]Dept. Chemistry, Gakushuin Univ., Mejiro, Tokyo 171, Japan

It has been widely accepted that type B1 CAI was formed through partial melting of precursor minerals [1-3]. However, combined petrological [4], chemical [5], and isotopic [6-8] studies on typical type B1 CAI from Allende, HN3-1, have revealed that it shows various disequilibrium features and that all of the four major minerals in HN3-1 should contain either visible or invisible relicts. REE patterns of mineral separates appear to be formed through crystallization from liquid but with positive Yb anomalies in Mel and An, oxygen isotopic compositions of mineral separates are widely distributed along Allende "mixing" line with minor difference between Mel and An, and Ca isotopic composition is different among Mel, Tpx, and An.

HN3-1 is a typical type B1 CAI from Allende, which comprizes nearly equal amounts of melilite (Mel), Ti-rich clinopyroxene (Tpx) and anorthite (An) with numerous spinel (Sp). In order to search the carriers of chemical and isotopic anomalies, color mapped photos were taken with ultra-high speed wide-area multi-analyzer (CMA) of entire area and many discrete areas of two thin sections of HN3-1. CMA photographs show that some Tpx grains contain compositionally distinguishable rectangular or triangle areas, 100 to 200 um in size. They have different compositions from surrounding areas on oxide-oxide diagrams, thus they should be relicts. Furthermore, Tpx 9 has concentrically zoned Ti distribution but the grain can be divided into two portions as to Al, Mg, and Si contents both of which portions show weak compositional zoning. This shows that compositionally different two Tpx grains had coalesced before melting and Ti was redistributed during melting and/or subsequent cooling.

Mel should also contain relicts which carry Yb anomaly, however, there are not any evidence of visible relicts on CMA photographs. Cations in Mel might have redistributed at high temperatures because of large diffusion rate. EPMA analyses revealed that Sps have small but systematic compositional difference for the occurrence; those in a single grain of Tpx, those in a single An grain, those forming a framboid, and those forming a pallisade have slightly different composition. This suggests that Sp has retained the primary composition including oxygen isotopes. Although An should contain relicts carrying Yb anomaly as well as Mel, there is no evidence of relicts.

Present results show that type B1 CAI did not largely melted. Not only the visible relicts shown in the CMA photographs but also most Tpx could be relicts as to oxygen framework though they partly exchanged cations with Mel at high temperatures. This shows that Tpx did not crystallize from a liquid, rather previously existed grains recrystallized to form larger grains as they now are. Oxygen isotopic composition demonstrates that the precursor of Mel and An originated in the solar system and Sp and Tpx in the another star or supernova. Large oxygen isotopic anomaly in Tpx may have been inherited from earlier generation which slightly changed during melting. Though the liquidus temperature of Mel is much higher than that of Tpx, considerable amounts of Mel melted probably because of finer grain size to form the Mel mantle.

References: [1] EPSL, 52 (1981), 16 [2] LPSC, XIV (1983), 596 [3] LPSC, XV (1984), 631 [4] LPSC, XVIII (1987), 694 [5] ibid., 698 [6] LPSC, XVII (1986), 526 [7] Meteoritics, 22 (1987), 326 [8] ibid.,483, and LPSC, XIX (1988), 951

Texture and chemical composition of pyroxenes in some carbonaceous chondrites and comparison with those in the unequilibrated ordinary chondrites

Noguchi, T., Nagahara, H. and Kushiro,I.
Geological Institute, Univ. of Tokyo

Texture and chemical composition of pyroxenes in chondrules in the carbonaceous chondrites were studied by SEM and EPMA. Most of the chondrules observed are type I chondrules of McSween (1983). The meteorites studied are Allende (CV3), Y-790112 (CR), ALH-77003 (CO3), ALH-77307 (CO?3) and Y-74662 (CM2).

(1) Texture

In type I chondrules, modal variation of olivine and pyroxene vary widely (McSween, 1983). There is a textural variation of pyroxenes in accordance with modal variation of these minerals.

In granular olivine (with pyroxene) chondrules, low-Ca pyroxene crystals set outer part of chondrules. These pyroxenes are euhedral with Ca-rich pyroxene rim. Crystallization sequence of pyroxene is low-Ca pyroxene (protopyroxene)→Ca-rich pyroxene. Together with this sequence, there is another sequence;(low-Ca pyroxene→) Ca-poor pyroxene→ Ca-rich pyroxene (Fig.1).

In porphyritic (olivine) pyroxene chondrules, texture of pyroxenes is similar to that in the ordinary chondrites. Glass amount in chondrules of this kind varies. In Allende, many chondrules have smaller amount of glass in chondrules than other meteorites studied. In glass-rich chondrules, many dendrites exist in the glass. In these chondrules, crystallization sequence is, in most cases, Low-Ca pyroxene (protopyroxene)→ Ca-rich pyroxene.

There are some kinds of unique chondrules. For example, there are holocrystalline chondrules which seem to have been slow cooling, however growth compositional zoning of Ca-bearing pyroxene is from Ca-poor pyroxene to Ca-rich pyroxene. From their zoning these chondrules crystallized rapidly. These unique chondrules are of small amount.

In porphyritic (olivine) pyroxene chondrules in Allende, metallic iron - iron oxide spherules in chondrules react with surrounding low-Ca pyroxene phenocrysts and Fe-rich olivine is formed around these spherules ; low-Ca pyroxene and metallic iron in other kind of chondrules also reacted to form ferrous olivine (Housley and Cirlin,1983). Such a reaction relation is not observed in other carbonaceous chondrites studied.

Another specific texture is "banding" or "lines" in BEI (contrast is enhanced by CMA) in low-Ca pyroxenes (originally protopyroxene, inverted to twinned clinopyroxene) (Fig.2). The "banding" or "lines" are parallel to the (100) polysynthetic twin boundaries. This texture is too fine to be determined whether they are due to compositional difference or orientaion contrast. However these "banding" or "lines" are finer than optical twinning. The texture may have be formed by introduction of FeO along twin boundaries. Similar texture is shown in many ordinary chondrites (Tsuchiyama et al.,1987; Noguchi,this volume).

(2) Chemical composition

Chemical compositon of pyroxenes in chondrules is shown in the En-Fs-Wo diagram (Fig.3). Though the compositions are very similar (most of them are less than Fs_5) in the diagrams, minor elements content distribution is different in these meteorites. Fig.4 shows a relationship between Al_2O_3 and TiO_2 content in Ca-rich pyroxenes, which indicates that there are two trends. Many of Ca-rich pyroxenes in Allende form a trend which has higher TiO_2/Al_2O_3 ratio than the other. In contrast, most of Ca-rich pyroxenes in Y-790112 and Y-74662 form a trend which has lower TiO_2/Al_2O_3 ratio. Al_2O_3 vs. Cr_2O_3 diagram shows reverse relationship, that is, lower Cr_2O_3/Al_2O_3 ratio in Allende and higher ratio in Y-790112 and Y-74662. Trend of higher TiO_2/Al_2O_3 is similar to that of coarse-grained type B CAI and trend of lower TiO_2/Al_2O_3 ratio is similar to that of the unequilibrated ordinary chondrites. Each meteorite has, more or less, Ca-rich pyroxenes of both trends. Then, above differences may have resulted from the difference of bulk composition of chondrules.

References: McSween(1983) In Chondrules and their origins, 195-210: Howsley and Cirlin(1983) In Chondrules and their origins, 145-161: Tsuchiyama et al.(1987) paper presented to 12th Symps. Antarc. Meteor., 51-53.

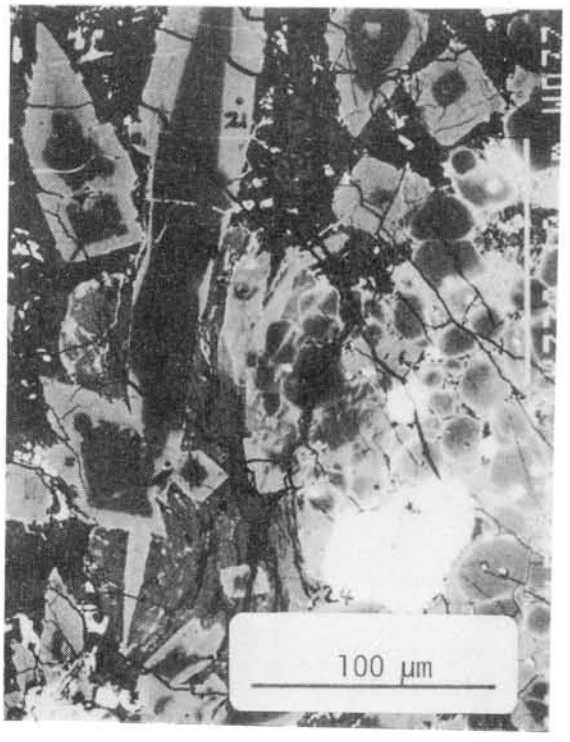

Fig.1 BEI of a chondrule in Allende. Low-Ca pyroxene is rimmed by Ca-rich pyroxene.

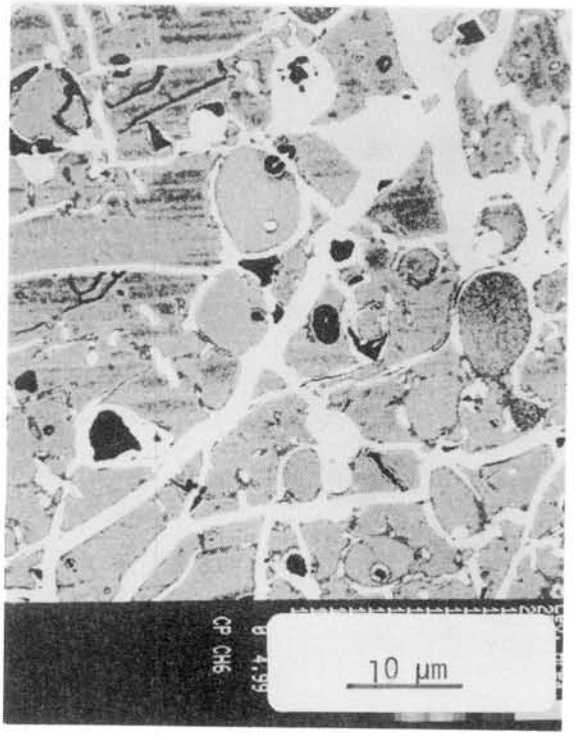

Fig.2 BEI of low-Ca pyroxene phenocryst in a chondrule (Y-790112). "Banding" or "lines" are shown in pyroxene.

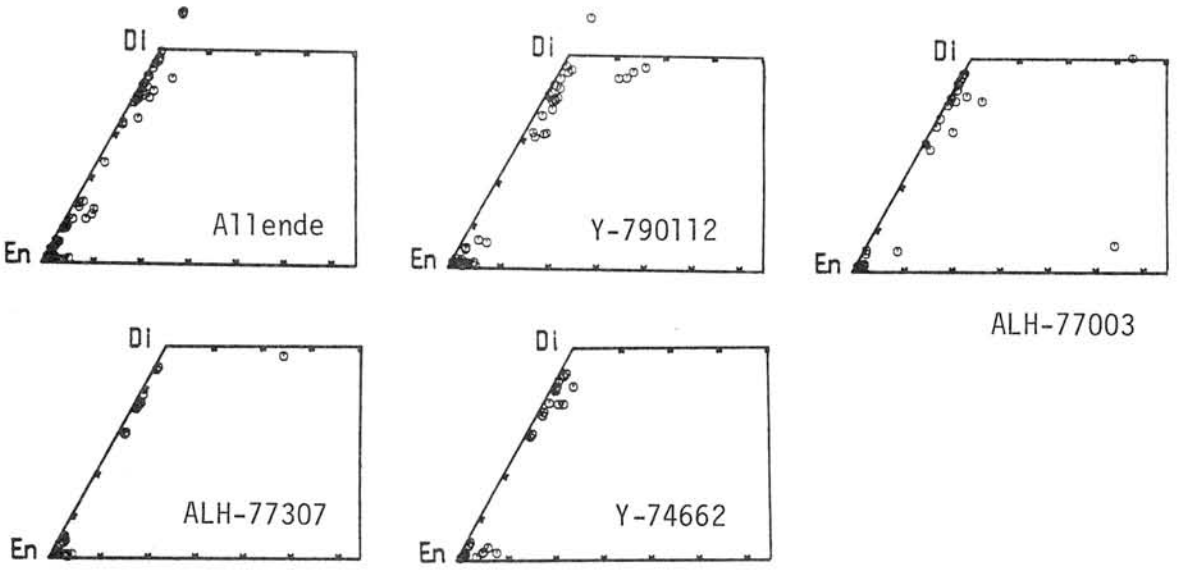

Fig.3 En-Fs-Wo diagrams of the meteorites studied.

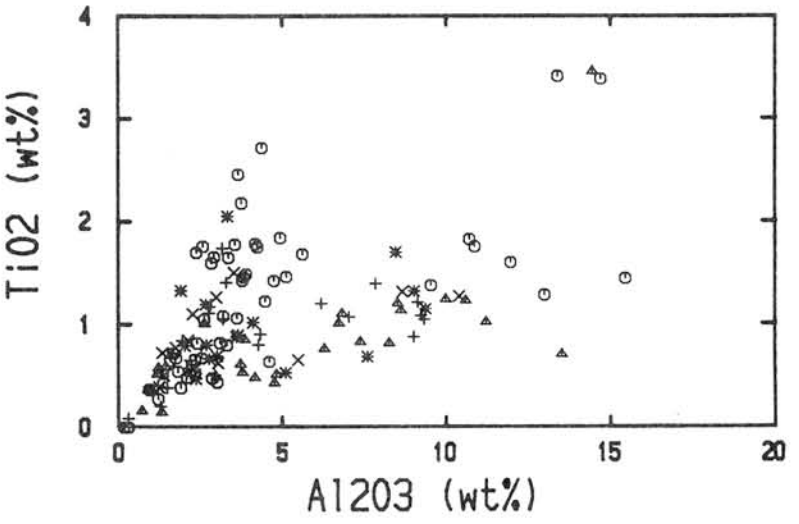

Fig.4 Al_2O_3 vs. TiO_2 plot of the meteorites studied. Symbols are followng: ⊙ Allende, △ Y-790112, + ALH-77003, × ALH-77307, ✳ Y-74662.

ORIGIN OF POSITIVE CORRELATION OF MN WITH FE IN MATRIX FE-RICH OLIVINE OF PRIMITIVE TYPE 3 ORDINARY CHONDRITES

S. MATSUNAMI: NATURO UNIVERSITY OF EDUCATION, NARUTO, TOKUSHIMA 772, JAPAN.

Ferrous olivine is the most abundant and ubiquitous mineral in the matrix and rim materials of UOC. Especially, formation of matrix Fe-rich olivine in several primitive type 3 ordinary chondrites seems to be records of condensation and reaction processes in the early solar system (Huss et al., 1981; Nagahara, 1984) and to give clues to understanding of origin of chemical fractionation of refractory lithophile elements in chondrites (Grossman & Wasson, 1983; Matsunami, 1984) and establishment of redox state of Fe in chondritic materials. There are two significant ideas on the origin of matrix intermediate to Fe-rich olivine: (I) solid-solid reactions between enstatite, silica, and metallic Fe-Ni (Ikeda et al., 1981; Nagahara, 1984; Nagahara & Kushiro, 1987) under high f_{O2} conditions mostly at low temperatures and (II) non-equilibrium vapor → solid condensation from nebular gas with nearly solar abundance under relatively high f_{O2} conditions (Kornacki & Wood, 1984; this work). The silica saturation assumed in the former may be the results of fractional condensation of forsterite from nebular gas (Nagahara & Kushiro, 1987). Mode of occurrences of matrix ferrous olivine in primitive chondrites seems to offer supporting evidences of the former interpretation (Nagahara, 1984; Matsunami, in prep.). The latter idea is based on mineral chemistry of matrix olivine in Allende CV3 and the least metamorphosed type 3 ordinary chondrites, those of lower petrologic subtypes, having low TLS (Sears et al., 1980, 1982). In this paper the existing ideas and data of features of matrix olivine are discussed in order to examine the possibilities of the two interpretations of matrix olivine formation with the use of consideration of mineral chemistry data such as Fa mole % and the relation between MnO and FeO contents and the theoretical calculations of non-equilibrium condensation of (Mg, Fe, Mn)-olivine from nebular gas.

Among characteristics of composition of matrix olivine, the MnO content appears to be important. Olivines in opaque matrix commonly contain a significant amount of MnO as much as 1.2 wt%. Particularly, the MnO content of ferrous olivine ($Fa_{>\sim 30}$) increases remarkably with increasing FeO content (Figs. 1A and 1B). Comparisons of the MnO contents of matrix olivine with that of chondrule olivine are also shown. The positive correlation of MnO with FeO is markedly clear in ferrous olivine than magnesian olivine. The correlation coefficients range from 0.66 to 0.91. The ratios of MnO to FeO in ferrous olivines appear to be distributed nearly around solar ratio (MnO/FeO~0.01). The MnO/FeO ratio of chondrule olivine is generally higher than that of matrix ferrous olivine. The individual ferrous olivine grains are sometimes chemically zoned. With the increase of FeO contents from the cores to the rims, the MnO contents also increase remarkably (Fig. 2).

Comparisons of MnO and FeO contents between matrix Ca-poor pyroxene, silica-rich spherules from matrix materials of Sharps (H3.4) and Chainpur (LL3.4) chondrites, and matrix ferrous olivine are shown in Fig. 3. It is revealed that compositions of matrix ferrous olivine are mainly plotted outside the Ca-poor pyroxene - silica-rich spherule - metallic Fe region. If we accept the idea (I), this strongly suggests that matrix ferrous olivine would have formed through reactions involving more Mn-rich pyroxene than those mainly observed in matrix or that magnesian, Mn-poor olivine, that would have simultaneously formed with matrix ferrous olivine, might have been lost by an unknown fractionation mechanism. Of course, we need more detailed data of reaction experiments of the Pyroxene-Silica-Fe system on the MnO distribution between Mn-bearing, Mg-rich pyroxene (reactant) and Fe-rich olivine (product) to produce the observed positive correlation of MnO with FeO in order to further examine the validity of the idea (I).

In contrast to the idea (I), the idea (II) assumes the delay of nucleation of metallic Fe-Ni at the cooling stage of the nebular gas, resulting in the Fe-enrichment in the cooling gas to lead to direct non-equilibrium vapor → solid condensation of

(Mg, Fe, Mn)-olivine (Blander & Katz, 1967; Yamamoto & Hasegawa, 1977; Kozasa & Hasegawa, 1988). Computer simulations of olivine condensation are conducted by the use of non-equilibrium homogeneous condensation theory of many-component system, including depletion of monomers in the gas (Mg, Fe, Mn, SiO). Condensation of "early condensates", enstatite and metallic Fe-Ni and reaction of olivine with gas to form enstatite are neglected for simplicity. A nebular gas with solar abundance (H, O, Mg, Fe, Mn, Si: Anders & Ebihara, 1982) is assumed to have relatively high P_{H2O}/P_{H2} ratio ($\sim$0.5), based on the considerations of stability of Fe-rich olivine. The value of surface energy of olivine is adopted from experimental data of Cooper & Kohlstedt (1982). In this calculations, analogous to the BCF theory, sticking probabilities of Mg, Fe, Mn, and SiO are determined by taking surface diffusion distance (x_s), chemical potential difference ($\Delta\mu$) and olivine stoichiometry, into consideration. Concentrations of gas species and nucleation rate of olivine are time-dependent because of monomer depletion resulting from growth of olivine grains. Using these assumptions, the distributions of grain-size and (Mg, Fe, Mn)-composition of olivine are calculated under various physical conditions: $P_{total} = 10^{-4}$, 10^{-5}, 10^{-6} atm; $\tau_{cool} = 10^{11} \sim 10^{6}$ sec, where $T=T_{e0}\exp(-t/\tau_{cool})$ is assumed for thermal history of the nebula gas, being T_{e0} equilibrium condensation temperature of forsterite. The MnO-FeO relation of olivine condensates are plotted for the case of $P_{total} = 10^{-5}$ atm in Fig. 4. From these results, it seems to be possible that remarkably variable olivine composition with nearly constant MnO/FeO ratio are obtained by the non-equilibrium vapor → solid condensation. It is suggested that the positive correlation of MnO with FeO and compositional zoning of matrix Fe-rich olivine may be evidences supporting the idea (II). It is also suggested that compositions and grainsizes of relict olivine (Nagahara, 1981) and olivine grains in fine-graind aggregates (FGA) (Watanabe et al., 1987) can be explained as a series of the products of the non-equilibrium condensation process.

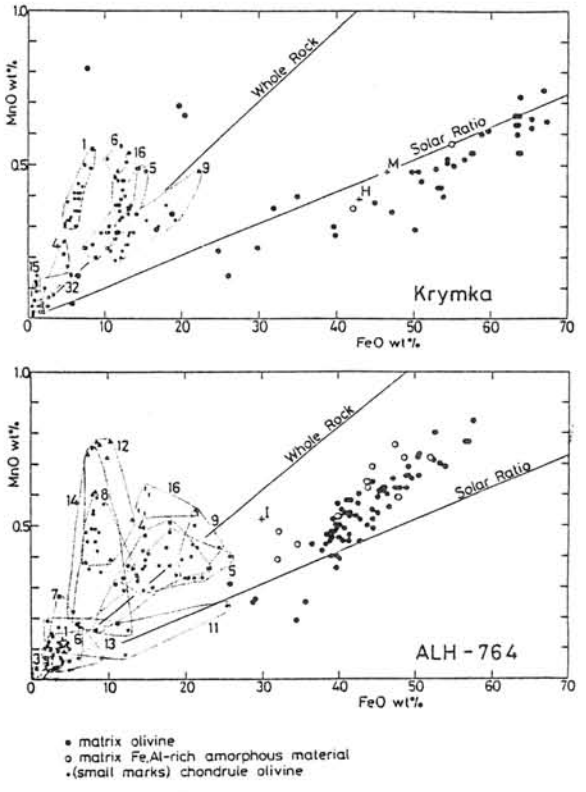

Figs. 1A and 1B

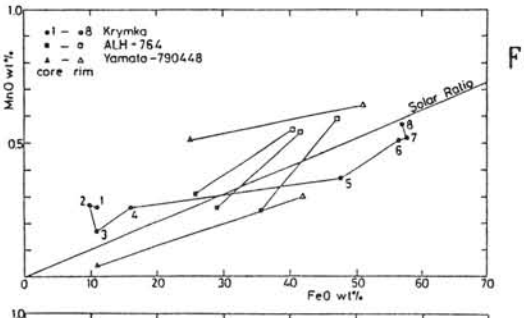

Fig. 2

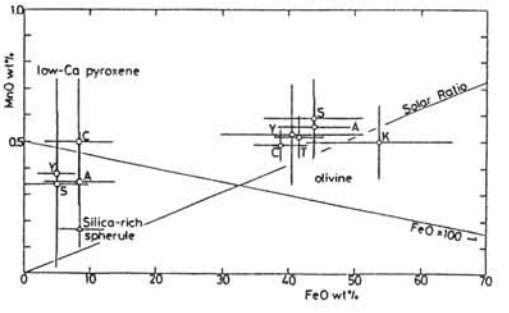

Fig. 3

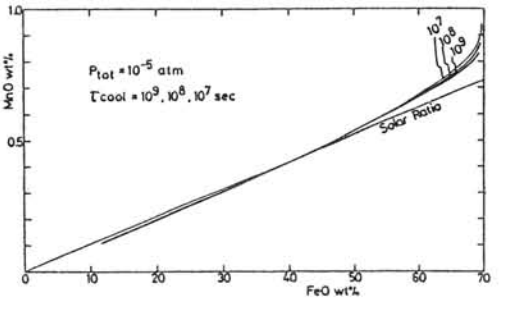

Fig. 4

THE EVOLUTION OF CHONDRULES

Hewins, Roger H.

Geological Sciences, Rutgers Universtiy, New Brunswick, N.J. 08903, USA

Events Prior to Chondrule Formation Chondrule melt droplets contained several kinds of solid inclusions: forsteritic olivine (1) which also makes up most of some chondrules, type C chondrules of (2); relict grains of ferroan olivine (3,4) which are shocked (5,6); other chondrules (e.g. in Chainpur and Allende); matrix lumps (7) comparable to chondrite matrix containing ferroan olivine, etc (8,9); and the central portions of some olivine crystals (10). Before the formation of the chondrules observed in chondrites, a variety of events must have taken place. Evaporation and condensation, possibly due to the heat of gas compression by angular momentum transfer in the accretion disk (11), had already fractionated cosmic material giving the range of olivine compositions. Forsterite reacted to pyroxene in reduced regions and to ferroan olivine in more oxidized regions. Condensed (and possibly residue) grains had clustered into particles with a range of bulk compositions. Impact events had taken place, either on planetesimal surfaces (6) or possibly as a result of infall of presolar grains (12) colliding at cosmic velocities with particle-rich zones in the disk. Chondrules may have formed before the observed generation of chondrules, but alternatively small quickly-cooled chondrules may have been incorporated into larger comtemporaneous droplets.

Chondrule Melting Dynamic crystallization studies have involved heating times from 2 minutes to 17 hours (13,14). In our experiments (15,16,17) we have found 30 minutes soaking at the initial temperature is required to get a reasonable match to natural chondrule textures, but shorter heating times might be possible with coarse-grained precursor materials. Initial temperatures close to, but above and below, the liquidus are required in experiments to control the number of nuclei and hence produce the range of textures in natural chondrules. Refractory chondrules (granular olivine) were not totally melted, but FeO- and SiO_2-rich ones (barred olivine, radial pyroxene, etc) generally were (18). Revision of liquidus temperatures calculated in (18) for chondrules of known textures suggests a 1700°C upper limit to chondrule initial heating (19). Comparison with experiments (16,17) suggests however that glassy chondrules should be more abundant, which probably means that initial grain sizes were too small and/or quench temperatures too high in the experiments. Nevertheless, a heating event of significant duration is required for chondrules. The heating mechanism is uncertain, but may be related to early solar activity (20,21). The preservation of Na in chondrules requires oxygen fugacities higher than cosmic (22) which is consistent with elevated Fe contents of olivine. The similarity of Na contents of Type I and II chondrules requires the higher oxygen fugacity for ferroan chondrules to offset the effect of a greater degree of melting.

Chondrule Crystallization Cooling rates of about 500°C/hr are ideal for reproducing barred olivine textures in our experiments (15-17). Granular and porphyritic olivine textures can be produced at lower cooling rates, but at least 100°/hr is required to obtain composition zoning comparable to that of chondrule olivine in unequilibrated chondrites, type A zoning of (2), as well as the porphyritic texture. The cooling rate requires that chondrules be embedded in a thick cloud, rather than free to radiate to space. Final temperatures must be relatively low to preserve the zoned olivine and glass of such chondrules.

Chondrule Modification The dominant type of modification of chondrules is replacement of Mg by Fe. This process may have started when the droplets were still molten producing unusual olivine zonation patterns (23) and certainly continued well below the solidus in the form of ferroan olivine veins and rims produced prior to accretion to parent bodies (9). The latter alteration (24,25,26) is a continuation of the condensation process which produced ferroan chondrule precursors. An intermediate stage of Fe-Mg exchange is suggested for the chondrules with metamorphically zoned and homogenous ferroan olivine, types B and D of (2), which become important in less unequilibrated chondrites. It is difficult to prove that this is not a parent-body process, but the co-existence of both zoned and homogenized olivine in one chondrite suggests nebular metasomatism. The ambient temperature must be low enough to permit survival of glass but high enough to promote Fe-Mg exchange. Homogeneous olivine could also result from slow cooling of chondrule melts, but the ubiquitous presence of barred olivine chondrules requiring faster cooling argues against this possibility. In the case of C3 chondrules, nebular metasomatism also involves Na addition (24). Chondrules show a clear history of collision and abrasion (27) and there is a correlation of chondrule shape and composition (28,29). The increase in Fe contents of broken and abraded chondrules shows that nebular metasomatism accompanied chondrule collision. Magnesian spheres may have been formed later than ferroan chondrule fragments, or simultaneously on the hydrogen-rich margins of particle-rich zones. Prompt accretion is required to prevent homogenization of chondrite components (12) and variations in the amount of accreted ice, from zero (EC), trace (OC) to abundant (CC) suggest considerable nebular distances are involved.

Conclusions Chondrule formation requires heating over many minutes and cooling over a few hours. It involves a short-lived thermal event (or events) superimposed on the nebula-wide cooling resulting in condensation which continued after chondrules were formed.

References (1) Steele, I.M. (1986) Geochim. Cosmochim. Acta 50, 1379. (2) Miyamoto, M. et al. (1986) J. Geophys. Res., 91, 12804. (3) Nagahara, H. (1981) Nature, 292, 135. (4) Rambaldi, E.R. (1981) Nature, 293, 558. (5) Watanabe, S. eta 1. (1984) Mem. N.I.P.R. Spec. Issue 35, 200. (6) Ruzicka, A. (1988) Geochim. Cosmochim. Acta, submitted, part II. (7) Scott, E.R.D. et al. (1984) Geochim. Cosmochim. Acta 48, 1741. (8) Nagahara, H. (1984) Geochim. Cosmochim. Acta 48, 2581. (9) Peck, J.A. and Wood, J.A. (1987) Geochim. Cosmochim. Acta 51, 1503. (10) Nagahara, H. (1983) "Chondrules and

their origins" Ed. E.A. King, 211. (11) Boss, A.P. (1988) Lunar Planet Sci. XIX, 122. (12) Wood, J.A. (1984) Earth Planet. Sci. Lett. 70, 11. (13) Tsuchiyama, A. and Nagahara, H. (1981) Mem. N.I.P.R. Spec. Issue 20, 175. (14) Lofgren, G. and Russell, W.J. (1986) Geochim. Cosmochim. Acta 50, 1715. (15) Radomsky, P.M. and Hewins, R.H. (1987) Lunar Planet. Sci. XVIII, 808 (16) Bell, D.J. (1986) B.S. thesis, Rutgers Univ. (17) Connolly, H.C. Jr. et al. (1988) Lunar Planet Sci. XIX, 205. (18) Radomsky, P.M. and Hewins, R.H. (1987) Meteoritics 22, 484. (19) Radomsky, P.M. and Hewins, R.H. (1988) Meteoritics 23, in press. (20) Levy, E.H. (1988) "Meteorites and the early solar system" Eds. J.F. Kerridge and M.S. Matthews, in press. (21) Huss, G.R. (1988) Lunar Planet. Sci. XIX, 521. (22) Tsuchiyama A. et al. (1981) Geochim. Cosmochim. Acta 45, 1357. (23) Ruzicka, A. (1988) Geochim. Cosmochim. Acta, submitted, part I. (24) Ikeda, Y. (1982) Mem. N.I.P.R., Spec. Issue 25, 34. (25) Palme, H. and Fegley, B.Jr. (1987) Lunar Planet. Sci. XVIII, 754. (26) Palme, H. and Wark, D.A. (1988) Lunar Planet. Sci. XIX, 897. (27) Kitamura, M. and Watanabe, S. (1986) Mem. N.I.P.R., Spec. Issue, 41, 222 (28) Dodd, R.T. (1971) Contrib. Mineral. Petrol. 31, 201. (29) Wlotzka, F. (1983) "Chondrules and their origins", Ed. E.A. King, 296.

Lamellae-bearing "pigeonite" in "equilibrated" ordinary chondrites (H4-6) and other texture in pyroxenes in ordinary chondrites (type 3-4): implication to the thermal history

Noguchi, T.
Geological Institute, Univ. of Tokyo

In recent years, autometamorphism of the ordinary chondrites has been discussed by some researchers from the observation of microstructure of pyroxenes by TEM (eg. Ashworth,1981; Watanabe et al.,1985). In order to elucidate the thermal history of the ordinary chondrites, pyroxenes in the unequilibrated ordinary chondrites and "equilibrated" ordinary chondrites were studied by using SEM and EPMA (Noguchi,1987).

In the course of the study, lamellae-bearing pyroxenes have been observed ubiquitiously in H4-6 chondrites (Y-74371, Jilin, Y-74115, Y-74193, Y74079, ALH-77139). Noguchi (1987) reported that crystallization sequences of pyroxenes in the ordinary chondrites were mainly two types; (1)low-Ca pyroxene (protopyroxene)→Ca-rich pyroxene, (2)low-Ca Pyroxene→Ca-poor pyroxene→Ca-rich pyroxene. Lamellae are observed in Ca-poor pyroxenes of type (2) of the above classification. These Ca-poor pyroxenes are thought not to have been formed by later shock melting and crystallization from such melt.

Some of their composition are shown in Table 1. Their CaO content vary from 1.20 to 4.36 weight %. Although it is difficult to determine whether they are pigeonite or orthopyroxene from only CaO content. From BEI images of which contrast is enhanced by CMA (computer aided microprobe, JXA 733 MkII), it is shown that they have thin lamellae (submicrometer in thickness) parallel to (001). It is suggested that most of them are pigeonite. Their crystallographic relations are not clear because TEM observation has not yet been done. Lamellae thickness of pigeonite in type 3 chondrites (Ashworth and Barber,1977;Topel-Schadt and Muller,1985) is thinner than those in type 4-6. However, the thickness does not increase clearly from type 4 to 6. It is suggested that cooling rates when "pigeonites" exsolved lamellae were similar in type 4-6.

Chemical composition of pyroxenes changes in accordance with petrologic types (Noguchi,1987). If their compostion changed during "metamorphism" below 1000^{o}C, Ca-rich pyroxene (augite-diopside) should have exsolved along with "pigeonite". However, the thickness and spacing of lamellae in "pigeonite" suggest that diffusion distance during metamorphism was at best a few micrometers in Ca-rich pyroxenes. Thus, it is difficult to change pyroxene composition only by subsolidus equilibration (metamorphism). Rather it would have been accomplished by crystallization and subsequent cooling of chondrule formation. There is another specific texture of low-Ca pyroxenes in higher subtype of type 3s (>3.6) and some of type 4s (from their composition, they seem to be as primitive as the highest subtype of type 3s (3.8-3.9)(Tsuchiyama et al.,1987;Noguchi,1987). FeO content of low-Ca pyroxene (twinned low-Ca clinopyroxene, originally protopyroxene) increases along the (100) polysynthetic twin boundaries. Spacing of high-FeO resions decreases in accordance with

petrologic types.

Similar texture is observed in newly grown pyroxenes from a melt pocket in a brecciated LL4 chondrite Y-75279 (Fig.2), which did not experience severe re-heating after melt pocket formation by shock heating. This indicates that relatively slow cooling rate at high temperature can produce similar texture to that in type 3.6-4 chondrites without reheating event ("relatively slow cooling rate" here may have been much rapid than cooling rate suggested by metallographic coolingmeter or fission track method).

In summary, chemical composition and texture of pyroxene in the ordinary chondrites may be accomplished by crystallization during relatively slow cooling of chondrule formation. Slow cooling might be accomplished by high dust/gas ratio or dense nebular gas where chondrule formation took place. Accretion temperature of the ordinary chondrites is still unknown.

References: Ashworth(1981) Proc. Roy. Soc. Lond. A374, 179-194 Ashworth and Barber(1977) Phil. Trans. Roy. Lond. A286,493-506: Noguchi(1987) paper presented to 12th Symps. Antarc. Meteor., 51-53: Topel-Schadt and Muller(1985) Earth Planet. Sci. Lett. 74, 1-12: Tsuchiyama et al.(1987) paper presented to 12th Symps. Antarc. Meteor., 51-53: Watanabe et al.(1985) Earth Planet. Sci. Lett. 72, 87-98.

sample name	Y-74115			Y-74079
sample No.	2	3	4	56
SiO_2	55.72	56.34	55.66	55.51
TiO_2	.16	.13	.14	.30
Al_2O_3	.19	.19	.22	.62
FeO	10.63	10.57	10.03	9.23
MnO	.39	.45	.48	.37
MgO	30.62	31.46	30.87	29.01
CaO	2.14	1.20	2.58	4.36
Na_2O	.07	.04	.07	.14
Cr_2O_3	.07	.08	.10	.55
V_2O_3	.06	-	-	-
NiO	.04	.03	-	-
tatal	100.09	100.49	100.78	100.09

Table 1 Chemical composition of "pigeonite".
They were analysed by defocused beam (10 μm).

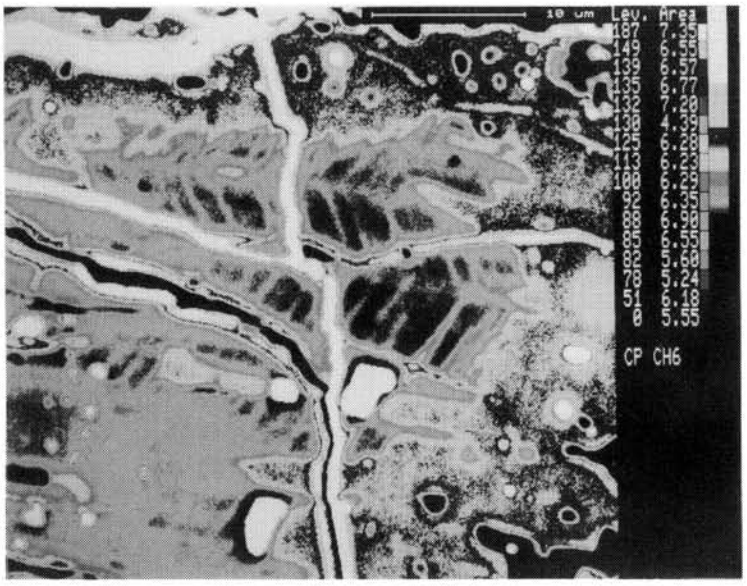

Fig.1 BEI of "pigeonite" shows exsolution lamellae. Lamellae are herringboned by twinnig of "pigeonite". (Y-74115, H5)

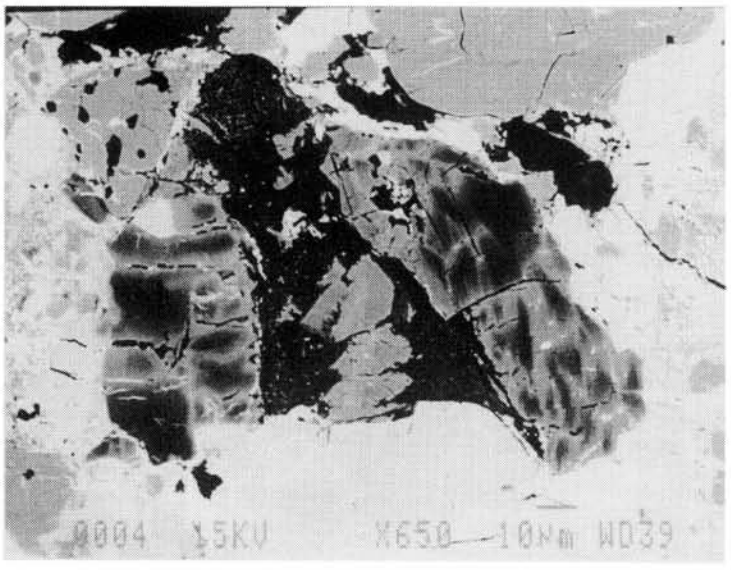

Fig.2 BEI of newly grown low-Ca pyroxenes in a melt pocket in a brecciated chondrite. Pyroxene shows compositional fractuation. (Y-75279, LL4)

CHONDRULE-LIKE OBJECTS IN TERRESTRIAL VOLCANIC ROCKS.

Sánchez-Rubio, G.

Instituto de Geología (UNAM), Ciudad Universitaria,
04510 México, D. F., MEXICO.

Reports on terrestrial rocks with characteristics similar to chondrites are scarce and chondrules are said to be non-existent on Earth, despite the fact that some years ago chondrites were said to be much like tuffaceous rocks.

Round mineral objects that look like chondrules were detected during a geologic investigation of the Amealco Volcano, in central Mexico. These objects occur in rocks of dacitic composition that exist inside a caldera depression.

Numerous feldspar phenocrysts appear embedded in a gray glassy matrix with conspicuous flow banding. Most phenocrysts show anhedral to subhedral forms and round shapes are not rare. Under the microscope, hornblende, orthopyroxene and Fe-ore granules can also be detected.

Assimilation of crystalline plutonic rocks by magma often leaves residual material with signs of the disaggregation and melting processes that took place within the magma. For instance, a structure similar to that shown by barred chondrules forms when melting occurs along planes of twinning (as in feldspars) or follow a main crystallographic orientation. Many other structures form as result of the complex interplay of melting and recrystallization processes that occur within the magma.

Further instances of chondrule -like objects appear in rocks of basaltic composition that exist in the high plateau of nort-central Mexico.

These chondrule-like objects are never as perfect in shape as real chondrules in meteorites. Mineral composition is also different. Nevertheless, terrestrial chondrule-like objects do illustrate that igneous processes are quite capable of producing mineral objects similar, in many ways, to real chondrules.

CHEMICAL AND MINERAL COMPOSITIONS OF FUSION CRUSTS ON ANTARCTIC CHONDRITES

Tazawa, Y.* and Sasaki, T.
*Dept. Physics, Kyoto University, Sakyo, Kyoto 606.
Sakuranomiya Osaka City High School, Miyakojima, Osaka 534.

We have been studying fusion crusts of Antarctic meteorites in order to find chemical and mineralogical alterations in the crusts due to ablation during atmospheric entry, which must have happened to "Cosmic Spherules".

Unfortunately, in our previous study, the INAA results for abundances of trace elements (e.g., rare earth elements: REE, siderophile elements: SPE, etc.) could not be discriminated between fusion crusts and their adjacent regions. Some probable reasons of this are: (1) analyzed samples of the crusts and their adjacents were filed off using a diamond file, so that they were separated insufficiently, (2) less than several miligrams of the samples were analyzed, so that results were very susceptible to the inhomogeneity among local constituents, (3) in the ablation process, most of elements may be redistributed among constituents of the crust but cannot be evaporated preferentially, etc.

To answer these problems, we studied how elements and minerals have been rearranged in the fusion crusts and their neighbors. Polished sections with distinguishable fusion crusts taken from Y-7304 (L6), Y-74155 (H5), Y-790448 (LL3) and ALH-77272 (L6) were studied by using an EPMA at Naruto University of Teacher Education, and EDX/SEM at Gakushuin University and Institute of Cosmic Ray Research, University of Tokyo. An enlarged back scattered electron image (BEI) of the fusion crust of Y-7304 (L6) is shown in Fig. 1 (Scale bar = 100 um). Olivine (Ol), pyroxene (Px), plagioclase (Pl), troilite (Tr) and chromite (Cm) are seen as major mineral constituents. Micro dendrites

Fig. 1

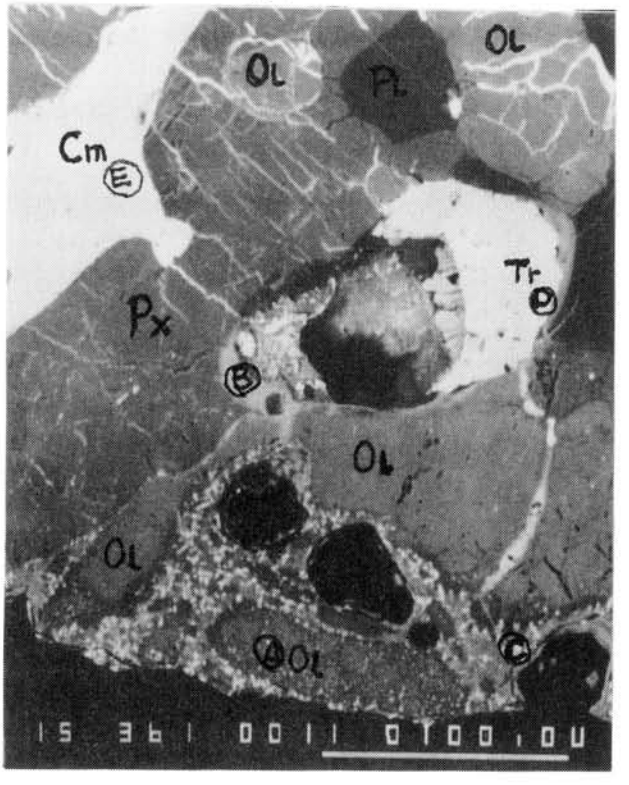

which surround olivines are also seen in the outermost region of the crust. EPMA results for the points marked by A, B, C, D, and E in Fig. 1 are listed in Table 1. Main results are as follows: (A) Micro dendrites occar in glassy parts located at the outermost region of the crusts. In many cases, the glassy parts include and/or contact with olivines seemed to have been re-crystallized. These glass and olivines have chemical composition similar to unaltered olivines in the inner region except for slight enrichments in minor elements, e.g., Al, Ca, Na, K, and Ni, and/or change in the Fe/Mg+Fe ratio. Some of the dendrites show decrease in SiO_2 (38.4% → 35.2%), MnO (0.5% → 0.3%), MgO (39.1% → 11.0%), and increase in Cr_2O_3 (0.1% → 0.5%), FeO (21.5% → 41.1%), relative to the inner olivine composition, and also show additional compositions, e.g., TiO (from Pl ?), Al_2O_3 (from Pl ?), CaO (from Pl,Px ?), NaO (from Pl ?), K_2O (from Pl ?) and NiO (from metal ?). In general, these additional components seem to increase the more, the outer the olivinitic costituents are found in. (B) Pyroxenes are mostly unaltered. (C) Because of complex structure and chemistry, alteration of plagioclases is more uncertain. In one of the large plagioclases and some other ones, however, they increase in Si, Al, Na, and K, and decrease in Fe, Mg, and Ca as their sites go away from the surface. (D) Large numbers of cracks filled by Fe-oxides/hydroxides are seen in silicate minerals. they are developed in the intermediate region more than in the outermost region. Color of them are mostly reddish/yellowish-brown, so that they seem to be weathering productions.

TABLE 1

	A	B	C	E		D
SiO_2	39.7	46.3	46.0	0.1	Fe	59.4
TiO_2	-	0.2	0.1	2.8	Ni	2.6
Al_2O_3	0.1	4.5	4.0	5.7	Co	-
Cr_2O_3	-	0.3	-	53.6	Cr	0.1
FeO	19.2	36.1	19.2	29.7	Mn	-
MnO	0.4	0.5	0.4	0.7	S	39.6
MgO	41.4	6.9	14.4	2.6	Si	0.1
CaO	0.1	2.3	3.2	-	Ti	-
NaO	0.1	1.2	1.8	-	Al	-
K_2O	-	0.2	0.2	-		101.8
NiO	0.1	-	0.2	0.1		
	101.1	98.5	89.5	95.5		

Acknowledgments. We thank H. Nishimura and S. Matsunami for making an EPMA available to us, H. Nagasawa and T. Fukuoka, and K. Yamakoshi for making EDX/SEM available to us.

CHEMISTRY OF Y-74025 CHONDRITE

Fukuoka, T.[1] and Kimura, M.[2]

1. Dept. of Chemistry, Gakushuin University, Mejiro, Tokyo 171
2. Dept. of Earth Sciences, Ibaraki University, Mito 310

Yamato 74025 (Y-74025) meteorite was classified as unique chondrite (1), enstatite chondrite (type ?) (2) and E6 chondrite (3), previously. Kimura (4) carried out the mineral and petrological investigations of Y-74025 and discussed the relationships between Y-74025 and the unique meteorite such as winonaites (5), Iodranites etc. He suggested that Y-74025 belongs to winonaite or related chondrite group. In this study, to discuss the classification of Y-74025 based on the chemical features, we analized more than 20 major, minor and trace elements in two chips of the meteorite which were provided from the National Institute of Polar Research of Japan, by instrumental neutron activation analysis (INAA).

The preliminary analytical results are shown in Table 1 together with the results of GSJ standard rock, JB-1 and Allende powder sample. The C1 chondrites (non-volatile) normalized abundance pattern of REE and Sc of Y-74025 (weighted mean) are plotted on Fig. 1.

The chemical abundances of two chips of Y-74025 show the chemical hetelogeneity (especially Sm). This suggests the hetelogeneous distributions of some minerals. The C1 chondrites (non-volatile) normalized abundance pattern of REE (weighted mean) (Fig. 1) is not similar to those of winonaites (5) and Lodran (6). The chemical abundances (weighted mean) are basically chondritic (e.g. Fig. 1) and close to those of E6 chondrite with lack of siderophile elements (except for Ni).

REFERENCES:

(1) Kojima,H. and Yanai,K. (1984) Abstract 9th Sym. Antarctic Meteorites, 11.

(2) Yanai,K. and Kojima,H. (1987) Photographic Catalog of the Antarctic Meteorites, 298p.

(3) Natl Inst. Polar Res. (1987) Science in Antarctica, 6 Antarctic Meteorites, 440p. (inJapanese).

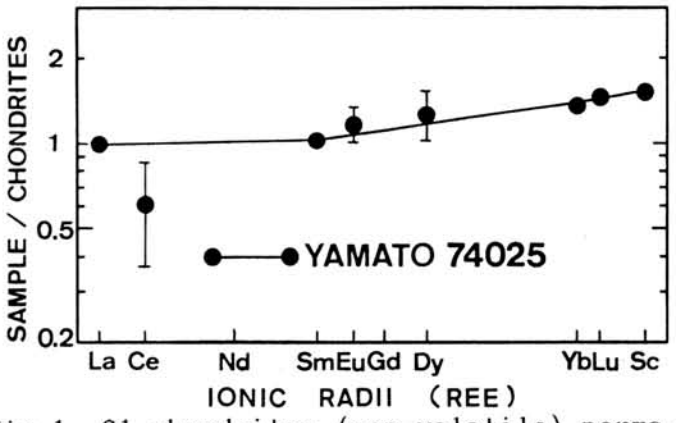

Fig.1. C1 chondrites (non-volatile) normalized abundance pattern of REE and Sc of Y-74025 chondrite (weighted mean).

Table 1. Preliminary results of chemical abundances by INAA

		YAMATO 74025			JB-1	Allende	Error*
		A	B	Wtd.mean			(%)
Wt	mg	88.2	108.4		93.1	78.1	
Ti	%	0.084	0.060	0.071	0.743		20-30[2]
Al	%	1.50	1.41	1.45	7.62		1-2
Fe[1]	%	14.7	15.0	14.9	=6.30	25.0	0.5
Mg	%	16.5	16.9	16.7	4.64		2-5
Ca	%	1.41	1.87	1.66	6.07		4-8
Na	%	0.797	0.737	0.764	=2.07	0.381	0.5-1
Mn	%	0.168	0.167	0.167	0.112		0.5-1
Cr	%	0.196	0.199	0.197	=0.0414	0.314	0.5
Sc	ppm	10.4	12.8	11.7	=28.9	13.0	0.5
V	ppm	36	41	39	208		2-5
La	ppm	0.29	0.33	0.31	=38.8	0.56	6-7
Ce	ppm	0.5	0.5	0.5	=63	0.9	20-40
Sm	ppm	0.146	0.250	0.203	=5.02	0.338	1-2
En	ppm	0.101	0.076	0.087	=1.59	0.12	10-20
Dy	ppm	0.44	0.38	0.41	3.94		16-20[3]
Yb	ppm	0.26	0.29	0.28	=2.4	0.30	7-10
Lu	ppm	0.050	0.043	0.046	=0.37	0.083	8-15
Hf	ppm	0.18	0.20	0.19	3.46	0.35	10-17[4]
As	ppm	1.21	1.31	1.27	2.38	2.12	8-14
Co	ppm	323	369	348	=39.1	698	0.5
Ni	%	1.63	1.63	1.63	0.0172	=1.55	0.5[5]
Os	ppb	244	162	199	-	=674	9-13
Ir	ppb	292	201	242	-	=853	1
Au	ppb	126	128	127	-	=157	2

* Errors for INAA are due to counting statistics.
1) Total iron as Fe. 2) Except for JB-1 (4%). 3) Except for JB-1 (3%). 4) Except for JB-1 (2%). 5) Except for JB-1 (3%).

(4) Kimura, M.(1987) Abstract 12th Sym. Antarctic Meteorites, 47.
(5) Prinz, M. *et al.* (1980) Lunar Planet. Sci., 11, 902.
(6) Fukuoka, T. *et al.* (1978) Lunar Planet. Sci., 9, 356.

CHEMICAL AND PETROLOGICAL STUDIES ON A LIGHT-COLORED FRAGMENT IN THE HEDJAZ CHONDRITIC BRECCIA

K. Misawa(1,3), N. Nakamura(1), S. Watanabe(2) and M. Kitamura(2) (1) Department of Science of Material Differentiation., Graduate School of Science & Technology, Kobe Univ., Nada, Kobe 657 (2) Department of Geology & Mineralogy, Faculty of Science, Kyoto Univ., Sakyou, Kyoto 606 (3) Present address, Institute for Cosmic Ray Research, Univ. of Tokyo, Tanashi, Tokyo 188

INTRODUCTION Shock induced melting (or metamorphism) is one of the most important events to understand collision of planetesimals and parent body brecciation in the early solar system. Numerous types of clasts in chondritic meteorites formed as a result of impact melting [1]. Fredriksson et al. suggested that the Hedjaz meteorite can be classified as a complex L-group chondritic breccia and concluded that Hedjaz exhibits no evidence of metamorphic equilibration after accretion [2]. We report REE, K, Rb, Sr, Ba, Ca and Mg abundances determined by mass spectrometric isotope dilution technique along with the results of petrographic, SEM-EDS studies of a light-colored lithic fragment in Hedjaz.

RESULTS & DISCUSSION Light-colored fragment mainly consists of olivine, pyroxenes (pigonite and subcalcic augite) and plagioclase. Accessory whitlokite, appatite, ilmenite and chromite are existed. The structure of the fragment clearly indicates that it crystallized from a melt, apparently slowly enough to allow crystallization of the plagioclase (Fig. 1). The Fe/Fe+Mg content of most of olivine grains is uniform (Fa23). Compositionally, olivine and pyroxenes are similar to ferromagnesian silicates in L-group chondrites (Fig. 2). Plagioclases are Ca-rich(An80-86). This feature is not similar to those of Y74160 (LL7) [3] or Brachina [4] but rather resemble to those of noritic clasts found in the Tieschitz H3 chondrite [5]. In Fig. 3, chondrites-normalized trace element abundance pattern of the Hedjaz light-colored fragment is shown. The REE and Ba abundances are 1.02-1.21 x chondrites with a large positive Eu anomaly (63 %). Sr is enriched (2.38 x chondrites), on the other hand, K and Rb are strongly depleted (0.224-0.436 x chondrites) relative to REE (Fig. 4). Compact polycrystalline mineral assemblages of above mentioned can form in magmatic systems (impact melt piles) either as adcumulate or melting residues. By analogy with the cumulate eucrites [6], a flat REE pattern with a positive Eu anomaly observed in the Hedjaz light-colored fragment can be interpreted as having formed in a solid/liquid fractionation event. It thus seems likely that cumulate textures and a positive Eu anomaly were produced by crystal settling or floatation. We suggest that L-chondrite breccia acquired shock-melting very early in solar system history, prior to gravitational reassembly.

ACKOWLEDGMENTS We thank Dr. P. Pellas for providing us with the Hedjaz samples.

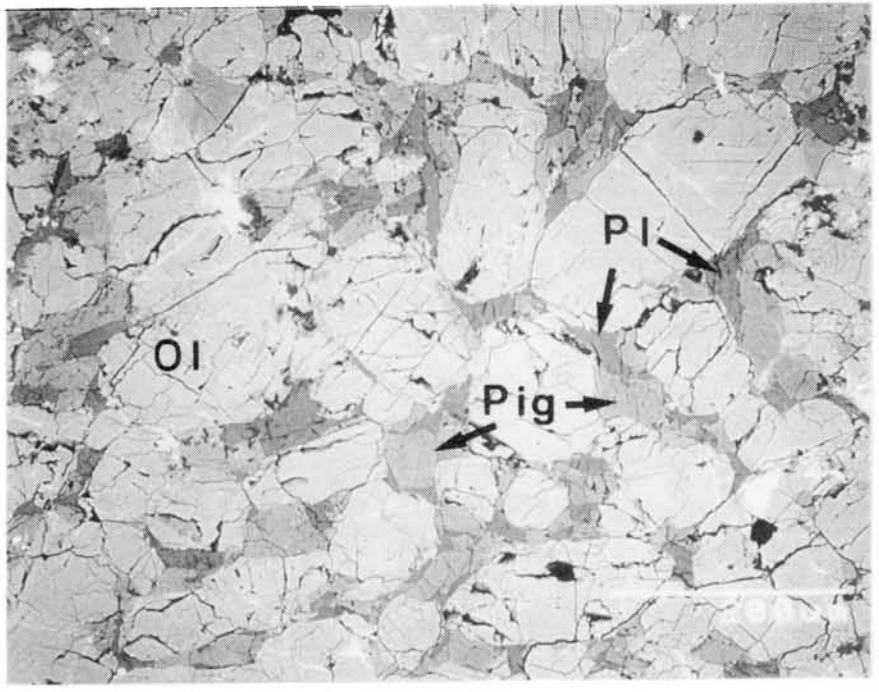

Figure 1 (a).

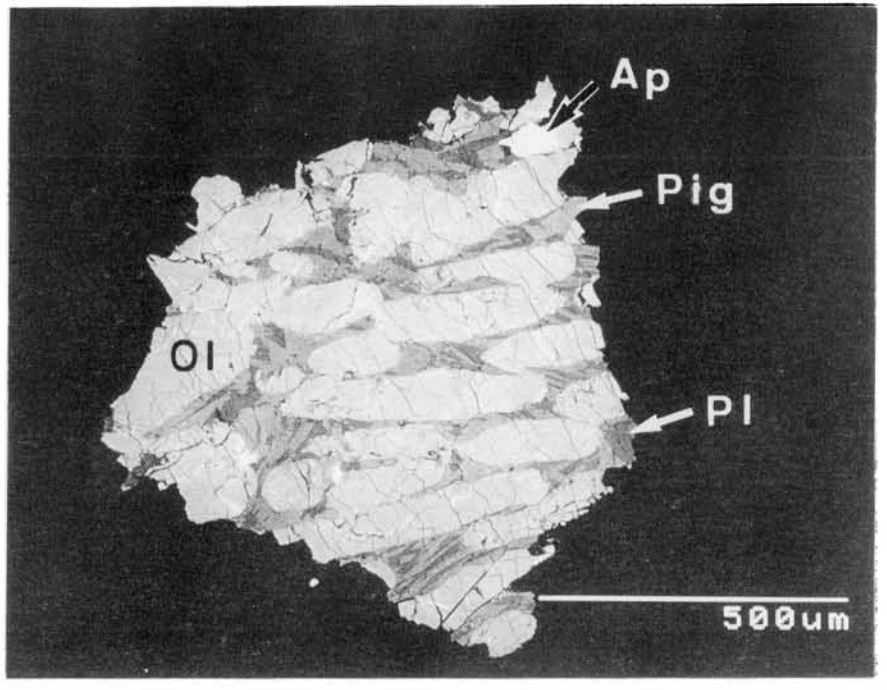

Figure 1 (b).

Fig. 1.
Photomicrographs of back scattered electron images of the Hedjaz light-colored fragment. This fragment consists of two lithologies. (a) Lithology I: Euhedral to subhedral olivines and pyroxenes. Plagioclase occurs between olivine and pyroxene crystals. (b) Lithology II: Typical skeletal or elongated olivine and pyroxene crystals in the fragment. Elongated olivines exhibit coincidental extinction.

Figure 2.

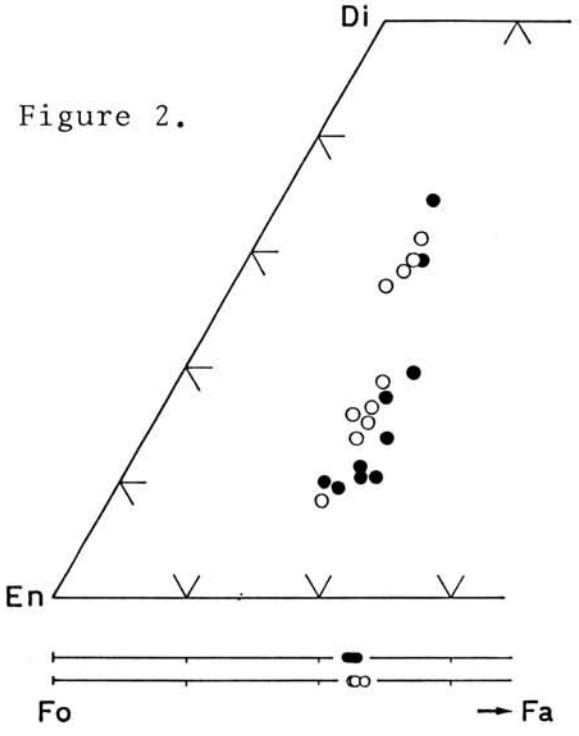

Figure 3.

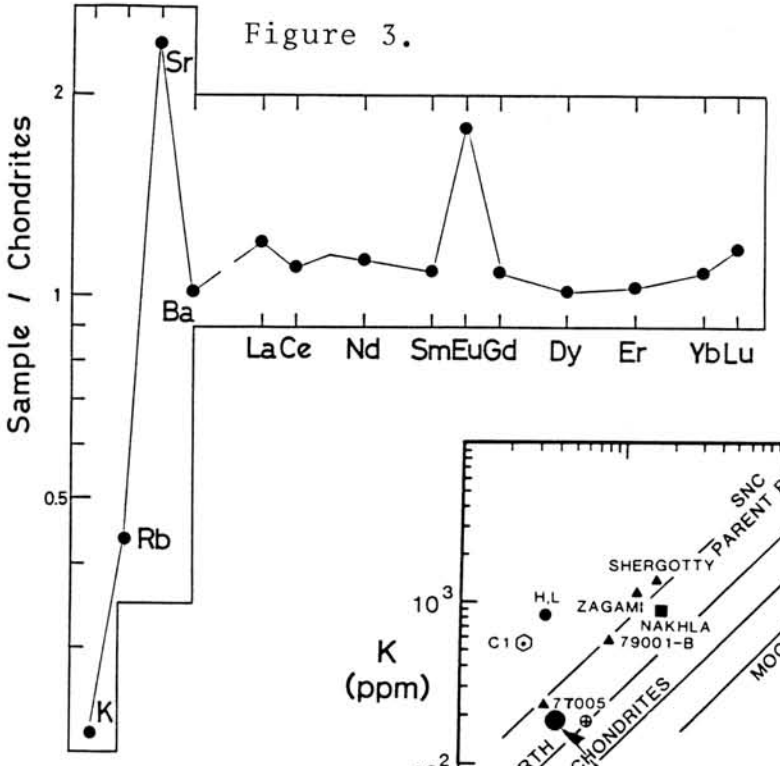

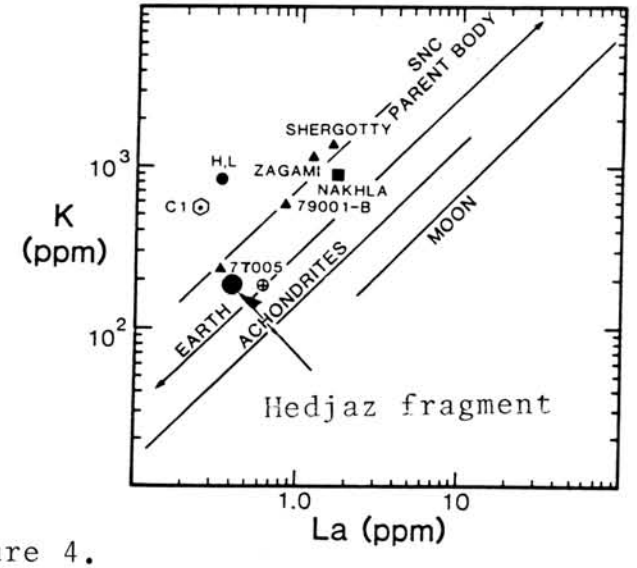

Figure 4.

Fig. 2.
Chemical compositions of pyroxenes and olivines in the Hedjaz light-colored fragment. Open and solid circles show the chemical compositions of pyroxenes or olivines in lithology I and lithology II, respectively.

Fig. 3.
Chondrites-normalized trace element abundance pattern of the Hedjaz light-colored fragment. Alkaline elements, K and Rb, are strongly depleted relative to alkali earths and REE. A positive Eu anomaly (63 %) is clearly observed.

Fig. 4.
Relationship between volatile element K and refractory rare earth element La for Hedjaz fragment, CI, H, and L chondrites, Earth, Moon, achondrites, and SNC parent body (based on [7]).

REFERENCES [1] e.g., Rubin A.E. Rev. Geophys. 23, 277-300 (1985) [2] Fredriksson K. et al. Meteoritics 21, 159-16 (1986) [3] Takeda H. et al. EPSL 71, 329-339 (1984) [4] Prinz M. et al. LPS XIV, 616-617 (1983) [5] Huchison R. Phys. Earth Planet. Interiors 29, 199-208 (1982) [6] e.g., Consolmagno G.J. & Drake M.J. GCA 41, 1271-1282 (1977) [7] Smith M.R. et al. JGR 89, B612-B630 (1984)

FURTHER STUDIES OF TRACE ELEMENT DISTRIBUTION IN CHONDRULE CORES AND RIMS OF THE TIESCHITZ(H3.6) CHONDRITE

Noda, S.[1], Nagamoto, H.[1], Nishikawa, Y.[1], Misawa, K.[2] and Nakamura, N.[1,2]

(1) Department of Earth Sciences, Faculty of Science and (2) Department of Sciences of Material Differentiation, Graduate School of Science and Technology, Kobe University, Nada, Kobe 657, Japan

Rims and cores of chondrules in unequilibrated chondrites have been studied by many workers (1-6). However, trace element chemical features, particularly for detailed REE patterns of chondrule core and rim are poorly known. In this study, in order to investigate trace element characteristics, and obtain constraints on physico-chemical conditions of chondrule formation, eight pairs of core and rim of Tieschitz (H3.6) chondrules were analyzed for REE, K, Rb, Sr, Ba, Ca and Mg by precise (direct-loading) mass spectrometric isotope dilution technique (7). Analytical precisions are considered to be better than 3 % for LREE, alkali and alkali earth, and 5 % for HREE. Part of our results were reported in the last symposium (8).

As pointed out by Nagamoto et al.(1987) (8), the K abundances in bulk Tieschitz chondrules are significantly depleted to compare with those of typical ordinary chondrites (830 ppm). Figure 1 shows K vs. CI-normalized (Rb/K) diagram for cores and rims of Tieschitz chondrules. It is found that rims is relatively enriched in K (283-706 ppm), but cores is significantly depleted in K (104-217 ppm). Similar result is reported for surfaces and interiors of Semarkona (LL 3.0) and Chainpur (LL 3.4) chondrules (4, 9). Rb/K ratios of the rims show large variation around CI (Rb/K) ratio, but the cores indicate systematically the higher Rb/K ratio than CI-chondrite. Fig. 2 (a) and (b) show K vs. Na diagrams for rims and glass materials of cores which were measured by EPMA. Since alkali metals in chondrule cores are mainly concentrated in glass materials, the ratio of Na/K in the glass materials is considered to represent those of bulk core. Glass materials of cores are enriched in Na and depleted in K compared to CI-chondrite. On the other hand, rims show K enrichments and Na depletions, indicating complementary distribution of alkali metals (at least for K) between cores and rims. It is considered that alkali metal enrichment in rims represents characteristics of precursor materials which could have been derived from parts of the materials vaporized from chondrule cores.

Fig. 3 shows the REE patterns of cores and rims of the same chondrules. REE abundances of cores are higher than those of rims. Most chondrule rims have mainly fine grained opaque materials. Chondrule rims have 1-2 x CI REE abundances and show uniformly flat patterns with positive Eu anomalies except for T-39, which consists of coarse grained materials. The rim of chondrule T-36 has positive Ce and Eu anomalies, suggesting that REE composition in this rim or its precursor material was established under oxidizing condition.

On the other hand, chondrule cores have more variable REE abundances ranging from 1 to 4 times CI-chondrite with Eu anomalies. Some samples show enrichment in HREE. REE abundance variations and Eu anomalies are not related with textural types of chondrules. The variable REE abundances with positive and negative Eu anomalies of cores suggests that the precursors of chondrule cores were not formed under sufficiently

uniform physico-chemical conditions. The depletion of alkali elements suggests that these chondrules were formed from an alkali-poor precursor and/or they lost alkalis during the chondrule-formation melting.

Chondrule rims and cores show different trends in a CI-normalized (K/Mg) vs. (Nd/Mg) diagram (Fig. 4). Rims indicate CI-chondritic abundance relatively, but substantially volatile free in cores. The relative enrichment of both refractory element (Nd) and the moderately volatile element (K) in rims, and larger variation of refractory and depletion of the moderately volatile in cores suggest that precursor materials of rims and cores were different, but possibly related in their formation process.

From the above results, it is suggested that rims and cores have different characteristics of alkali and Eu anomaly, but two genetically related chondrule precursors can be considered. We suggested that alkalis and the relatively volatile REE (Eu) had been lost from cores during formation of precursor materials of the core, and were partly incorporated into the rims. Hence, precursor of chondrule cores represent residual materials which lost alkalis and relatively volatile REE (Eu).

We are indebted to Dr. R. Hutchison, British Museum (Natural History), for providing us the Tieschitz specimens.

REFERENCES

(1) Allen, J. S., Nozette, S. and Wilkening, L. L. (1980) GCA 44, 1161-1175. (2) King, T. V. V. and King, E. A. (1981) ICARUS 48, 460-472. (3) Matsunami, S. (1984) Mem. Natl. Inst. Polar Res., Spec. Issue 35, 126-148. (4) Wilkening, L. L., Boynton, W. V. and Hill, D. H. (1984) GCA 48, 1071-1080. (5) Rubin, A. E. and Wasson, J. T. (1987) GCA 51, 1923-1937. (6)Nagahara, H. (1984) GCA 48 2581-2595. (7)Nakamura, N. (1988) submitted (8)Nagamoto, H., Nakamura, N., Nishikawa, Y., Misawa, K. and Noda, S. (1987) Papers presented to the 12th symposium on Antarctic Meteorite, 84-86. (9) Grossman, J. N. and Wasson, J. T. (1987) GCA 51, 3003-3012.

Figure captions

Fig. 1. The relationship between K contents and CI-normalized (Rb/K). Open circles and closed circles refer to chondrule cores and chondrule rims, respectively.

Fig. 2. Plot of K and Na contents in glass inside chondrule core (open circles) and chondrule rim material (closed circles).

Fig. 3. The REE patterns of individual chondrule cores and rims from Tieschitz. Symbols are the same as in Fig. 1.

Fig. 4. Plot of CI-normalized (K/Mg) vs. (Nd/Mg). Chondrule cores (open circles) and rims (closed circle) are shown in different area.

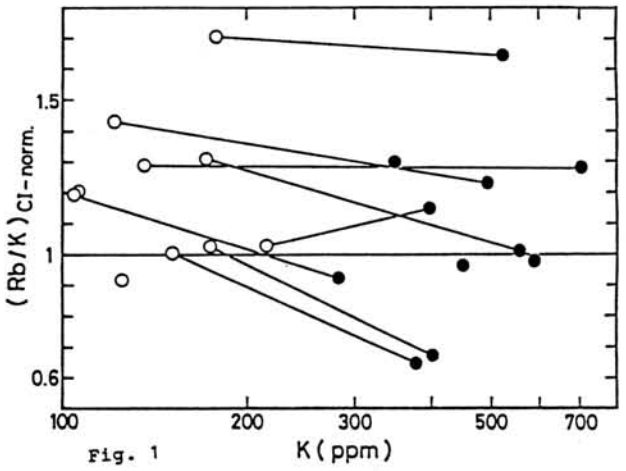

Fig. 1

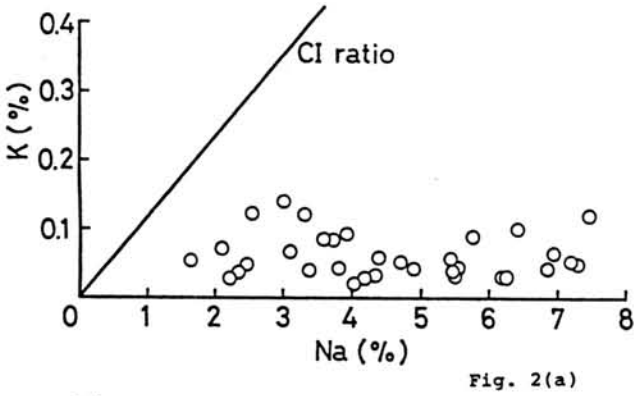

Fig. 2(a)

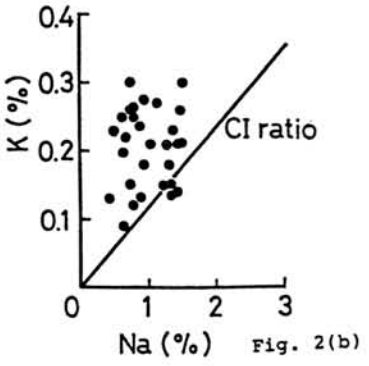

Fig. 2(b)

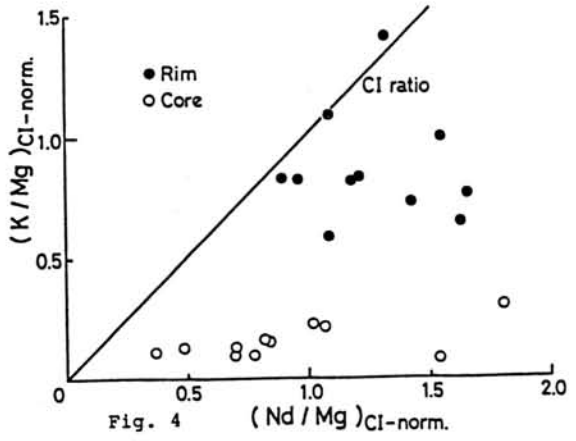

Fig. 4

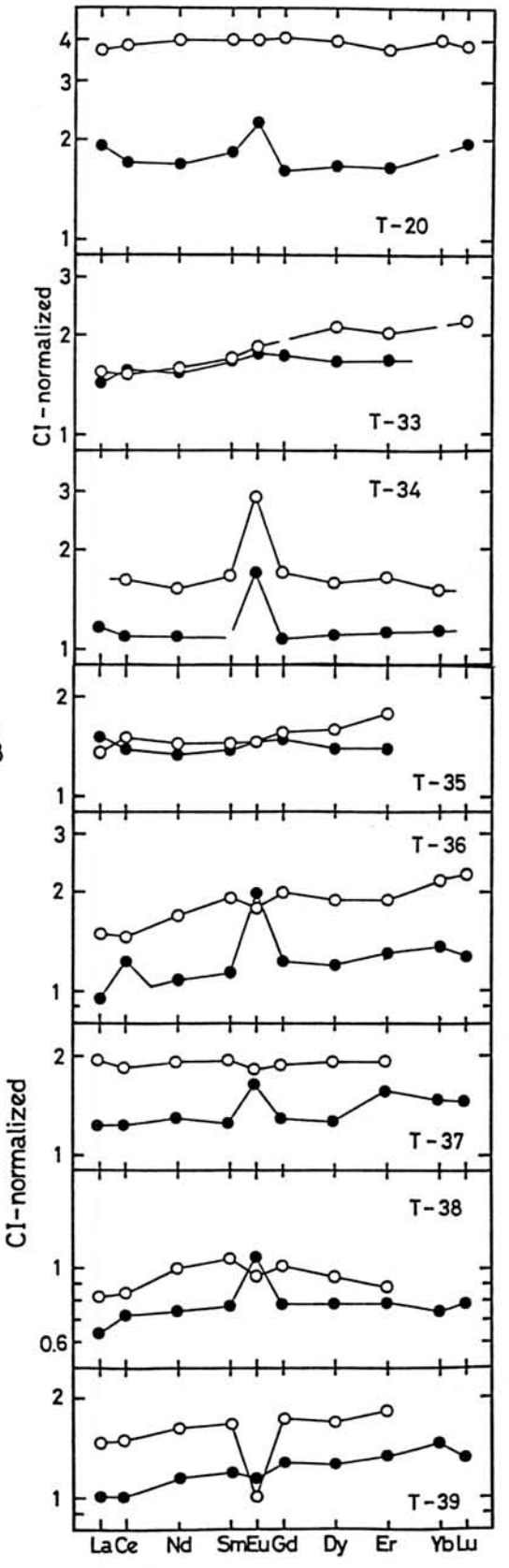

Fig. 3

24

NEUTRON ACTIVATION MEASUREMENT OF IRIDIUM CONCENTRATION IN YAMATO CV CHONDRITE

Yabushita,S. and Wada,K.
Deprrtment of Applied Mathematics & Physics and Department of Nuclear Engineering,Kyoto University,Kyoto 606,Japan.

Iridium content of extra-terrestrial objects is important in relation to the Ir rich clayer at the Cretaceous/Tertiary boundary found by Alvalez et al.[1] It has been proposed by a number of authors that the Iridium in the clay layer represents material brought to the earth by an asteroid or a comet. If it is so, the Ir content in such a body can be inferred from a measurement on the Ir content of extra-terrestrial objects such as meteorites or chondrites.

The sample we used for measurement is Y-793321,which is a CV chondrite. The sample was irradiated by neutron beams using the Experimental Reactor of Kyoto University Reactor Laboratory. A specimen of known weight was also irradiated in the same nuclear reactor. In order to remove noise due to radioactive elements of short half-lives, both the chondrite and the specimen were left to decay for nearly two months. The specimen was dissolved and diluted twice using micropipettes. Radioactivity of the chondrite and the specimen were then measured by a high sensitivity gamma ray detector.

The Ir content so obtained is 590 ng per gramme of the chondrite. This value may be compared with 570 ng/g obtained by Kallemeyn et al.[2]

REFERENCES

1) Alvarez,L.W.,Alvarez,W.,Asaro,F. and Michel,H.V.,1980.Science, 208,1095.

2) Kallemeyn,G.W. and Wasson,J.T.,1981.Geochim.Cosmochim.Acta,45,1217.

Wednesday, June 8, 1988

0900 - 1720 ***Symposium, Auditorium***

Abundances and distribution of trace elements in enstatite chondrites

Ebihara, M

Department of Chemistry, Faculty of General Studies, Gunma University, Maebashi, Gunma 371
(present address: Department of Chemistry, Faculty of Science, Tokyo Metropolitan University, Fukasawa, Setagaya, Tokyo 158)

As discussed previously (1, 2), abundances and distribution of trace elements largely reflect the formational and metamorphic processes meteorites experienced. Following the study on Y-691 (EH3) (2), possibly the least metamorphosed enstatite chondrite ever collected, experiments were extended to both unequilibrated and equilibrated enstatite chondrites (Qingzhen (EH3), Indarch (EH4), Abee (EH4), St. Mark's (EH5), Atlanta (EL6), Blithfield (EL6)) to see how the metamorphic activities changed abundances and distribution of trace elements in enstatite chondrites. Phase separation was carried out by using acid (nitric acid and aqua regia).

The bulk samples and the acid-residual samples of enstatite chondrites were analyzed at first by instrumental neutron acivation analysis (NAA) for some major and minor elements and then by radiochemical NAA for ten rare earth elements (REEs) (La, Ce, Nd, Sm, Eu, Gd, Tb, Tm, Yb, Lu) and eleven siderophile and chalcophile elements (Re, Ir, Pd, Au, Ag, Se, Te, Zn, In, Cd, Tl). Analytical methods and procedures are the same as those described previously (2). Few iron was confirmed to be present in acid-insoluble silicates, corresponding to characteristically low abundance of FeO in silicates in enstatite chondrites. Essentially no Co was detected in these fractions. These results suggest that phase separation was performed satisfactorily in the sense that acid-soluble phases were hardly present in the acid-residual fraction.

Figure 1 shows the C1-normalized abundance patterns of REEs in acid-soluble and -insoluble phases. As pointed out already (2), about 15 % of light REEs and 30 % of heavy REEs were confirmed to be allocated to acid residual phases of Y-691, for which abundance pattern is almost flat in the light REE span and gradually increases from Gd to Lu. These features in abundance patterns can be noticed for Qingzhen and Indarch, but distribution fractions of REES in acid-residual phases become smaller. In Abee and St. Mark's, essentially no REEs except Eu were found to be present in acid residues. Europium in acid-residues is attributable to plagioclase, which is hard to be dissolved in acid treatment, along with pyroxene and some glasses. Apparently REE abundance patterns in acid-residual fractions have a strong correlation with petrologic types of enstatite chondrites.

In the previous paper (1), two possible scenarios were presented for explaining the REE abundances in acid-residues of Y-691. Either scenario basically can also explain the

correlation stated above but needs some modefications, especially for explaining Eu anomalies in acid-residues of Abee and St. Mark'. Both Indarch and Abee are conventionally classified as EH4. REE abundance patterns in acid-residues, however, suggest that these meteorites experienced metamorphic activities of different degrees: Indarch was less metamorphosed than Abee. Essentially no difference was confirmed in REE abundance patterns between Abee and St Mark's acid residues.

references
(1) Ebihara, M. and Honda, M. (1987) Meteoritics 22, 179-190.
(2) Ebihara, M. (1988) Proceeding of 12th Symposium on Antarctic Meteorites, in press.

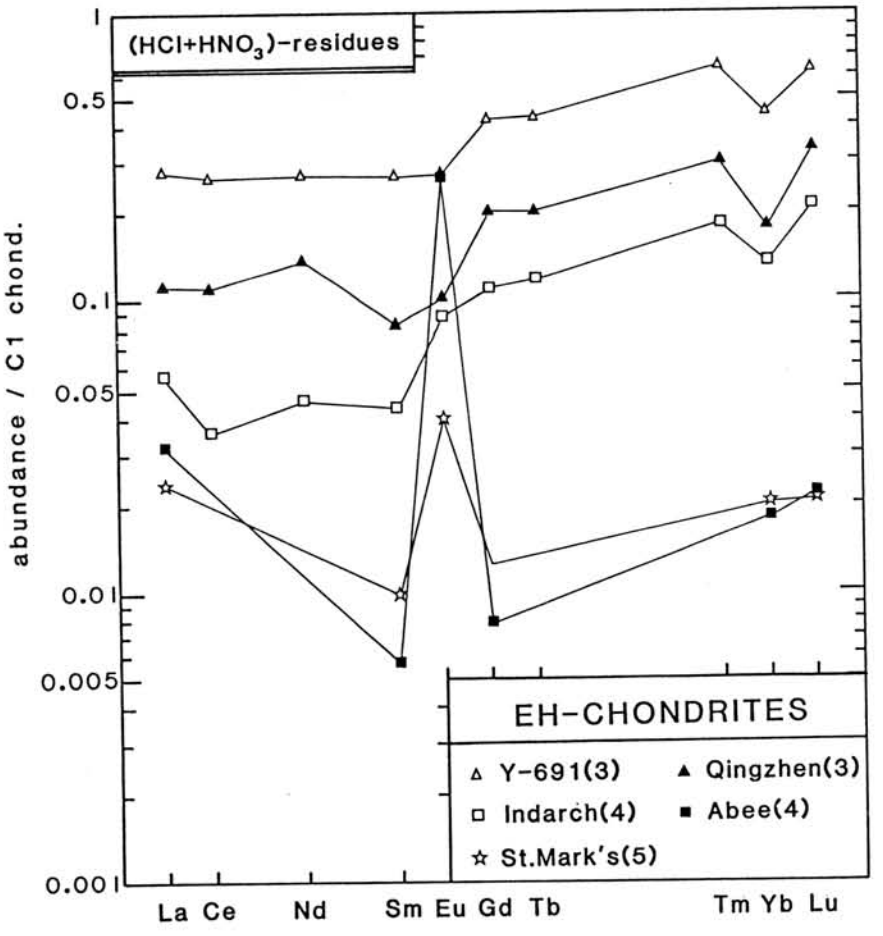

Fig. 1 REE abundance patterns in acid-residual fractions of unequilibrated enstatite chondrites.

THE CORRELATION OF MAGNESIUM ISOTOPE ABUNDANCE AND CHEMICAL COMPOSITION IN TYPE 3 CHONDRITES

Uyeda Chiaki and Okano Jun

Institute of Geological Science, College of General Education, Osaka University

Isotopic abundances of magnesium in primitive meteorites have been measured and compared with those in a terrestrial laboratory standard olivine. The results revealed that magnesium in a number of primitive meteorites have an excess of ^{24}Mg[1]. The relation between $\Delta 24$ for the individual chondrule and its chondrule texture was studied[2], where $\Delta 24$ is the excess of ^{24}Mg with respect to the laboratory standard. It was found that $\Delta 24$, which were ranging from several to thirteen permil, were large for glassy and barred olivine, while for porphyritic and radial pyroxene chondrules $\Delta 24$ show small values. The results of laboratory experiment reported by Tsuchiyama et al, which were carried out to reproduce chondrule textures, showed that the textures were dependent on the heating temperatures and the cooling rates.[3] Comparing the results of this reproducing experiment and the results on the ^{24}Mg excess, it is seen that the intensively heated and rapidly cooled chondrules have a relatively large excess of ^{24}Mg. It is also seen that textures with large abundance such as porphyritic chondrules tend to show small $\Delta 24$ values. A model of chondrule formation to account for these relations was presented.[2]

However, $\Delta 24$s of the chondrules with a specific texture are still scattered within ten permil, and the difference in chemical or mineral composition of each chondrules were assumed to be the cause of this scattering. In the present work, the amount of $\Delta 24$ for each chondrule is compared with its ratios of major elements such as Mg+Fe/Si or Fe/Mg to check this idea.

The atomic ratios of major elements were obtained in the following way. Mass spectra of five terrestrial minerals, three chondrules of Allende meteorite and four chondrules of Julusburg meteorite were obitained by SIMS (Hitachi IMA-2A) and the ratios of the secondary ion intensities of the major components were calculated. EPMA (JEOL JCXA-73) measurements were carried out on the same samples and the atomic ratio of the major components were determined. The results were shown in Table I. In order to convert the secondary intensity ratios to the atomic ratios, caribration lines for Mg/Si and Fe/Si were obtained as shown in Fig. 1. With these caribration lines, the atomic ratios of Mg/Si and of Fe/ Si can be obtained from the corresponding secondary ion intensity ratios with the accuracy of about 10%.

Mg isotope abundance was measured by SIMS. The primary ions were 9keV O_2^+,with beam current of about 1-1.5μA. The spot size was 80-120μm. At each spot of Mg isotope measurement, mass spectra were taken to obtain the atomic ratio of the major components.

The relation between measured $\Delta 24$ and atomic ratios for each chondrules are ploted in Fig.2, where (a) and (b) are plotted for ratios of Mg+Fe/Si and Fe/Mg, respectively. The correlation coefficient of $\Delta 24$ against Mg+Fe/Si in Fig.2-(a) is 0.68, and the value of $\Delta 24$ tends to increase with Mg+Fe/Si ratio. Three chondrules whose Mg+Fe/Si values are larger than 2.0 probably contains metal iron fragments. The correlation between Fe/Mg ratio and $\Delta 24$ is rather obscure. However, when Fe/Mg is below 3.0, iron rich silicate tend to have small amount of $\Delta 24$.

The relations seen in Fig.2 indicate that chondrules composed of high temperature minerals tend to have high $\Delta 24$ values. This supports the previous assumption that chondrule

formation process has a close relation with the excess ^{24}Mg contamination process, and that chondrules formed from intense heating conditions tend to have relatively large $\Delta 24$ values.

We thank Professor H.Nishimura and Ms.H.Sakaguchi of Naruto University of Education for useful instructions and suggestions in measurements using the EPMA.

TABLE.1 Mg/Si and Fe/Si ratios measured by EPMA and SIMS.

SAMPLE	Mg/Si EPMA		SIMS		Fe/Si EPMA		SIMS	
	$\bar{m}$	σ_m	$\bar{m}$	σ_m	$\bar{m}$	σ_m	$\bar{m}$	σ_m
(TRRESTRIAL)								
AUGITE(KOUCHI)	.780	.009	.94	.004	.189	.005	.28	.001
ENSTATITE(NORWAY)	1.781	.009	2.80	.21	.210	.005	.31	.03
OLIVINE(HAWAI)	.853	.004	1.10	.05	.127	.001	.23	.04
FOLSTERITE(OKI)	.850	.003	1.31	.20	.117	.003	.21	.03
FOLSTERITE(EHIME)	1.872	.001	2.85	.18	.114	.001	.18	.01
(ALLENDE METERITE)								
PORPHYRITIC-1	1.40	.20	1.61	.33	.087	.021	.16	.02
ENSTATITE-1	1.94	.02	2.40	.05	.023	.002	.17	.04
OLIVINE(SINGLE)-1	.95	.01	1.34	.03	.033	.004	.10	.01
(JULESBURG METEORITE)								
PORPHYRITIC-1	.90	.016	1.11	.06	.068	.034	.23	.01
BARRED OLIVINE-1	.91	.190	1.52	.18	.295	.068	.44	.05
RADIAL PYROXENE-1	.95	.28	1.21	.43	.28	.09	.40	.06
RADIAL PYROXENE-1	.88	.02	1.11	.09	.12	.01	.21	.02

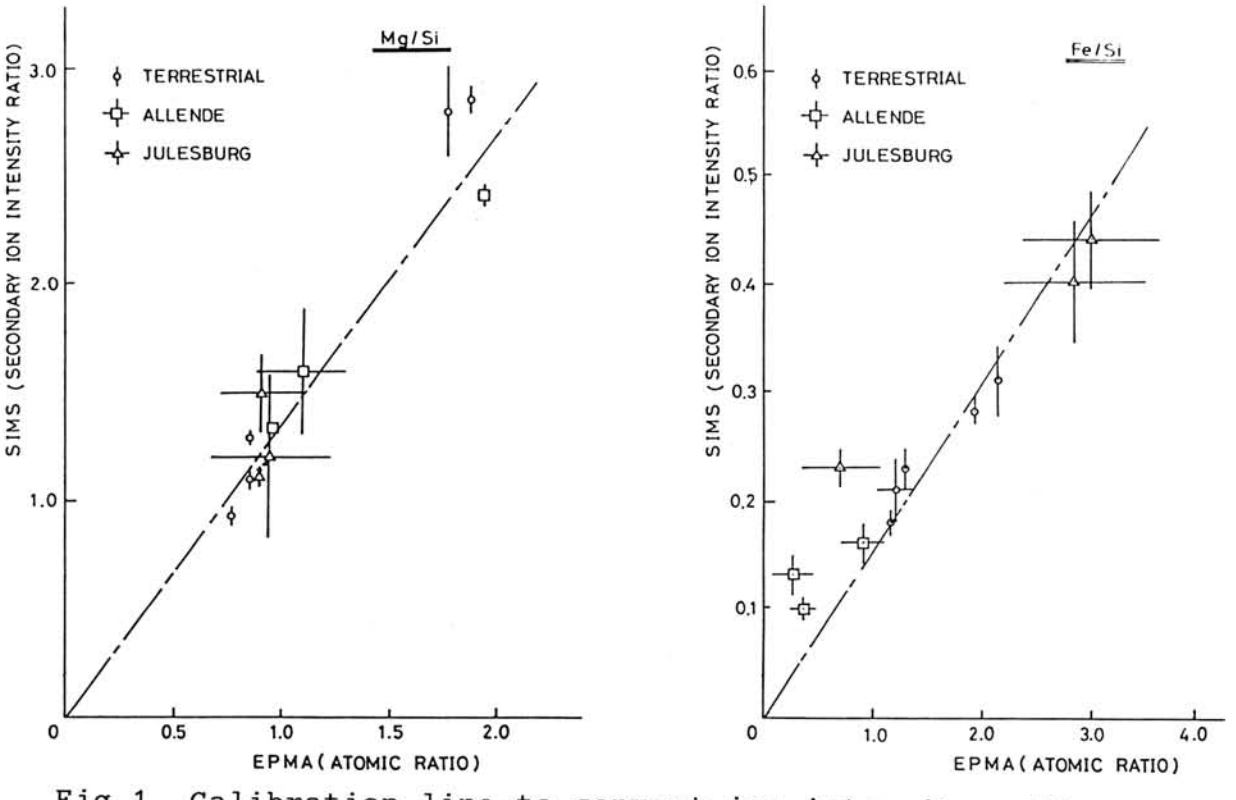

Fig.1 Calibration line to convert ion intensity ratio to atomic ratio.

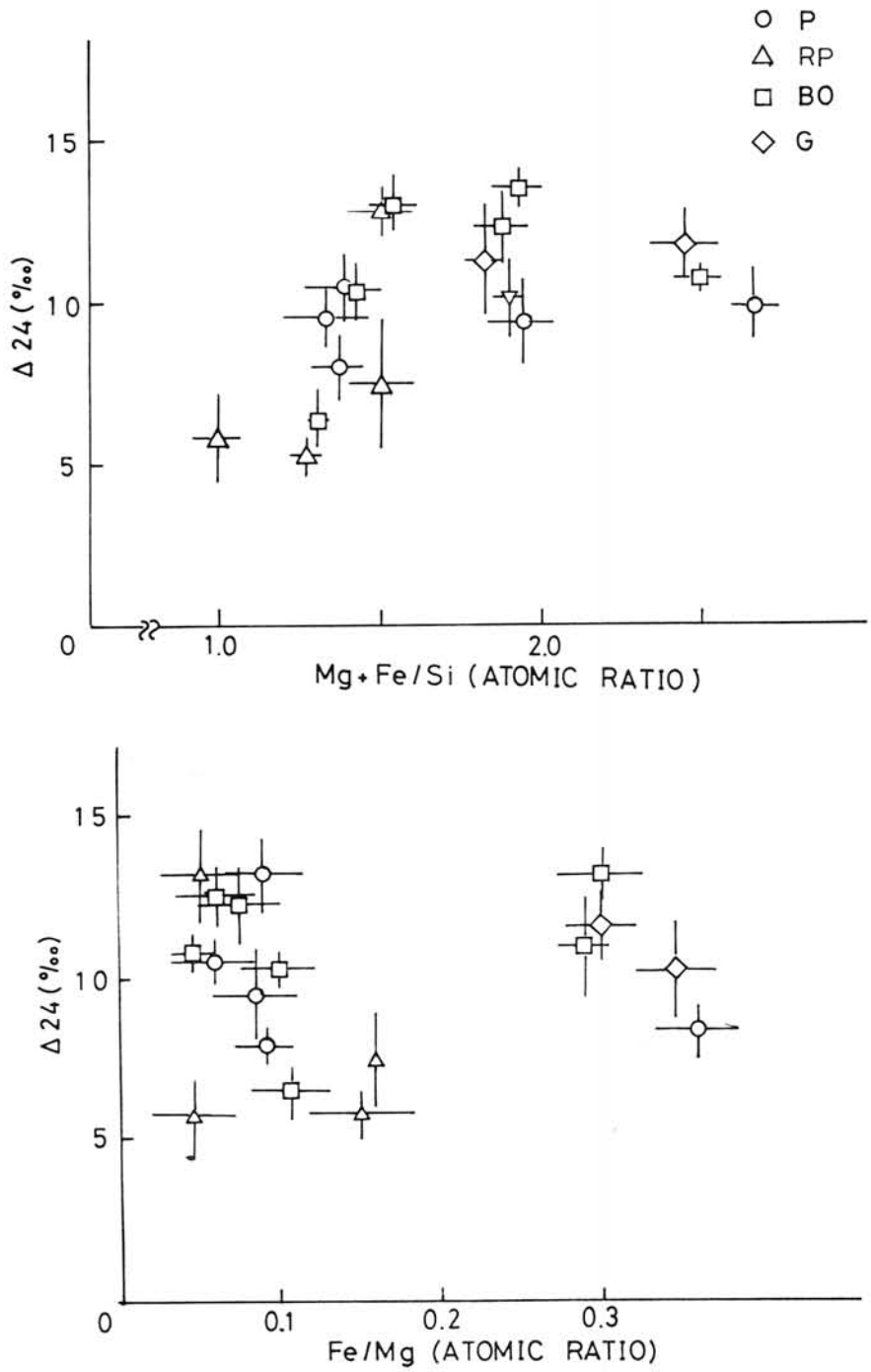

Fig.2 Relation between ^{24}Mg excess and major chemical composition for individual chondurules.

Refferences

1)H.Nishimura and J.Okano:Secondary Ion Mass Spectrometry, SIMS IV,
ed.A.Bennighoven et al., Springer-Verlag, p475(1984)
2)C.Uyeda, M.Suzuki and J.Okano:Proc.ISAS Lunar and Planetary Symposium XII,p62 (1987)
3)A.Tsuchiyama, H.Nagahara and I.Kushiro:Earth Planet Sci . Lett.,48,155-165

Isotopic Studies on Diogenites, Based on the Rb-Sr Systematics

Kazuya Takahashi*, Hiroshi Shimizu and Akimasa Masuda
Department of Chemistry, University of Tokyo, Hongo, Tokyo 113
*Institute of Physical and Chemical Research, Wako, Saitama 351

Previously, we reported the chronological data for several diogenites and we obtained an age of 4.398 ±0.024 b.y.[1]. This age is younger than that of eucrite (around 4.5 b.y.) and it indicates that the diogenite was formed at later stage than eucrite. We also reported that diogenites can be classified into some groups according to their REE (Rare Earth Elements) patterns. In this study, the analyses of Rb-Sr systems and REE abundances have been newly carried out on some diogenites (Tatahouine 2, Roda and Shalka 1,2), to discuss their genesis. Fig. 1 shows the isochron plot obtained from six diogenite samples. The data of Johnstown samples and Tatahouine 1 are taken from our previous study but Tatahouine 2 newly studied is another fragment of the same chip as Tatahouine 1. The data on Tatahouine 1 and 2 are close to each other in Fig. 1. The isochron yields an age of 4.396 ±0.012 b.y. This result confirms our previous one. This age is considered to indicate that the parental region of diogenite had kept igneous activity for one hundred or more million years after the accretion and the formation of eucritic layer.

On the other hand, the data of Roda and Shalka suggest that there exist some groups genetically distinguished from the others in the diogenite association. In Figs. 2 and 3, the isotopic data of Roda and Shalka are shown. The data of Roda does not fall on the isochron formed by Johnstown and Tatahouine, but the data of Roda is plotted rather close to the isochron of Juvinas eucrite (dotted line). And, as shown in Fig. 4, the REE pattern of Roda is similar to that of pyroxene fraction of Juvinas eucrite. It is considered that Roda would be closely related with eucrite. And the similarity in the REE pattern between Roda and Johnstown matrix samples suggests some genetic relationship with each other, although Johnstown samples form the isochron with an age of 4.396 b.y. For Shalka, the REE pattern and Rb-Sr isotopic data are distinct from other diogenites. Shalka 1 is the main part and Shalka 2 is the clast with similar appearance to the Opx clast in Kapoeta howardite. As shown in Fig. 3, the Rb-Sr data on Shalka 1 fall on the point distinct from both of 4.52 and 4.396 b.y. lines. And the REE pattern has some unique characteristics as shown in Fig. 4. Namely, this REE pattern is characterized by the enrichment of light REE. These observations suggest that Shalka was formed through different process from other diogenites. Birck and Allegre (1981)[2] also analyzed Shalka and their data are shown in Fig. 3. It seems that our data and those by Birck and Allegre would form a line. It is possible that we can get an internal isochron for Shalka. The line formed by our data and those of Birck and Allegre yields 2.7 ±0.6 b.y.(dashed line in Fig. 3). Shalka 2 shows the similar REE pattern, and appears to fall close to the Kapoeta OPx-clast in Fig. 3 within the experimental errors.

In summary, Johnstown and Tatahouine constitute one group in

the diogenite association and these were formed around 4.396 billion years and two opx clasts, in Kapoeta and Shalka, also belong to this group, in the point that their REE patterns resemble the REE pattern of Johnstown opx-clast. Roda is considered to have been formed by the process related with eucrite 4.5 billion years ago. The REE pattern of Shalka suggests the complicated history for its genesis and we are planning to carry out a further study to obtain the more convincing age for the formation of Shalka. We are going to study some samples (another fragment of Tatahouine or some Antarctic diogenites) to discuss the genesis of diogenite in detail.

References:

[1] Takahashi et al.(1987), Papers presented to the Twelfth Symposium on Antarctic Meteorites, 96-97.
[2] Birck and Allegre (1981), Earth and Planetary Science Letters, 55, 116-122.
[3] Shimizu and Masuda (1981), Mem. Natl. Inst. Polar Res., Spec. Issue, 20, 211-220

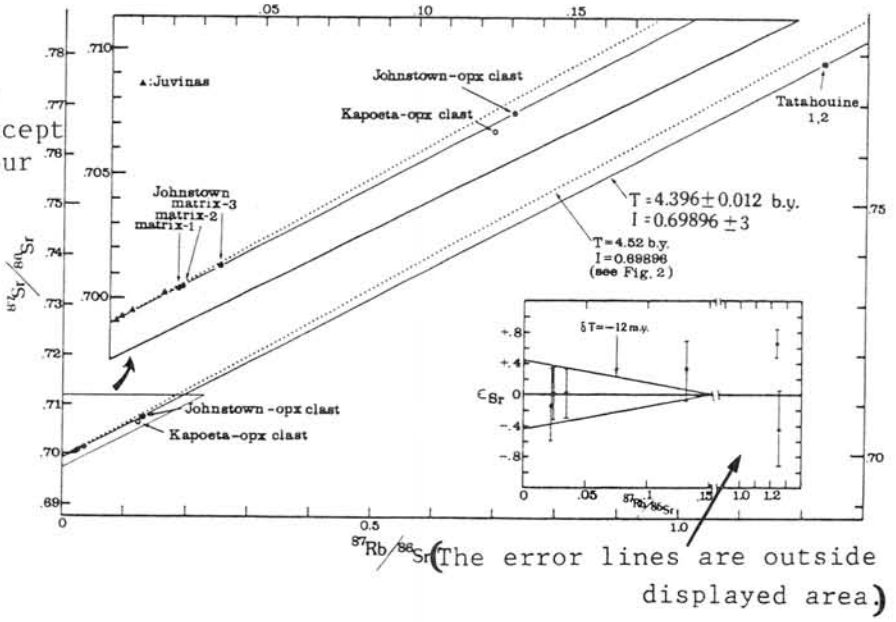

Fig. 1
The isochron plot for diogenites. The data except Tatahouine 2 are from our previous report[1].

(The error lines are outside displayed area.)

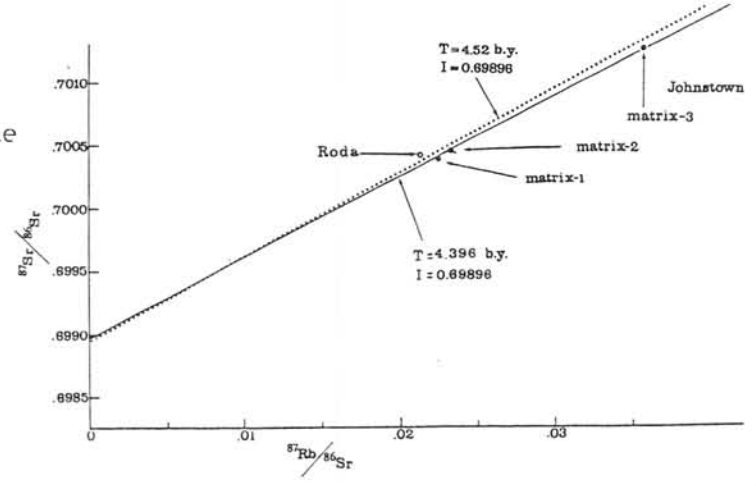

Fig. 2
The Rb-Sr data of Roda. This plot corresponds to the area for $^{87}Rb/^{86}Sr$ smaller than 0.035 in Fig. 1.

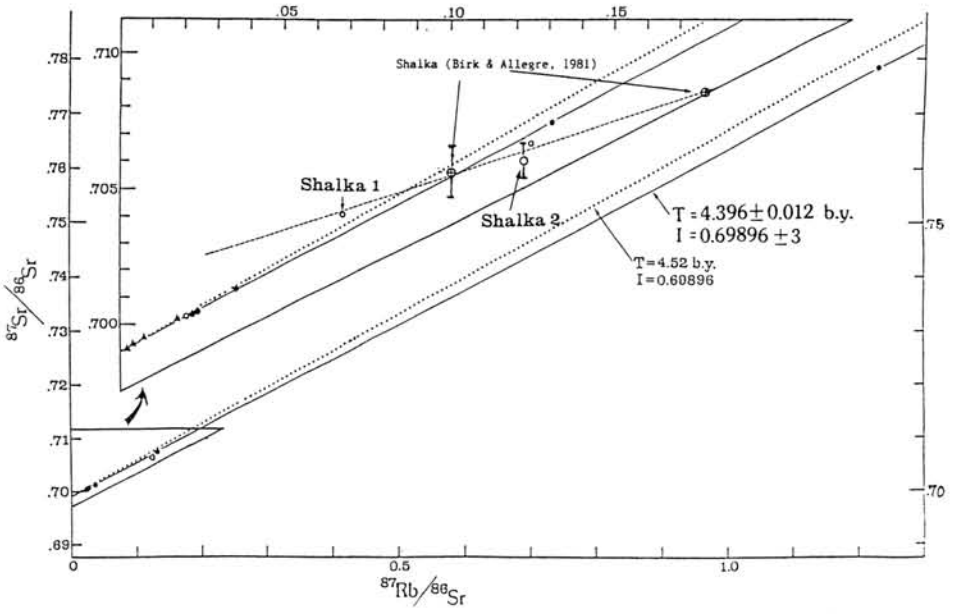

Fig. 3 The Rb-Sr data of Shalka.
The dashed line represents an isochron with an age of 2.7 b.y.(see text).

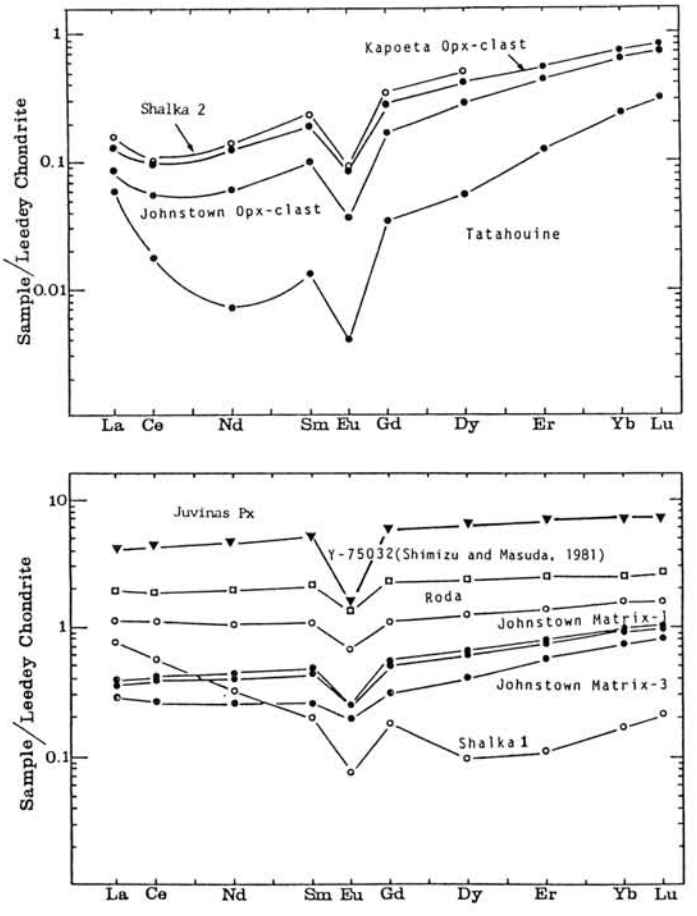

Fig. 4 The REE pattern of diogenite samples. The data of Y-75032 are from Shimizu and Masuda (1981)[3].

HOWARDITE, EUCRITE AND DIOGENITE (HED) METEORITES FROM ANTARCTICA AND ELSEWHERE: CHEMICAL CLUES TO THEIR ORIGIN

Paul, R. L.*, Lipschutz, M. E.*, Kruse, H.§ and Sack, R. O.†

*Department of Chemistry, †Department of Earth and Atmospheric Science, Purdue University, W. Lafayette, IN 47907 USA. §Max-Planck-Institut für Chemie (Otto-Hahn-Institut) D-6500 Mainz, FRG.

Petrologic differences between Antarctic and non-Antarctic HED meteorites suggest some difference in their genetic history [1]. To examine this in more detail, we determined by radiochemical neutron activation analysis (RNAA) 15 thermally-labile trace and ultra-trace elements and/or those whose geochemical behavior is known to provide important genetic information (Ag, Au, Bi, Cd, Co, Cs, Ga, In, Rb, Sb, Se, Te, Tl, U, Zn). We also estimated average major and minor element contents (hence, mineral modes and compositions) by electron microprobe analysis of thin sections of nearly all samples studied by RNAA. The samples studied included 25 Antarctic and 9 non-Antarctic eucrites or clasts in them, 2 Antarctic and 3 non-Antarctic howardites and 5 Antarctic and 7 non-Antarctic diogenites or clasts.

The major results include

a. Antarctic and non-Antarctic eucrites (presumably also howardites and diogenites) derive from different regions in the same parent body, apparently 4 Vesta [2].

b. On average, Antarctic eucrites contain higher levels of labile elements indicating higher closure or lower formation temperatures.

c. Trends for nearly all labile trace elements in eucrites reflect volatilization and loss from the parent magma [3]: Rb and Cs contents also reflect monotonic lithophile fractionation while no coherent Ga trend is evident.

d. As previously shown [4], howardites are mixtures of eucrite and diogenite end-members, which are better approximated by Antarctic samples than by non-Antarctic ones.

e. Eucrites and howardites apparently constitute a compositional continuum while a definite hiatus exists between the latter and diogenites.

f. Contrary to previous thought, late volcanism apparently took place on at least one asteroidal-sized object, the HED parent body. During this volcanism, mobile trace-element-rich emanations deposited in the surface howardite and lower-lying diogenite layers [4] indicating that impact mixing penetrated entirely through the intermediate eucrite layer.

Depending on the presentation time available, we will show data illustrating these points seriatim.

References: [1] Takeda, H., Mori, H., Delaney, J. S., Prinz, M., Harlow, G. E. and Ishii T. (1983) Proc. Eighth Symp. Antarctic Meteorites, 181-205; [2] McCord, T. B., Adams, J. B. and Johnson, T. V. (1970), Science 168, 1445-1447; [3] Mittlefehldt, D. W. (1987) Geochim. Cosmochim. Acta 51, 267-278; [4] Dreibus, G. and Wänke H. (1980) Z. Naturforsch. 35a, 204-216.

Acknowledgement: This research was sponsored by the U.S. National Science Foundation (grant DPP-8415061) and National Aeronautics and Space Administration (grant NAG 9-48).

Rare earth and major element fractionations in evaporation of chondritic matter

Shigekazu Yoneda*, Hiroshi Shimizu** and Akimasa Masuda**

* College of Humanities and Sciences, Nihon University
** Department of Chemistry, Faculty of Science, The University of Tokyo

Introduction: The equilibrium condensation theory (Grossman, 1972) has well explained the Allende CAI compositions rich in the refractory elements, e.g. Ca and Al, and the thermal history of the primitive solar nebula. But, the oxygen isotopic anomalies found in the carbonaceous chondrite inclusions (Clayton et al, 1973) suggested the heterogeneity of the solar nebula, and the relict grains (Nagahara, 1981; Rambaldi, 1981) showed the incomplete melting or vaporization of the precursors. Also, the evaporation experiments were recently performed to investigate the differentiation of the materials in the primitive solar nebula at the high temperature (e.g. Hashimoto, 1983; Nagahara and Kushiro, 1987). In this study, the REE and the major element fractionations are examined by evaporation of chondritic matter, and the origin of inclusions and chondrules are investigated.

Experimental: About 1g pellets prepared from the powder of Jilin meteorite (H5 chondrite) were used as starting materials. Experimental conditions are shown in Table 1. RF means the residual fraction, that is the evaporation residue percentage relative to the starting material. Condensates were collected on the glass piece (10cm x 10cm) set 10-30cm over the evaporation crucible or boat. Rb, Sr, Ba and REE abundances were determined by the isotope dilution method using thermal ionization mass spectrometry.

Results and Discussion:

1. Major elements abundances measured by EPMA

Major element abundances measured by EPMA are plotted on Si-Mg-Fe and Si-Mg-(Ca+Al) diagrams (Fig. 1). Condensation and evaporation paths after Grossman (1972) and Hashimoto (1983) are also drawn on Fig. 1. Two condensates of run 10 were collected separately; the first 40 minutes condensate named A (C10A) and the last 60 minutes condensate B (C10B). Major element composition of the evaporation residues changes; for example, the residue of run 2 (R2) becomes rich in Ca and Al along the evaporation path, whereas each composition of the condensates is uniform. The condensate composition is normally Fe-rich. The order of contents of elements in the bulk of condensate is Fe > Si, Mg> Ni > Ca, Al. At the later stage of evaporation like C10B, however, Fe scarcely exists in the residue. Thus, the condensate condensed from its vapor is also Fe-poor.

2. Major element fractionations measured by SIMS

Major element fractionations were examined by depth analysis of the condensate using the secondary ion mass spectrometer (SIMS). Results of SIMS studies concerning K, Mg, Si and Fe in C10A are shown in Fig. 2. The vertical axis shows the ratio of secondary ion beam intensity to total one, and the horizontal axis refers to the time exposed to the primary ion beam. Time 0 corresponds to the last condensed part, and the time at 2 hours corresponds to the first condensed part because the secondary ion beam intensity of every element vanishes here.

At first, the alkali metal element K which has high volatility almost entirely evaporates. Vaporization of Si takes place next to K. The vaporization sequence of Si and Fe is opposite to the result of Hashimoto (1983). Hashimoto (1983) used the synthetic materials of Fe, Mg, Si, Ca and Al, so the reason for this reversal in sequence of opposite seems to have something to do with the difference in the starting materials. The Fe vaporization extends for almost two hours because the metal phase gathers together and sinks into silicate melt and then it becomes hard to evaporate. Although Mg appears to be the last element in vaporization in C10A, not only Mg but also Si yet evaporate in the later part C10B.

3. Rare earth elements in the residues

The REE pattern of the run 10 residue (R10) is shown in Fig. 3. The R10 pattern has the negative Ce anomaly, suggesting the vaporization of Ce with the volatile form of CeO_2 because of locally high oxygen fugacity made by the evaporation of large amount of silicates (Nagasawa and Onuma, 1979). The Ce negative anomaly is also observed at run 9 even in the atmosphere of H_2. Thus,

the experiments in this study is understood to simulate the evaporation of the chondritic materials under the oxidizing condition surrounded by the vapor from themselves.

Some Allende inclusions and chondrules are investigated in this study, and one of them named Allende 2-A has the similar REE pattern to R10; very low amount of Rb and the negative anomaly both of Ce and Eu (Fig. 3). Davis et al. (1982) found that the Allende inclusion named HAL had the large negative anomaly of Ce, and concluded that it had been formed in the extremely oxidizing circumstances (in the supernova ejecta of helium-burning zone or in the "chondritic gas" which was formed by entirely vaporization of chondrites). Two possibilities could be supposed for the origin of formation of the Allende 2-A inclusion: (1)the residue formed in the oxidizing vapor having vaporized from itself, (2)the condensate formed in the "chondritic gas" at the high temperature.

4. Rare earth elements in the condensates

The REE pattern of the run 10 condensates, C10A and C10B, are shown in Fig. 4. REE contents in C10B are more abundant than those in C10A because of the REE enrichment in the residue. Rb is found to have almost entirely evaporated in the first half. The REE pattern of the "giant olivine chondrule (GOC)" found by Tanaka et al. (1975) is also shown in Fig. 4. The REE pattern of GOC is very similar to C10A and B having the large positive anomaly of Ce and Eu (and Ba) except for the little difference of the slope from Nd to Lu. This suggests that GOC experienced the circumstances of the high temperature and high oxidizing condition. If GOC is assumed to have formed as a condensate from the "chondritic gas", the following processes, taking into account the low Rb content, are considered to have taken place with the decrease of temperature of the oxidizing high-temperature gas: (1)REEs except Ce and Eu condensed with Ca and Al etc. as high temperature condensates, (2)this high temperature condensates were removed from the cooling gas, (3)GOC condensed, (4)GOC was removed from the gas before such alkali metal elements as Rb condensed. Alternatively, if GOC is assumed to be formed by the evaporation metamorphism, considering that Rb abundance is similar to that of C10B and the olivine composition is Fo_{79}, i.e. Mg-rich, the following processes are conceivable: (1)Rb and Fe almost entirely vaporized by heating of the chondritic matter, (2)by further heating, the vapor similar to the gas which formed C10B was generated, (3)GOC condensed from this vapor. It is difficult to conclude whether the GOC was formed by condensation or evaporation. But it might merit attention that the former must consider the removing mechanism twice, while the latter need not presume a removing mechanism.

Summary: The REE patterns similar to those of Allende 2-A and GOC which were supposed to have been formed under oxidizing conditions were obtained by the evaporation experiments of the chondritic matter in the laboratory. The origin of GOC could be explained by the evaporation metamorphism.

References: Clayton, R. N. et al.(1973) Science, 182, 485; Davis, A. M. et al.(1982) G.C.A., 46, 1627; Grossman, L.(1972) G.C.A., 36, 597; Hashimoto, A.(1983) Geochem. J., 17, 111; Nagahara, H.(1981) Nature, 292, 135; Nagahara, H. and Kushiro, I.(1987) Proc. 20th ISAS Lunar and Planetary symposium, 66; Nagasawa, H. and Onuma, N.(1979) L.P.S., X, 884; Rambaldi, E. R.(1981) Nature, 293, 558; Tanaka, T. et al.(1975) Nature, 256, 27

Table. 1 Experimental conditions

Run	Heating Method	min.	Atmosphere(Torr)	RF(%)
1	electron beam	2	Ar 2×10^{-4}	72.6
2	"	5	"	30.2
3	CO_2 laser	1	vacuum 7×10^{-6}	96.0
4	"	2	" 4×10^{-5}	95.5
5	W filament	30	" 8×10^{-6}	56.2
6	Mo boat	360	" 2×10^{-6}	98.6
7	"	30	" 8×10^{-6}	61.9
8	"	60	H_2 2×10^{-4}	77.6
9	"	60	H_2 0.7	77.4
10	"	100	vacuum 2×10^{-5}	2.7

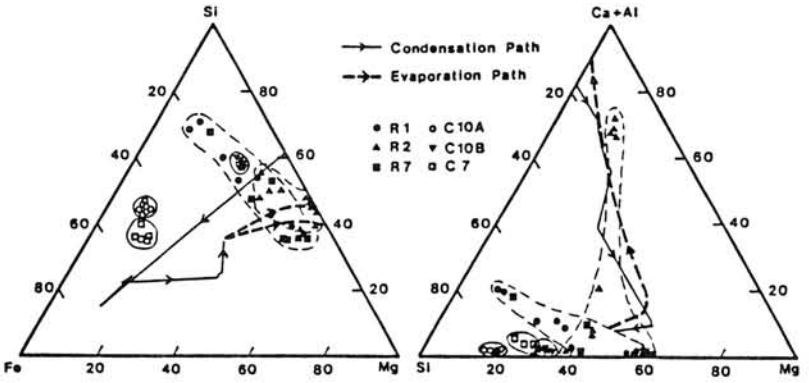

Fig. 1 Major element compositions

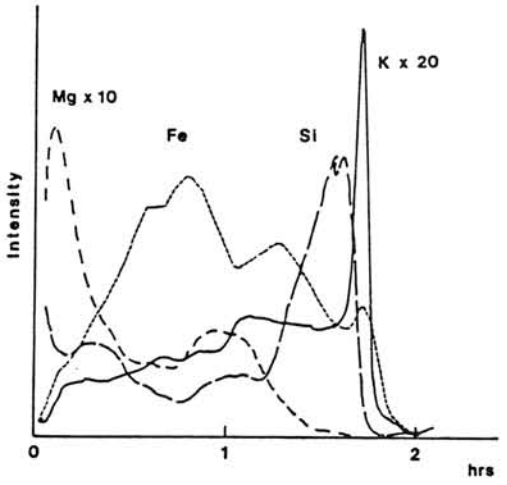

Fig. 2

Major element fractionations in the run 10 condensate A (C10A)

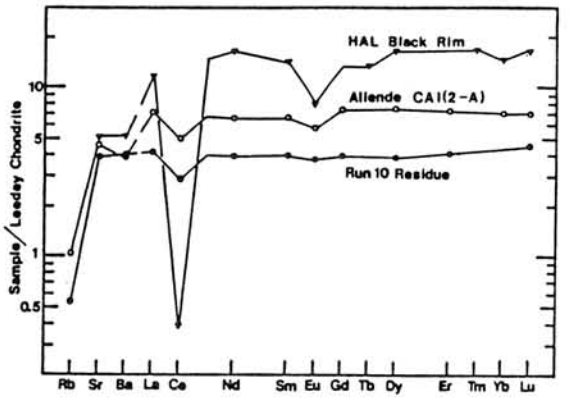

Fig. 3

REE patterns of the run 10 residue (R10) and Allende inclusions

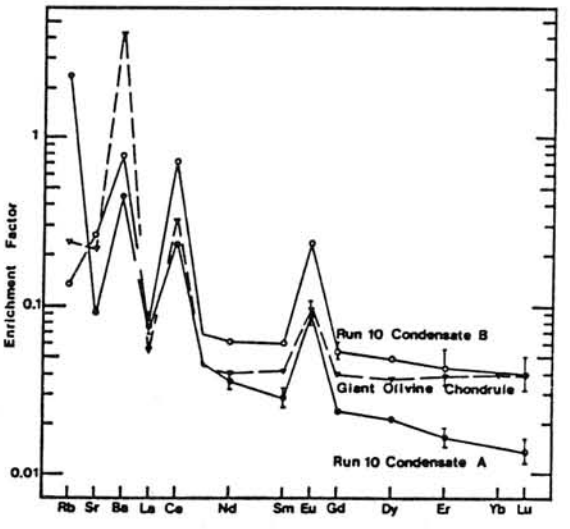

Fig. 4 REE patterns of the run 10 condensates and the "giant olivine chondrule (GOC)"

FRACTIONATION EXPERIMENTS OF CHONDRITIC MATERIAL

Hiroshi ISOBE*, Akira TSUCHIYAMA and Masao KITAMURA
Department of Geology and Mineralogy, Kyoto University, Sakyo, Kyoto, 606
* Present address: Department of Environmental Safety Research, Japan Atomic Energy Research Institute, Tokai, Ibaraki, 319-11

It is considered that the HED meteorites (howerdite, eucrite, and diogenite) and/or pallasite have genetic relations and correspond to each layer of a single parent body (e.g. [1,2]). Two models for the formation process of the parent body have been proposed but still in a controversy; (1) the parental body was formed by fractional crystallization from a single magma ocean on the parent body [1], and (2) by a partial melting of a hypothetical source region [3,4].

In the present study, phase relations of a chondritic material (Table 1) have been determined on the assumption that the bulk composition of the parent body is chondritic. Compositional variations of melts and minerals by temperature have been also determined because the previous experiments using chondritic materials [5,6,7] were too preliminary to discuss the problem. The present experiments shows that a two stage fractionation model is possible for the formation of the HED meteorite parent body.

Two types of starting materials were used, a chondritic material (type-1 experiments) and the diogenite-eucrite mixture (type-2 experiments) (Table 1). The reason why the type-2 experiments were done will be discussed later. Both starting materials were prepared from mixtures of oxides and carbonates for ten elements. Total contents of alkalis are about 0.2 wt.%, which is the same as those of the HED meteorites. They do not contain metallic iron and iron sulfides because of difficulty in the experiments. Oxygen fugacities were controlled by H_2/CO_2 gas mixtures and kept constant between the IW and FMQ buffer curves to keep the $Mg/(Mg+Fe^{2+})$ ratios of the charges constant. Fe-saturated Pt wires were used for holding the charges. Temperatures were ranging from 1070 to 1600°C with intervals of about 30°C. Run durations were chosen to achieve equilibration between crystals and melt. Run products were observed under a SEM with back-scattered electron imaging and analyzed with an EDX system.

Type-1 experiments. The following results were obtained by the type-1 experiments using the chondritic starting material.

(1) Melts with the chemical compositions of eucrite or diogenite [8] were not formed at any temperatures.

(2) The compositional trend of the melts by the temperature crossed the tie line of eucrite and diogenite compositions at around 1400°C (Fig. 1 and Table 1).

Type-2 experiments. It is shown from the type-1 experiments that the diogenite-eucrite association was not formed by a single stage fractionation from the chondritic material. In this type-2 experiments, it was assumed that the diogenite-eucrite association was formed by a fractionation of the melt (55 wt.%

diogenite - 45 wt.% eucrite mixture) which was derived from the chondritic material. Then, the experiments were carried out using the 1400°C melt of the type-1 experiment as a starting material. The results are follows.

(1) The chemical composition of the melt at 1180°C is very similar to those of noncumulate eucrites (Fig.1).

(2) The chemical compositions of olivine and pyroxene are similar to those of diogenite.

According to the above results, a two stage fractionation from a chondritic material is possible for the formation of the layered structure of the HED meteorite parent body. If this was the case, the first fractionation must took place at about 1400°C to form the melt with the composition of the diogenite - eucrite mixture. The solid residues (olivine + metallic iron) might be pallasite. The heating at about 1400°C is consistent with the lack of alkali elements in the HED meteorites. The second stage of the fractionation must took place at about 1200°C to form diogenite and eucrite. The two stage fractional crystallization is possible to take place even in a continuous heating-cooling event.

References : [1] Mason, B. (1967) Am. Sci., **55**, 429-55. [2] Takeda, H. (1979) Icarus, **40**, 453-70. [3] Stolper, E. (1977) Geochim. Cosmochim. Acta, **41**, 587-611. [4] Stolper, E., McSween, H. Y. and Hays, J. F. (1979) Geochim. Cosmochim. Acta, **43**, 589-602. [5] Seitz, M. G. and Kushiro, I. (1974) Science, **183**, 954-57. [6] Kushiro, I. and Mysen, B. O. (1979) Mem. Natl. Inst. Polar Res., Spec. Issue, No.15, 165-70. [7] Takahashi, E. (1983) Mem. Natl. Inst. Polar Res., Spec. Issue, No.30, 168-80. [8] Dodd, R. T. (1981) 'Meteorites', Cambridge Univ. Press

Table 1 Chemical compositions of starting materials, partial melts of the experiments, and Stannern noncumulate eucrite

	(1)	(2)	(3)	(4)	(5)	(6)	(7)
Na_2O	0.14	0.0	0.1	0.26	0.5	0.6	0.62
MgO	31.90	18.1	17.4	17.99	8.7	7.3	6.97
Al_2O_3	3.23	6.2	6.8	6.11	10.8	12.5	12.33
SiO_2	45.29	50.6	51.9	51.17	50.7	50.0	49.70
K_2O	0.01	0.0	0.0	0.03	0.1	0.1	0.06
CaO	2.98	5.8	6.1	5.18	9.5	10.4	10.67
TiO_2	0.14	0.3	0.3	0.35	0.6	0.7	0.98
Cr_2O_3	0.70	0.8	0.8	0.96	0.2	0.2	0.34
MnO	0.49	0.6	0.6	0.53	0.5	0.5	0.53
FeO	15.11	17.5	16.1	17.42	18.3	17.7	17.78

(1) Starting material for the type-1 experiments.
(2) Melt at 1410°C in the type-1 experiment.
(3) Melt at 1400°C in the type-1 experiment.
(4) Starting material for the type-2 experiments.
(5) Melt at 1220°C in the type-2 experiment.
(6) Melt at 1180°C in the type-2 experiment.
(7) Stannern, noncumulate eucrite.

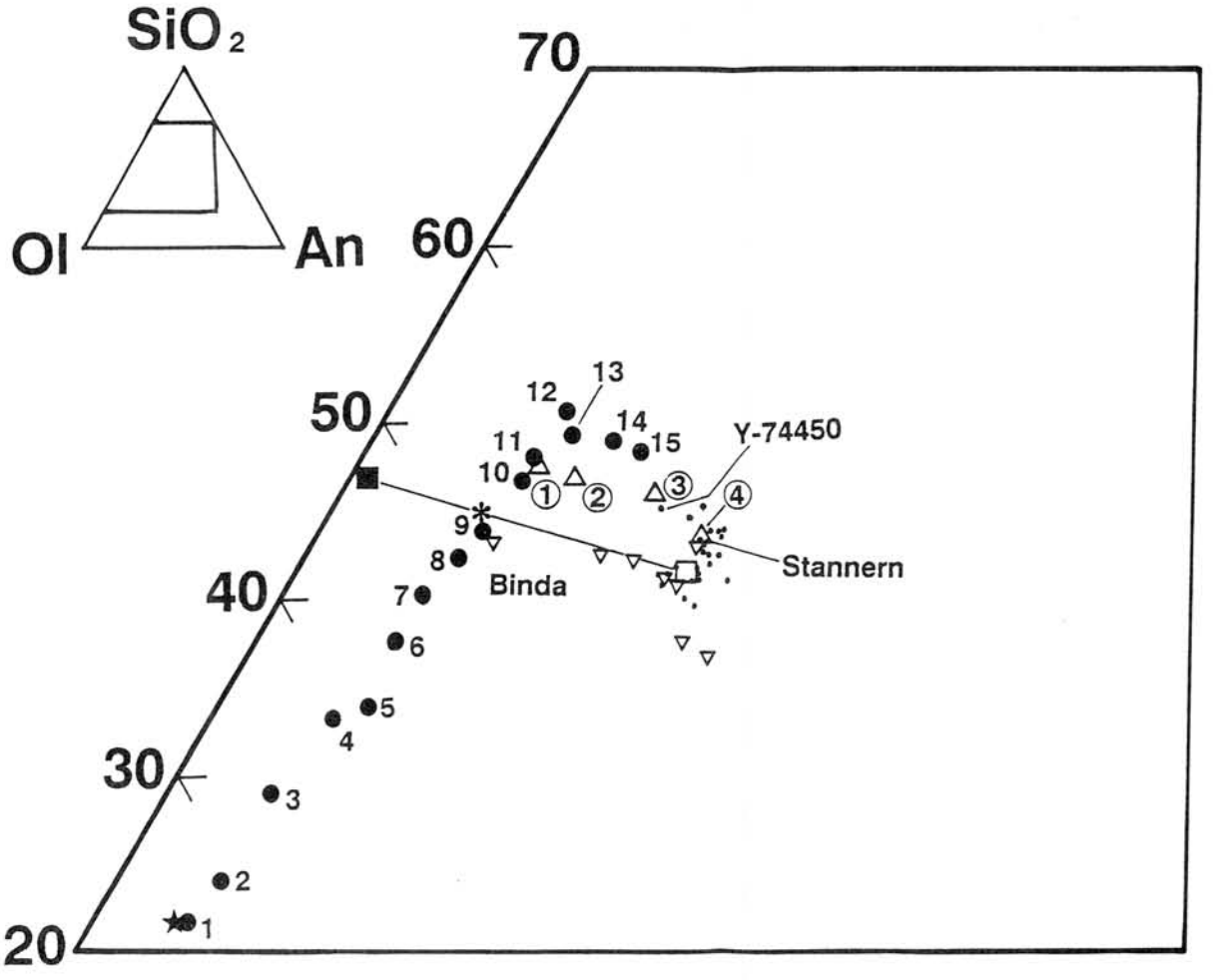

Figure 1. 'Pseudo-liquidus' diagrams for the compositions after [3].

★: Starting material for the type-1 experiments.
●: Melt compositions in the type-1 experiments.
1=1600°C, 2=1570°C, 3=1540°C, 4=1510°C, 5=1490°C
6=1470°C, 7=1450°C, 8=1430°C, 9=1410°C, 10=1400°C
11=1380°C, 12=1350°C, 13=1330°C, 14=1300°C, 15=1280°C
✸: Starting material for the type-2 experiments.
△: Melt compositions in the type-2 experiments.
1=1330°C, 2=1280°C, 3=1220°C, 4=1180°C
■: Diogenite average.
□: Noncumulate eucrite average.
▽: Cumulate eucrites.
•: Noncumulate eucrites.

Experimental studies on rare earth elements partitioning between olivine and silicate melt using chondrite as a starting material, in relation to pallasites

Tsutomu Saito, Hiroshi Shimizu and Akimasa Masuda

Department of Chemistry, The University of Tokyo

Chondrite-normarized REE patterns of olivine in pallasites are convex-downwards, or "V-shaped" (Schmitt et al.,1963; Masuda,1968). These REE patterns differ from the REE partition coefficient patterns commonly observed for olivine-silicate melt systems. In the latter case, the partition coefficient increases with the increase of atomic number of REE (Matsui et al.,1977; McKay,1986) and the coefficients are below unity. But, the "V-shaped" REE partition coefficient pattern is conceived to appear under some conditions.

In order to investigate the condition under which the "V-shaped" REE pattern may appear, we have determined REE partition coefficients between olivine and silicate melt, which were prepared by partial melting of L6 chondrite, ALH-76009, at 1 atom total pressure with low oxygen fugacities controlled by CO-CO_2 gas mixtures. The liquidus of this system is 1450°C. Fig. 1 shows the conditions of temperature and oxygen fugacities, which are set on the analogy of the conditions of formation of eucrites (Stolper,1977). Fig. 2 shows the dependence of the shape of REE partition coefficients on temperature at oxygen fugacity 1 log unit lower than the Fe-FeO boundary. At low temperature of 1320°C, the partition coefficient increases with the increase of atomic number, while at higher temperatures "V-shaped" patterns are observed and the degree of convexity increases with increasing temperature. As shown in Fig. 3, Mg/(Fe+Mg) ratio of olivine produced near liquidus in our experiment is very similar to that of olivine in major part of pallasites. It should be noted that olivine produced at higher temperature, similar in major chemical composition to those in pallasites, has "V-shaped" REE pattern.

In conclusion, our results imply that the majority of pallasites were produced at very high temperature, near the liquidus of source material. REE patterns of olivine with more ferrous component (Fa>14) in pallasite will also be reported.

References:

Buseck,P.R. and Goldstein,J.I. (1969) Geol. Soc. Amer. Bull. 80, 2141-2158.

Masuda,A. (1968) Earth Planet. Sci. Lett. 5, 59-62.

Matsui,Y., Onuma,N., Nagasawa,H., Higuchi,H. and Banno,S. (1977) Bull. Soc. Fr. Mineral. Crystallogr. 100, 315-324.

McKay,G.A. (1986) Geochim. Cosmochim. Acta 50, 69-80.

Schmitt,R.A., Smith,R.H., Lasch,J.E., Mosen,A.W., Olehy,D.A. and Vasilevskis,J. (1963) Geochim. Cosmochim. Acta 27, 577-622.

Stolper,E. (1977) Geochim. Cosmochim. Acta 41, 587-611.

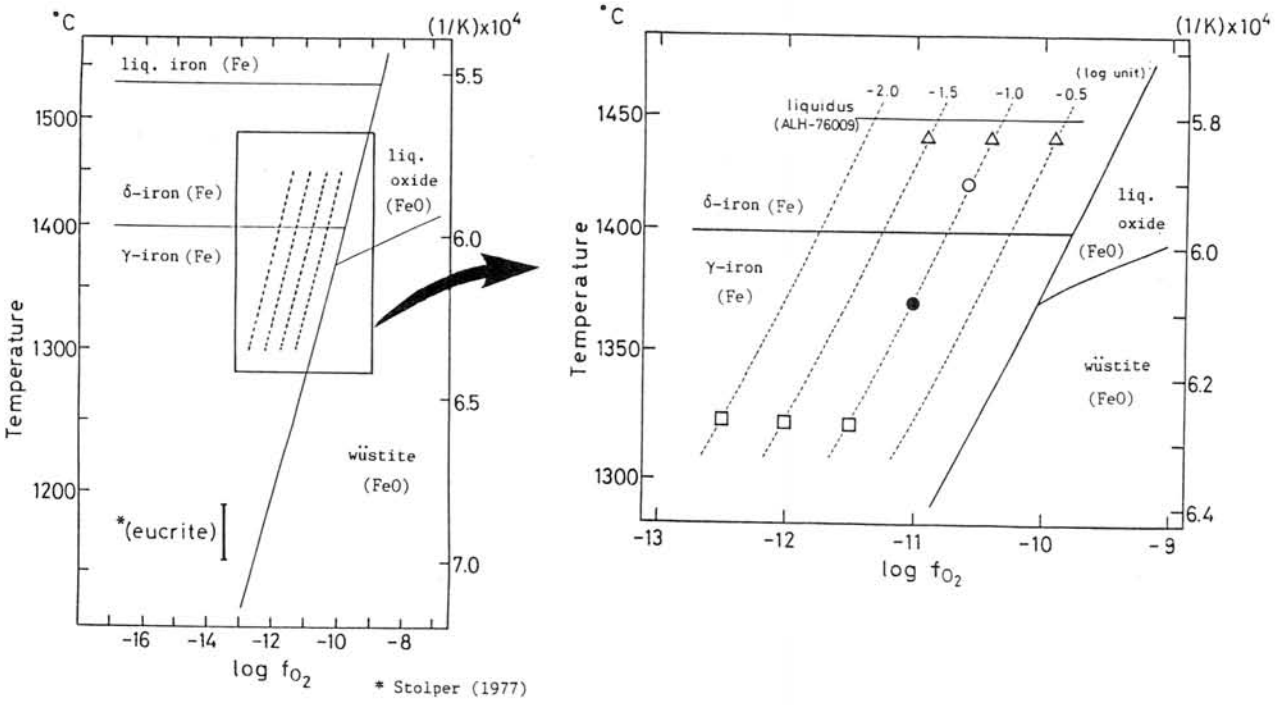

Fig. 1 The experimental conditions of experiments, temperature and oxygen fugacities.

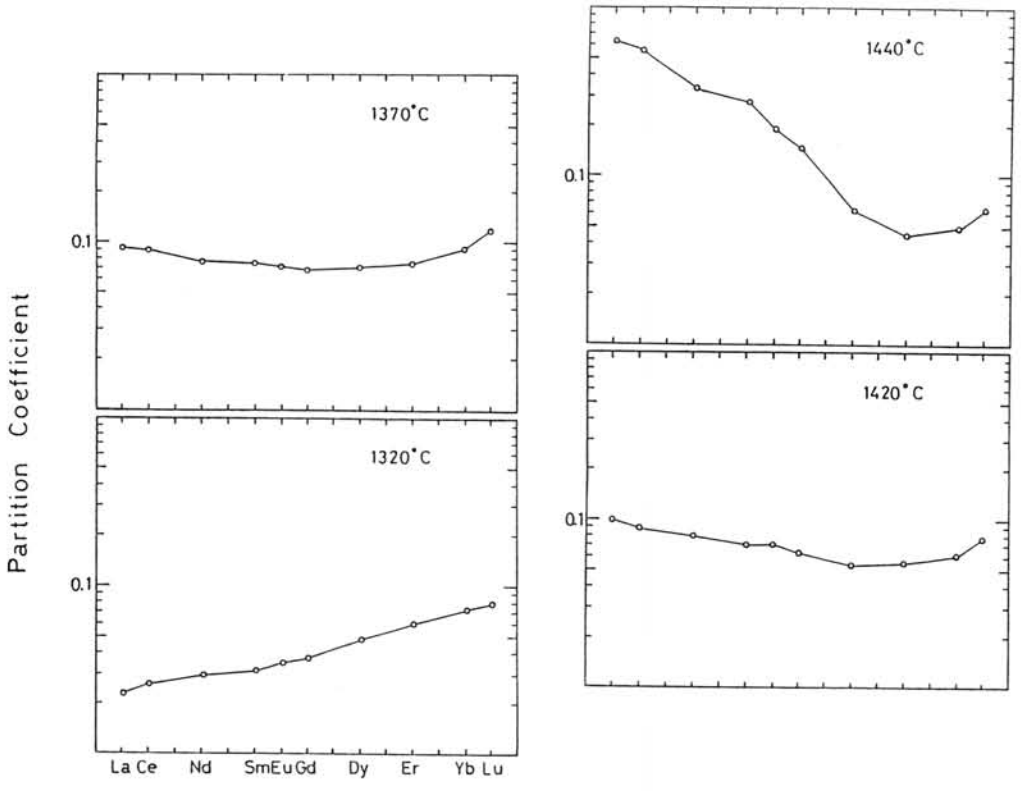

Fig. 2 REE partition coefficient patterns at different temperature.

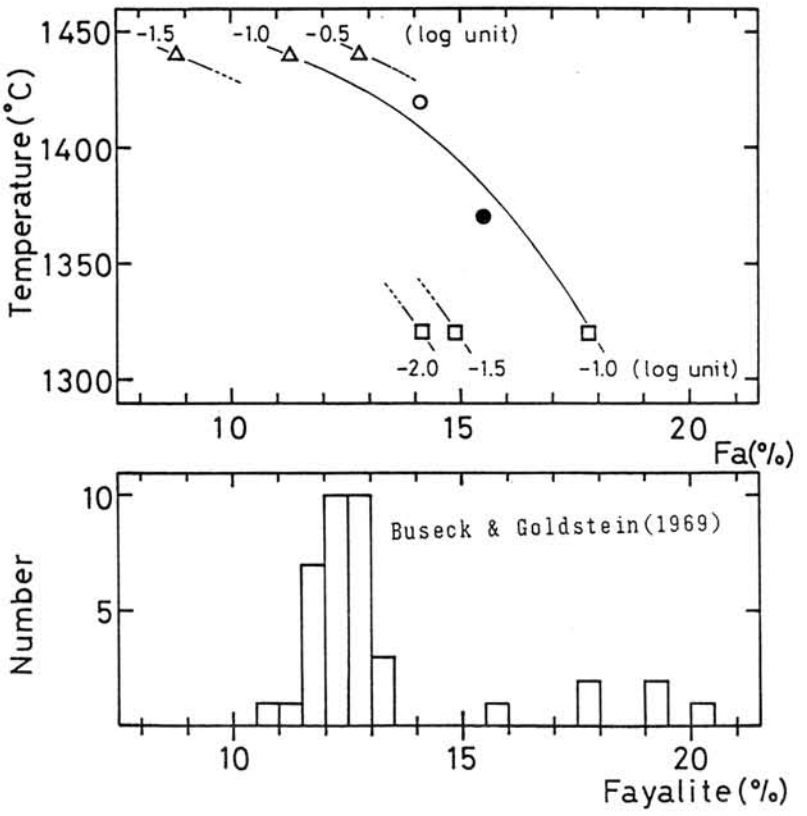

Fig. 3 Mg/(Fe+Mg) ratio (mole percent of fayalite) of olivine produced in this experiments and in pallasites.

VOLATILIZATION STUDIES OF ALKALI METALS ON A CHONDRITIC MATERIAL (PART I)

Shimaoka, T. and Nakamura, N.

Department of Earth Science, Faculty of Science, Kobe University, Nada, Kobe, 657, Japan

Volatilization studies on a chondritic material have been undertaken to investigate the behavior of alkali metals during the formation process of chondrule precursor and/or melting process of chondrule.

The schematic illustration of the volatilization apparatus is shown in Fig. 1. Two kinds of starting materials were prepared using the Etter (L5) meteorite; A (fine: ϕ < 10 μm) and B (coarse: ϕ = 50-90 μm). About 50 mg of the starting material was heated in a Ta crucible at constant heating rate (29°C/min) up to a desired temperature (1100-1450 °C), and was held at the temperature for a certain duration time (0.017-180 minutes) under constant total pressure (7.7×10^{-6} Torr). For most runs the experiments were terminated by turning off the power of furnace. One set of runs was cooled at controlled cooling rate (10 °C/min). The volatilization residues were then analyzed for Na, K and Rb using stable isotope dilution mass spectrometry and atomic absorption (Na only). The petrographic texture of each residues was also examined using the scanning electron microscope with a back-scattered electron (BSE) detector.

Experimental results of Rb for the starting material A are given in Fig. 2. The data points are approximately regressed to a straight line for each set of temperature. This suggests that the volatilization rate of alkali metals were basically controlled by the surface area of the charges and the concentrations of the alkali elements [1]. Fig. 3 shows the relation of the temperature with the apparent volatilization rates (V) estimated from the slopes of the lines. In this figure, it is interesting that V is not a simple function of 1/T but there is an irregularity at ~1300°C for both cases of A and B. From a scanning electron microscopic observation, these irregularities can be understood in terms of abundances of vesicles in the melt. That is to say, the run products at 1200°C have more abundant vesicles and/or the larger effective surface area than those at 1300°C. This can be considered to be caused by the lower degree of melting at the lower temperature. Similar irregularity is also found for Na and K, but the degrees of irregularities were different, which give rise to elemental fractionations among alkali metals.

In Fig. 4 elemental ratios of the Rb/K or Na/K in run products normalized to those in starting material are plotted against the K content in run products. From present results including more runs under various conditions, the following characteristic differences of V between three alkali elements are found:

(1) For kinetically controlled run (at short duration and large cooling rate),

$$V_{Na} > V_K = V_{Rb}$$

(2) For thermodynamically controlled run (at long duration and large cooling rate or at short duration and small cooling rate),

(a) $T > 1300°C$,

$$V_{Na} > V_K > V_{Rb}$$

(b) $T < 1250°C$,

$$V_{Na} > V_{Rb} > V_K$$

The fractionation features of three alkali elements discussed above is clearly different from those obtained from the thermal volatilization studies on lunar basalts [2,3] and those expected from the thermodynamic data for individual alkali oxides [4]. However, for example, the unfractionated features of Rb/K ratio found in Allende chondrules [5] could be understood by considering that alkalis in alkali-rich precursors of chondrules were derived from the materials formed by kinetically controlled thermal processes. These peculiar fractionations of alkali metals are considered to be important to understand alkali-fractionations observed in chondrules as well as other planetary materials.

Reference: [1] Tsuchiyama, A., Nagahara, H. & Kushiro, I., (1981), Geochim. Cosmochim. Acta, 45, 1357-1367. [2] Gibson, E. K. Jr. & Hubbard N. J., (1972), Proc. Lunar Sci. Conf. 3rd., 2003-2014. [3] Gibson, E. K. Jr., Hubbard, N. J., Wiesmann, H., Bansal, B. M. & Moore, G. W., (1973), Proc. Lunar Sci. Conf. 4th., 1263-1273. [4] Brewer, L., (1953), Chem. Rev. 52, 1-75. [5] Misawa, K. and Nakamura, N. (1988), Geochim. Cosmochim. Acta, in the press.

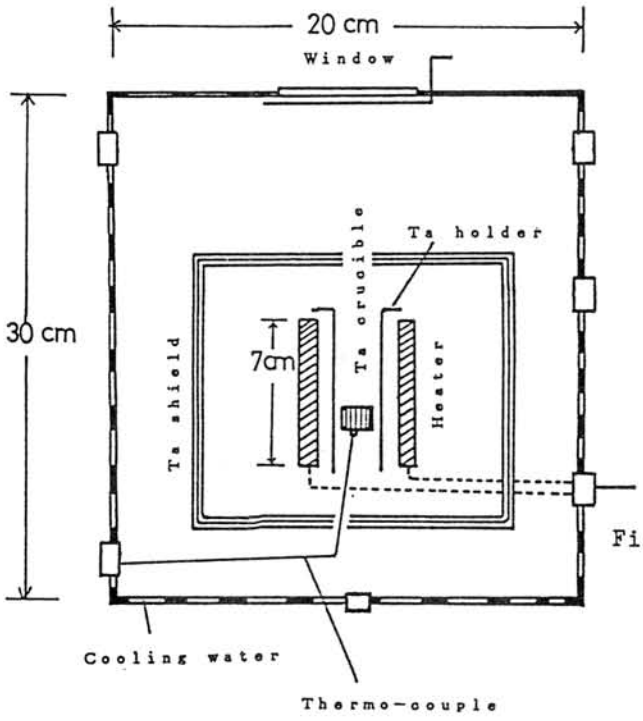

Fig. 1 The schematic illustration of the volatilization apparatus

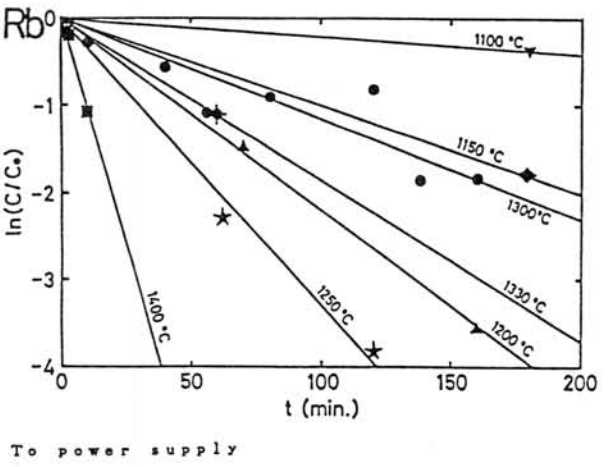

Fig. 2 The plot of the residual fraction of Rb in run products vs. run duration (t)

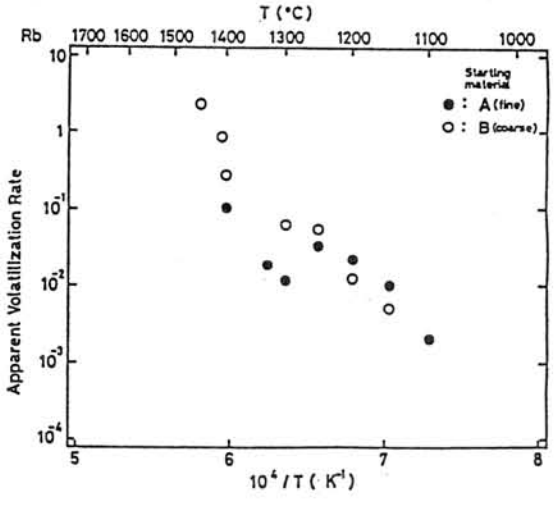

Fig. 3 The relation of the heating temperature with the apparent volatilization rate

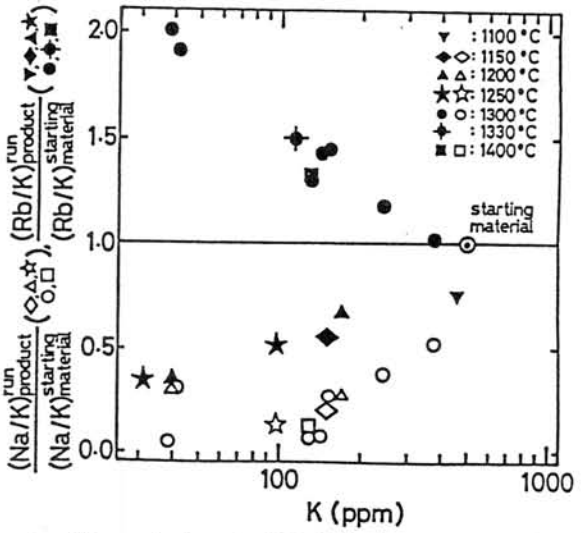

Fig. 4 The plot of (Rb/K) (normalized to starting material) vs. K content

VOLATILIZATION STUDIES OF ALKALI METALS ON A CHONDRITIC MATERIAL (PART II): CHEMICAL COMPOSITIONS OF RESIDUAL MELTS.

Noboru NAKAMURA and Taro SHIMAOKA

Department of Earth Sciences, Faculty of Science, Kobe University, Nada, Kobe 657, Japan

In our companion paper (1), we reported analytical results of alkali metals for vaporization residues of the ETTER (L5) chondrite. As shown in Fig. 1, the apparent vaporization rate of alkali metals is approximately a function of the heating temperature and the specific surface area of melt but exhibits an irregularity at 1300 C. Particularly, a marked fractionation trend of Rb to K observed for the heated sample (A) suggests that chemical parameters were one of the important factors which control the vaporization of alkali metals. In this work, we have examined chemical compositions of heated samples (1), specifically glass materials representing partial melts (1), using SEM-EDX.

As shown in Table 1, starting materials (metal-removed ETTER powder) (1) contains plagioclase (An13) as a carrier of alkali metals, olivine (Fo77), orthopyroxene (En78), clinopyroxene (En47Wo45Fs8), troilite and other minor minerals. The solidus and liqidus temperatures of plagioclase are estimated to be 1225 and 1285°C (dry condition), respectively. The glass materials of sample A heated at 1200°C are significantly higher in Al and Ca but lower in Fe than those of sample A and B heated at 1300°C. In addition, compositions of

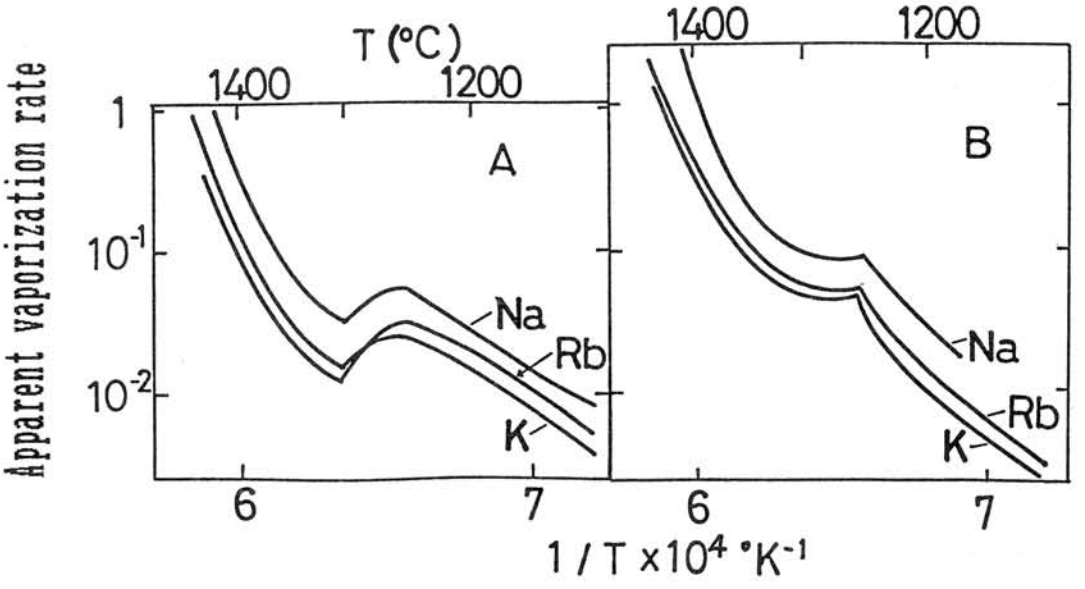

Fig. 1. Schematic illustration of apparent vaporization rate vs heating temperature. (A, <10 um; B, =50-90 um.)

non-volatile elements of glasses from starting material A at 1300°C (heating time: 40, 60, 80, 120, 140 and 160 minutes) were also found to be quite similar each other. Therefore, it is likely that the melting and vaporization of alkalies were prevailing under an equilibrium chemical condition.

In view of chemical compositions as well as SEM observations, following melting and vaporization processes are considered; The heated sample have degassed H_2O + C below 900°C (2) but reached to the heating temperatures without further loss of volatiles such as alkalis. The samples heated below 1300°C have started incongruent melting and de-sulfurization within a few minutes. Fine-powder sample (A) might have lost iron together with sulfur during desulfurization. For the temperature range of 1200-1300°C, a large degree of partial melting of plagioclase and minor olivine and pyroxene have occured during heating, and volatilization of alkali metals was accelerated by vesiculation of melt but the complete melting of plagioclase above 1285°C now made difficult to retain vugs within the heated samples and even for desulfurization, and then the apparent vaporization rate temporarily dropped down. The partial melts were quenched by turning off the power but a minor amount of melt have crystallized as overgrowth olivine and pyroxene. Vaporization mass loss were 2-3% at 1100-1300°C or larger than 5% at higher temperature.

In any case, for major chemical data (Table 1), any chemical factors which might be specifically related to differential vaporization loss of Rb to K at 1300°C does not seem to be pointed out.

Table 1. Chemical compositions of the starting material and glasses of heated samples.

	Starting material			Glass of run product		
	Bulk#	Plagioclase		A,1200C	A,1300C	B,1300C
		Ca-rich	Ca-poor	70-160m	40-160m	20-40m
SiO_2(%)	42.1	66.2	68.4	51.8	52.2	53.0
Al_2O_3(%)	2.4	21.0	21.0	15.7	12.2	13.5
CaO(%)	2.0	2.44	0.22	11.9	10.7	10.0
MgO(%)	26.5	0.1	0.0	4.2	3.8	3.8
FeO(%)	16.5	0.3	0.4	15.1	18.7	17.8
TiO_2(%)	0.13	0.0	0.0	0.5	0.5	0.6
MnO(%)	0.32	0.0	0.0	0.4	0.4	0.4
Cr_2O_3(%)	0.58	0.0	0.1	0.3	0.5	0.1
Na_2O(%)	0.86	9.7	5.8			
K_2O(%)	0.07	0.2	3.9	# recalculated for		
FeS(%)	6.1			silicate + FeS (ref. 8)		
$\pm H_2O$ + C(%)	1.1					

Since run products at 1300°C contain much abundant troilite grains compared with run products (A) of 1200°C or run products (B) of 1300°C within glassy matrix, dissolution of sulfur by decomposition of FeS into melt was considered. We then analyzed sulfur in glass materials by SEM-EDX using glass standards which had been calibrated for sulfur contents (110, 535, 890, 1510 ppm) (4). Preliminary results are shown in Fig. 2. It is interesting that only the run products (A) at 1300C have extremely high sulfur concentrations (2000-3000 ppm), indicating that the melts (A) at 1300°C were oversaturated with sulfur (5). Under reducing condition, alkali metal sulfides have a great stability with increasing order of NaS < RbS < KS for a silicate melt (6,7). Thus, as one of possibilities it is considered that the Rb/K fractionation at 1300°C mentioned above was due to high concentration of sulfur in melts. However, as shown in Fig. 1, the relative vaporization rate of Rb and K above 1250°C is not expected one. Hence, thermochemical data given in literatures may not be directly applicable to the present results and/or some other chemical factors should be invoked to interprete the observed Rb/K fractionation.

Refernces:
(1) Shimaoka, T. & Nakamura, N. (1988) This volume (2) Hashimoto, A. et al. (1979) EPSL 43, 13-21. (3) Gooding, J.L. & Muenow D.W. (1977) Meteoritics, 12, 401-408 (4) Ueda, A. & Sakai, H. (unpublished) (5) Katsura, T. & Nagashima S. (1974) GCA 38, 517-531 (6) Lewis, J.S (1971) EPSL 11, 130-134. (7) Hall, H., T. & Murthy, V.R.(1971) EPSL 11, 239-244. (8) Rubin A.E. (1983) Meteoritics 18, 179-196.

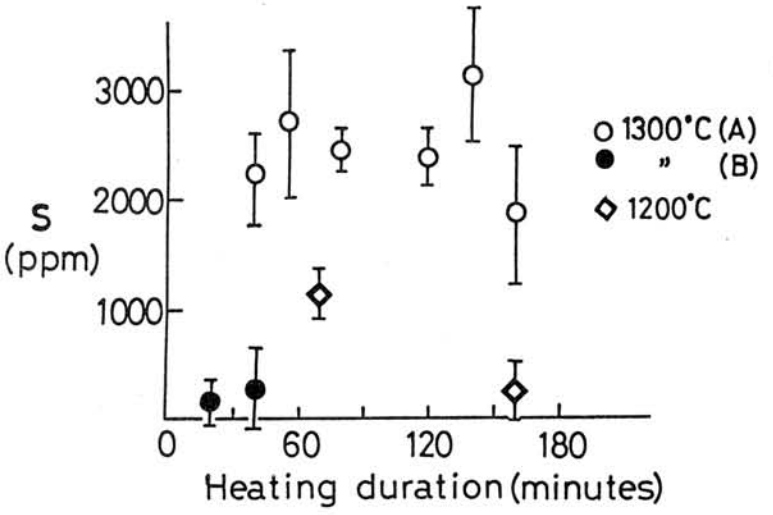

Fig. 2.
Sulfur contents in glasses of heated samples.

VAPORIZATION AND CONDENSATION EXPERIMENTS IN THE SYSTEM PLAGIOCLASE - HYDROGEN

Hiroko Nagahara and Ikuo Kushiro: Geol. Inst., Univ. Tokyo, Hongo, Tokyo 113, Japan

Vaporization and condensation experiments of olivine in hydrogen gas under highly vacuum conditions revealed that olivine vaporized "congruently"; i.e. both residue and gas had olivine compositions, strictly speaking, however, it is incongruent because Mg/(Mg+Fe) ratios of residue and gas were different; various phases including forsterite, enstatite, a silica mineral(s) , ferrous olivine, ferrous pyroxene, and metallic iron, condensed at different temperatures from the same gas of olivine composition [1]. In order to investigate whether or not plagioclase solid solution system has the similar relationship to olivine, vaporization and condensation experiments of plagioclase were carried out in hydrogen gas at low pressures.

Plagioclase (An_{79} with 0.4 wt% FeO and 0.1 % MgO; PL1 hereafter) and albite (almost pure; AB, hereafter) were used as starting materials. Vacuum furnace was newly constructed; its essential design is similar to that of Geophysical Lobaratory of Carnegie Institution [2]. Pressure was controlled by bleeding hydrogen gas and temperature was automatically controlled. Starting materials were put in a graphite capsule which was sustained by Mo wire; all of them are set in the furnace. Total pressure varied from about 10^{-6} to 10^{-1} torr (in the former case, no hydrogen was supplied), temperature from 1350 ^{o} to 1080 ^{o}C, and duration from 10 to 48 hrs.

The results show that vaporization kinetics of plagioclase solid solution system is quite different from that of olivine solid solution system. At 1350 ^{o}C, PL1 melted to form Al_2O_3 and anorthite on the surface of the residue and the inside contains two phases with non-plagioclase compositions. At 1300 ^{o}C, PL1 vaporized incongruently; Na (and K and Fe) preferentially vaporized to form Ca-enriched residues. The Na-depleted portion does not keep a stoichiometry of plagioclase, thus amorphous, though it has not yet been determined by TEM or X-ray method. Na_2O content decreases gradually from the center of the grain to the surface, CaO contents vice versa, and SiO_2 content is almost uniform. Preferential Na O vaporization and CaO enrichment took place at all pressures studied (10^{-1} to 10^{-4} torr with hydrogen gas and 10^{-6} torr without hydrogen). Width of Na O depleted zone decreases with decreasing total pressure, about 200um at 10^{-1} torr and 50um at 10^{-6} torr after similar experimental durations. On the other hand, Al_2O_3 behavior varied depending on total pressure; it enriched with CaO in the Na_2O depleted portion at higher pressures but did not show any change at lower pressures. At 1200 C, PL1 appears to show no change after 48 hrs. In the experiments with AB, Na_2O vaporized to form Al and Si-rich residues regardless of total pressure.

Plagioclase solid solution shows different behavior from olivine solid solution during vaporization, which may be due to difference of structure; i.e. plagioclase has a structure closer to liquid than that olivine has. In plagioclase, each element behaves differently depending on its volatility; on the contrary, elements form components (M_2SiO_4, M:Mg,Fe) in the vaporization of olivine. The present results suggest that chondritic materials which are essentially mixtures of olivine, pyroxene and plagioclase, would have Mg, Ca, and Si-rich and volatile and Fe-poor compositions after partial vaporization in the nebula. Al content of the residue varies depending on total pressure of the nebular gas.

[1] Nature, 331,516 (1988) [2] EPSL, 75,139 (1985)

An Experimental Study on Heating-Melting of Zhaodong Chondrite

Hou Wei, Wang Daode, Xie Hongsen, Wang Mingzai

Institute of Geochemistry, Academia Sinica, Guiyang, China

This work was carried out stage by stage. In first stage, eleven heating experiments of Zhaodong chondrite(L_4) were done at 30 kbar and various temperature from 840°C to 1800°C,taking this chondrite's fragments as starting material and filling interval and around fragments with it's powder in order to know change of texture of chondrite and temperature reaching melt. The order of experiments is from Z-101 to Z-111. In the second stage, powder sample of Zhaodong chondrite(C-1) was melted under 30 kbar and 2050°C in 40 minutes. A YJ-3000 ton press fitted with a wedge-type cubic anvil was employed for all experiments. The sample was suddenly cooled by cutting off the heating electric supply. The method of calibration of pressure and temperature of sample chamber are omitted here[1].

In product of Z-101(840°C), recrystallization of glassy (mainly in chondrule) occurs, metal and troilite begin to melt and form micro-eutectic texture. In Z-109(1610°C),the eutectic texture begins disappearing and small metal sphere is often in troilite sphere. Probe analyses show metal contains some S, but Ni and Co content of troilite is more than that of starting material. The silicate of Z-109 occurs melting and skeletons of olivine and Ca-poor pyroxene crystallize from melt,but lumps of Si,Al-rich melt do not separate from original melt until C-1 (2050°C). In the product of C-1, the metal and troilite occur strong element-exchange and form a type of mixture of polyphase with different proportion of Fe,Ni,Co,S(table 1). The silicate phase of sample has completly melted and product may be divided into two parts: 1) Yellow-brown transparent glass is visible to the naked eye. Probe analyses show this glass is Si,Al-rich and its chemical composition is: SiO_2 60.64, TiO_2 1.85, Al_2O_3 28.64, Cr_2O_3 0.20, FeO 3.84, MnO 0.04, MgO 3.24, CaO 0.57, Na_2O 0.59, K_2O 0.38. 2) Skeletons of olivine and Ca-poor pyroxene and the matrix intergranular of minerals. This matrix is dark

and heterogeneous in chemical composition in probe analyses.

Above experimental result shows that in process of Zhaodong chondrite heated,at first metal and troilite separate from silicate and form a aggregate with eutectic texture. Up to 1610°C the eutectic texture disappears and little element-exchange occurs in the two phases. At the same time,silicate phase begins to melt and only one original melt forms. Temperature going up 2050°C,metal and troilite form a heterogeneous mixed-melt, and a type of Si,Al-rich melt separates from the original silicate melt.

It is well known that experience no melt-fractionation chondrite preserve the feature on composition and structure of primitive terrestrial planet. However,this heating-melting experiment furnishes some evidences for formation and evolution history of stratified structure of terrestrial planet. Based on this experiment, it is inferred that when primitive planet heated, metal and sulphide gradually sinked into the center of planet after separated from silicate, temperature and pressure gradually went up,and their element-exchange was gradually stronge, lastly the core formed. Because the temperature and pressure of core of all these planet are more than 2000°C and 30kbar respectively,these cores are composed of mixed-melt of metal and sulphide. The immiscibility of two types of silicate melt phase in this experiment shows that some Si,Al-rich melt could derive from melting original mantle,then aggregated,floated and covered the surface of planet.Lastly the original crust formed. Therefore, the formation of original crust of terrestrial planet may be attributed to melt-fractionation of the original mantle.

Table 1. Electron Probe Analyses of Metal and Sulphide in C-1

No.	Fe	Ni	Co	S	Total
1	83.68	10.40	0.04	1.83	96.31
2	72.29	22.26	0.42	0.62	95.59
3	60.17	2.75	0.08	29.66	92.66
4	59.07	32.75	0.37	3.76	95.95
5	56.14	1.95	0.10	42.53	100.72

Note: No.1,2,3 and No.4,5 are in two metal-sulphide sphere respectively.

Reference:
(1) Hou Wei et al., Geochemica,1985,No.4,337-343(CHN).

A PRELIMINARY REPORT ON THE NITROGEN ISOTOPE MEASUREMENTS USING A QUADRUPOLE MASS SPECTROMETER

Sugiura, N. and Hashizume, K.
Geophysical Institute, Tokyo University, Tokyo, Japan

A new static system for nitrogen isotope measurements was constructed based on the system described by Frick and Pepin (1981). The mass spectrometer in our system is a quadrupole mass spectrometer (QMS240) whose mass resolution is low but is able to scan quickly over a wide mass range. Nitrogen in a sample is converted to nitrogen molecules by combustion, and the isotopic ratio is determined by measuring m/e=29 and =28. Because of the low mass resolution of the QMS, contributions of CO and C_2H_4 to m/e=28 and those of 13CO, C_2H_5 and N_2H to m/e=29 have to be subtracted. The interferences due to hydrocarbons can be roughly estimated from the measurements of hydrocarbons at m/e=26 and 30. The contribution of CO to m/e=28 is more difficult to estimate, but as far as the amount of CO_2 is small, its contribution may be neglected. The contribution of N_2H is estimated from the correlation of m/e=29 and m/e=2 and concluded to be negligible.

A couple of examples of the 29/28 ratio of the air measured with our system are shown in Fig.1. Due to the interference of hydrocarbons, the apparent 29/28 ratio increases with time, especially when the sample size is small. But if the correction for the hydrocarbon is made, the ratio is approximately 0.00704. Since the expected value of 29/28 for the air is 0.00732, the discrimination of our system is about 4%. The standard deviation of the 29/28 ratio is less than 0.5% at a sample size of 2 ng of nitrogen.

Since the nitrogen isotope anomalies observed in meteorites are as large as several tens of percent, and since the concentration of nitrogen in meteorites is larger than 10 ppm (Kung and Clayton, 1978), our system is quite capable of detecting isotope anomalies of nitrogen in meteorites. We will report some results of actual measurements of nitrogen isotopes in meteorites at the meeting.

U.Frick and R.O.Pepin, Earth Planet. Sci. Lett. 56(1981)64-81.
C-.C. Kung and R.N.Clayton, Earth Planet. Sci. Lett. 38(1978) 421-435.

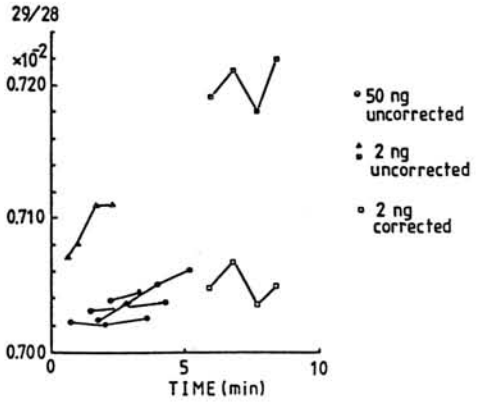

NOBLE GAS DEGASSING FROM METEORITES INFERRED FROM ^{40}Ar-^{39}Ar ANALYTICAL DATA

Kaneoka, I.
Earthquake Research Institute, University of Tokyo, Bunkyo-ku, Tokyo 113.

Meteorites contain noble gases in different amounts, reflecting their trapped conditions and secondary degassing histories. To estimate the composition of trapped noble gases, it is also significant to evaluate the effect of degassing from meteorites. By applying the ^{40}Ar-^{39}Ar analytical data, it is possible to evaluate the rate of degassing of noble gases.

Based on the ^{40}Ar-^{39}Ar analytical data, we can get information on the time of a shock event for a meteorite. By analysing the release patterns of Ar from a meteorite, we can identify the degassing properties of Ar from the meteorite whether it was an event of relatively short period such as a shock event or not(1). Assuming that a meteorite was formed about 4.5 b.y. ago and degassing from the meteorite occurred only by an event of a short period, we can estimate the degassing rate of radiogenic ^{40}Ar at that time. It will also be conjectured that the trapped ^{36}Ar in a meteorite would have been degassed during the event. The amounts of trapped ^{36}Ar in meteorites which show signs of degassing due to shock events seem to correlate with the retention rate of radiogenic ^{40}Ar. Further, meteorites with lower degrees of metamorphic properties (type 3 or 4) generally show no sign of serious shock events. Thus, we can roughly estimate the originally trapped amount of ^{36}Ar in meteorites based on the degree of ^{40}Ar retention rate.

The amounts of trapped ^{36}Ar also seem to correlate with those of heavier noble gases. Hence, we have a possibility to estimate the original amounts of trapped noble gases in a good condition even if they were partially lost. If the degassing occurred in a more complicated way, however, we cannot apply the procedure described above directly.

Reference

(1) Kaneoka, I. (1984) Characterization of Ar-degassing from Antarctic meteorites.
Mem. Natl Inst. Polar Res., Spec. Issue, No.35, 272-284.

Penetration of solar energetic particles into the planetary region after dissipation of the solar nebula

Sho SASAKI

Geophysical Institute, Faculty of Science, University of Tokyo, Tokyo 113, JAPAN

Some meteorites contain large amounts of noble gases with solar-type elemental and isotopic patterns and these gases are considered to have come from implantation of solar wind during meteorites formation. Venus has ^{36}Ar 100 times as much as the Earth and Wetherill (1981) considered that the large amount of Ar also could be explained by implantation of solar wind into collisionally-ejected fine particles around Venus.

When the primordial solar nebula exists, the solar wind cannot intrude into the planetary region, and fine dust particles once should have escaped in accordance with escape of the solar nebula. But in the later stage after the escape of nebular gas, dust grains are formed through mutual collision of planetesimals. Producing smaller and smaller grains by collision between dusts, they would form a dust disk whose thickness is determined by the average inclination of orbit of planetesimals. In order to clarify whether the implantation can serve as noble gas sources, we investigate the penetration of solar energetic particles into disk-like dust cloud around the sun. We estimate the absorption of energetic particles by dust grains assuming dust size, abundance and distribution in a simple manner. Dust particles absorb the solar wind in a similar way to absorb light. The flux intensity I is governed by the relation $dI/dx = - I/\ell$. The absorption length (i.e. mean free path) of energetic particles, ℓ, is $4d\bar{\rho}/3\rho_d$, where d is dust size, $\bar{\rho}$ is mean dust density and set to be 2000 (kg/m^3) and ρ_d is spatial mass density of dusts and expressed as a function of radial distance from the sun a and height from the disk midplane z. We assume

$$\rho_d(a, z) = 5.85\ 10^{-9}\ f\ \left(\frac{a}{1AU}\right)^{-q} \exp\left\{ - \left(\frac{z}{h}\right)^2 \right\}$$

where f is relative dust abundance to that before planetesimal formation. The penetration of the solar wind are determined by f/d and q. Another parameter is the inner boundary of the dust

cloud. Since dust evaporation due to solar radiation flux should determine the position, we have $0.05 \sim 0.1$ (AU).

Figure 1 shows that when f/d 1 (m^{-1}) the solar wind is strongly absorbed at the inner boundary and the energetic particles cannot penetrate into the equatorial region of Venetian or terrestrial zone. But the wind can penetrate into the region far from the equatorial plane, and even when f/d 1 some fraction of solar gas should be trapped. As for the explanation of ^{36}Ar of Venus, we estimate amounts of trapped solar ^{36}Ar between $0.65 \sim 0.75$ (AU) and the results are shown in Fig. 2. We assume that the solar wind flux is 100 times as large as the present one and that irradiation duration is 10^6 (yr). So long as f/d 0.1, sufficient amount of ^{36}Ar is provided. But by this mechanism, the ratio of trapped ^{36}Ar of the Earth to that of Venus becomes about 0.4, which could not satisfy the present ratio ~ 0.01.

Ref. Wetherill, G. W. (1981). Icarus, 46, 70-80.

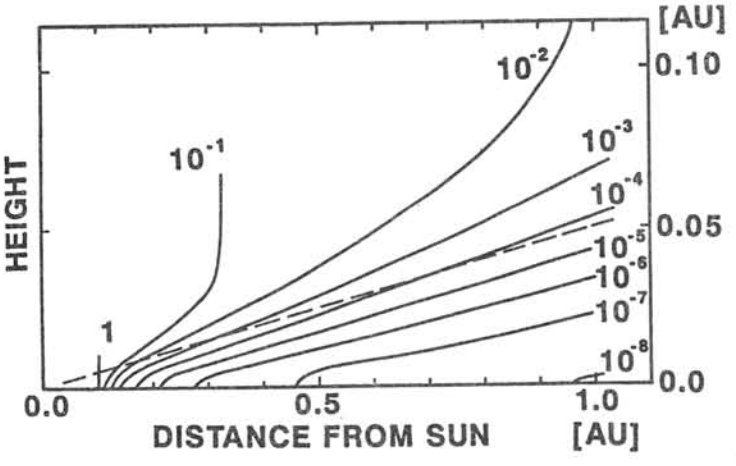

Fig. 1 Decrease in the wind flux in a dusty cloud. The dust-existing boundary is put to be 0.1 (AU). We assume f/d = 1, q = 2.75 and h = 0.05a. Values are normalized to fluxes at 0.1 (AU). The dashed line denotes h = 0.05a where mass density of dust is 1/e of that at the midplane. Far from midplane, the flux decreases in inverse proportion to r^2.

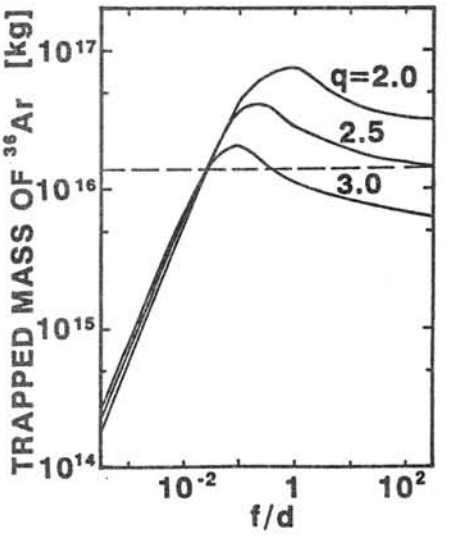

Fig. 2 Mass of trapped ^{36}Ar between $0.65 \sim 0.75$ (AU) for various f/d and q. Solar wind flux is 100 times larger than the present one and duration of flux is 10^7 (yr). Dashed line shows the present amount in Venus.

NOBLE GASES IN SHOCK-PRODUCED DIAMONDS

Matsuda, J.[1] and Nagao, K.[2]

1.Department of Earth Sciences, Faculty of Science, Kobe University, Nada, Kobe 657.
2.Institute for Study of the Earth's Interior, Okayama University, Misasa 682-02.

The amounts of noble gases have been determined in synthetic diamonds: those by shock transformation of graphite and those synthesized under static pressure. The shock-produced diamonds (NOF diamonds) and the raw material graphite were provided with the courtesy of Mr. Araki by Nippon Oil & Fats Co., Ltd. The NOF diamonds were black powder of grain size 2-4 μm. Other shock-produced diamonds (DP diamonds) were from Du Pont. These diamonds were also black powder of grain size 12-22 μm. The synthetic conditions of DP diamonds and their raw material were not known. The diamond produced under static high pressure was provided with the courtesy of Mr. Yazu by Sumitomo Electric Industries, Ltd. This diamond is a single crystal and synthesized in a molten metal bath (1).

The amounts of noble gases in the NOF diamonds were higher than those in the starting material graphite by about one to two orders of magnitudes, suggesting that noble gases in the ambient atmosphere had been emplaced in the shock-produced diamonds. These noble gases were mainly released at 1700-2000°C. The high temperature release of noble gases indicates that noble gases were tightly trapped inside the diamond structure or in void that were completely sealed by the diamonds and were released only at the graphitization. The release pattern of noble gases in DP diamonds is similar to that for NOF diamonds, but the release fractions of light noble gases in the latter are larger than those in the former. It seems likely that small grains of NOF diamonds release gases at comparatively low temperatures. The elemental abundance ratios of noble gases were similar to those in air, suggesting that there was no mass fractionation at the emplacement of noble gases during the phase transition. The diamond produced under hydrostatic pressure had much smaller noble gases than those in the shock produced diamonds.

The distribution coefficient for Ar, defined as the Ar content normalizing to 1 atm ambient Ar pressure, of the NOF diamonds is lower than that of CVD diamonds (2) by one order of magnitude. However, we did not know the temperature and pressure dependence on the trapping efficiency of noble gases into the shock-produced diamonds, yet. It is interesting to note that the distribution coefficient of Ar for the laboratory-produced carbon condensate (3) is similar to that for the shock-produced diamonds. The physical adsorption, known as being able to trap large amounts of noble gases, is the trapping mechanism of noble gases for the carbon condensate, which is quite different from that for the shock-produced diamonds because noble gases are loosely bound and elementally strongly fractionated in the adsorption. The distribution coefficients of shock-implanted Ar

in silicate were 10^{-3} to 10^{-1} $cm^3STPg^{-1}atm^{-1}$ for shock pressure between 2 and 40 GPa (4). The highest of these values is of the same range as the value obtained for the shock-produced diamonds. The implanted noble gases in silicate are released below 1200°C and shows two or more trapping sites, which is different from our results for shock-produced diamonds.

References: (1)Wentorf, R.H.Jr. (1971) J. Phys. Chem., 75, 1833. (2)Fukunaga, K., Matsuda, J., Nagao, K., Miyamoto, M. and Ito, K. (1987) Nature, 328, 141. (3)Niemeyer, S. and Marti, K. (1981) Proc. Lunar Planet. Sci., 12B, 1177. (4)Bogard, D.D., Hörz, F. and Johnson, P.H. (1986) Proc. Lunar Planet. Sci. Conf. 17th: J. Geophys. Res., 91, E99.

SOME COSMOGENIC NUCLIDES IN CHONDRITES AND IRON METEORITES

H. Nagai, M. Honda, M. Imamura[1], K. Kobayashi[2], K. Yoshida[3], Y. Miyaki and Y. Chonan
Department of Chem.,Nihon U.,Setagaya,Tokyo 156
1.Inst. for Nuclear Study, U.Tokyo, Tanashi,Tokyo 188.
2.Res.Center for Nucl.Sci. & Technol.,U.Tokyo,Bunkyo-ku, Tokyo 113
3.Dept. of Chem.,U.Tokyo,Bunkyo-ku Tokyo 113

Last year, we presented results of determinations of ^{10}Be and ^{26}Al in metallic irons and stones by the AMS method (Nagai et al,1987 and Honda et al,1987). Based on the relation between $^{26}Al/^{10}Be$ in metals and $^{26}Al/^{53}Mn$ or the shielding index, k_2', the $\Delta A'$ value for 10Be produced in metal was estimated at 22. this figure is close to the $\Delta A'$ of ^{38}Ar in metals. Here k_2' and $\Delta A'$ are defined in a general formula

$$\text{Production rate} = f * k_1' * (\Delta A')^{-k_2'}$$

where f is a normalizing factor for the product of $\Delta A'(A,Z)$ and $\Delta A'$ is A(target)-A(product)+4, the empirically corrected delta A value. The k_1' indicates a general production level and k_2' corresponds to a common shielding index (Honda,1988).

In this report, we show that saturation activities of ^{10}Be in stone phases of chondrites also can be expressed in terms of $\Delta A'$ and f for ^{10}Be. A compilation of ^{10}Be data is shown in Table 1, which also includes our older AMS data since 1983. We also show that ^{10}Be production in metal phases can be compared with that of ^{53}Mn and related to shielding indexes obtained from stable products.

Based on $\Delta A'=7$ for ^{53}Mn, ^{10}Be in chondrites can be expressed employing $\Delta A'(^{10}Be)=12$ in a range of $k_2'=1.8$-2.3 (Fig. 1). In this process, several examples of multi-exposure histories of chondrites are detected, for example, with Y74028,Y74116,Y74118 and Y74165, all similar to the case of Y7301. Figure 1 also shows that the ratios of ^{10}Be and ^{53}Mn in the metal phases of chondrites, as well as in iron- and stony iron- meteorites, can be directly related to the common shielding indexes, and the $\Delta A'$ for ^{10}Be in metal can be estimated at 22, the same figure as in our previous report (Nagai et al,1987).

It is known that many antarctic meteorites have relatively low ^{26}Al content: as low as half the common levels. This cannot be directly correlated to their long terrestrial ages. However, in many cases it reflects their lower shielding because of smaller size or their multi-stage exposure histories. These issues can be resolved by an examination of ^{53}Mn and ^{36}Cl in metals and ^{10}Be and ^{26}Al in stones and metals. This situation may be attributed to relatively higher recoveries of smaller-sized objects in antarctic areas.

(References)
Honda et al, Meteoritics,18,315-6(1983); Honda et al, abstract of this symposium, June 1987; Nagai et al, Meteoritics,22,467-469(1987); Honda, Meteoritics 23,Mar.(1988).

Table 1 ^{10}Be determinations in chondrites and meteoritic irons

Name	Class	ID	^{10}Be found (dpm/kg) Chondrite	^{10}Be found (dpm/kg) Metal	Prod.R. ^{53}Mn*	Shield k'_2	^{21}Ne (10^{-8} cc/g)
CHONDRITE							
Y74028	L6		6.7±0.7		60		
Y74117	L6		15.0±2.0		240		
Y74455	L6		17.5±1.1	5.94±0.27	300	1.90	5.6
Y74663	L6		17.2±1.1 17.0±1.1	5.55±0.29	280	1.79	3.1
Y75108	L6		18.4±2.5		407	2.27	9.8
ALH77299	H3		15.8±1.0	4.58±0.25	320	1.95	9.67
Barwise	H5		14.6±0.5#	6.3 ±1.0 #	463	2.0	1.6
Beardsley	H5			4.37±0.17#	593	2.4	1.51
Bruderheim	L6	16-2	25.4±1.7	4.71±0.33	530	2.25	10.8
		B156	23.1±1.0	5.09±0.26	491	2.22	10.8
Kesen	H4			6.15±0.30	485	2.25	2.9
Peace River	L6	4	21.2±0.8	5.08±0.97	403	2.1	15
STONY IRON and IRON METEORITE							[^{4}He/^{21}Ne]
ALH762	IA			3.83±0.32	556	2.70	
Bencubbin	Mes			5.90±0.28	525	2.43	
Braunau	IIA			3.44±0.24	512	2.62	244
Emery	Mes			5.9 ±0.5	422	2.11	205
Grant	IIIB	G-320		3.32±0.16	(400)	2.87	319
Henbury	IIIA	H193.488		1.43±0.10	331	2.83	
Majarhati	Pal	14.9cm		5.99±0.27	515		
Odessa	IA	H91.3		1.30±0.05	190	2.9	
		H91.202		0.54±0.02			
Tawallah Valley	IVB			5.26±0.20			340
Tocopilla	IIA			2.28±0.17			310
Treysa	IIIB	A,Surface		5.23±0.24	(470)	2.55	257
Trenton	IIIA	AII-22+2		3.51±0.11	590	2.83	325
Udei Station	IA			3.8 ±0.3	575	2.6	259

* P(^{53}Mn) : atoms/min·kgFe from K.Nishiizumi(1987)
# not corrected for exposure time

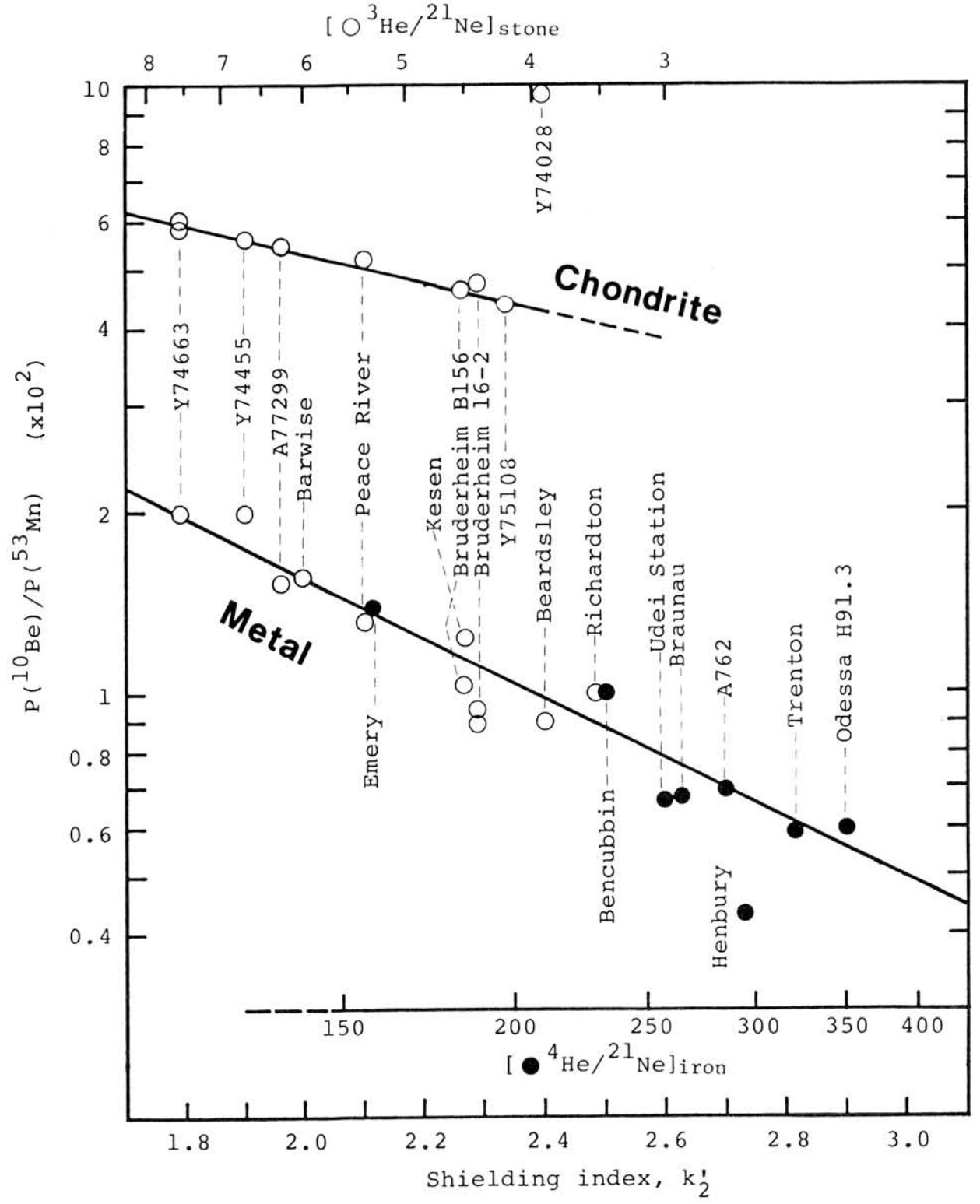

Fig.1 Ratios of ^{10}Be and ^{53}Mn productions effected by shieldings.

$^4He^+$ ion implantation experiments into minerals and their implications for planetary sciences

T.Futagami[1], M.Ozima[1], Y.Nakamura[2]

1)Geophysical Institute, University of Tokyo. Tokyo 113.Japan
2)Institute of Space and Astronautical Science. Sagamihara 229.Japan

Amari and Ozima[1] reported that extraterrestrial helium in deep ocean sediments was concentrated by more than ten times in the magnetic fraction (probably magnetite) than in the non-magnetic fraction. The amounts of ^4He in μm-sized lunar dust grains reported by Eberhardt et al.[2,3] and Signer et al.[4] show that ilmenite grains contained more than ten tiems ^4He of the solar wind origin than silicate minerals, such as olivine and pyroxene. These differences in concentrations of the solar wind origin ^4He between magnetite, ilmenite and other phases must be attributed to some processes of implantation or to some post-implantation processes.

1) Differences in ^4He abundances may be accounted for by differences in trapping efficiences. Maximum ^4He concentrations which are trapped by magnetite and ilmenite may be one order of magnitude higher than maximum concentrations trapped in other phases, such as silicates.
2) Differences in ^4He abundances may be accounted for by differences in ^4He retentivity. Implanted ^4He may diffuse out much more easily of silicates than of magnetite and ilmenite.

We undertook two kinds of experiments which simulated solar wind α-particle implantation into rocks or minerals in order to examine the above two possibilities. Wetherill[5] proposed a hypothesis that the ^{36}Ar on the Venus was of the solar wind origin. Noble gas implantation experiments in laboratories would be useful to test the above hypothesis on the origin of the planetary atmospheres.

Experiment-I: We have investigated how amounts of ^4He trapped per unit irradiated surface area varied with irradiation ion dose. We have irradiated platelet targets of magnetite, olivine, and ilmenite with a 3.6KeV $^4He^+$ beam at room temperature. Subsequently, the amounts of ^4He gases which were extracted under vacuum by melting individual samples were analyzed with a peak height method by a mass spectrometer. The results are shown in Fig. 1. The following characteristics are recognized.

1) Three kinds of mineral targets are saturated with ^4He atoms at the almost same critical dose of $\sim 2\times10^{16}$ $^4He^+/cm^2$. There are not large differences among these minerals in the ^4He saturation concentrations.

2) At the dose smaller than the critical value about 100% of irradiated $^4He^+$ is retained in the targets.

Subsequently, we will compare ^4He saturation concentrations with ^4He abundances in lunar grains. The ^4He concentrations ($\sim 10^{16}$ atoms/cm^2) in lunar ilmenite are comparable to the above experimentally determined saturation concentration, while ^4He concentrations ($10^{14} \sim 10^{15}$ atoms/cm^2) in lunar olivine are one or two order of magnitude lower than the saturation concentration. Fig. 1 shows that ilmenite and olivine begin to be saturated with ^4He atoms at the almost same critical dose. If we assume that ilmenite and olivine grains have been on the lunar surface exposed to α-particles of the same dose, lunar olivine grains as well as ilmenite grains must have been irradiated with the α-particle dose enough for saturation. It would be allowed to consider that ^4He abundances in lunar olivine were lower than the saturation concentration because most of implanted ^4He atoms diffused out of olivine grains.

Experiment-II: We have investigated whether or not there are significant differences in degassing patterns of 3.6KeV-implanted ^4He atoms among some minerals(olivine, magnetite, and rutile) by the use of stepwise heating, in order to know qualitatively how easily implanted ^4He atoms diffuse out of minerals. The results are shown in Fig. 2. The peak of ^4He thermal release patterns for magnetite and rutile is located at 600°C, while the peak for the two kinds of olivine is located at 300°C. Implanted ^4He atoms are easier to diffuse out of olivine than out of magnetite and rutile.

From these results, we can conclude that implanted ^4He atoms diffuse more easily out of olivine than out of oxides of Fe and Ti(magnetite, rutile, and ilmenite). It seems that the differences in ^4He concentrations between magnetite or ilmenite and other phases, such as olivine can be attributed to differences in the easiness with which implanted ^4He atoms diffuse out of minerals.

References

[1]Amari and Ozima (1985) Nature, 317, 520
[2]Eberhardt et al. (1970) Proc. Apollo 11 Lunar Sci. Conf, 1037
[3]Eberhardt et al. (1972) Proc. 3rd Lunar Sci. Conf, 1821
[4]Signer et al. (1977) Proc. 8th Lunar Sci. Conf, 3657
[5]Wetherill (1981) Icarus, 46, 70

Fig. 1 Relation between irradiation dose and trapped ^4He amounts. The dotted line corresponds to the case where 100% of irradiated $^4He^+$ ions is trapped in targets.

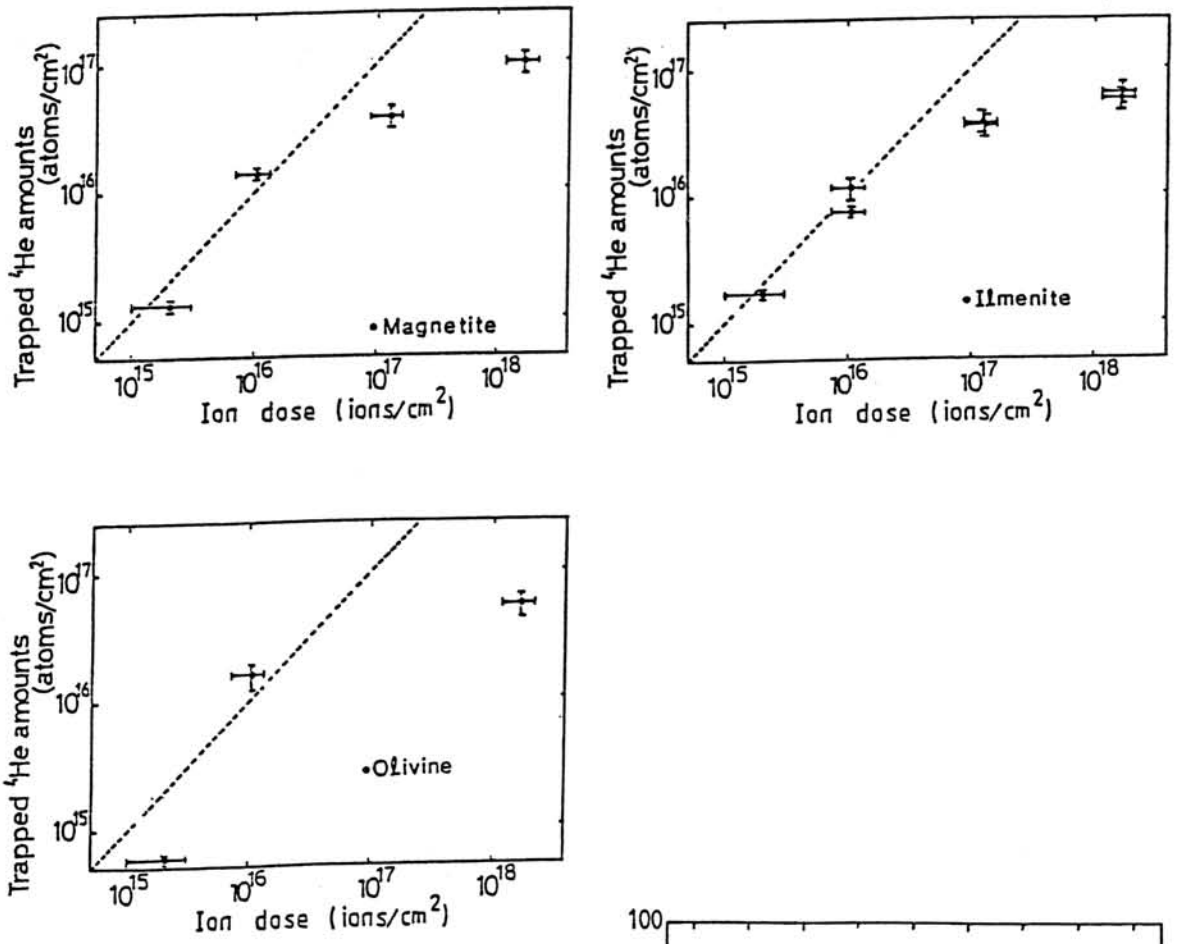

Fig. 2 Results of stepwise heating experiments.

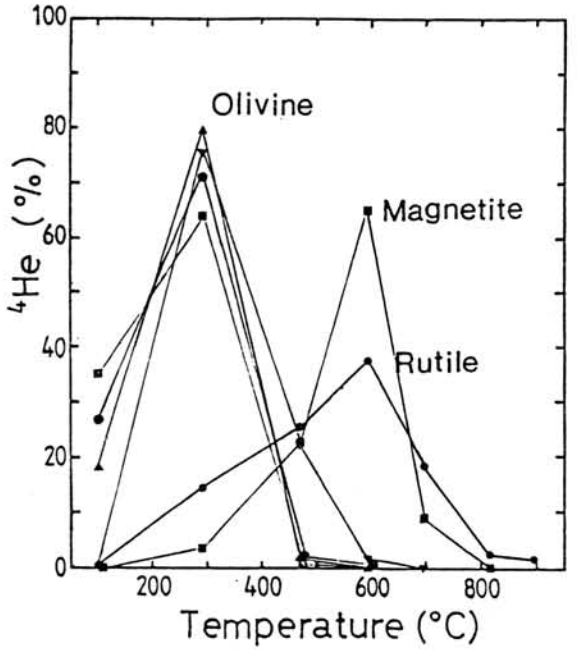

COMPARATIVE STUDY IN COSMIC-RAY AND TERRESTRIAL AGES OF ANTARCTIC METEORITES.

Miura, Y., Rucklidge, J.*, Beukens, R.*, Nagao, K.** and Koga, H.

Dept. of Min. Sci. and Geol., Fac. of Sci., Yamaguchi Univ., Yamaguchi, 753, Japan. *) IsoTrace Lab., Univ. of Toronto, Toronto, M5S1A7, Canada. **) Inst. Earth's Interior, Okayama University, Misasa, Tottori, 682-02, Japan.

Cosmic-exposure and ^{14}C terrestrial ages in the same ten Antarctic meteorites are discussed in various chemical groups and petrologic types. The present results are summarized as follows (cf. Figs. 1 to 2).

Ten various types and groups of Antarctic meteorites offered from the National Institute of Polar Research in Japan are used in this study; that is, Y-791500 (H3), Y-74647 (H5), Y-74014 (H6), Y-74191 (L3), Y-791630 (L4), Y-75271 (L5), ALH-77231 (L6), Y-790448 (LL3), Y-74097 (Diogenite) and Y-791717 (C3) for meteorite ages. The Bruderheim (L6) and Nio-3 (H3) chondrites are used as comparison references [1,2].

The exposure ages of the meteorites are calculated from the ^{3}He and ^{21}Ne isotopic data [3]. Carbon-14 terrestrial ages of the Antarctic meteorites have been measured by the IsoTrace accelerator mass spectrometry (AMS) [1,2,4]. The ^{14}C terrestrial age of 1 gram sample was determined from ^{14}C concentrations collected at melt and re-melt temperatures, compared with the ^{14}C concentration of the known falling-time chondrites. The Yamato chondrites have wide range of terrestrial age from 510 (in the Y-791630) to 29,940 (in the Y-790448) years BP. Allan Hills meteorite of the ALH-77031 chondrite shows older age of about 30×10^3 years, which is nearly consistent with the previous comparative data that the Allan Hills meteorites have older terrestrial age than the Yamato chondrite [1,2,5,6]. Among various chemical groups of H, L, LL and C, there are no regular relationships in terrestrial age data. This indicates that Antarctic meteorites are mixtures of the various falling-times which are concentrated accidentally to several regions in the Antarctica by glacer movement.

The pairing problem that some Antarctic meteorite fragments have been fallen from the same meteoroid origin before entering to the Earth is also discussed. The Yamato-74013 diogenite group meteorites indicate similar terrestrial age of 16 to 19×10^3 years obtained from the counting method [1,2,5,6,7]. The present AMS ^{14}C terrestrial age indicates that the Y-74097 diogenite (1×10^3 years) has younger terrestrial age than the previous reported data.

The four meteorite ages between types 3 and 6 are completely different in the Antarctic chondrites. Type 6 chondrites show the longest cosmic exposure ages, whereas the type 3 chondrites have relatively the shortest cosmic exposure ages. The types 4 and 5 chondrites show the shortest exposure and terrestrial ages with younger (i.e. the most metamorphosed) gas-retention ages. Thus,

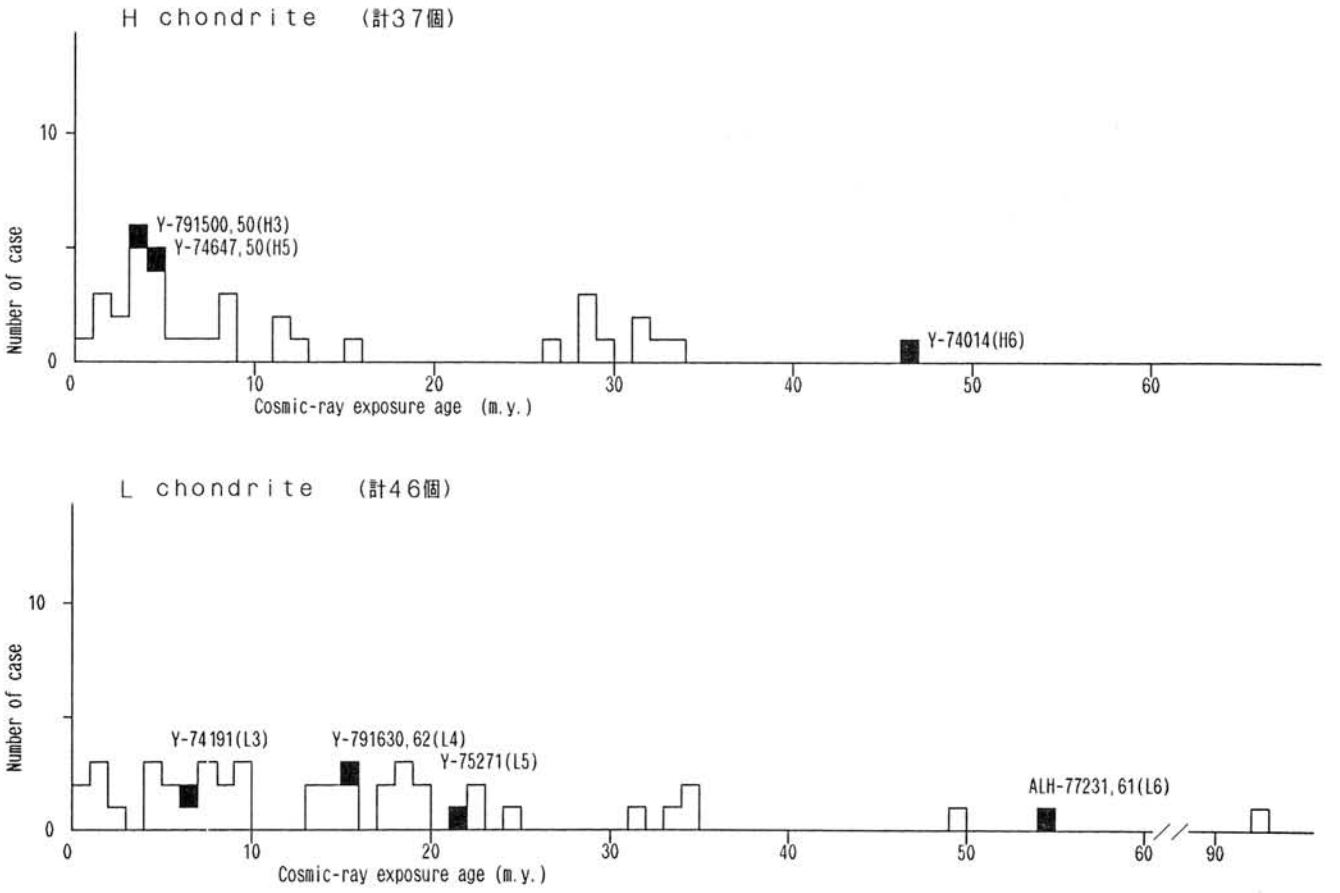

Fig. 1. Histogram of cosmic-exposure ages of H and L Antarctic meteorites. The present data are shown in black areas, together with reference data [3,5].

the tentative formation model of the chondrites is that the types 3 and 6 chondrites are the fragments from the core and margin, respectively, in the the meteoroids if these fragment came from the similar parent body [8,9].

The different terrestrial ages among ^{14}C, ^{36}Cl and ^{26}Al can be explained as the heterogeneity of the meteoroids; that is, (1) large size of the meteoroids in space (more than 1 m in diameter), and (2) imperfect saturation of the ^{26}Al and ^{36}Cl radioisotopes by cosmic-ray bombardment which are usually contained in the major constituent minerals in the meteorites [1,3,5,6,8,9].

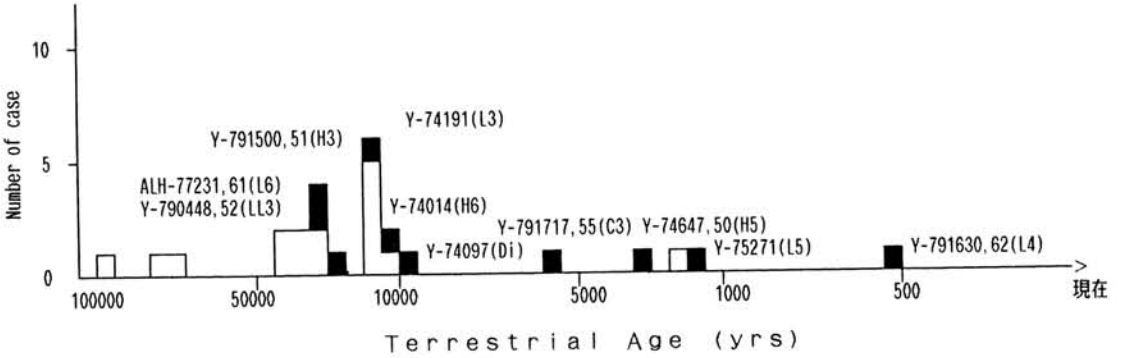

Fig. 2. Histogram of ^{14}C terrestrial ages in Antarctic meteorites. The present data are shown in black areas, together with the previous reported data [1,3,5,6,7].

References

1) R. P. Beukens, J. C. Rucklidge and Y. Miura (1987): Mem. Natl Inst. Polar Res., Spec. Issue (in press). pp. 5.
2) Y. Miura, J. Rucklidge, R. Beukens and E. Fireman (1987): Proc. 12th International Symposium on Application of Ion Beams in Material Science (in press). pp.6.
3) K. Nagao, K. Ogata, N. Takaoka and K. Saito (1983): Mem. Natl Inst. Polar Res., Spec. Issue, 30, 349-361.
4) A. E. Litherland, J. C. Rucklidge, G. C. Wilson, W. E. Kieser, L.R. Kilius, and R. P. Beukens (1984): SIMS IV, Chemical Physics, 36, (Springer-Verlag), 170-174.
5) J. O. Annexstad, L. Schultz, and H. Wanke (1986): International Workshop on Antarctic meteorites (Houston, LPI), pp. 119.
6) E. Fireman (1983): Mem. Natl Inst. Polar Res., Spec. Issue, 30, 246-250.
7) K. Kigoshi and E. Matsuda (1986): International workshop on Antarctic meteorites (Houston, LPI), 58-60.
8) Y. Miura (1987): Lunar Samples and Antarctic Meteorites (Tokyo), 1-6.
9) Y. Miura et al. (1988): Proc. Origins of Meteorites and the Solar System (Tokyo), pp.3 (in press).

DISCUSSION OF C-14 "WEATHERING AGES" OF SOME YAMATO AND ALLAN HILLS METEORITES

Miura, Y.*, Beukens, R. P.** and Rucklidge, J. C.**

Yamaguchi Univ.* Univ. of Toronto**

Carbon-14 released when heating a meteorite below 1000C has been used by several authors to yield an age known as the "Weathering Age". For meteorites which have spent their time on earth buried in the Antarctic ice, it has been assumed that the carbon was adsorbed on the surface during passage through the atmosphere, and has decayed steadily since that time. The activity of this carbon should yield the terrestrial age: Anything less has been interpreted as C-14 added during the weathering process.

We have found that carbon released at 1000C contains a fraction (28.6 percent) which is due to spallation in outer space, and that a further correction must be applied to compensate for crucible contributions. When these corrections are made, the "Weather Ages" of 8 Yamato and 1 Allan Hills meteorite range from being roughly equal or less than the terrestrial age determined from the C-14 released when the meteorite is melted, though one sample had an activity substantially greater than modern, I.E. a negative age. The "Weathering Ages" are difficult to interpret from a simple point of view, though there does seem to be a general correlation with the weathering classification. It is clear that contamination from unknown sources may occur, and we will discuss the various possibilities.

Noble gases in K-T boundary clay: Evidence for meteorite impact

Nobuo Takaoka(1) and **Yasunori Miura**(2)

(1) Dept.Earth Sciences, Yamagata University, Yamagata 990

(2) Dept.Mineral.Sci.Geol., Yamaguchi University, Yamaguchi 753

Many reports on K-T boundaries have been devoted from various disciplinaries for understanding events happened between the Cretaceous and Tertiary periods since Alvarez et al.[1] determined a high Ir concentration in the K-T boundary at Gubbio, Italy and proposed a hypothesis that a large asteroid impact caused mass extinction at the end of the Cretaceous. In spite of extensive studies, any experimental evidence does not clinch the question what happened at the end of the Cretaceous. Some of experimental results such as Ir enrichment, shocked mineral and isotopic ratios for Sr and Os can be explained by both extraterrestrial and terrestrial causations [2]. Because noble gas isotopes are less abundant on the earth and can be detected with high sensitivity by modern mass spectrometry, they are sensitive tracers for extraterrestrial matters. Large difference in the isotopic ratio between the terrestrial and the meteoritic noble gases could enhance the sensitivity to identify the meteoritic gas. Therefore, the noble gas is diagnostic for the existence of debris of the asteroid if it never melted.

Noble gas abundances in K-T sediments from Stevns Klint in Denmark have been reported by Eugster et al.[3].They analysed carbon residues prepared by acid etching and found slight enrichment in ^{3}He relative to the atmospheric ratios but no anomalies for other isotopes. Wolbach et al.[4] have analysed carbon residues in clay samples from three K-T boundary sites including Stevns Klint, and found no trace of meteorite noble gases.

We report the result of noble gas analysis of the K-T boundary clay from

Stevns Klint. The sampling site, and mineralogical and ESR studies of this sample have been reported elsewhere [5].

The clay sample(SK-2-4) of 51.67 g was etched by 6N HCl and condense HF. After the HF-etching for 2 days, the sample was washed in distilled water and dried. The sample weight decreased to 16.38 g by the HCl-HF etching. In the acid etching, we never heated the sample nor used any oxiding chemicals such as HNO_3 , because heating degases loosely trapped gases and the oxidizing chemicals remove carbonaceous materials.

Part of the residues(5.08 g) was used for noble gas analysis. Techniques of noble gas analysis have been given by Takaoka[6]. Noble gas data corrected for blank, instrumental background and mass discrimination are shown in Table 1. Large enrichment of ^{3}He (69 R_a) and slight depletion of ^{20}Ne are found compared to the atmospheric ratios.

High ^{3}He / ^{4}He ratios up to or beyond 1×10^{-4} have been reported in terrestrial deep-sea sediments,diamonds and lavas. The high He ratios in the deep-sea sediments[7] and the diamonds[8] are accompanied by high Ne ratios. The high He ratios found in the lavas is attributed to cosmogenic ^{3}He produced by cosmic-ray interactions with lavas at high mountains [9].

The high He ratio and the low Ne ratio in the present sample are inconsistent with the isotopic signature reported for both deep-sea sediments and diamonds. Since the sampling site at Stevns Klint is not at altitudes but on a sea shore, and was underground in the past, cosmic-rays could not intrude the K-T boundary. These suggest the existence of a noble gas component that is different from that identified in the terrestrial matters mentioned above. The noble gas of the same trend as found in the present K-T sample is found in meteorites: it is the cosmogenic gas or the planetary-type gas. The present result indicates that the K-T sediments from Stevns Klint contain the meteoritic noble gas,a result favoring the asteroid impact

hypothesis.

From the isotopic ratios, the fractions of cosmogenic ^{4}He and ^{22}Ne are 0.05 and 4.1 % respectively, if He and Ne in SK-2-4 are mixtures between atmospheric and cosmogenic gases. In case of mixtures between atmospheric and planetary gases, the fractions of planetary He and Ne are 69 and 23 %, respectively. The latter case is hardly practical because of the large fractions of planetary gases.

Table 1. Isotopic abundances of He and Ne in K-T boundary clay

Sample	^{4}He	^{3}He / ^{4}He	^{20}Ne	^{20}Ne /^{22}Ne	^{21}Ne /^{22}Ne
SK-2-4	>300	$(97\pm3)10^{-6}$	>3	9.43 ± 0.08	(0.0358)
Atmospheric	---	1.4×10^{-6}	---	9.800	0.0290
Spallogenic	---	0.2	---	0.85	0.92
Planetary	---	1.4×10^{-4}	---	8.2	0.024

Concentrations of He and Ne are given in unit of 10^{-9} cm^3 STP/g.

References: [1] L.W.Alvarez et al., Science 208, 1095(1980). [2] A.Hallam, Science 238, 1237(1987). [3] O.Eugster et al., Earth Planet.Sci.Lett. 74, 27 (1985). [4] W.S.Wolbach et al.,Science 230,167(1985). [5] Y.Miura,ESR dating and dosimetry, ed.M.Ikeya and T.Miki,p.469,Ionics,Tokyo(1985); Y.Miura,Lunar Planet.Sci. XVII, 555(1986). [6] N.Takaoka, Mass Spectr. 24,73(1976). [7] S. Amari and M.Ozima,Terra Cognita 6,102(1986). [8] M.Honda,Terra Cognita 6,104 (1986).[9] G.Kurz,Geochim.Cosmochim.Acta 50,2855(1986);H.Craig and R.Podera, Proc.Nat.Acad.Sci.83,1970(1986).

ANOMALOUS DATA ON THE K-T BOUNDARY SAMPLES

Y. Miura and M. Imai

Fac. of Science, Yamaguchi University, Yamaguchi, 753, Japan.

Cretaceous and Tertiary boundary (designated as K-T boundary in this study) problem has been discussed previously from the geological research, mainly by fossils [1].

Although geochemical bulk data of "Ir anomaly" reported by Alvarez et al. (1980) [2] suggest the extraterrestrial origin of the K-T bounary, the exact formation process discussed by mineralogical study has been started recently by Miura et al. (1985) and Miura (1986) [3,4].

The K-T boundary sample at Kawaruppu-river, Hokkaido has been collected in this study, in order to compare with the typical K-T boundary samples of Gubbio, Italy and Stevens Klint, Denmark. The experimental data of silicas and calcites in these K-T boundary samples have been obtained from the X-ray unit-cell dimension, ESR signal and total linear absorption coefficient.

The following tentative results have been obtained in the Kawaruppu K-T boundary samples:

(1) volume percentages and grain-sizes of the constituent minerals within the K-T boundary are changed abruptly, together with abrupt changes of the physical properties of unit cell parameters, X-ray absorption coefficient and ESR signal A (g=2.0050).

(2) abrupt change of physical properties is not the same within the K-T bundary sample-series.

(3) the abrupt change of the physical properties has been observed in the Denmark, Italy and Japan-Hokkaido K-T boundary samples. The exact point-level of the abrupt change is nearly consistent with the compositional change of trace elements, such as Pt-group and siderophile elements.

(4) Danish K-T samples show the typical abrupt changes, but the Italian K-T samples have effects from much more terrestrial activities. Compared with these typical K-T boundary samples, Japanese K-T boundary samples indicate the two or three different patterns. The mixed patterns of the Japanese K-T boundary samples are very difficult to explain as the real K-T boundary samples, if it is not compared with the typical K-T boundary sample patterns.

Anomalous change of physical properties of calcite and quartz in the Cretaceous-Teretiary (K-T) boundary which is completely different with the typical terrestrial limestones from the Akiyoshi-Kaerimizu boring cores, has been obtained in the samples from Denmark, Italy and Japan. Anomalous high total dose in Danish calcite is due to inclusion of Ir elements, which can be obtained from trace analysis with the JXA-8600 micro-probe. The calcites from Italy and Hokkaido, Japan with highly terrestrial alteration show slight changes of ESR data within the successive K-T boundary samples.

References
1) Alvarez, L.W., Alvarez, W., Asaro, F. and Michel, H.Y. (1980): Science, 208, 1095-1107.
2) Saito, S., Yamanoi, T. and Kaiho, K. (1986): Nature, 323, 253-255.
3) Miura, Y. (1986): Lunar and Planetary Science (NASA-LPI), 17, 555-556.
4) Miura, Y., Ohkura, Y., Ikeya, M., Rucklidge, J. and Takaoka, N. and Nielsen, T. (1985): ESR Dating and Dosimetry (Ionics, Tokyo), 1, 469-476.

THERMOLUMINESCENCE OF ANTARCTIC METEORITES FROM JAPANESE COLLECTION

Haq, M.[1]; Hasan, F.[2]; Vanzani, V.[3]; Sartori, S.[3]; and Englert, P.A.J.[1]. [1]Department of Chemistry, San Jose State University, San Jose, CA 95129; [2]Department of Chemistry and Biochemistry, University of Arkansas, Fayetteville, AR 72701; [3]Department of Physics, University of Padova, Padova, Italy.

Ordinary Chondrites have been studied in great detail using Thermoluminescence (TL). The natural TL shows a correlation with Al-26 (Hasan et al;1987) and like other cosmogenic nuclides is influenced by shielding and depth (McKeever and Sears;1980). The natural TL provides information regarding terrestrial ages of meteorites (McKeever;1982, Sears and Durrani;1980, Melcher;1981). The Antarctic meteorites tend to have lower natural TL than Non-Antarctic counterparts because of longer terrestrial ages (Hasan et al;1987).

The natural TL shows no correlation with static loading or petrological types (McKeever and Sears;1980) whereas the TL sensitivities are greatly influenced by metamorphic and shock history of ordinary chondrites (Guimon et al;1985, Keck et al;1986, Haq et al;1987). The TL sensitivities for petrological type 3 are much lower than those of type 4,5 or 6 (Sears;1980). The Antarctic H Chondrites show lower TL sensitivities than those of non-Antarctic because of higher degree of weathering (Haq et al; 1987). The differences in TL properties may imply that the Antarctic chondrites are sampling different regions of the parent body (Haq et al;1987).

In the present work TL properties of 8 Antarctic meteorites from the Japanese collection are studied for cosmic ray interaction products in a collaborative effort. Cosmogenic nuclide studies in bulk meteorite material and separates are in progress.

The meteorite samples (300-500 mg) were gently crushed in an agate mortar. 30 mg non magnetic portion was used for TL and the remaining for cosmogenic nuclide measurements. The non magnetic portion was further ground to reduce the grain size to approx 100 mesh. The TL was measured in 3 aliquots of 4+/-1 mg. After natural TL measurement these samples were irradiated with Sr-90 source and used for the induced TL measurements. The techniques are described by Sears and Weeks (1983).

The results are shown in Table 1 and Table 2. The natural TL glow curves consist of two broad peaks one at low temperature (LT, approx 250°C) and the other at high temperature (HT, approx 400°C). The natural TL are reported as peak ratios LT/HT (i.e normalized to HT). The equivalent dose is referred to the ratio of natural TL at 250°C and induced TL at 250°C multiplied by the test dose administered. The Yamato meteorite data are comparable to those of Allan Hills meteorites (Hasan et al;1987). Y 74193,84 has the highest LT/HT ratio (5.60) whereas Y 75028 has the lowest ratio (0.21).

The TL sensitivities are shown in Table 2. The TL sensitivities are normalized to the TL sensitivity of Dhajala (H3.8). The TL sensitivities cover a range of 0.03-2.94. Such a large spread is expected because of the variation in petrological types and class. The L3 chondrites ALHA 77167 and ALHA 77260 show the lowest TL sensitivities, whereas Y 81132 (H6) has the highest TL sensitivity.

On the basis of TL properties the 5 Yamato meteorites show close resemblance to Allan Hills and other Antarctic meteorites.

References: Guimon et al (1985) Geochim. Cosmochim. Acta,49 ,1515. Hasan et al (1987) J. Geophys. Res.,E7305. Haq et al (1987) Geochim. Cosmochim. Acta (submitted). Keck et al (1986) Earth Planet. Sci. Lett., 77, 427. McKeever and Sears (1980) Mod. Geol., 137. McKeever (1982) Earth Planet. Sci. Lett., 58 ,419. Melcher (1981) Geochim. Cosmochim. Acta,45, 615. Sears and Durrani (1980) Earth Planet. Sci. Lett., 46, 159. Sears and Weeks (1983) J. Geophys.Res, 88, B301. Sears (1980) Icarus, 44, 190.

Table 1: Natural TL properties of Antarctic Meteorites

Meteorite	Type	LT/HT	E.D. [K rad]	Al-26+ [dpm/kg]
ALHA 71677.73	L3	6.25+/-1.6	29.7+/-0.3	37+/-2
ALHA 77260.75	L3	4.08+/-0.8	23.9+/-11.8	37+/-2
ALHA 77273.61	L6	0.59+/-0.04	10.6+/-0.9	
Y 75028.103	H3	0.19+/-0.004	3.63+/-0.1	
Y 75028.104	H3	0.24+/-0.03	4.34+/-0.6	
Y 74193.84	H5	5.60+/-0.6	103+/-9.6	
Y 781869.71	H5	1.48+/-0.1	21.5+/-5.4	
Y 81132.71	H6	3.49+/-0.2	73+/-6.6	

+From Nishiiziimi (1984).

Table 2: Induced TL properties of Antarctic Meteorites

Meteorite	Type	TL Sensitivities (Dhajala=1.0)	T(max) [°C]	FWHM [°C]
ALHA 77167.73	L3	0.03+/-0.006	134+/-6	82+/-4
ALHA 77260.75	L3	0.05+/-0.006	130+/-6	86+/-8
ALHA 77273.61	L6	2.3+/-0.3	185+/-4	134+/-4
Y 75028.103	H3	0.27+/-0.004	190+/-4	142+/-2
Y 75028.104	H3	0.17+/-0.02	184+/-4	142+/-4
Y 74193.84	H5	1.8+/-o.3	184+/-6	132+/-5
Y 781869.71	H5	1.01+/-0.2	187+/-2	131+/-4
Y 81132.71	H6	2.9+/-0.4	178+/-4	124+/-1

Errors quoted are one sigma based on triplicate measurements.
ALHA-Allan Hills, Y-Yamato.

TERRESTRIAL AGES OF ANTARCTIC METEORITES USING THE THERMOLUMINESCENCE LEVELS INDUCED IN THE FUSION CRUST

Bhandari, N. and Sengupta, D.

Physical Research Laboratory, Ahmedabad 380 009, India.

The terrestrial age (T_E) of meteoritic finds is an important parameter, which enables one to evaluate the frequency of falls, its time variation, and in turn, the mechanism of their injection in earth crossing orbits in interplanetary space. A quick and reliable determination of terrestrial ages will be particularly useful in understanding ice dynamics as well as the mechanism of meteorite concentration in Antarctica.

Activity levels of cosmogenic radionuclides when compared to their production rate in space, is used to estimate the time since their fall, when the cosmic ray production ceased. However, these production rates depend on size of the meteoroid, shielding depth of the sample and degree of saturation which are normally not known independently (1,2). Also because of short terrestrial ages of meteorites (10^3-10^5a) compared to the mean life of radionuclides used (^{26}Al≅1 Ma, ^{53}Mn≅5 Ma), the error in computation of terrestrial age is large. The cosmic ray induced thermoluminescence (TL) in the meteorite, in space, also decays after its fall. However the extent of its decay has not provided a reliable method for estimating terrestrial ages (3). Ninagawa et al. (4), instead, suggested that the TL induced in the meteorite fusion crust after its fall, due to cosmic ray exposure and ambient radioactivity on earth, could provide a measure of their terrestrial ages.

$$\text{Thus } T_E = \frac{\text{TL acquired}}{\text{TL dose/a}}$$

We report here our results on six Antarctic meteorites collected from Allan Hills, Meteorite Hills and Mount Baldr (Table 1).

Table 1: TL data and the estimated terrestrial ages by the fusion crust method.

Meteorite	Class	Latitude and Longitude	Altitude (m)	E.D. (240-260°C)	E.D. (360-380°C)	Dose rate (mGy/a)	TL T_E (yrs)	Cosmogenic T_E (yrs)
DHAJALA	H3	22°22'N,71°25'E	65	0.12	0.16	1.89	85	11$^+$
KIRIN	H4	44°N,126°30'E	65	0.09	0.28	1.89	175	11$^+$
ALHA 77256	DIO	76°45'S,159°20'E	2000	7	42	0.80	5.2×10^4	1.1×10^4
ALHA 77257	UREI	76°45'S,159°20'E	2000	33	123	0.79	1.6×10^5	3.7×10^5
ALHA 77231	L6	76°45',159°20'E	2000	13	37	0.80	4.6×10^4	-
EETA 79001	SHER	76°15'S,156°30'E	2000	7	57	0.92	6.2×10^4	3.2×10^5
MBRA 76001	L6	77°35'S,160°,9'E	2000	6	14	0.80	1.7×10^4	3.2×10^4
META 78028	L6	79°41'S,155°45'E	1500	15	67	0.63	10.6×10^4	3.3×10^4

$^+$known ages.

Surface chips containing the fusion crust from relatively unweathered meteorites (5), were chipped, grinded and polished from all sides. They were subsequently washed in an ultrasonic bath, crushed and then treated with 1N HCl to remove any

weathered material. The grains in the size range of 45-110 microns were sieved and deposited on stainless steel discs with sil-spray. Fusion crust samples of Dhajala and Kirin (both of which fell in 1976) were used as reference. The natural and the beta induced glow curves were read using a standard TL experiment set-up described in detail earlier (6). In spite of their low TL sensitivity (about a factor of 2-6 times lower than the interior) the TL levels in the fusion crust were found to be adequate to estimate the acquired dose (ED) reliably. Some of the glow curves obtained at a heating rate of 5°C/sec and the ED profile are shown in Fig. 1. The ED values were obtained using second glow normalisation.

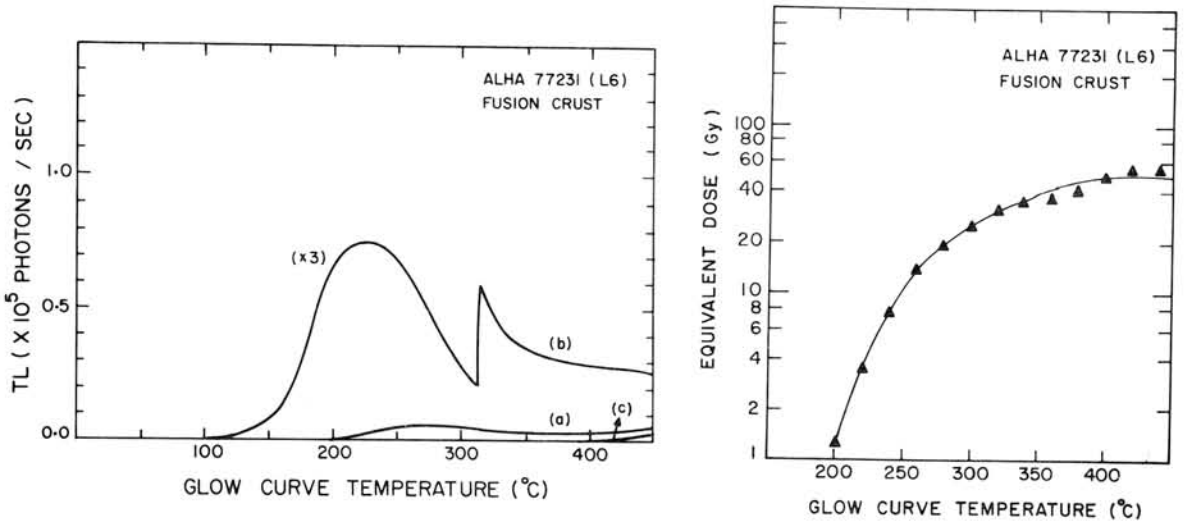

Fig. 1. Typical TL glow curves (a) Natural, (b) Beta induced TL for a test dose of 500 Gy, (c) Black body and ED profile for ALHA 77231 fusion crust sample.

The fusion crust samples from Dhajala and ALHA 77231 were studied for any changes in TL sensitivity due to multiple heating in the laboratory as well as anomalous fading of the TL signals for long (100 days) storage periods. The measurements showed no appreciable effect of multiple heating, or fading (<5%) in the plateau region over 100 days at room temperature. The latter thus clearly indicates that the long term TL fading (anomalous fading) in the fusion crust is negligible.

The Antarctic meteorites spend a part of their terrestrial residence time on surface of ice [T_S] and a part buried deep in the ice [T_D] as they travel from the region of fall to the region of recovery (7). Thus the terrestrial age could be represented as

$$T_E = T_S + T_D$$

Dynamical consideration suggest that $T_D \ll T_S$. Hence $T_E \approx T_S$. The annual dose received by these meteorites should thus mainly

result from the cosmic ray irradiation on the surface of ice. The dose rate due to the cosmic rays at the Antarctic altitudes of 1500-2000 m and geomagnetic latitude of 70°S is estimated to be 0.6 - 0.8 mGy/a (8,9). The contribution to the dose rate due to internal radioactivity (U, Th and K) in meteorites and the surrounding ice is negligible (<10%). The results obtained are summarised in Table 1 and leads to the following conclusions.

(i) The acquired dose for known falls like Dhajala and Kirin with $T_E \sim 11a$ is close to zero. When coupled to an indoor dose rate of 1.6 mGy/a (10) this provides an age of 85 a and 175 a respectively, well within the experimental uncertainty in detecting the low light levels of 1000 photons/sec.

(ii) The signal in the fusion crust of Antarctic meteorites is 10-100 times higher than in these recent falls. The ages computed from acquired dose values in the plateau region (T^*>300°C) exhibit a range of 10-100 Ka for the six Antarctic meteorites studied. The observed trend is generally consistent with the ages based on cosmogenic radionuclides (11,12,13) as given in Table 1.

The present work thus indicates the feasibility of the TL dating of the fusion crust as a rapid and simple method for terrestrial age estimation.

References: (1) Evans, J.C, and Reeves, J.H. (1987) Earth Planet Sci. Lett., 82, 223. (2) Bhandari, N. et al. (1984) Proc. Ninth Symp. Ant. Nat. Inst. Polar Res., Tokyo, 44-1. (3) Melcher, C.L. (1981) Geochim. Cosmochim. Acta, 45, 615. (4) Ninagawa, K. et al. (1983) Nuovo Cemento, 38, 33. (5) Marvin, U.B. and Mason, B. (1982) Smithsonian Contrib. Earth Sci., 24, 85. (6) Singhvi, A.K. et al. (1982) Nature, 295, 313. (7) Cassidy, W.A. et al. (1977) Science, 198, 727. (8) Herbst, W. (1964) in Natural Radiation Environ. (eds. J.A. S. Adams and W.M. Lowder), 781. (9) Prescott, J.R. and Stephan, L. (1982) PACT, 6, 17. (10) Nero, A.V. et al. (1982) in Natural Radiation Environ. (eds. K.G. Vohra et al.) Wiley Eastern Ltd., 473. (11) Nishiizumi K. and Arnold, J.R. (1982) Workshop on Ant. Glaciol. and Met. (eds. C. Bull and M.E. Lipschutz), LPI Tech. Rep. 82-03, 12 (12) Sarafin, R. et al. (1985) Earth Planet Sci. Lett., 75, 72 (13) Fireman, E.L. (1983) Proc. Eighth Symp. Ant. Met., 246.

Thursday, June 9, 1988

0900 - 1530 *Symposium, Auditorium*

1530 - 1630 *Special Lecture*

Doctor Robert Hutchison

(British Museum, Natural History)

MECHANICAL AND MORPHOLOGICAL CHARACTERIZATION OF SHOCK EFFECTS IN ANTARCTIC METEORITES (I)

Fujii, N.[1], Y. Horii[1] and H. Takeda[2]
1) Dept. Earth Sci., Faculty of Sci., Kobe Univ., Nada, Kobe 657
2) Mineral. Inst., Faculty of Sci., Univ.Tokyo, Bunkyo, Tokyo 113

Shock effects recorded in meteorites are of importance to reveal collision processes on parent bodies including metamorphism, melting, lithification and brecciation. Most of shock effects have been described by mineralogical-/petrochemical approaches, i.e. breccias and deformation of lithic fragments, texture and crystalographic features in olivine, low-Ca pyroxene, plagioclase, metal and troilite, and some isotopic studies.

In this paper, we intended to chracterize shock effects by means of mechanical and morphological approaches. The samples used are four LL-chondrites (Y-790144, Y-790345, Y-790519, and Y-790964), two H-chondrites (Y-82122 and Y-82163) and euclite (Y-792769). All samples are embedded in resin and cut so as to make at least three mutually perpendicular surfaces with each area of larger than 30 mm^2 and used for mechanical and morphological analyses, and a thin section for each sample was made for petrological analysis. The rest of samples are mainly used for the dislocation analysis by using the oxidation decolation technique.

LL-chondrites studied are characterized by the presence of vesicles and the amount of vesicles increases in following order: Y-790345, Y-790519, Y-790964, and Y-790144 (Sato, et al., 1982). The microscopic observations in thin sections of Y-82122 and Y-82163, indicate that brown glass exists near vesicles and most of grain boundaries as well as cracks which cut through single crystal olivine and pyroxene, fine-grained portion and closely spaced cracked portion distribute heterogeneously, and large grains of euhedral olivines and pyroxenes sometimes show undulating extinction. These features are similar to those of the shocked LL-chondrites. In shocked H-chondrites, the shape irregurality of metallic grains seems to be controlled by the distribution of cracks and brown glasses, and the dislocation density and crack distribution seem to be affected by some annealing processes, which should be investigated by the further analysis.

Among various methods related to mechanical and morphological characterizations of shock effects, we introduce following parameters: the dislocation density and subgrain size of olivines, the Vickers hardness and the distribution of cracks for large crystals, mechanical and petrological effects of glasses filled in cracks, surface irregularities of vesicles and fractures of fragmented portion and shape irregularity of metals and troilites. At this moment, we could not obtain the quantitative relationships among these parameters nor correlate with the intensity of shock, further investigations are in progress.

WEATHERING OF SOME ANTARCTIC METEORITES: INFORMATION FROM ABSORPTION BANDS NEAR 3 μm

Miyamoto, M.*, Kojima, H.**, and Yanai, K.**

* College of Arts and Sciences, University of Tokyo, Komaba, Tokyo 153
** National Institute of Polar Research, Kaga, Itabashi-ku, Tokyo 173

Weathering is one of the important problems involved in studying Antarctic meteorites, although recent progress in meteorite studies owes much to the Antarctic meteorite collection. We developed a new method to quantify the degree of weathering by using absorption bands near 3 μm, because we are often compelled to select the least weathered meteorites from among the Antarctic collection. The degree of weathering of Antarctic meteorites may be combined with terrestrial age data to yield additional information on meteoritic terrestrial histories.

Absorption bands (hydration bands) near the 3 μm wavelength region are sensitive to the presence of hydrates or hydroxyl ions, because the bands are due to OH streching vibrations. The integrated intensity of hydration bands may be dependent on the degree of weathering, because terrestrial weathering produces hydrous minerals.

Antarctic meteorite samples used in our study were supplied by the National Institute of Polar Research and were powders from the cutting of the meteorites [1]. The volume of powder produced is probably large enough to represent the overall nature of the meteorite, since the powder is produced by cutting across many different sections of the meteorite.

Spectral reflectance measurements (2.5-25 μm) were made with a Fourier transform infrared spectrophotometer in a dry air atmosphere, equipped with a diffuse reflectance attachment. Details of measurements are described in Miyamoto [2]. The definition of the integrated intensity of absorption bands near 3 μm is the same as that in [3]. Diffuse reflectance measurements do not require that a sample be mixed with KBr powder. This is favorable to studying hydration bands near 3 μm, because KBr tends to absorb water. Results of reflectances may be applied to the study of planetary surface materials.

Table 1 shows integrated intensities of hydration bands near 3 μm of some Antarctic meteorites and non-Antarctic meteorites Allende(C3) and Nuevo Mercurio(H5). Both non-Antarctic meteorites show relatively weak integrated intensities when compared with the Antarctic meteorites, which is consistent with their histories, that is, neither was exposed to the weather after falling. Some Yamato meteorites measured show relatively weak hydration bands near 3 μm compared with the Allan Hills meteorites measured (Fig. 1). This implies that the Allan Hills meteorites are more weathered than the Yamato meteorites.

Many investigators have reported that the Allan Hills meteorites show greater terrestrial ages than other Antarctic meteorites, on the basis of cosmic ray produced nuclide data [e.g., 4,5]. Our results are consistent with their results, because more hydrous minerals would be produced over longer terrestrial ages. Further studies combined with terrestrial age data are required to study terrestrial history of Antarctic meteorites. Nishiizumi and Elmore [5] have shown that there is no clear correlation between the terrestrial age of Allan Hills meteorites and their degrees of weathering on the A-B-C scale [1].

Jarosewich [6] discussed quantitatively the degree of weathering of Antarctic meteorites on the basis of chemical analysis data. Severely weathered meteorites denoted as C on the A-B-C scale usually show higher values for H_2O, C and FeO (which includes weathered metal) and lower values for Fe-metal and FeS than the averages for their class of meteorites. He showed that ALH-77278 (LL3) and ALH-77299 (H3) contain considerable large amounts of H_2O inspite of their classification of A on the A-B-C scale. He also showed that ALH-77271 (H5) and ALH-77003 (C3) contain considerable large amounts of H_2O. Our results show that integrated intensities of ALH-77299, ALH-77271, and ALH-77003 are relatively strong and seem to be consistent with H_2O contents.

Degrees of weathering of some meteorites determined using the A-B-C scale appear to be inconsistent with those determined using other studies such as the integrated intensity near 3 μm, terrestrial age, or H_2O content. One explanation for this apparent discrepancy may be explained by differences in weathering between different portions of a meteorite. The degree of weathering of a meteorite sample varies as a function of distance from the surface of the meteorite, because weathering proceeds from the surface to the center of a meteorite. In this study, we have tried to investigate the average degree of weathering of each meteorite. Abundant powders from cutting appear to be useful for getting "averaged" samples. Future studies shoud address the variation in degree of weathering with location inside the meteorite.

The ALH-765 and ALH-78132 eucrites show relatively strong integrated intensities (Table 1) in spite of A on the A-B-C scale. Both polymict eucrites are similar in integrated intensity and this is consistent with the fact that they are thought to be samples of a single meteorite [7].

Our results show that integrated intensities near 3 μm vary widely (Fig. 1) among meteorites whose degree of weathering is reported to be A. Additionally, the integrated intensity of Y-75097 is nearly identical to that of Nurvo Mercurio, which fell in 1978, implying that Y-75097 has undergone a minimal degree of weathering. Optical observation confirmed that Y-75097 is one of the least weathered Antarctic meteorites. This suggests that the integrated intensity near 3 μm is useful for selecting the least weathered meteorites from among the Antarctic meteorite collection. It is neccesary to study many Antarctic meteorites in order to enlarge the data base used for selection.

References: [1] K. Yanai and H. Kojima (1985) Meteorites News, Vol. 4, No. 1, Natl. Inst. Polar Res., Tokyo. [2] M. Miyamoto (1987) Icarus 70, 146-152. [3] M. Miyamoto (1987) Papers presented to the 12th Symposium on Antarctic Meteorites, 125-126, Natl. Inst. Polar Res., Tokyo. [4] M. Honda (1981) Geochem. J. 15, 163-181. [5] K. Nishiizumi and D. Elmore (1985) Papers presented to the 10th Symposium on Antarctic Meteorites, 108-109, Natl. Inst. Polar Res., Tokyo. [6] E. Jarosewich (1984) Smithsonian Contributions to the Earth Sci., No. 26, 111-114. [7] J. S. Delaney, M. Prinz, and H. Takeda (1984) Proc. Lunar Planet. Sci. Conf., J. Geophys. Res. 89, C251-C288.

Table 1. Integrated intensities of absorption bands near 3 μm of some meteorites.

Meteorite name	Class	The degree of weathering: Integrated intensity	The degree of weathering: A-B-C scale*
ALH-77299	H3	77	A
Yamato-75028	H3	82	-
Yamato-74156	H4	34	A
Yamato-74647	H5	31	A
ALH-77182	H5	90	C
ALH-77271	H5	64	C
ALH-768	H6	88	B/C
Yamato-74191	L3	53	A
Yamato-75097	L6	28	-
ALH-769	L6	56	B
ALH-769,10	L6	59	B
ALH-78103	L6	49	B
ALH-78251	L6	53	B
MET-78003	L6	80	B
Yamato-790448	LL3	86	-
Yamato-790964	LL	36	-
ALH-77003	C3	78	A
ALH-765	EUC	124	A
ALH-78132	EUC	154	A
Allende	C3	19	
Nuevo Mercurio	H5	23	

* Yanai and Kojima (1985)

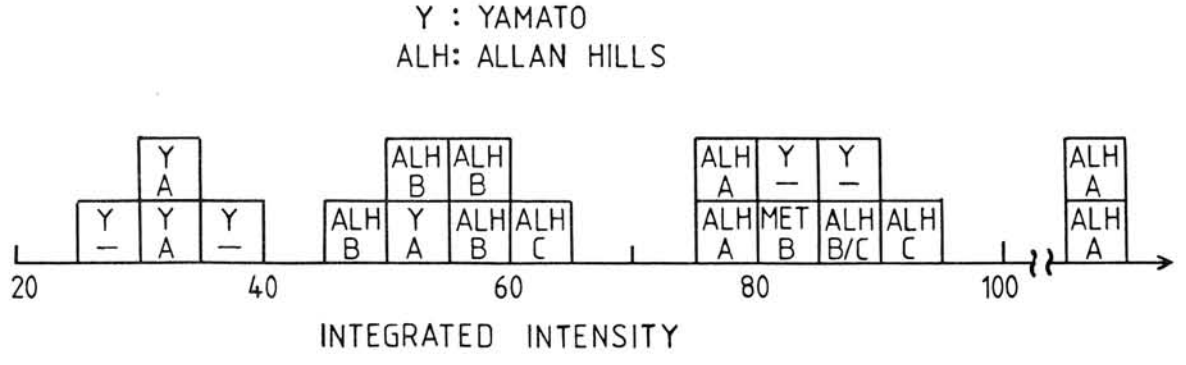

Fig. 1 Integrated intensities (cm^{-1}) of hydration bands near 3 μm of some Antarctic meteorites. ALH: Allan Hills meteorites; Y: Yamato meteorites; MET: Meteorite Hills meteorite. A, B, C, or B/C shows the degree of weathering on the A-B-C scale. "-" means that the degree of weathering is not reported.

MAGNETIC PROPERTIES OF THE MIXTURES OF FE-NI ALLOYS SIMULATED TO Y-74354, Y-74362 AND Y-74190 CHONDRITES

Nagai, H.[1], Momose, K.[2] and Funaki, M.[3]

1) Department of Physics, Faculty of Science, Shinshu University, Matsumoto 390.
2) Department of Geology, Faculty of Science, Shinshu University, Matsumoto 390.
3) National Institute of Polar Research, Tokyo.

In order to study magnetic properties of meteorites, we have investigated the thermo-magnetic behaviours of Fe-Ni alloys [1]. The present work aims to investigate the magnetic properties of the mixtures of Fe-Ni alloys simulated to Y-74354(L6), Y-74362(L6) and Y-74190(L6) chondrites.

The alloys were prepared by melting constituent elements of 99.99% purity in an induction furnace under argon atmosphere. The mixtures of Fe-Ni alloys were produced in accordance with the EPMA analysis data of Nagahara[2]. The mixture samples are made from several series of Fe-Ni alloys and their compositions are nearly equivalent to the metallic components of chondrites.

The original thermo-remanent magnetization (TRM) was acquired by heating these mixtures at 850°C for 2 hours and cooling them to room temperature in geomagnetic field in vacuum of 10^{-3}Pa. Changes of TRM by cooling at 77K in zero magnetic field and geomagnetic field were measured.

The experimental results of RM are listed in Table 1. The intensities of RM obtained by cooling at 77K in zero magnetic field decreased by about 20%. No significant differences in the directions of TRM were found by cooling at 77K in both the geomagnetic and zero magnetic fields. The decrease of RM intensity by cooling in zero magnetic field is caused by the martensitic transformation from fcc to bcc [1]. The partial phase changes by cooling are observed by Mössbauer effect as shown in Fig.1.

Fig.1 shows the decrease of the non-magnetic fcc phase (marked by arrow) after cooling at 77K in the mixture sample.

Thermo-magnetic measurements of mixture samples simulated to the meteorites are plotted in Fig.2. The magnetic properties will be discussed in detail, comparing with the results of meteorites.

References:

[1]Momose,K. and Nagai,H.(1983) Mem. Natl. Inst. Polar Res., Spec. Issue 30 447

Momose,K., Nagai,H. and Muraoka,Y.(1984) Mem. Natl. Inst.Polar Res., Spec. Issue 35 298

Momose,K. and Nagai,H.(1985) J. Geomag. Geoelectr., 37 817

Momose,K. and Nagai,H.(1986) J. Geomag. Geoelectr., 38 721

Nagai,H., Momose,K. and Funaki,M.(1987) J. Geomag. Geoelectr., 39 431

[2]Nagahara,H.(1979) Mem. Natl. Inst. Polar Res. Spec. Issue 15 77

Table 1. Remanent magnetizations of alloy mixtures simulated to 74354(L6), 74362(L6) and 74190(L6) chondrites.

[74354(L6)]

	Original TRM	Cooling at 77K in geomag. field	2nd TRM	Cooling at 77K in zero field
D	350.85°	354.5°	352.62°	345°
I	46.93°	53°	57°	50.8°
J x10^{-3}	8.547	8.667	8.18	6.169
J/J_0	($=J_0$)	1.013	($=J_0$)	0.754

[74362(L6)]

	Original TRM	Cooling at 77K in geomag. field	2nd TRM	Cooling at 77K in zero field
D	335.54°	338.64°	332.2°	324.14°
I	49.53°	53.32°	50.71°	51.44°
Jx10^{-3}	8.162	11.794	8.130	6.802
J/J_0	($=J_0$)	1.44	($=J_0$)	0.837

[74190(L6)]

	Original TRM	Cooling at 77K in zero field	2nd TRM	Cooling at 77K in geomag. field
D	23.16°	24.69°	17.23°	21.40°
I	56.63°	56.21°	54.94°	56.78°
Jx10^{-3}	20.04	16.209	18.768	18.471
J/J_0	($=J_0$)	0.809	($=J_0$)	0.984

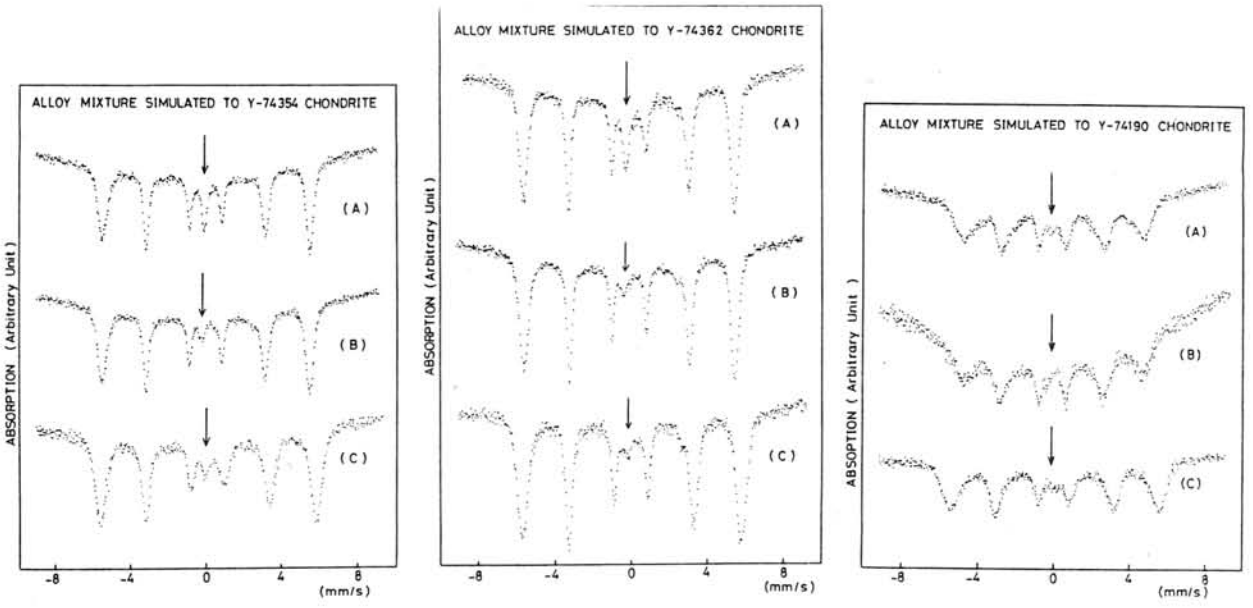

Fig.1 Mössbauer spectra of mixture samples simulated to Y-74354(L6), Y-74362(L6) and Y-74190(L6) chondrites.
(A): measured at room temperature (T_0) after cooling from 850°C to T_0.
(B): measured at T_0 after cooling at 77K.
(C): measured at 77K.

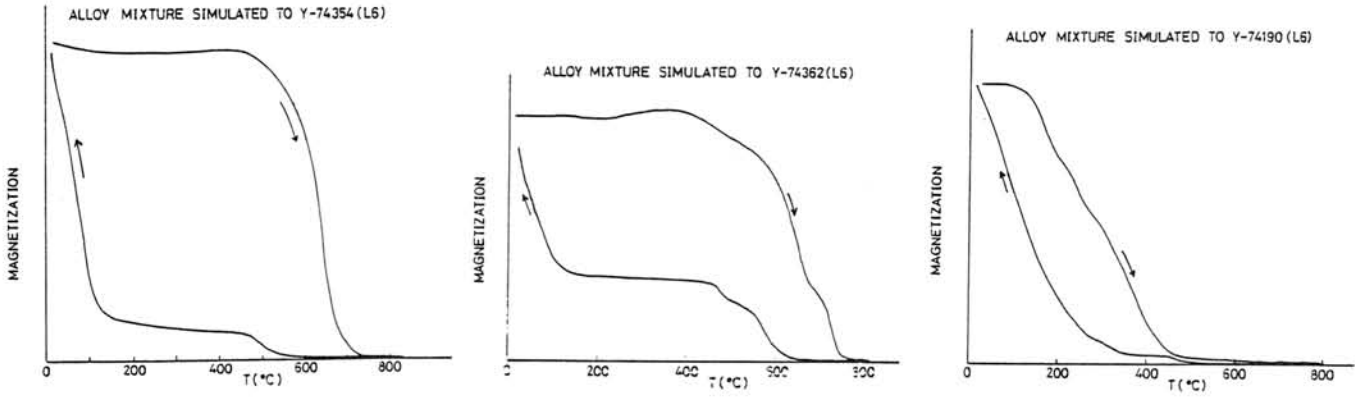

Fig.2 Thermo-magnetic curves (J_s-T) of mixture samples simulated to Y-74354(L6), Y-74362(L6) and Y-74190(L6) chondrites.

Studies on Magnetic Properties and Mössbauer spectroscopy of the Nova Petropolis iron meteorite

Minoru FUNAKI[1], Jaques DANON[2] and Takesi NAGATA[1]

1: National Institute of Polar Research, Tokyo
2: National Observatory, Rio de Janeiro, Brazil

Nova Petropolis is a medium octahedrite (IIIA) of about 300kg in total weight. Thermomagnetic curves of this meteorite indicated phase transition temperature at 755° ($\alpha \rightarrow \gamma$) in heating curve and 600°C ($\gamma \rightarrow \alpha$) in cooling curve and minor amount of Curie point at 520°C. The phase transition temperatures relate to those of 7%Ni FeNi. The Curie temperature may be disordering temperature of tetrataenite (γ') phase due to existent only in the 1st run heating curve. A magnetic mineral having high magnetic coercive force is supposed from the result of magnetic hysteresis analysis.

Natural remanent magnetization (NRM) of bulk samples of the Nova Petropolis ($1.2 \times 10^{-2} Am^2/kg$) consists of very stable and unstable components. The stable component is harder than 100 mT against AF demagnetization, but it was demagnetized steeply by thermal demagnetization between 400 and 630°C as shown in Fig. 1. The directions of stable NRM component of small bulk samples from the interior Nova Petropolis scatter widely having no relation to Widmanstätten structure. The samples having oxidized surface are magnetized to a same direction.

Fig. 1 Thermal demagnetization curves of NRM for interior Nova Petropolis

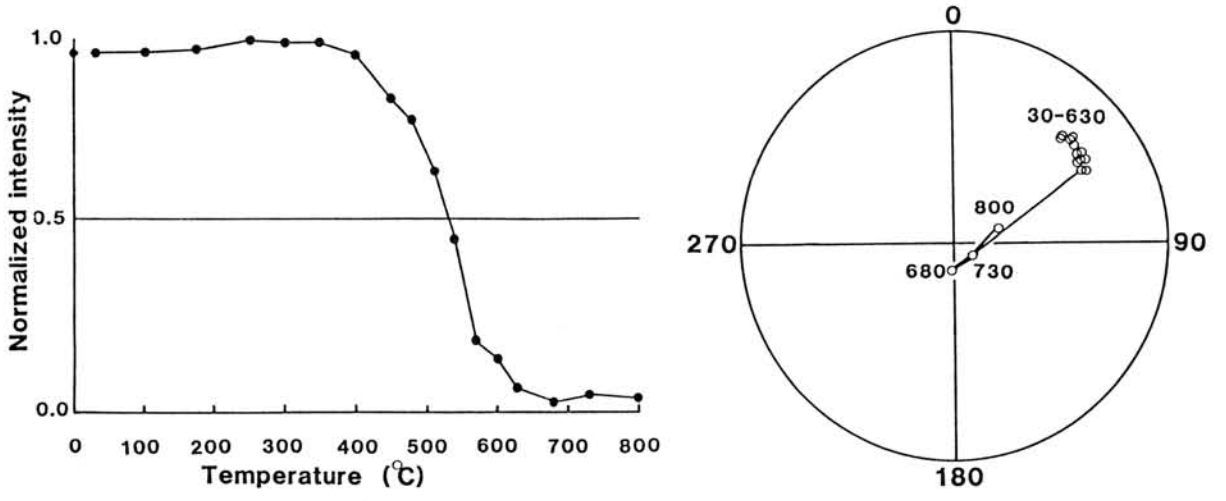

Configration of well developted Neumann bands were observed by the Bitter pattern in the every kamacite field with 10-100μm in intervals. The bands alined more than several millimeters (similar to the hexahedrite) with some discontinuity as shown in Fig. 2. There is no well crystalized γ' phase which is visible by Bitter pattern, although that weak pattern was recognized in the plessite field and a part of high nickel lamelae.

Thin high nickel lamellae were prepared from this meteorite. The Mössbauer absorption spectrum at room temperature of the lamellae indicated a mixture of 15% α-FeNi, 62% γ-FeNi, 20% paramagnetic (30% Ni) FeNi and 3% iron oxide. Ordering phase of FeNi was not observed clearly in these lamellae.

From these experimental results we reached general conclusions as follows. Nova Petropolis consist of 7%Ni kamacite, taenite and tetrataenite. Small amount of fine-grained (poorly crystallized) tetrataenite phase is in presence in plessite field and a part of high nickel lamellae. As the amount of tetrataenite phase is very small, it cannot be detected by the Mossbauer spectroscopy. The meteorite might acquire stable NRM component after heavy shocks suffered by its collisions.

Fig. 2 Developted Neumann band and its deformation

NATURAL REMANENT MAGNETIZATION OF MAGNETIC GRAINS IN ST. SÉVERIN AND Y-75097 ORDINARY CHONDRITES

M. FUNAKI[1], J. DANON[2] and T. NAGATA[1]

1: National Institute of Polar research, Tokyo
2: National Observatory, Rio de Janeiro, Brazil

Usually natural remanent magnetization (NRM) of meteorites is measured by astatic, spinner or SQUID magnetometers. The NRM has an integrated value of individual NRMs of magnetic grains in a meteorite. Although the Bitter pattern configuration indicates strong NRM regions on the polished surface of FeNi grains in meteorite under a microscope, the magnetic polarity cannot be determined by this method. If the magnetic polarity of those grains can be identified, it gives useful informations for understanding of NRM acquisition mechanism of meteorites. We identified the magnetic polarity and the magnetic field lines radiated from the S pole on fine magnetic grains using characteristic of the north seeking magnetotactic bacteria under a microscope.

The magnetotactic bacteria in the northern hemisphere have a characteristic of swimming toward the S pole (north seeking bacteria). We determined the N and S poles of several Fe-Ni grains in the St. Séverin (LL6) and Y-75097 (L5-6) chondrites by means of the bacteria and the Bitter pattern methods.

The results indicated that the strong NRM regions are formed along some parts of limb on taenite grains, Figure 1 indicates the strong NRM regions of a representative taenite grain in the St. Séverin. The main NRMs are carried by tetrataenite in this case. The swarming regions of the north seeking bacteria on this grain are shown in Fig. 2. From these figures the N and S poles can be elucidated. The NRM directions of each FeNi grains are likely to scatter in the St. Séverin and Y-75097 chondrites on the microscopical scale. These magnetic morphological structures suggest that the strong and steady magnetic field as the earth's magnetic field may not participate in the forming of FeNi grains and the chondrite parent body.

Fig. 1
Configuration of the Bitter pattern (dark spots) of a FeNi grain from the St. Severin

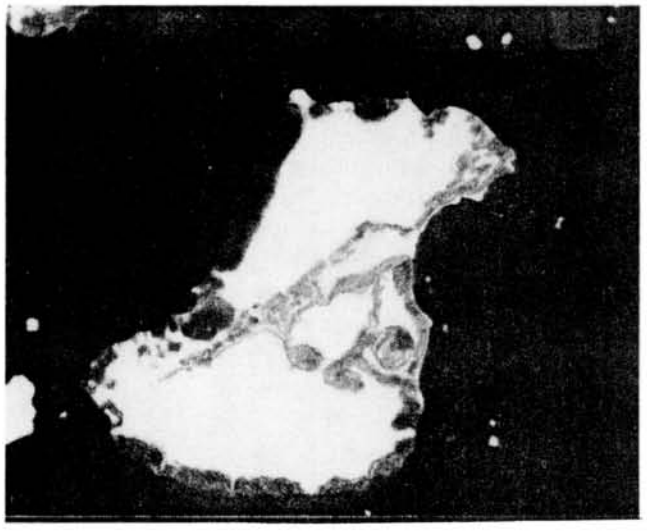

Fig. 2
Swarming regions of the north seeking bacteria (dark spots) of the FeNi grain.

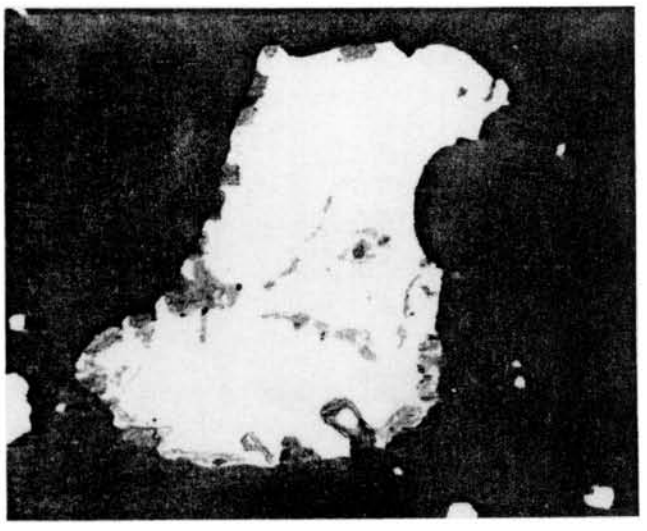

Magnetic Analysis of Antarctic Chondrites and Achondrites on the Basis of a Magnetic Binary System Model

Takesi NAGATA and Minoru FUNAKI
National Institute of Polar Research, Tokyo

1. Introduction

Magnetic characteristics of meteorites may have to be considered to be substantially different from those of terrestrial rocks, because their main ferromagnetic constituents, i.e. Fe-Ni metallic particles, comprise several distinctly different phases and some of them are in a metastable state. A simple model that ferromagnetic particles are uniformly dispersed in non-magnetic matrix, which can approximate most terrestrial rocks, may not be able to be applied on most meteorites. Hence, the second approximation of meteorite magnetism could be based on a magnetic binary system model.

2. Non-interactive Binary System Model

A non-interactive magnetic binary system model (Nagata and Carleton, 1987) could be considered as the basis of a second approximation magnetic analysis of meteorites. Fig. 1 shows a theoretical relation between content (m) of a uniaxially anisotropic hard component (a) in the meteoritic metal and observed value of I_R/I_S, where I_R=saturated IRM and I_S=saturation magnetization. Fig. 2 illustrates an example of theoretical dependence of coercive force (H_C) and remanence coercive force (H_{RC}) on m. Since the dependence of H_{RC} on m is largely different from that of H_C on m in the binary system model, $H_C^{(a)}$ and $H_{RC}^{(a)}$ of (a)-component, $H_C^{(b)}$ and $H_{RC}^{(b)}$ of magnetically soft component (b) and m can be estimated from the measured values of I_S, I_R, H_C and H_{RC}.

Fig. 1

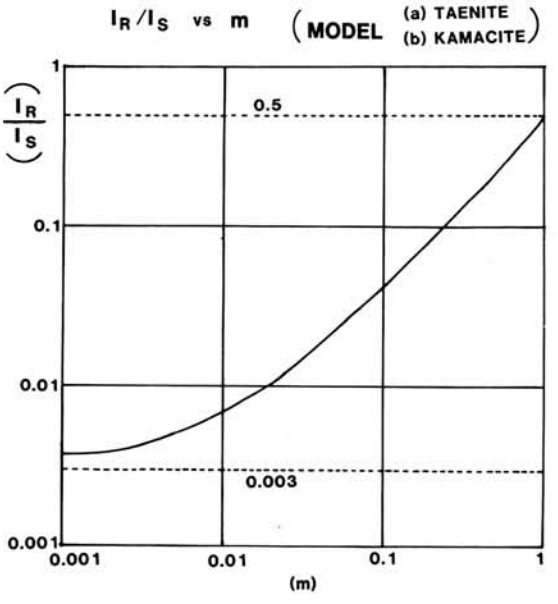

Fig. 2

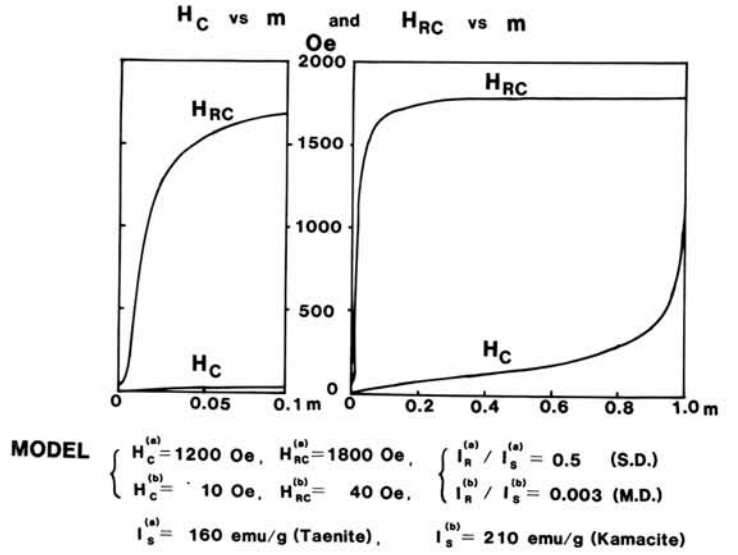

3. Magnetic Binary Structure of Chondrites

Table 1 gives examples of the parameters of magnetic binary structure of H, L and LL chondrites. The upper line numerical figures for individual samples are the parameters for the original meteorite sample before any heat treatment, while those of the lower line show the parameters of the same sample after heating twice up to 800°C, for a thermal annealing.

The metallic components of both St. Séverin and Olivenza LL chondrites contain about 40% tetrataenite (γ'-FeNi), but the content of γ'-FeNi in the original state is much reduced or almost completely broken down by the heat treatmant as shown in the table, where (b)-component is mostly kamacite. A similar break-down of γ'-FeNi component by the heat treatment can be observed in Y-74647, Y-74191, Y-74354 and Y-74362 chondrites. In the case of Y-7301, however, (a)-component after heating may represent fine single-domain (SD) particles of ordianry taenite which are newly produced, though the original (a)-component may be identified to γ'-FeNi phase. In the case of Y-790250 and Y-790448, it seems likely that relative amount of SD particles considerably increases oweing to the heat treatment.

Table 1. Examples of Magnetic Binary Structure of Chondrites

Meteorite		I_s (emu/g)	I_R/I_s	H_{RC}/H_C	m	H_C (a) (Oe)	H_C (b) (Oe)
St. Séverin (LL_6)	(B)	2.80	0.1785	3.54	0.417	1239	47
	(A)	3.95	0.0053	11.58	0.006	1240	6
Olivenza (LL_5)	(B)	2.7	0.1974	4.17	0.457	2160	62
	(A)	4.4	0.0034	3.40	~0	(-)	10
Y-74647 (H_{4-5})	(B)	35.7	0.0087	55.1	0.015	1284	9
	(A)	35.8	0.0014	10.0	~0	(-)	10
Y-7301 (H_4)	(B)	20.2	0.0064	84.1	0.009	3607	6
	(A)	17.1	0.0275	5.62	0.064	227	15
Y-74191 (L_3)	(B)	14.3	0.0147	28.30	0.031	901	14
	(A)	14.1	0.0064	21.80	0.006	975	9
Y-75354 (L_6)	(B)	21.8	0.0326	39.70	0.077	1925	15
	(A)	19.8	0.0043	15.1	~0	(-)	11
Y-74362 (L_6)	(B)	9.5	0.0382	23.77	0.093	1401	14
	(A)	11.4	0.0026	40.8	~0	(-)	6
Y-790250 (LL_4)	(B)	1.80	0.0256	8.03	0.059	465	22
	(A)	1.38	0.1500	2.31	0.355	238	20
Y-790448 (LL_3)	(B)	4.8	0.0231	10.76	0.052	518	18
	(A)	5.5	0.1016	2.55	0.245	303	27

(B): Before heat treatment. (A): After heating twice to 800°C.

4. Magnetic Binary Structure of Achondrites

Table 2 gives examples of the parameters of magnetic binary structure of eucrites and diogenites. It seems likely that metallic grains in these achondrites also consist of a magnetically hard (a)-component and a soft-(b) component, where (a)-component can be identified to SD particles of kamacite or taenite. In ALH-76005, Y-74037, Y-74097 and Y-74648, in particular, the heat treatment results in a considerable increase of relative amount of SD-particle component, while m-value is kept roughly invariant in the other 4 achondrites.

Table 2. Examples of Magnetic Binary Structure of Achondrites

Meteorite			I_S (emu/g)	I_R/I_S	H_{RC}/H_C	m	H_C (a) (Oe)	H_C (b) (Oe)
Y-74159	(Eu)	(B)	0.175	0.0543	6.32	0.103	263	11
		(A)	0.171	0.0567	7.79	0.108	410	13
Y-75011	(Eu)	(B)	0.27	0.0096	15.40	0.013	337	10
		(A)	0.52	0.0113	11.42	0.017	534	14
ALH-76005	(Eu)	(B)	0.17	0.0100	32.97	0.014	564	7
		(A)	0.157	0.0503	9.84	0.095	388	10
ALH-77302	(Eu)	(B)	0.028	0.1071	8.02	0.211	276	6
		(A)	0.024	0.1417	5.74	0.279	227	6
ALH-77005	(Sh)	(B)	0.173	0.1301	6.30	0.256	158	4
		(A)	0.145	0.1703	5.44	0.337	183	4
Y-74037	(Di)	(B)	0.218	0.0206	1.96	0.046	98	33
		(A)	0.250	0.0580	4.33	0.140	292	18
Y-74097	(Di)	(B)	0.318	0.0126	10.77	0.025	193	5
		(A)	0.435	0.0218	6.02	0.049	246	17
Y-74648	(Di)	(B)	0.20	0.0375	4.08	0.089	372	19
		(A)	0.50	0.2180	1.87	0.500	282	28

(B): Before heat treatment. (A): After heating twice to 800℃.

5. Magnetically Interactive Binary Structure

The thermal demagnetization curves of natural remanent magnetization (NRM) of chondrites exhibit considerably large fluctuation in intensity as well as in direction in most cases. This result suggests that individual ferromagnetic phases possessing respective NRM are mutually interacted in chondrites. A possible interaction between (a)- and (b)-components may be particularly effective. Possible interaction behaviours among magnetized particles or domains will be discussed in individual cases.

MELTING AND DEFORMATION OF A CHONDRITE BY SHOCK-LOADING

Masao KITAMURA, Akira TSUCHIYAMA, Seiko WATANABE,
Department of Geology and Mineralogy, Faculty of Science,
Kyoto University, Sakyo, Kyoto 606, Japan
Yasuhiko SYONO and Kiyoto FUKUOKA
Institute for Materials Research, Tohoku University,
Katahira, Sendai 980, Japan

Shock deformation is one of the most important processes during the accretion of planets and in the formation of meteorites. Shock deformation of rock-forming minerals has been extensively studied. However, few experiments have been carried out on rocks. Recently, Arai et al. (1987) studied shock melting of a mineral mixture with solar abundance in major elements. In their experiment, the material was completely melted with a flyer speed of 3 km/sec. In the present study, shock experiments of a chondrite and its powders were carried out under shock pressure lower than that by Arai et al. (1987), to elucidate the deformation process of the constituent minerals and melting process of the specimen.

[Experiments] An H6 chondrite (Cedar) was chosen as a starting material, because unequilibrated chondrites are heterogeneous and include glass, and among equilibrated chondrites L6 has shock veins. Three types of specimens with different porosities were prepared from the chondrite; (I) a rock chip (the porosity is almost 0), (II) powder of the chondrite with porosity of about 28 %, (III) powder with porosity of about 43 %. The type I specimens were sealed in a steel capsule after covering the specimen by Cu in order to protect contamination of Fe and Cr from the capsule. The types II and III specimens were sealed in copper capsules.

Six shock experiments were carried out using a powder gun of Tohoku University. Two different speeds of a flyer were chosen for each type of the specimen; 1.20 and 1.94 km/sec, which correspond to the pressure on the capsule of 25 and 45 GPa, respectively. The actual pressure on the specimen could not been estimated because shock impedances of the specimens have not been obtained. Thin sections of the recovered specimens were prepared for optical microscopy, back-scattered electron imaging (BEI) and electron microprobe analysis (EPMA).

[Results and Discussion] The type I specimens do not show any melting textures but shock veins were observed (Fig. 1). The veins, running at about 40° with the direction of the shock propagation, are filled with tiny grains of the constituent minerals of the chondrite (Fig. 2). Maskelynite (shock glass) was observed everywhere in the specimen. The maskelynite shows significant evaporation of Na during the point analysis of EPMA.

In the type II and III specimens, the shock veins were not found clearly. A BEI study revealed that interstices among large grains of olivine, pyroxene and plagioclase (maskelynite) show textures of both partial melting and evaporation (Fig. 3).

Eutectic melting of Fe and FeS was also observed. The type III specimens have the similar porosity to the specimen of the experiment by Arai et al. (1987). Therefore, the pressure for the melting of the chondritic materials with the porosity of about 45 % must be between 1.9 km/sec and 3 km/sec of the flyer speeds.

Although the effect of porosity to the melting was not clarified quantitatively in the present experiments, the partial melting and the evaporation must be accelerated by the porosity.

Arai,M., Sawamoto,H., Urakawa,S., Kato,M., Mizutani,H. & Kumazawa,M. (1987) Abstract in "Koatsu-toronnkai". 3C13.

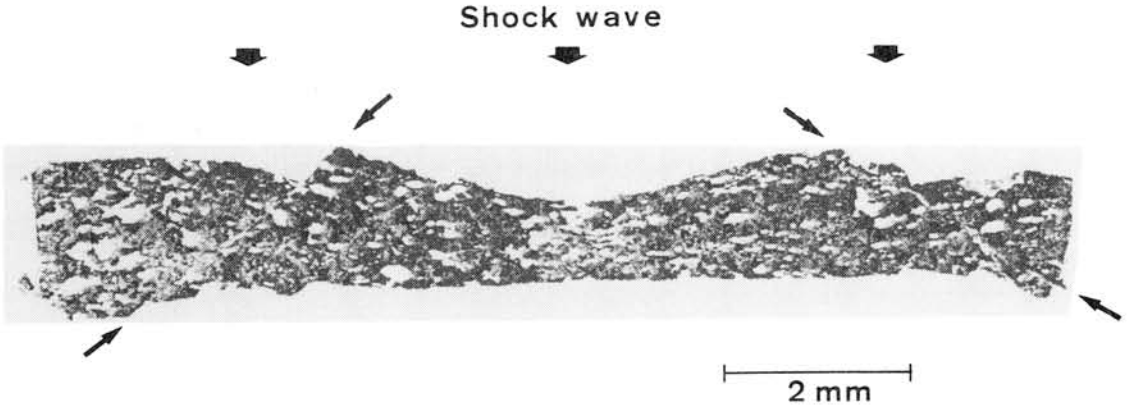

Fig.1. BEI of the Type I specimen (1.94 km/sec of the flyer speed). Note the shock veins running at about 40° with the direction of the shock propagation.

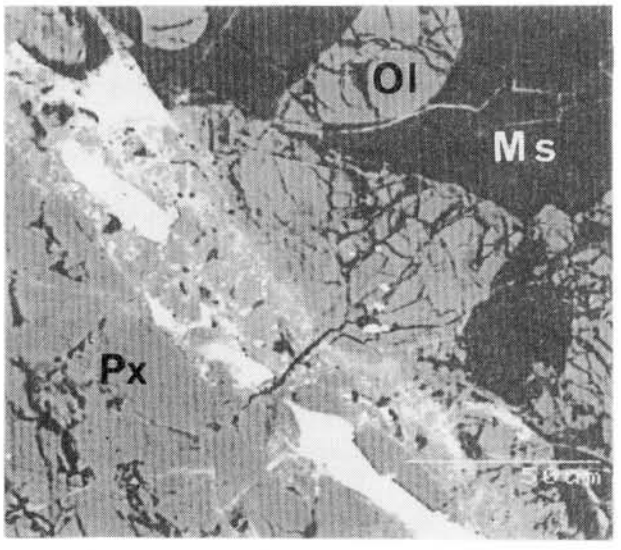

Fig. 2. Enlarged BEI of the shock vein of Fig. 1.

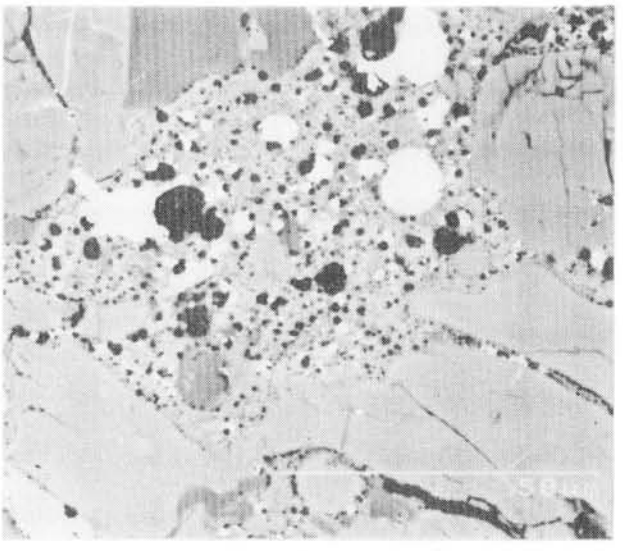

Fig. 3. BEI of the type III specimen (1.94 km/sec).

A NEW GAS CONDENSATION FURNACE AND ITS APPLICATION TO CONDENSATION IN THE SYSTEM Mg_2SiO_4-H_2.

Tsuchiyama, A.

Dept. Geology & Mineralogy, Kyoto University, Sakyo, Kyoto 606.

Condensation of minerals has played an important role in the primodial solar nebula. In the present study, a new vacuum furnace has been designed for studying condensation process in the nebula. Special attention was paid to obtaining a large amount of condensates which makes it easier to carry out their characterization, such as phase determination and chemical analysis. Condensation experiments were carried out by using this furnace in the system forsterite-H_2, which is one of the most simplest but important system.

The furnace consists of two vacuum chambers, one for samples and the other for a heater of tantalum (Fig.1). The sample chamber is evacuated by a turbo molecular pump to obtain clean vacuum up to 10^{-10} bar, and a constant $p(H_2)$ is maintained by bleeding of H_2 gas. Evaporation sources are placed at the bottom of a tantalum crucible in the sample chamber, and heated up to about 1800°C. A cold finger of molybdenum is put into the crucible for an evaporated gas to condensate. A molybdenum mesh, a sample holder for characterization by a TEM, is placed at the top of the cold finger. The condensation temperature measured by a W5Re-W26Re thermocouple can be changed by moving the cold finger. Metal wires (Mo or Ni) are also attached along the cold finger to examine change of condensates by temperature.

Condensation experiments were carried out by using forsterite evaporation source at $p(H_2)$ ranging from 1.6×10^{-5} to 1.4×10^{-7} bar. In the experiments, forsterite vaporized congruently at about 1635°C. Condensation temperatures were ranging from 850 to 1400°C. Condensation took place on the the chamber wall, which was kept at the room temperature, as well as on the cold finger. The following results were obtained. (1) Condensation takes place only at high pressures in which gas molecules collide with each other in the crucible. (2) Phases and average chemical compositions of the condensates are controlled mainly by the condensation temperature. (3) Chemical fractionation takes place in the furnace (Fig.3). With decreasing temperature the condensates are changing from forsterite flakes (Fig.2a), forsterite whiskers (Fig.2b), very fine mixtures of forsterite and silicon, Si-rich and O-poor amorphous material (Fig.4a) to Mg-rich and O-poor amorphous material (Fig.4b). (4) The forsterite whiskers grow by the VLS (Vapor-Liquid-Solid) mechanism [1] in which gas molecules are trapped into eutectic melt droplets on the top of the whiskers (M in Fig.2b) and then a whisker is grown from each melt droplet. (5) Large amounts of condensates (about 100 mg or more) can be obtained by the experiments for further studies of isotope and minor element compositions of condensates (phases included in the very fine mixtures, silicon and forsterite, were determined by the powder X-ray diffraction method in the present experiments).

Whiskers are found rarely in meteorites and cosmic dusts. However, their morphology might have been changed into bulky crystals by equilibration after the condensation because of their morphology. If condensation of whiskers took place commonly in the primodial solar nebula, current scenarios on the nebula should be reconstructed because the physical and chemical properties of whiskers, such as densities of their aggregates and chemical reactivity, are different from those of normal grains.

Reference: [1] Wagner,R.S. & Elis,W.C. (1965) Trans. Metal. Soc. AIME, **233**, 1053.

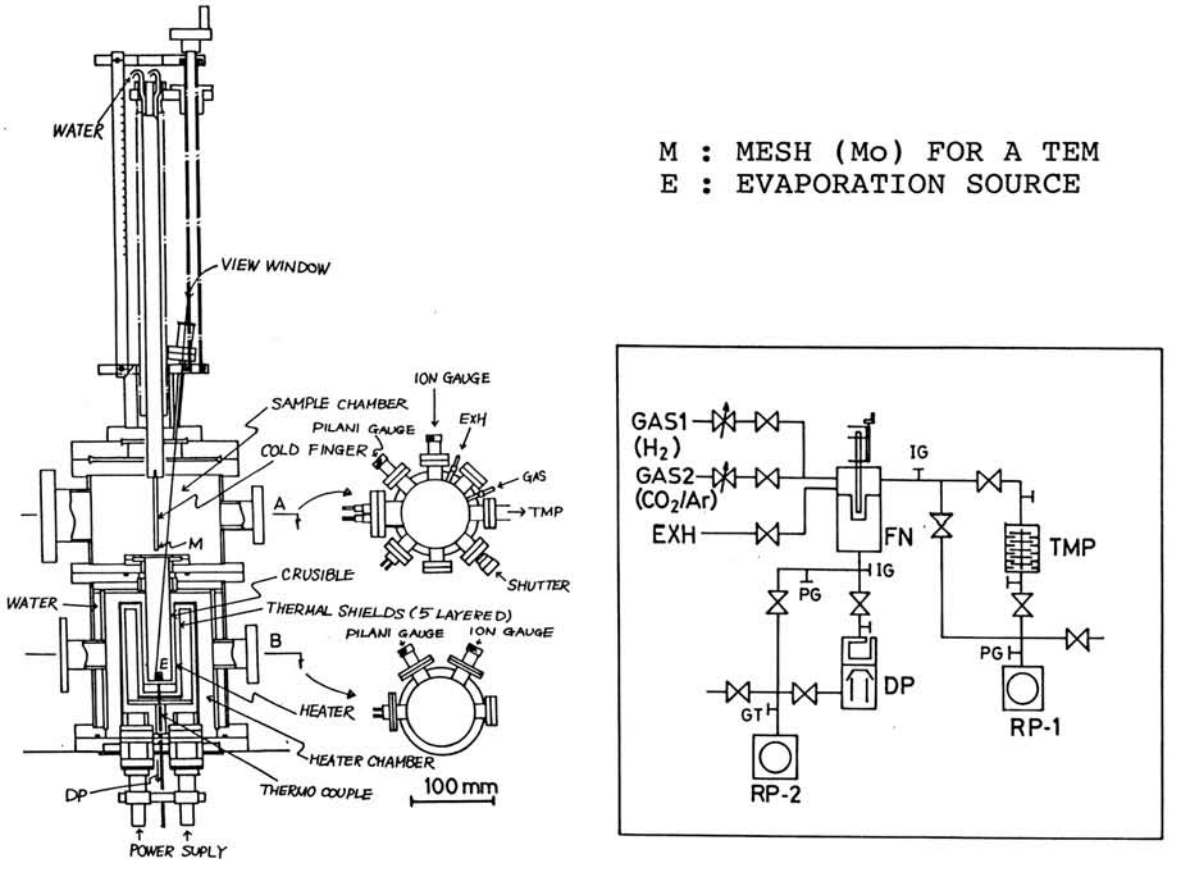

Fig.1. A gas condensation furnace.

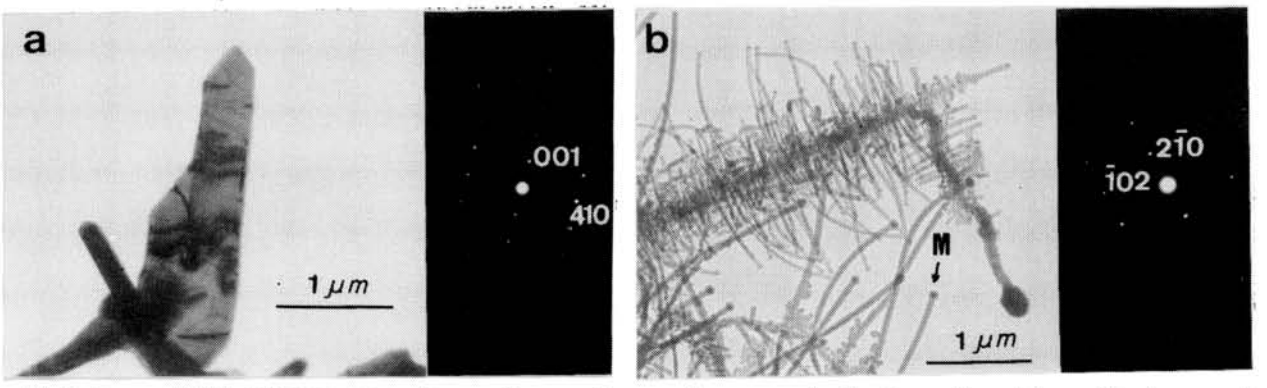

Fig.2. TEM micrographs of condensates. (a) Forsterite flakes at 1060°C. (b) Forsterite whiskers with melt droplets (M) at 850°C.

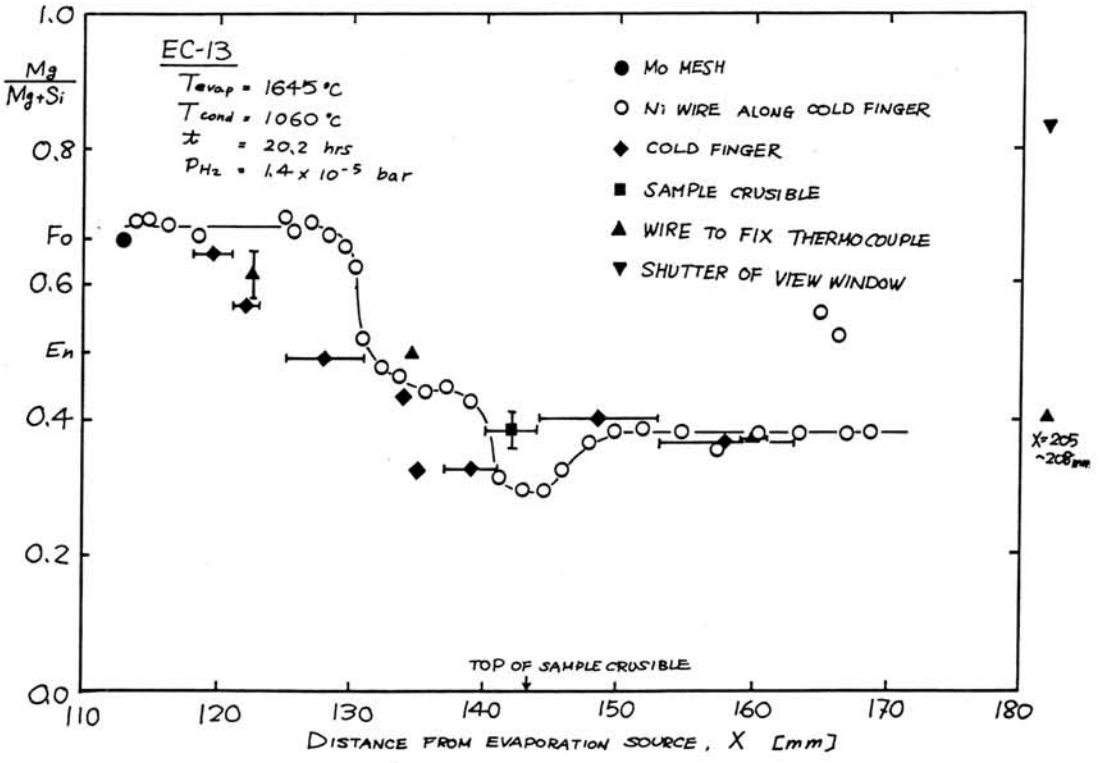

Fig.3. The average Mg/(Si+Mg) ratio of condensates as a function of the distance from the evaporation source, X.

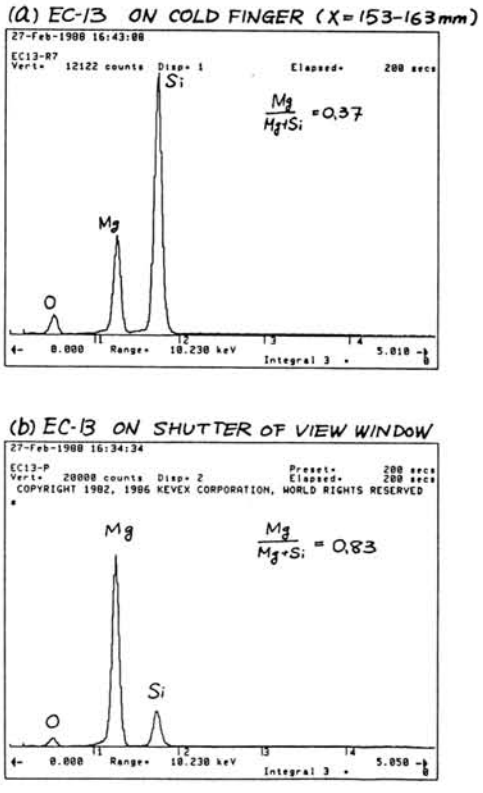

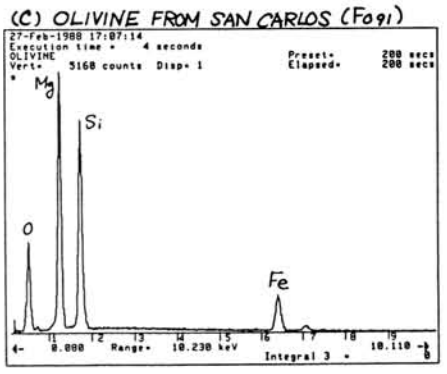

Fig.4. Specific X-ray spectra of condensates by using an ultra thin window EDX detector. Olivine from San Carlos (Fo_{91}) as a reference.

YAMATO-82162: A NEW KIND OF CI CARBONACEOUS CHONDRITE FOUND IN ANTARCTICA

Kazushige Tomeoka*, Hideyasu Kojima#, and Keizo Yanai#, * Mineralogical Institute, Faculty of Science, University of Tokyo, Hongo, Bunkyo-ku, Tokyo, 113; # National Institute of Polar Research, 9-10, Kaga 1-chome, Itabashi-ku, Tokyo 173

INTRODUCTION: Among nearly seven thousand meteorite samples found in Antarctica, Yamato-82162 (Y-82162) is probably the first sample that can be classified as a CI chondrite [1]. However, this meteorite shows many mineralogical features that apparently differ from the known CI chondrites, suggesting that it has a unique formation history compared to other CI chondrites. We present here the results of petrographic, scanning electron microscope (SEM), and transmission electron microsocope (TEM) studies of the Y-82162 chondrite.

GENERAL PETROGRAPHIC FEATURES: Y-82162 is a breccia composed of millimeter to submillimeter clasts. The clasts consist almost entirely of extremely fine-grained, optically black matrix. No chondrules and aggregates of anhydrous silicates are found. Magnetite occurs in a variety of forms characteristic of CI chondrites: (1) framboidal aggregates [2], (2) plaquettes (stacks of dicks) [3], (3) spherulites [4], and (4) polygonal to subrounded particles (0.2 to 2.0 μm in diameter). Like many CI chondrites, Mg-Fe-Mn-bearing carbonates, mostly breunnerite and magnesian siderite, are common as relatively large grains (~100 μm), many of which contain minute grains bearing Fe and S, probably Fe-sulfide. Ca-phosphate occurs in association with the carbonates.

A marked differece from the CI chondrites is that most S in Y-82162 occurs as Fe-(Ni) sulfides, primarily pyrrhotite and less pentlandite. Volumetrically, the sulfides constitute ~10 % of the meteorite and are much more abundant than magnetite (~0.5 vol%). They occur in lath-like and euhedral grains (50 to 200 μm in the largest dimension) and also in fine grains (<1 to 5 μm). In the Alais, Ivuna, and Orgueil CI chondrites, Mg-, Ca-sulfates are common as fracture-filling veins [5-7], but they are absent in Y-82162. Dolomite that is also common in the CI chondrites is rare.

MATRIX AND PHYLLOSILICATES: Recently, Tomeoka and Buseck [8] showed that the matrix of the Orgueil CI chondrite consists of a heterogeneous, submicron mixture of serpentine, saponite, and S- and Ni-bearing ferrihydrite ($5Fe_2O_3$ $9H_2O$). The serpentine and saponite are coherently intergrown and occur in poorly crystallized platelets, in intimate association with the ferrihydrite. Because of the submicron mixture of those minerals, microprobe analyses of the Orgueil matrix show correlations between Fe, Ni, and S and also inverse correlations of these elements with Si, Mg, and Al. However, the matrix of Y-82162 shows no such obvious correlations, suggesting that its mineralogy is different from Orgueil.

Our TEM observations of the Y-82162 matrix show that it consists in large part of fine-grained phyllosilicates. The phyllosilicates generally have larger grain sizes than those in Orgueil, but their crystallinity is very poor. Ferrihydrite is much less abundant in Y-82162 than in Orgueil. Noted is that extremely fine grains (<<1000 A in diameter) of Mg-Fe silicates, probably pyroxene and/or olivine, Fe-Ni sulfides, both pyrrhotite and pentlandite, and Mg-Fe carbonates are abundant and are intimately associated with the phyllosilicates.

Phyllosilicates that are relatively coarsely crystallized ("coarse

phyllosilicates") occur in isolated clusters (10 to 300 μm in diameter). The coarse phyllosilicates are more abundant and occur in much larger clusters than in Orgueil. In the Fe-(Si+Al)-Mg ternary diagram [8], analyses of the Y-82162 phyllosilicates plot between serpentine and smectite solid solution lines but mostly concentrate near saponite. Compared to the phyllosilicates in Orgueil, they are significantly richer in Na (up to 5 wt% as Na_2O) and Al (up to 6 wt% as Al_2O_3).

CONCLUSIONS: Although the general petrology of Y-82162 most resembles the CI chondrites, its detailed mineralogy differs. The low H_2O content and the high abundance of Fe-sulfides suggest that Y-82162 has been affected by a heating event after the formation of phyllosilicates and possibly other hydrous minerals. Alternatively, this meteorite may not have experienced the late aqueous alteration stage that resulted in veins of sulfates in other CI chondrites; thus it may represent the mineralogy prior to the aqueous alteration responsible for the sulfate formation. Especially, the high abundance of the coarse phyllosilicates and the sparsity of ferrihydrite appear to support this hypothesis. More detailed mineralogical investigations are in progress, and those studies combined with chemical and isotopic analyses would shed further light on this matter.

REFERENCES:

[1] H. Kojima and K. Yanai (1987) Abstr. 12th Symposium on Antarctic Meteorites, 8-1.
[2] J.F. Kerridge (1970) Earth Planet. Sci. Lett. 9, 299.
[3] J. Jedwab (1971) Icarus 35, 319.
[4] J.F. Kerridge, A.L. Mackay, and W.V. Boynton (1979) Science 205, 395.
[5] E.R. DuFresne and E. Anders (1962) Geochim. Cosmochim. Acta 26, 1085.
[6] K. Bostrom and K. Fredriksson (1966) Smithson. Misc. Collect. 151, 1.
[7] S.M. Richardson (1978) Meteoritics 13,141.
[8] K. Tomeoka and P.R. Buseck (1988) Geochim. Cosmochim. Acta (in press).

A PRELIMINARY REPORT OF MINERALOGY OF Y-82162 (CI)

Seiko WATANABE, Akira TSUCHIYAMA and Masao KITAMURA
Department of Geology and Mineralogy, Faculty of Science, Kyoto University, Sakyo, Kyoto 606, Japan

Two thin sections of a carbonaceous chondrite (Yamato 82162; CI) were studied by optical microscopy, back-scattered electron imaging and EPMA analysis. Y82162 shows clastic texture having veins. Chondrules are absent. Coarse materials dispersed in matrices are (1) clusters of phyllosilicates, (2) aggregates and separate grains of pyrrhotite and probably hydroxides, and (3) probably carbonate grains.

Matrix. Matrix is complex mixture in submicron scale of more than two kinds of phyllosilicates and/or poorly crystalline materials, sulfides, and so on. Each minerals could not be characterized, because the grain sizes are too small even for BEI. Only planar analyses (about 30 μm x 30 μm) were carried out to obtain average composition. The H_2O and CO_2 contents and Fe^{2+}/Fe^{3+} ratio could not be estimated by conventional EPMA analyses. Matrix composition slightly differs among the clasts (Fig. 1). Analytical results are consistent with predominance of serpentine and saponite (Tomeoka & Buseck, 1988).

Clusters of phyllosilicate. Coarse (10 μm - 200 μm) phyllosilicate-clusters in irregular shapes (Fig. 2a) are dispersed throughout the thin sections. Some of them include pyrrhotite. Chemical compositions of the clusters (Fig. 1) show that the Na content is higher than those of the matrix, the phyllosilicates in CI and CM chondrites, and the upper limit of smectite. Candidates for the phyllosilicate are Na-rich glauconite and Na-analogue of phlogopite. Chemical composition of the clusters is consistent with their formation by hydrous alteration from olivine and/or pyroxene + albite.

Small equant clusters consisting of phyllosilicates (several μm) were observed (Fig. 2b). The shape of the clusters is considered to be pseudomorph of a precursing euhedral crystal. Their composition corresponds to olivine + pyroxene + small amount of albite + possibly H_2O, and can be explained by hydrous alteration. The precursing mineral may be olivine based on the morphology.

Hydroxides. Fe-oxide occurs as separate grains, aggregates of small spherules (~ 1 μm), and large spherules. Composition of the phase can be explained as FeO(OH). This is considered to be formed by hydrous alteration from magnetite or hematite. Oxide or probably hydroxide grains (few tens μm) of Ca, Mg, and Fe surrounding pyrrhotite are common.

Others. Several Mn-rich aggregates were found. Pseudomorphous grains now consisting of tiny grains (~ 0.1 μm) are in the aggregates. MgO, Fe_2O_3, and some CO_2 were detected with Mg/Fe atomic ratio about 3.5. Precursing mineral may be

$(Mg,Fe,Mn)CO_3$. Groundmass among the pseudomorphous grains consists of similar tiny grains and Mn-rich grains ($\sim$ 1 μm). Chemical analyses of these grains gave MnO (or Mn_2O_3), S (or SO_3), CaO, little SiO_2, MgO, and Fe_2O_3 with Mg/Fe about 3.5. The grains may be Mn_3O_4, MnO_2, MnO H_2O, or $Mn_2O_3 \cdot H_2O$.

Small whitlockite (1 μm - 10 μm) are also frequent. An orthopyroxene ($Wo_3En_{93}Fs_4$) grain (Fig. 2a) was found.

Veins. Some veins were analyzed qualitatively using an EDX with an ultra thin window. The results suggest magnesite.

Above characteristics of Y-82162 do not conflict with that this meteorite experienced hydrous alternation.

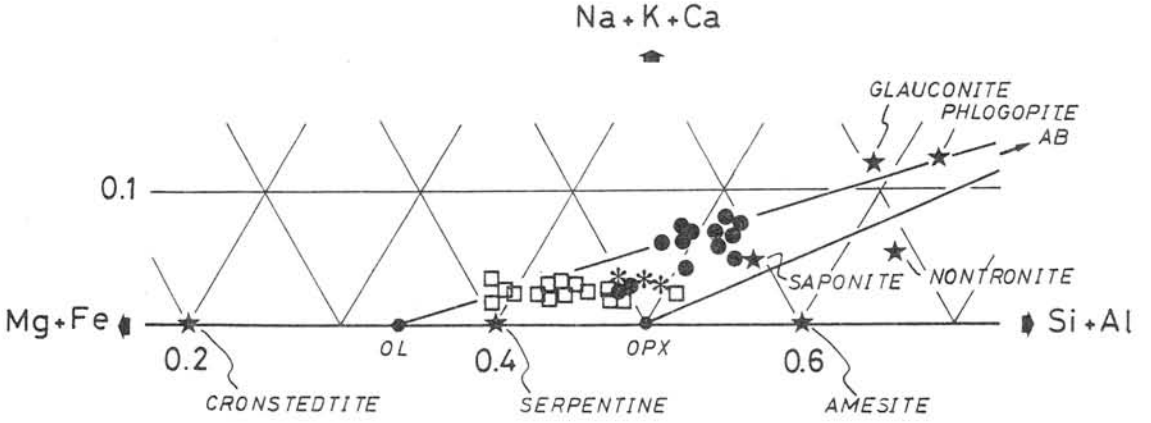

Fig.1 (Na+K+Ca)-(Mg+Fe)-(Si+Al) atomic ratio of matrix (□), coarse (●) and small equant (✱) phyllosilicate-clusters determined by EPMA.

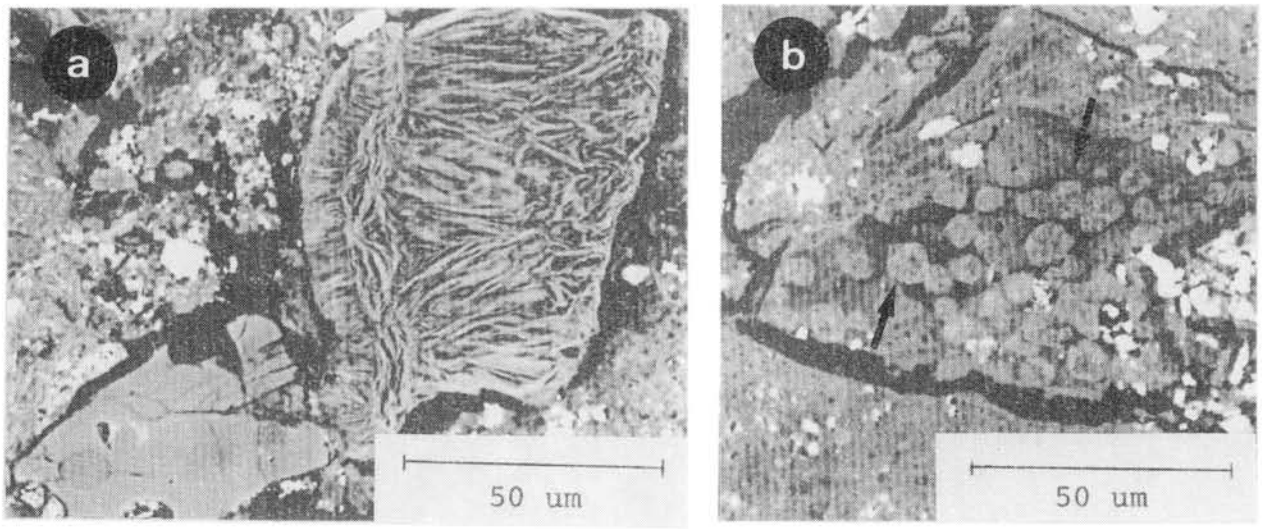

Fig.2 (a) BEI of coarse phyllosilicate-cluster (right) and orthopyroxene (left). (b) BEI of small equant clusters of phyllosilicate.

YAMATO-86720: AN EXTENSIVELY ALTERED AND THERMALLY METAMORPHOSED CM CARBONACEOUS CHONDRITE?

Kazushige Tomeoka*, Hideyasu Kojima#, Keizo Yanai#, * Mineralogical Institute, Faculty of Science, University of Tokyo, Hongo, Bunkyo-ku, Tokyo 113; # National Institute of Polar Research, 9-10, Kaga 1-chome, Itabashi-ku, Tokyo 173

INTRODUCTION: Yamato-86720 (Y-86720) is a carbonaceous chondrite that consists largely of dark, fine-grained matrix, and thus it resembles CI chondrites. However, its petrology and mineralogy apparently do not conform to CI chondrites. This meteorite may be a highly altered CM chondrite in that it contains replaced chondrules and aggregates, but it shows many mineralogical characters that differ from CM chondrites. We report here the results of our detailed petrographic and transmission electron microscope studies of the Y-86720 chondrite.

GENERAL PETROGRAPHY: Y-86720 has an unusually high abundance of Fe-sulfides, primarily troilite (nearly 10 vol% of the meteorite). Troilite occurs in large laths (50 to 200 μm in length and 10 to 50 μm in width) and also in rounded or irregularly-shaped fine grains (<1 to 20 μm in diameter). The latter are widely dispersed throughout the matrix. Many of the large sulfide grains are finely fractured and disaggregated. The sulfides are commonly replaced by ferrihydrite-like material that contains small amounts of Si and Mg. Magnetite occurs in fine grains, but no such framboidal aggregates as in the CI chondrites are found. Chondrules, aggregates, and inclusions that range in size from 100 μm to 1 mm are completely replaced by brownish, translucent material.

MATRIX: Microprobe analyses of the matrix using defocussed electron beam plot close to the CI area in the Fe-Si-Mg ternary diagram of McSween [1], which is consistent with that Y-86720 is a highly altered CM chondrite. The analyses are relatively high in their summations compared to other CI and CM matrices. The matrix shows large variations in Fe contents (from 10 to 50 wt% as FeO) with lesser variations in Mg/(Si+Al) ratios. The Fe contents are particularly high in the areas where the Fe-sulfides are concentrated. The matrix has numerous voids; they are common near the sulfide grains. These compositional and textural features suggest that Y-86720 has been thermally metamorphosed.

Our TEM observations show that the matrix consists of fibrous phyllosilicate-like material that is very poorly crystallized and shows only broad diffraction rings. Fine grains (<1000 A) of Mg-Fe silicates, probably pyroxene and/or olivine, occur in intimate association with the fibrous material. These mineralogical and textural features are reminiscent of the Y-82162 chondrite [2].

CHONDRULES AND AGGREGATES: The brownish, translucent material that replaced chondrules and aggregates contains major Si and variable Fe and Mg, and minor Al and Na, and it is probably a phyllosilicate(s). It has a range of (Mg+Fe)/(Si+Al) ratios between smectite and serpentine. However, like the matrix it shows consistently high summations in its microprobe analyses relative to ordinary phyllosilicates, again suggesting dehydration and recrystallization. We found an inclusion (~600 μm in diameter) that contains an unusually high Al silicate and abundant ilmenite grains as well as the phyllosilicate; it may be a pseudomporph of a calcium- and aluminum-rich inclusion.

CONCLUSIONS: These results, taken together, suggest that Y-86720 is a CM chondrite that was extensively affected by aqueous alteration; the degree of alteration is one of the highest among the CM chondrites. Although overall mineralogies are distinct, Y-86720 and Y-82162 show certain common features [2], particularly the low H_2O contents and the high abundance of Fe-sulfides, suggesting both have experienced similar heating events after the aqueous alteration.

REFERENCES:

[1] H.Y. McSween (1979) Geochim. Cosmochim. Acta 43, 1761; ---- (1987) Geochim. Cosmochim. Acta 51, 2469.
[2] K. Tomeoka, H. Kojima and K. Yanai (1988) (A companion paper in this volume).

COMPOSITIONAL STUDY OF CARBONACEOUS CHONDRITES WITH CI-CM AFFINITIES

Gregory W. Kallemeyn
Institute of Geophysics and Planetary Physics, University of California, Los Angeles, CA 90024

A compositional study is underway on three Antarctic meteorites: Belgica 7904, Yamato 82162 and Yamato 86720. Oxygen isotope studies (Mayeda et al., 1987) show Belgica 7904 and Yamato 82162 fall in the CI range. Previously Belgica 7904 was classified as CM (Yanai and Kojima, 1985) or anomalous CM (Kallemeyn, 1986; Skirius et al., 1986). A petrographic study of Yamato 82162 (Kojima and Yanai, 1987) supports a close relationship to CI chondrites. The preliminary report on Yamato 86720 (Yanai and Kojima, 1987) suggested it may also have an affinitiy to CI chondrites. Preliminary data are reported here for some 28 elements determined by neutron activation analyses in replicate samples of Belgica 7904 and Yamato 86720, and a single sample of Yamato 82162.

Plotted in Fig. 1 are ratios of refractory Al and volatile Zn to moderately volatile Mn for the three chondrites and for CI and CM falls analyzed by this lab. Kallemeyn and Wasson (1981) showed that these ratios were useful in classifying carbonaceous chondrites. Yamato 82162 forms a tight cluster with the CI falls, while Belgica 7904 falls near the tight cluster of CM falls. Yamato 86720 plots far from both clusters. Refractory element ratios plotted in Fig. 2 show both Yamato 82162 and Yamato 86720 clustering with CI, while Belgica 7904 again clusters with CM. With the volatile chalcophile Se plotted against refractory Al (Fig. 3), Yamato 82162 and Belgica 7904 once again form distinct clusters with CI and CM falls, while Yamato 86720 plots intermediate. Plotted in Fig. 4 are moderately volatile Au and refractory Ir to Ni ratios. Yamato 86720 and Belgica 7904 plot with the CM falls. Because of its very low Au content Yamato 82162 does not plot very close to the CI falls, but shows no affinity to CM. The CI falls show a relatively wide range of Au concentrations, and the value for Yamato 82162 may just be an extension of that range. Plots of other data not shown here tend to cluster Yamato 82162 with CI falls and Belgica 7904 with CM falls, although Belgica 7904 often plots just outside the cluster of falls. Yamato 86720 usually plots intermediate or with the CM falls.

The compostional data along with the oxygen isotope data tend to support a CI classification for Yamato 82162. Despite the CI-like oxygen isotope data for Belgica 7904, the compositional data seem to support a CM-anomalous classification. The compositonal data for Yamato 86720 weakly group it with CM chondrites, though it may be intermediate between CI and CM.

References: Kojima and Yanai (1987) 12th Sym. Ant. Met., 15; Kallemeyn and Wasson (1981) Geochim. Cosmochim. Acta, 45, 1217-1230; Mayeda et al. (1987) Mem. Natl. Inst. Polar Res., 46, 144-150; Yanai and Kojima (1985) Met. News, 4.

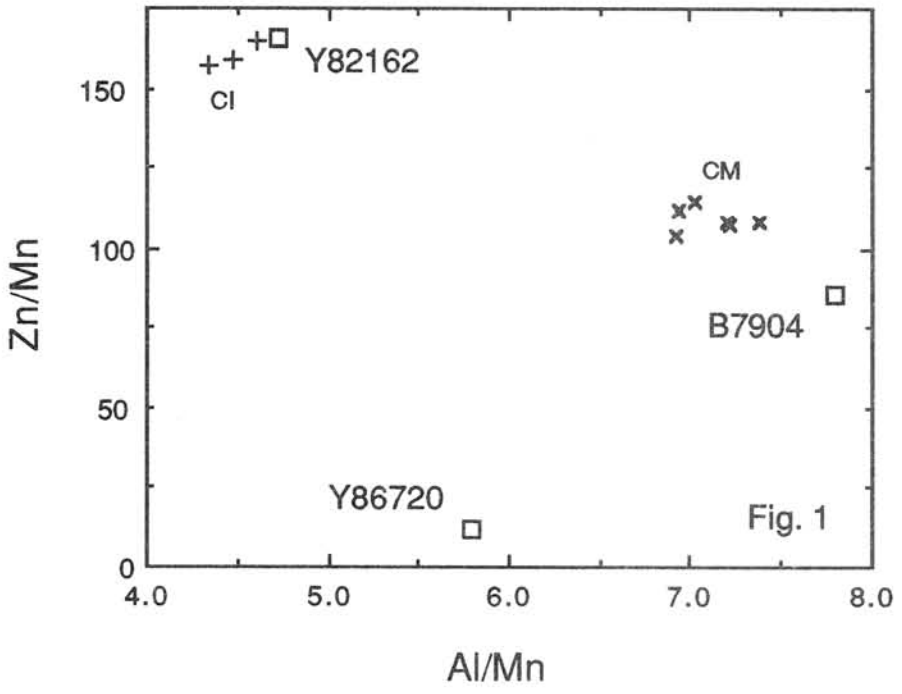
Y82162
CI
CM
B7904
Y86720
Fig. 1
Zn/Mn
Al/Mn
150
100
50
0
4.0
5.0
6.0
7.0
8.0

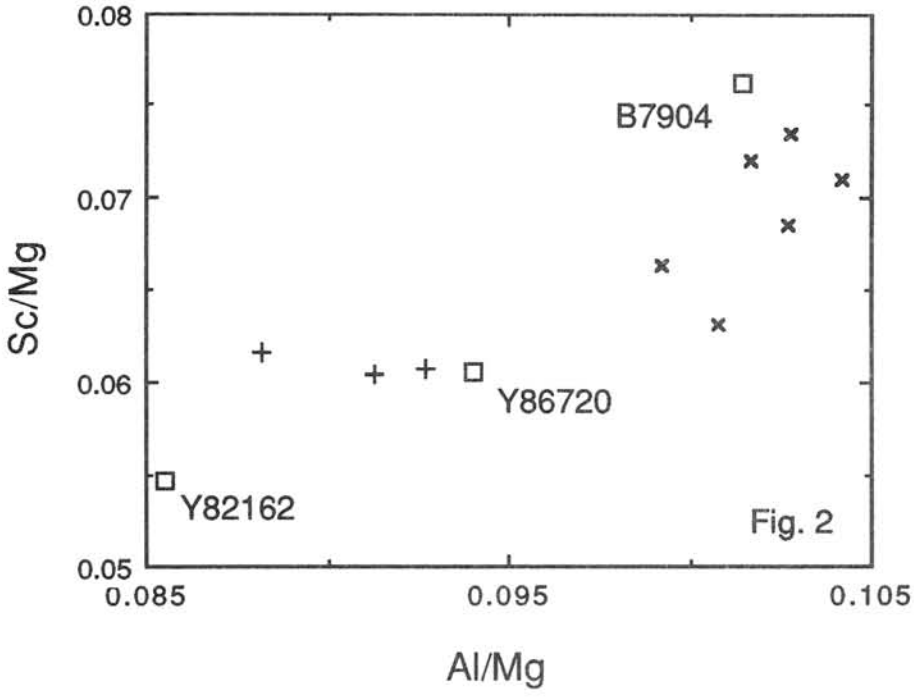
B7904
Y86720
Y82162
Fig. 2
Sc/Mg
Al/Mg
0.08
0.07
0.06
0.05
0.085
0.095
0.105

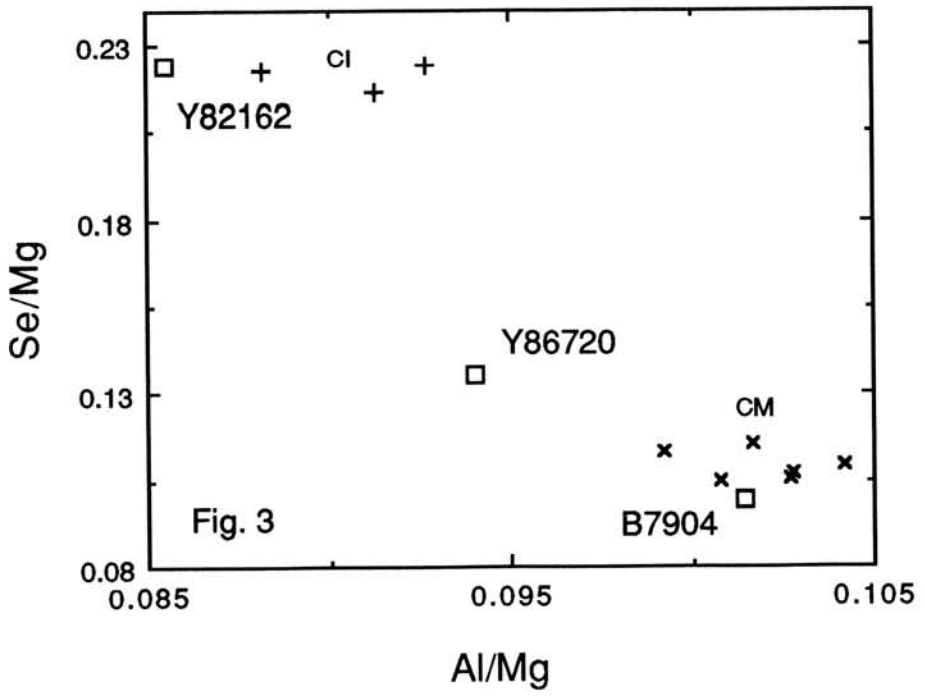
0.23
0.18
0.13
0.08
0.085
0.095
0.105
Se/Mg
Al/Mg
CI
Y82162
Y86720
CM
B7904
Fig. 3

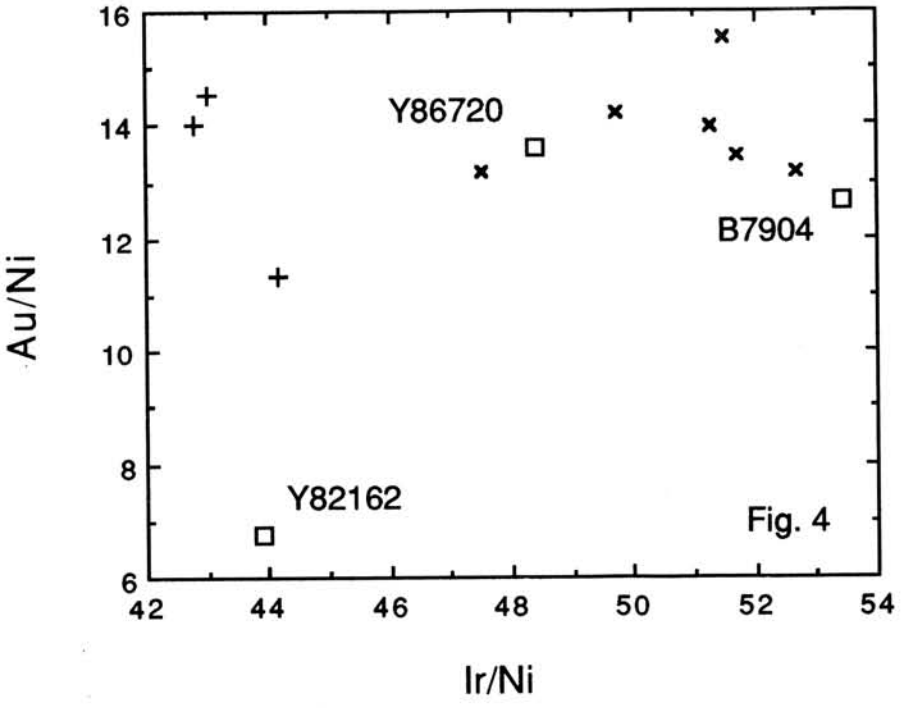
16
14
12
10
8
6
42
44
46
48
50
52
54
Au/Ni
Ir/Ni
Y86720
B7904
Y82162
Fig. 4

CRITICAL ANALYSIS OF THE APPLICATION OF THE SPHALERITE COSMOBAROMETER TO EH CHONDRITES.

El Goresy, A. and Ehlers, K.

Max-Planck-Institut für Kernphysik, P.O. Box 103980, 6900 Heidelberg, FRG.

Recent experimental investigations on the effect of pressure on the solubility of Fe in sphalerite (1) seem to offer a promising tool for estimation of total pressures in meteorites and ultimately estimation of sizes of meteorite parent bodies. The experimental data may also reveal information on the closure temperature of Fe diffusion in sphalerite (2). In order to test the application of the sphalerite cosmobarometer, sphalerite-bearing assemblages in the EH chondrites Yamato 691 (EH3), Qingzhen (EH3), and Indarch (EH4) were studied with the SEM and the electron microprobe. Recent investigations on these meteorites revealed that they were subjected to metamorphic events in their parent bodies (3). Niningerites in the three chondrites display reverse zoning indicative of Fe diffusion from troilite as a result of the thermal episodes (3). An important question is if the sphalerites readjusted their compositions to the PT conditions several times: a) subsequent to their accretion in the parent asteroid, and b) at least once more during the young thermal episode (1.4 BA for Qingzhen and 800 MA for Yamato 691).

Sphalerite in Qingzhen displays complex textural and chemical zoning characteristics. The cores of the grains contain bright and dark zones with various FeS-contents (47.1 and 49.7 mole % FeS respectively). The FeS-content decreases to 45.9 mole % to the rim to the neighbouring troilite. Exsolution lamellae of troilite were also encountered in several grains. The FeS-contents in these grains also decrease to a value as low as 45.5 mole % FeS near the contact to the lamellae. In Yamato 691, three different sphalerites were found: a) Unzoned primary sphalerite (48.5 - 50.2 mole % FeS), b) Zoned porous sphalerite with higher FeS-contents in the core (49.7 - 51.3 mole % FeS), a steep descending FeS profile to the adjacent troilite, and a minimum value of 44.7 mole % FeS at the contact to troilite, c) secondary homogeneous sphalerite formed during a late metamorphic episode (800 MA ago) characterized by low FeS-content (43.2 - 42.3 mole % FeS). The descending concentration profiles in sphalerites in Qingzhen and Yamato 691 were probably produced by reequilibration of the sphalerites with the neighbouring troilites at high pressures. However, the composition of the sphalerite cores may reflect primordial compositions after sphalerite condensation but before its burial in the parent asteroid. From compositions of the cores we obtain closure temperatures between 731 K and 641 K, and 798 K and 712 K for sphalerites in Qingzhen and Yamato 691, respectively. From compositions of sphalerite rims we estimate that the reequilibration took place at 0.21 kbar in Qingzhen and at 0.88 kbar in Yamato 691 (Figure 1). However, these values are very probably unrealistic since Qingzhen and Yamato 691 were metamorphosed at different times and much later after accretion (1.4 BA and 800 MA, respectively).

Sphalerite in Indarch displays complex textures indicative of multiple metamorphic events. Its FeS-content varies between 53.0 and 56.0 mole %. The grains contain open pores and are subdivided by platelets arranged parallel to (111) planes of the original sphalerite. This is strongly suggestive of sphalerite-wurtzite inversion at high temperatures. Consequently, its composition cannot be used to unravel the pressure-temperature history of this meteorite. The textures argue for a violent event 4.2 BA ago.

References: (1) Hutchison, M. N. and Scott, S. D. (1983) Geochim. Cosmochim. Acta, 47, 101. (2) Kissin, S. A. (1986) Meteoritics, 21, No. 4, 417. (3) Ehlers, K. and El Goresy, A. (1988) Geochim. Cosmochim. Acta (in press).

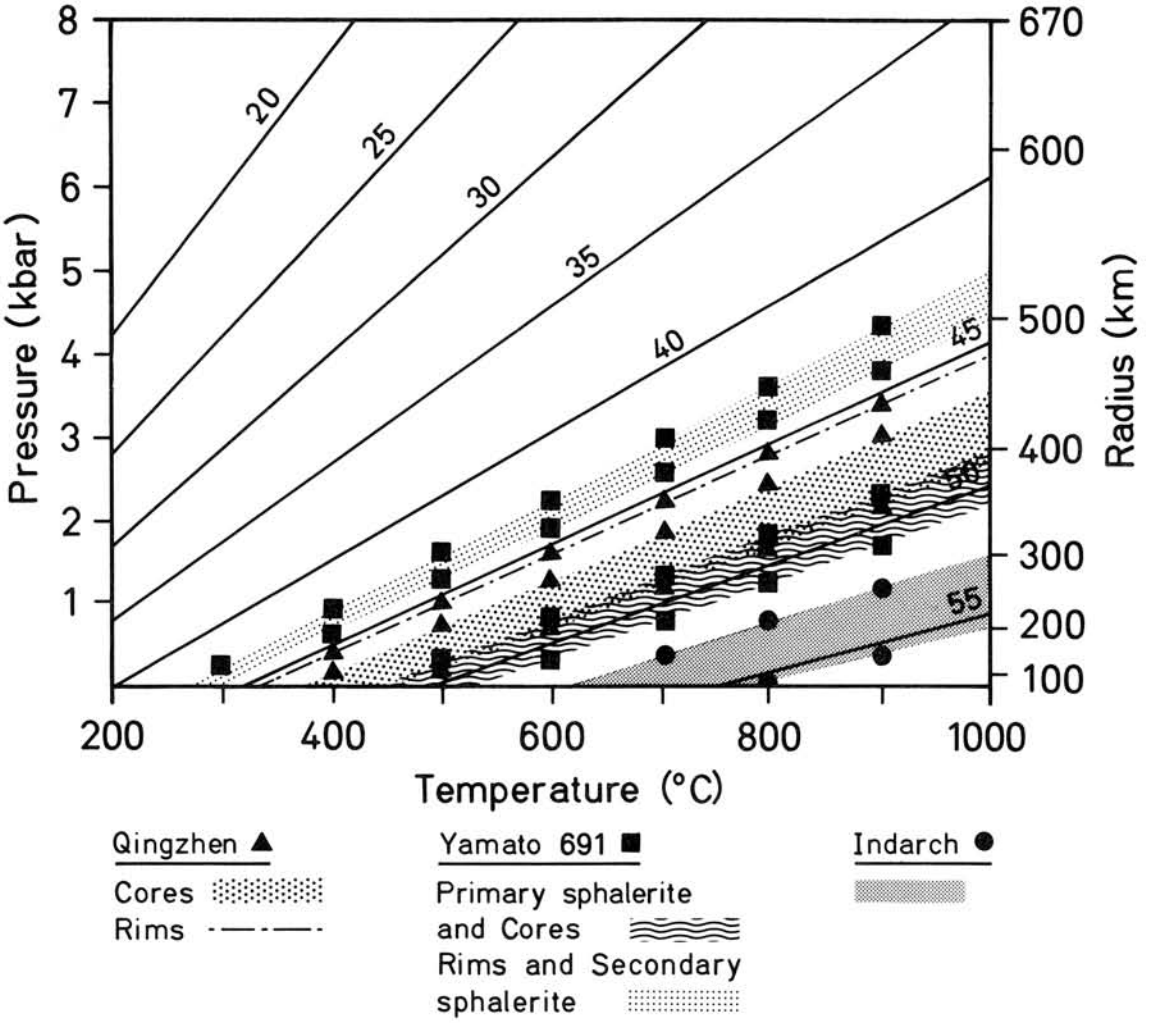

FIG. 1

CARBONACEOUS CHONDRITE OR SNC COMPOSITION FOR THE PHOBOS ?

Petr Jakeš[+], Zdenek Ceplecha [++]

\+ Geological Survey, Malostranské nám. 19, Praha 1 Czechoslovakia

++ Astronomical Institute of the Czechoslovak Academy of Sciences, Ondřejov, Czechoslovakia

During the days of this conference, a Soviet spacecraft has been launched to the Mars to measure the physical and chemical compositions and the properties of the Mars, one of its two moons the Phobos, and the space between the Earth and the Mars. There are about thirty different experiments on board of the spacecraft, some of them uniquely designed. Lima-D, for example, is an experiment programmed to measure the composition of Phobos´ surface by laser-beam excited mass spectra during the close approach of the spacecraft to the surface of the Phobos at a distance of around 50 meters.

The philosophy and working hypothesis of the mission to the Phobos are based on an assumption that the Phobos represents a captured asteroid of the C type and consequently that the Phobos is composed of carbonaceous chondrite. The arguments in support of the capture of a C-type asteroid include:

a) the extremely low albedo of the Phobos (around 0.05),
b) the relatively low density of the Phobos (2.2 ± 0.5 g.cm^{-3})
c) its irregular, "primitive" shape.

The case histories of two decades of planetary exploration have shown however, that none of the physical constrains presented in favour of the capture hypothesis is sufficiently rigid to exclude other models for the origin of the Phobos. Available data suggest also the possibility to relate the Phobos to SNC meteorites and to events which have sent SNC meteorites to trajectories towards the Earth. It is suggested that the Phobos was formed late in the history of the Mars (i.e. less than

$1,3.10^9$ years) by an impacting body of large size, probably by the same body which has sent SNC type Martian rocks to higher than Mars escape velocities. Collision ejection instead of non-disintegrative capture hypothesis is advocated.

a) The low albedo of the Phobos in such a hypothesis should be due to the presence of microsize particles representing an impact, or to condensed debris of basaltic composition settling at the surface after the collision. (The lowest albedo area on the Earth´s Moon is formed by debris of ghlassy basaltic compositions).

b) The density of the Phobos is not precisely determined but the given range offers either silicate or dirty ice compositions. Considering the upper densities, a combination of a silicate core and of a relatively thick regolith could be an explanation.

c) The irregular shape of the Phobos is a consequence of the suggested process.

d) Ceplecha (1979), using the example of the fireball of 10 Aug. 1972 tangentially approaching the Earth at low angle argued that non-disintegrative capture is a highly unlikely event.

e) The surface of the Mars´northern regions, the cratering of the Phobos, as well as the morphological features of the Phobos (e.g. grooves) suggest the origin in a higher gravity environment rather than at the present low-gravity one.

Though the authors are members of LIMA D (laser-induced mass spectrometry analysis) team,the view presented here is a private one, based on the notion that in a planetary research, expectations substantially differ from discoveries, and one should expect the unexpected.

MINERALOGY OF INTERSTITIAL RIM MATERIALS OF UREILITES AND THEIR ORIGIN

Ogata, H., Mori, H., and Takeda, H.

Mineralogical Inst., Faculty of Science, Univ. of Tokyo, Hongo, Tokyo 113.

Ureilites are carbon-bearing achondrites, consisting dominatly of coarse-grained pigeonite, olivine and carbonaceous matrix. In spite of their well developed plutonic textures, ureilites show oxygen isotope anomaly [1] and high planetary-type noble gas contents in the carbonaceous matrices [2]. Recently, interstitial pigeonitic materials are found in 11 ureilites [3, 4]. Y-74123 is suitable for a detail study of interstitial materials, because it is a relatively unshocked ureilite, most rich in olivine and interstitial pigeonitic materials [4, 5]. This work has been undertaken to gain better understanding of the nature of the interstitial materials and their origin. Rims around and glassy materials in cloudy pigeonites in Y-790981, which are considered to be produced by shock -induced partial melting [6] show similar chemical compositions to the Y-74123 interstitial materials [5]. Y-790981 also has been examined to compare with the interstitial materials of Y-74123.

Polished thin sections (PTS) of Y-74123 2-2, Y-74123 92-2 and Y-790981 42-2 were studied with an optical microscope, an electron probe (JEOL JCMA-733) and scanning electron microscope (JSM 840). Electron microscopy of ion-thinned samples made from fragments of Y-74123 and Y-790981 was carried out with a high resolution transmission electron microscope (TEM) and an analytical TEM.

Y-74123 is the most pigeonite poor ureilite [5]. Overall modal abundance of pigeonite is about 3 vol.%. They show a homogeneous chemical composition, $Ca_6Mg_{76}Fe_{18}$. Olivine core composition is Fa_{21} and the rims about 100-150 microns from the surface are reduced to more magnesian compositions by carbon. Dislocation recovery after shock has not been observed in Y-74123.

The Y-790981 olivine crystals show wavy extinction and subgrain boundaries and their core composition is Fa_{21} identical to that of Y-74123. The chemical compositions of the Y-790981 pigeonites within a crystal vary widely in the pyroxene quadrilateral because of the presence of glassy inclusions produced by shock, and the chemical compositions of the area without inclusions are clustered around $Ca_9Mg_{72}Fe_{19}$.

In Y-74123, the interstitial materials between olivine crystals show mostly thin film-like shape mantling olivine crystals and their thickness varies from 3 to 70 microns. The chemical composition of them shows relatively low-Ca and Al content. For example, the compositions of the material at the triple point juncture of three olivine crystals (Fig. 1a) are mostly $Ca_5Mg_{79}Fe_7$ to $Ca_{10}Mg_{88}Fe_{13}$ (Fig. 2) and the Al content is up to 1.2 wt.%. At a grain boundary between olivine and pigeonite, Ca-rich materials (augite) which include silica-rich islands extend into the olivine crystal (Fig. 1b). Some portions of the augite are Al-rich (6.6 wt.% Al_2O_3). Their chemical compositions are shown in Fig. 2.

Interstitial materials also are observed at a grain boundary of olivine and cloudy pigeonite in Y-790981 (Fig. 1c) in addition to the glassy materials. In cloudy pigeonite, bead-like pyroxenes are surrounded by fine thread-like Si, Al-glasses. In the bead-like pyroxene (Fig. 1c), light grey portion of the back-scattered electron image (BEI) is rich in Fe content, and dark grey is rich in Mg. Interstitial materials at the olivine rim are composed of high-Ca pyroxene, low-Ca pyroxene (Fig. 2) and

silica-rich glass with K_2O up to 1 wt% .

The TEM observation of the interstitial materials of Y-74123 shows that it consists of alternating pigeonite-augite lamellae on (001) (Fig. 3). The width of the pyroxene showing the lamellae texture is more than 3.5 microns thick, and any other phases are not observed in it. This microstructure is thought to have developed by the spinodal decomposition mechanism. The texture indicates the pyroxene may be sub-calcic augite and the wollastonite content is about 25. This value is in agreement with the data obtained by electron probe, The average (001) lamella wave length of the sub-calcic augite is 900 Å. The cooling rate estimated by a method based on an experimental calibration of augite exsolution lamella wave length vs. cooling rate [7] is 0.03°C/hour.

In a cloudy pigeonite of Y-790981, Ca-rich pyroxene, glass and chromite are formed (Fig. 4). A tiny metal grain and glass are also found adjacent to them. The glass is rich in Si, Al and Ca. Pigeonite lamellae sharing (001) with its host augite are observed at another part of the cloudy pigeonite. The bulk chemical composition of the augite-pigeonite lamellae obtained by broad beam scanning technique is $Wo_{30}En_{63}Fs_7$. Mori and Takeda [6] estimated the cooling rate of Y-790981 to be 3°C/hour by the same method.

The large size of the high-Ca pyroxene in the Y-74123 interstitial materials and the absence of any other phases nucleated in it (Fig. 3), in contrast to the Y-790981 cloudy pigeonite, in which many phases produced by shock partial melting coexist (Fig. 4), suggest the pyroxene had already crystallized when the excavation of parent mass took place.

The interstitial materials at olivine-pigeonite grain boundaries (Fig. 1b) have higher Al_2O_3 and CaO content than those at olivine-olivine grain boundaries (Fig. 1a) and are enclosed in olivine grains (Fig. 1b). Their bulk chemical composition obtained by broad beam analysis has higher Al_2O_3 and CaO than that of the core olivine and that of core pigeonite. From these fact, it may be inferred that some residual liquids of high Ca melts which lead the high Ca contents of ureilite olivines, might have been present at one time along grain boundaries, and later a part of them was removed and the rests were mixed with partial melts of olivines and pigeonites produced by heating events, probably by impacts, before the parent body breakup. When the grains of olivine and pigeonite are growing larger, they are acumulated into the grain boundaries and some of them are trapped in grains. The presence of exolved pyroxenes in the rim materials suggest that they were already solidified at the time of the breakup.

We thank NIPR for the meteorite samples and Mr. O. Tachikawa for the techical assistances.

References:

[1] Clayton R. N. and Mayeda T. Y. (1988) Geochim. Cosmochim. Acta 52, (in press).
[2] Begemann F. and Ott U. (1983) Geochim. Cosmochim. Acta 47, 975-977.
[3] Goodrich C. A. (1986) Lunar Planet. Sci. 17, 273-274.
[4] Ogata H., Takeda H. and Ishii T. (1987) Lunar and Planetary Science XVIII, 738-739, Lunar and Planetary Institute, Houston.
[5] Takeda H. (1987) Earth Planet. Sci. Lett. 81, 358-370.
[6] Mori H. and Takeda, H. (1983) Meteoritics 18, 358-359.
[7] Grove T. L. (1982) Am. Min. 67, 251-268.

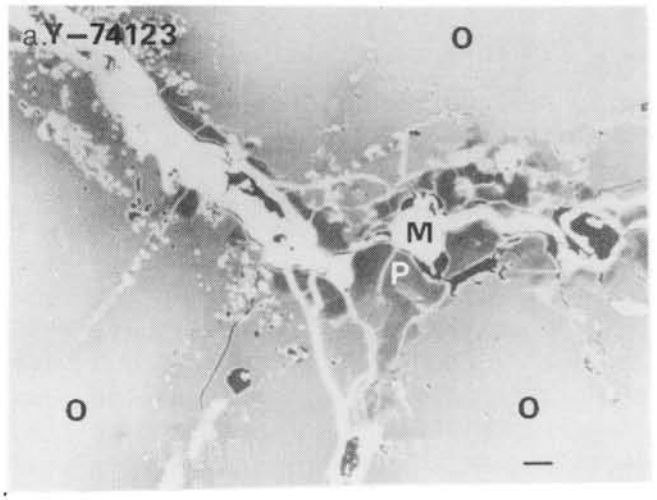

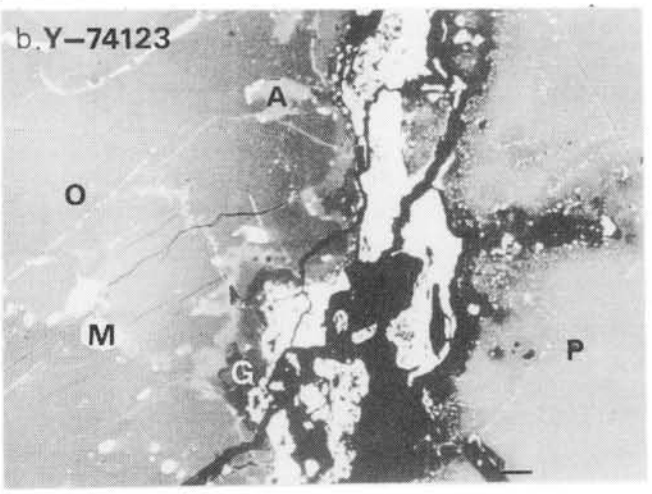

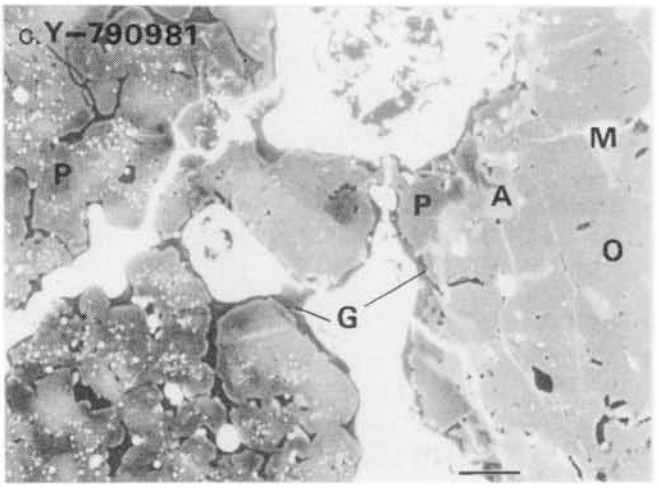

Fig. 1 BEI of interstitial materials. The scale bar is 10 microns. O:olivine M:metal P:pigeonite G:glass A:augite
a at triple point juncture of olivines
b at grain boundary between olivine and pigeonite
c at grain boundary between olivine and cloudy pigeonite

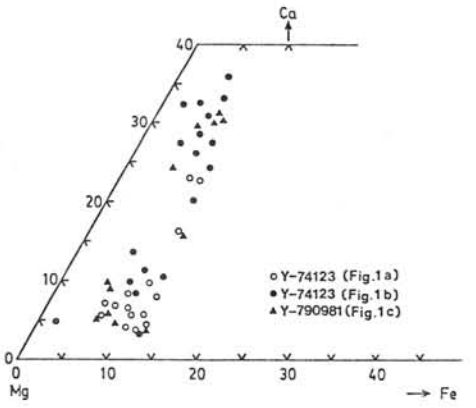

Fig. 2 Chemical compositions of interstitial pyroxenes of Fig. 1.

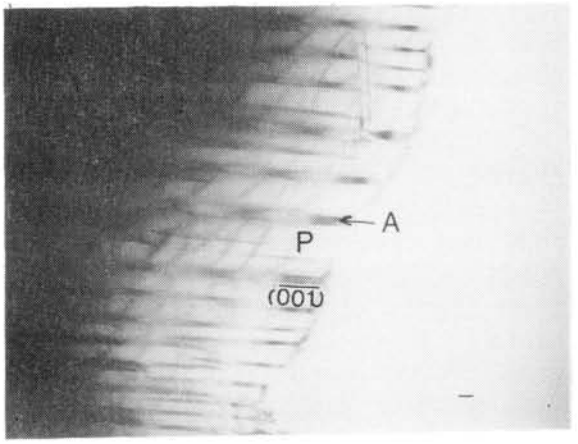

Fig. 3 Electron micrograph of (001) pigeonite(P)-augite(A) lamellae in interstitial materials of Y-74123. The scale bar is 1000Å.

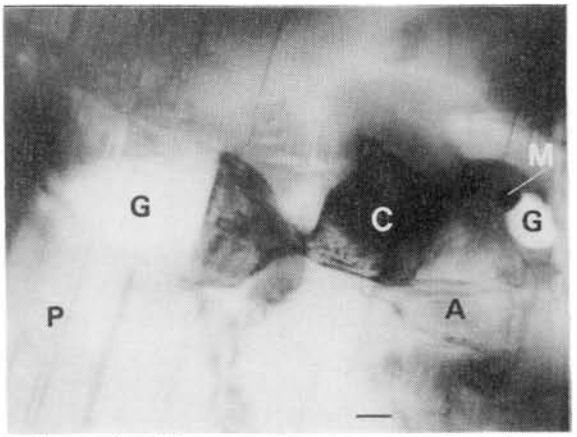

Fig. 4 Electron micrograph of augite(A), chromite(C), metal (M) and glass(G) in a cloudy pigeonite(P) of Y-790981. The scale bar is 1000 Å.

MINERALOGY OF SLOWLY COOLED EUCRITES AND THERMAL HISTORIES OF THE HED PARENT BODY.

Takeda, Hiroshi[1] and Tagai, Tokuhei[1] and Graham, A. L.[2]
[1]Mineralogical Inst., Faculty of Science, Univ. of Tokyo, Hongo, Tokyo 113.
[2]Dept. of Mineral., British Museum (Natural History), Cromwell Road, London

The degree of homogenization of eucritic pyroxenes (1,2) and resetting of Rb-Sr ages and ^{39}Ar-^{40}Ar ages of monomict eucrites (3,4) revealed that the HED (Howardites, Eucrites, Diogenites) parent body might have been active as recently as 2.8 b.y. ago. The discovery of partly inverted pigeonite to orthopyroxene in monomict eucrites (5) suggests that some eucrites experienced slow subsolidus cooling comparable to some cumulate eucrites. Because some cumulate eucrites such as Nagaria and Medanitos and a crystalline eucrite Y-791195 show exsolution pattern intermediate between true cumulate eucrites and monomict eucrites, we investigated these eucrites by mineralogical techniques to gain better understanding of geologic history of the HED parent body. The results will contribute to understand younger ages of cumulate eucrites (6) in the context of the above thermal histories. In this study, calcic plagioclases of four cumulate eucrites, Serra de Magé, Moama, Moore County and Y-791195 were also studied by the high resolution X-ray diffraction method to deduce their thermal histories.

Textures.

Nagaria and Medanitos are know as cumulate eucrites, but their growth textures and pyroxene exsolution textures are different from other cumulate eucrites. Medanitos is a brecciated monomict eucrites but pyroxene textures show some ranges suggesting slight polymict nature. The amount of plagioclase is smaller than the plagioclase cumulate eucrites and an original unbrecciated material may not belong to this group. Y-791195 is a crystalline eucrite rather similar to Nagaria. It shows a granular to microgabbroic texture. Short prismatic forms of plagioclase are rarely seen. Some parts of the crystalline texture are disturbed and recrystallized.

Pyroxenes.

The exsolution and inversion textures of pyroxenes in Nagaria, Medanitos and Y-791195 also share common features. They do not show characteristic textures of inverted pigeonite as is represented by Serra de Magé (1,7). Blebby augites decomposed from the host pigeonites after exsolving thick exsolution lamellae on (001) have not been observed. The width of the exsolution lamellae of Moore Co. is about 50μm. Nagaria has thickness of 15 to 20μm with 60 to 80μm intervals. The finer exsolution of Medanitos is similar to those of Juvinas, and width of even coaser ones is 1.2μm with 7.5μm intervals. Y-791195 has augite lamellae on (001) of about 10μm thick with 20 to 40μm intervals. Their chemical compositions of the host and lamellae pairs are given in Fig. 1. Medanitos is Mg-rich and Y-791195 is rather close to the ordinary eucrites. The inversion to orthopyroxene is detected in Nagaria, but some are only partly inverted.

Plagioclase.

The diffraction diagram of calcic plagioclase is characterized by the four kinds of reflections, namely a-, b-, c- and d-reflections. The b-, c- and d-reflections are sometimes associated by the diffuse streaks, which are closely connected with the experienced thermal history. The degree of

diffuseness of the b-reflection is sensitive to the cooling rate in the temperature range of 1200-1000°C and is dependent on the degree of Al/Si-ordering (9). Those of c-and d-reflections can be an indicator of the cooling rate in the temperature range of 400-150°C according to the results of Adlhart et al. (10,11) and they are also dependent on the albite content.

Moore Co. (An_{90}) shows sharp b-reflections and slightly diffuse c- and d-reflections but relatively sharp in spite of the high albite contents. Serra de Magé (An_{93}) shows sharp b-reflections and considerably sharp c- and d-reflections in spite of rather high anorthite contents. Y-791195 (An_{90}) shows sharp b-reflections and very weak and diffuse c- and d-reflections.

Discussion.

These textural evidences of Nagaria, Medanitos and Y-791195 indicate much faster growth and cooling than common cumulate eucrites. However, chemical zoning of plagioclase is minor suggesting much slower equilibrium crystal growth of plagioclase than ordinary eucrites. The texture and chemistry (Fig. 1) of these eucrites are similar to a recently described unique eucrite Pomozdino (8).

The cooling histories of common cumulate eucrites have been discussed previously on the basis of the pyroxene exsolution and inversion textures (1,7). Binda and Moama contain Mg-rich pigeonite, which decomposed into orthopyroxene and blebby augites at the pigeonite eutectoid reaction (PER) line. Serra de Magé experienced continuous slow cooling during exsolution and inversion episodes. After exsolving thick (001) augite lamellae, the pigeonite was decomposed into orthopyroxene and blebby augites at the PER line. Moore Co. has extremely thick (001) augite lamellae, but inversion and bulk decomposition to orthopyroxene were not completed and uninverted pigeonites contain very thin (001) exsolution lamellae, suggesting sudden changes of the cooling condition.

By combining the above results and the pyroxene studies (1,7), we conclude that Serra de Magé was constantly slowly cooled till room temperature. All meteorites above mentioned were cooled slowly enough at the temperature range of 1200-1000°C for Al/Si to be ordered. Moama seems to be a little more rapidly cooled than the Moore Co. and Serra de Magé. Y-791195 was much more rapidly cooled than others in the temperature range of 400-150°C. Partly inverted texture of Moore Co. suggests rather moderate cooling at the temperature range of inversion.

The younger ages of cumulate eucrites (6) do not necessarily indicate later crystallization. One interpretation was that the cumulate eucrites experienced prolonged slow cooling in the depth of the HED parent body. Another possibility is that thermal events that reset the ages of ordinary eucrites also resets the radiogenic clock of the cumulate eucrites. The presence of the eucrites intermediate between cumulate eucrites and ordinary eucrites such as studied in this paper suggests variety of geologic activities on the HED parent body. The impact excavation and rapid cooling on the surface or impact brecciation and heating at depth may give variety of thermal history in addition to the regular cooling in the lava or in the cumulate pile.

We thank National Inst. of Polar Res., British Museum for the meteorite samples and one of us (H.T.) thanks the support of the JSPS/Royal Society fellowship. The microprobe analyses were performed on JEOL 733 mark II, at Geol. Inst., Univ. of Tokyo.

References:
(1) Takeda H., Mori H., Delaney J.S., Prinz M., Harlow G.E. and Ishii T. (1983) Mem. Natnl. Inst. Polar Res., Spec. Issue, 30, 181-206.
(2) Takeda H. and Graham A.L. (1987) Rept. to Jap. Soc. Promotion of Sci., Tokyo.
(3) Birck J.L. and Allègre C.J. (1978) Earth Planet. Sci. Lett. 39, 37-51.
(4) Nyquist L.E. et al. (1988) Abstr. 51st Meteoritical Soc. Meeting, Fayatteville.
(5) Takeda H. and Nyquist L.E. (1985) Meteoritics, 20, 769.
(6) Tera F., Carlson R.W. and Boctor N.Z. (1987) Meteoritics, 22, 513-514.
(7) Harlow G.E., Nehru C.E., Prinz M., Taylor G.J. and Keil K. (1979) Earth Planet. Sci. Lett. 43, 173.
(8) Migdisova L.F., Kononkova N.N. and Zaslavskaya N.I. (1988) Lunar and Planetary Science XIX, 776-777, LPI, Houston.
(9) Tagai T. and Korekawa M. (1981) Phys. Chem. Mineral. 7, 77.
(10) Adlhart W., Frey F. and Jagodzinski H. (1980a) Acta Cryst. A36, 450.
(11) Adlhart W., Frey F. and Jagodzinski H. (1980b) Acta Cryst. A36, 461.

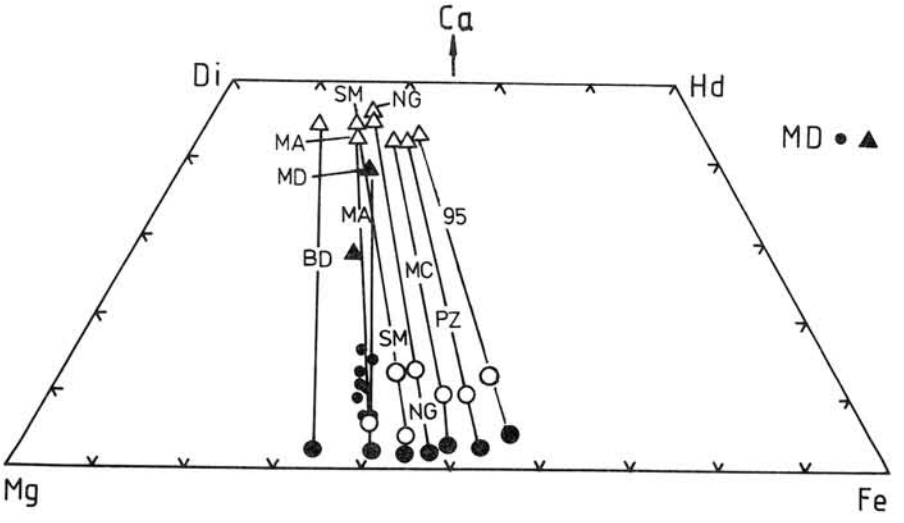

Fig. 1 Pyroxene quadrilateral showing chemical compositions of host (solid circles), lamella (triangles) and bulk pyroxene (open circles) of slowly cooled magnesian eucrites, Binda (BD), Moama (MA), Medanitos (MD), Serra de Magè (SM), Nagaria (NG), Moore Co. (MC), Pomozdino (PZ) and Y-791195 (95). Data of PZ is after Migdisova et al. (8).

Mineralogical study of the Yamato-791694 ataxite with reference to Santa Catharina

Saito, J., Tachikawa, O., Takeda, H. and Tagai, T.
Mineralogical Institute, Faculty of Science, University of Tokyo Hongo, Tokyo 113 Japan

Yamato-791694 is an anomalously Ni-rich ataxite (1) and classified into type IAB (2). We studied this meteorite because its bulk chemical composition (Ni: 35.5, P: 1.5%) is almost identical to the Santa Catharina, but their textures are different. Santa Catharina is known for containing oxygen but oxygen is detected in the specimen proved to be no oxides by an Mossbauer method (3). Because we anticipated that comparison of Y-791694 and Santa Catharina may provide a new insite into this problem of the Santa Catharina, we studied these meteorites by EPMA, AEM and Santa Catharina by Ion-Probe Microanalyser for detecting the deapth profile of oxygen. X-ray diffraction technique is also applied to detect any other minerals besides Fe-Ni phases in Santa Catharina.

A polished and etched surface of Y-791694 shows some heat-altered zone in the part of the surface of the specimen. Kamacite spindles less than one micron wide are moderately distributed in a vague orientation of kamacite-taenite resolution (Fig. 1). Neither cloudy zones nor martensitic plessite is seen. The iron nickel ratio of Y-791694 suggested no presence of tetrataenites as Nagata et al.(4) reported by Mossbauer study. Schreibersites are commonly seen on the specimen. One interesting thing is that the iron and nickel ratio of the screibersite is almost one by weight.

The polished sections of Santa Catharina showing no evidence of oxidation reveal two different areas (Fig. 2). Darker colored patches of tetrataenite which is studied by Danon et al. (about 20 to 100 microns in diameter) are distributed in shiny matrix of taenite with about 33 wt% Ni. These darker colored patches are further divided into relatively lighter colored and very darker colored areas of BEI. EPMA data shows these tetrataenite areas contain oxygen by employing the ZAF method for oxygen. No kamacite spindles are seen. The AEM images of the oxygen containing areas show the texture of aggregates of small grains. We cannot discuss definitly whether oxides or hydro-oxides exists by electron diffraction techniques, because the electron diffraction of these areas is too complex to detect diffraction spots of any other minerals except for Fe-Ni minerals. X-ray diffraction of the oxygen containing areas with minor matrix taenites did not show reflections of known iron oxide minerals.

About 3 to 10 wt.% of oxygen is detected in the oxygen containing areas, while the Fe/Ni ratio by wt.% stay about one. The oxygen content is not correlated to the distance from the cracks. It does not decrease gradually away from the cracks. This distribution trend of oxygen is clearly shown by Chemical Map Analysis (CMA) of oxygen K-alpha X-ray. This suggests that the terrestrial corrosion through the cracks by water is not the main sourse of oxygen of Santa Catharina. The deapth profiles of oxygen from the surface of the oxygen containing areas by ion-probe show no decreasing of oxygen content except for one case where gradual decreasing was observed.

These evidence suggested that the oxygen may be adsorbed in the tetrataenite structure. We carried out heating experiments (195 C, about 10^{-5} torr, 2-3hours) of small chips of Santa Catharina confirmed the

present content of oxygen. As is shown in Table. 1., oxygen content of the lighter colored tetrataenite areas deacreased drastically down to 1 to 2 wt.% after heating, whereas those of the darker colored areas stay nearly constant. After the same chip was exposed to the atmosphere for about 2 days, the oxygen contents increased again to nearly the original level. From these results, we suggest that the oxygen of the Santa Catharina may be adsorbed from the atmosphere in the tetrataenite.

Because only the slowly cooled tetrataenite portions adsorbed oxygens, we thought that this property might have been aquired preterrestrial events. Always constant ratio of Fe/Ni supports this hypothetis. Because of the fact that similar ataxite Y-791694 does not show oxygen adsorption, we can attribute this difference to the different thermal history. In spite of almost identical bulk chemical compositions in both Y-791694 and Santa Catharina, Y-791694 has kamacite spindles in a vague Widmanstatten orientation but Santa Catharina has no kamacite spindles. This evidence suggests that Y-791694 cooled in equilibrium near the solvus between gamma and alpha+gamma region, whereas Santa Catharina did not, in other words, Santa Catharina cooled faster than Y-791694 near the solvus. The presence of tetrataenites of the Santa Catharina and the absence of tetrataenite in Y-791694 suggest that Santa Catharina cooled slower (about a few degrees per million years) than Y-791694 below about 350 C. These differences of thermal history of Y-791694 and Santa Catharina are schematically shown in Fig. 3. Such a slow cooling is thought to cause decomposition imperfectly on the Fe-Ni phases and form the texture of small grain aggregates containing tetrataenites. We think that tetrataenites which is formed in such a condition may aquire the adsorbing property. The ordering of iron and nickel atoms in such a condition may help adsorbing oxygen.

In summary, we suggest that the oxygen of Santa Catharina is adsorbed the terrestrial atmosphere, and that the adsorbing property may have been aquired by some preterrestrial events, which cause faster (and inequilibrium) cooling than Y-791694 near the solvus and slower cooling than Y-791694 under about 350 C. The oxygen adsorbing properties may provide a new information on the oxygen contents of the Earth's core and its origin. Further study may be required to gain quantitative information of such a adsorbing property.

We thank National Institute of Polar Research and American Museum of Natural History for meteorite samples. We also thank Dr. H. Yurimoto for Ion-Probe study and Mr. H. Yoshida for Chemical Map Analysis. We are much indebted to Mr. T. Furuta for advising the techniques of oxygen analysis by EPMA and heating experiment.

References:

(1) Nagata, T. et al. (1984) Mem. Natl Inst. Poler Res., Spec. Issue, 35 302-318
(2) Ouyoung et al. (1986) Meteoritics 21 478-479 (abstract)
(3) Danon, J. et al. (1979) Nature 277 283-284
(4) Nagata, T. et al. (1986) 11th Symp. on Antarctic Meteorites (abstract) No. 60

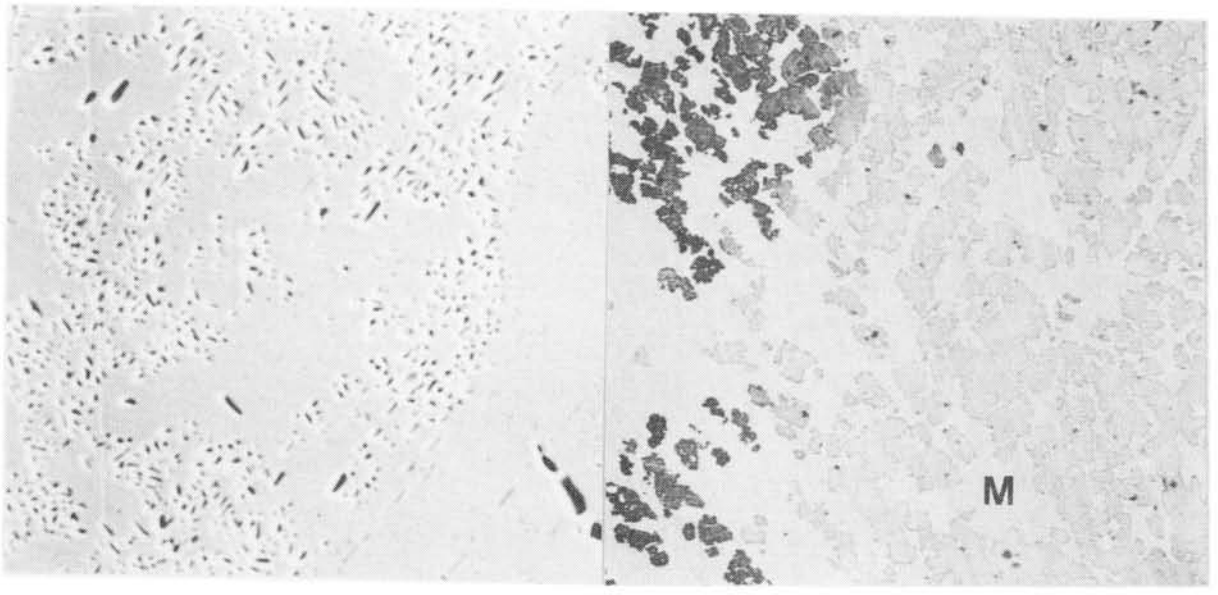

Fig. 1 SEI photograph of Y-791694 (nital etched) width: about 100 microns

Fig. 2 BEI photograph of Santa Catharina width: about 140 microns. M: matrix

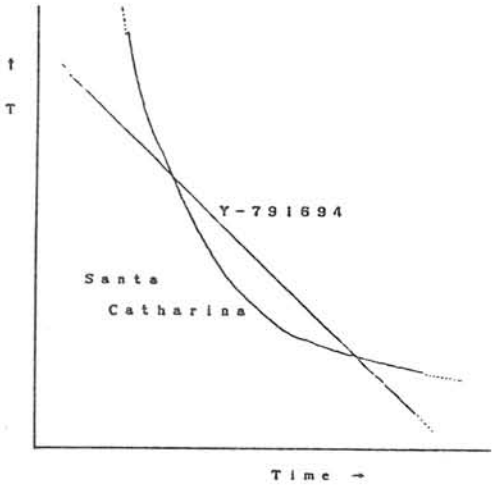

Fig. 3 Schematic figure depicting the difference of thermal history of Y-791694 and Santa Catharina

Table. 1 Chemical compositions of the lighter and darker colored oxygen containing areas of Santa Catharina analysed by EPMA (wt %, (*): darker colored oxygen containing areas)

	"Unheated"			"Heated"			After exposure of "Unheated"		
			(*)			(*)			
Fe	46.7	45.5	44.8	48.2	48.0	46.3	46.0	46.0	45.8
Ni	47.3	46.3	46.4	48.5	48.4	43.7	46.8	46.1	45.9
O	5.2	4.1	7.8	1.4	1.4	9.1	5.6	5.3	4.6
total	99.2	95.9	99.8	98.1	97.8	97.8	98.4	97.4	96.3

LOW-DENSITY PLAGIOCLASES FROM METEORITIC IMPACT CRATOR

Y. Miura

Department of Mineralogical Sciences and Geology, Faculty of Science, Yamaguchi University, Yamaguchi 753

Amorphous plagioclases formed by impact (i.e. diaplectic labradorite glass) have 4% larger volume (i.e. low-density) than the terrestrial standards, whereas those in meteorite (i.e. maskelynite) have smaller volume (i.e. high-density) [1-7]. But the amorphous plagioclases (i.e. diaplectic glass) hold the weak crystalline structure with a similar feldspar composition, which is called as "low-density plagioclases" in this study.

The low-density plagioclases are summarized as follows:

1) Definition:

Plagioclase crystal with lower density (2.54-2.60), mainly formed by meteoritic impact (i.e. shock waves), than normal density (2.62-2.76) in the terrestrial plagioclase crystallized mainly by igneous activities.

2) Texture and paragenesis:

Plagioclases with wholly or partly extintion under the polarized microscope. Pyroxene (cpx) and garnets are co-existed.

3) Crystal structures:

The similar plagioclase patterns with various intensities in powder diffraction patterns. Unit cell volume is lower (675-693 $Å^3$ in albite cell) than the normal terrestrial plagioclases. Lattice images in the high-resolution electron microscopy show irregular shapes with lattice arrangements, compared with the sharp regular lattice images in Nain labradorites.

4) Composition:

Plagioclases with 51 to 64 anorthite content (mol.%).

5) Occurrence:

The low-density plagioclases are observed in center-anorthosite regions of the Manicouagan impact crater.

6) Remarks:

The low-density plagioclases are similar density of synthetic glass with plagioclase compositions.

The low-density plagioclases are completely different with normal or higher density plagioclases from achondritic meteorites.

Impact events by meteorites also results in lower anorthite contents, together with normal igneous activities.

REFERENCES:

[1] Arndt, J. et al. (1982): Phys. Chem. Minerals, 230-239.
[2] Miura, Y. (1984): Mem. Natl Inst. Polar Res., Spec. Issue, 35, 226-242.
[3] Miura, Y. (1987): Lunar and Planetary Science XVIII(NASA-LPI), 649-650.
[4] Miura, Y. (1987): Lunar Samples and Antarctic Meteorites (Tokyo), 1-6.
[5] Miura, Y. (1987): Abstract on Min. Soc. Japan (Tokyo), 111.
[6] Miura, Y. (1988): Lunar and Planerary Science XIX, 792-795.
[7] Miura, Y. (1988): Abstract on Min. Soc. Japan (Kyushu, in press).

Special Lecture

Doctor Robert Hutchison

Advances in our understanding of the ordinary chondrites

Robert Hutchison, Mineralogy Department, British Museum (Natural History), London SW7 5BD, UK.

The two component model for the origin of the ordinary chondrites (Larimer and Anders, 1967) has been popular with meteoriticists for many years. The model proposes that the chondrites comprise a high temperature fraction - chondrules and remelted metal/sulphide - and a low temperature fraction which is host to volatiles. The low temperature fraction is composed of dust that obtained its volatiles by condensation from a protosolar nebula down to almost 400K. Post accretion metamorphism was isochemical and produced the textural range now observed (Van Schmus and Wood, 1967).

Since the model was put forward, various aspects of it have been questioned:

1. Could H6, L6 and LL6 have had type 3 precursor material?
2. Could metamorphism after cold accretion have produced the observed mineral assemblages?
3. Are chondrules nebular, as implied by the two component model?
4. Was the opaque, interchondrule matrix formed from nebular dust?

Type 3 (and 4) ordinary chondrites contain a variety of angular clasts and clast chondrules composed of Ca-rich, Na-poor igneous rock (Hutchison and Bevan, 1983). Such material is exceedingly rare in type 6 (and 5) meteorites (for example, Hutchison et al., 1986), but metamorphism has not erased its identity. Thus it appears that the precursor of type 6 chondrites was more uniform in composition than that from which type 3 formed. Type 6 precursor did not differ from type 3 only in the proportion of low temperature component, as Larimer and Anders (1967) and Laul et al. (1973) implied.

The structural polymorph of low-Ca pyroxene in type 3 chondrites is monoclinic and probably the inversion product of protopyroxene. In types 4 and 5, 'striated' pyroxene typically occurs; this is orthopyroxene containing some clino lamellae, which persist even to type 6. The pyroxene in H4 transforms to the structure typical of H5-6 in one week at 800°C (Ashworth et al., 1984). Thus prograde, thermal metamorphism must have been of exceedingly short duration, which is not compatible with the longer duration of most possible heat sources. Watanabe et al. (1985) reached a similar conclusion for the L-group chondrites. Hutchison et al. (1979), Christophe-Michel-Levy (1981), and Holmen and Wood (1986) presented evidence that various ordinary chondrites accreted hot. This calls into question the basis of the two component model because the temperature of accretion would have been greater than the condensation temperatures calculated for several volatile metals such as Tl and In.

Chondrules have variable contents of Ca, Al and other refractory lithophile elements which would be expected to condense together. Some of the fractionation of these elements from one chondrule to another cannot readily be accounted for by nebular processes; planetary, crystal-liquid, fractionation is implied (Hutchison et al., 1988). Some clast-chondrules and angular fragments have igneous textures, and one has a heavy rare earth element depleted pattern, with a positive Eu anomaly. Some

apparently planetary igneous materials clearly formed very early, and co-existed with chondrules when opaque matrix or rims (see below) was added. Droplet chondrules may be nebular in origin, bur other types appear to be planetary. Either all chondrules are planetary, or two processes of formation are required.

In highly unequilibrated ordinary chondrites, silicate chondrules, metal/sulphide chondrules, clast chondrules and other objects are often coated by fine-grained rims of opaque silicate-rich material, which may also occur as interchondrule matrix. Some chondrules were molten when their opaque rims were added. Opaque rims and matrices contain clastic olivines and low-Ca pyroxenes that probably were derived from fragmented chondrules. Rims and matrices contain fayalitic olivine (Nagahara and Kushiro, 1987) and a feldspathic component. This material could have been derived from the reaction of chondrule mesostases with FeO from the oxidation of metal. Chondrules that crystallized abundant protopyroxene would, on quenching, be susceptible to spontaneous disintegration because of 3% contraction along the c axis on rapid inversion to clino. This could have released Si-rich mesostasis to react with FeO to produce fayalite. Although rims and matrices probably were derived mainly from chondrules, there also was an interstellar component identifiable from anomalous stable isotope ratios (Sears et al., 1988).

It is concluded that there is little or no mineralogical evidence that the ordinary chondrites are directly of nebular origin. A planetary origin, with the admixture of a minor interstellar component, is favoured. This poses a problem for theories of chemical variation between chondrite groups and petrologic types, but the mineralogical constraints appear to be more strongly based on experiment than the chemical constraints.

I acknowledge the influence of colleagues in this work: S O Agrell, C M O Alexander, J R Ashworth, H J Axon, D J Barber, A W R Bevan, G M Biggar and A L Graham.

Ashworth et al. (1984) Nature 308, 259-261.
Christophe-Michel-Levy (1981) EPSL 54, 67-80.
Holmen and Wood (1986) Meteoritics 21, 399.
Hutchison and Bevan (1983) In: Chondrules and their origin, 162-179. Houston, Lunar Planet. Inst.
Hutchison et al. (1979) Nature 280, 116-119.
Hutchison et al. (1986) Meteoritics 21, 402-403.
Hutchison et al. (1988) Phil. Trans. R. Soc. Lond. A, (in press).
Larimer and Anders (1967) GCA 31, 1239-1270.
Laul et al. (1973) GCA 37, 329-357.
Nagahara and Kushiro (1987) EPSL 85, 537-547.
Sears et al (1988) Lunar Planet. Sci. 19, 1051-1052.
Van Schmus and Wood (1967) GCA 31, 747-756.
Watanabe et al. (1985) EPSL 72, 87-98.

Abstract Only

THE PETROLOGICAL STUDY ON THE TWO METEORITE SAMPLES (ALH-77226, ALHA-78103-24) COLLECTED IN ANTARCTICA

E Molan and Zheng Xiangshen
Institute of Geology, Academia Sinica, Beijing 100011

Two meteorite samples, ALH-77226 (A77) and ALHA-78103-24 (A78), found in Antarctica were given to the late professor Zhang Wenyou by Japanese geologists worked in East Antarctica, on them some of petrological and mineralogical investigations have been made recently.

The light grey sample A77 and the dark grey one A78 are all the aerolite with spherulites, however, of which the spherulytic structure and mineral association are slightly distinguishable. The spherulites in A77 are mainly round in shape and 25-30 per cents in volume and that in A78 are up to 30-35 per cents with circular, elliptic, or spindle shape. The spherulites can be divided into skeletal (including fan-, clubbed-, sheaf-like skeletal), grain packing, and cryptocrystalline. Different type of spherulites has different cooling history and the strain-slip cleavage of some spherulites are probably resulted from the mechanical impact.

The mineral associations of the two aerolithes are different. A78 consists of chrysolyte ($Fa_{25.45-25.96}$), bronzite ($Fs_{17.01-22.69}$) and some plagioclase grains ($Or_{6.8}Ab_{81.7}An_{11.5}$) as well as glass. A77 is composed of chrysolite ($Fa_{18.17-18.52}$) and bronzite ($Fs_{16.78-26.61}$) , glass also, but with no plagioclase, however, has diorite ($Wo_{46.67}En_{46.90}Fs_{6.43}$) and a kind of Ca-poor clinopyroxene ($Wo_{16.15-18.78}En_{68.66-68.70}Fs_{15.20-12.42}$). The content of ore minerals in meteorites, mainly kamacite and troilite filling within the grains of chrysolite and bronzite, is about 15 vol%.

The chemical compositions of samples list here:

	SiO_2	TiO_2	Cr_2O_3	Al_2O_3	FeO	CaO	MgO	MnO	K_2O	Na_2O
A77	37.33	0.01	0.02	1.99	16.67	1.87	23.18	0.37	0.15	0.80
A78	38.12	0.01	0.02	2.09	14.43	1.88	24.35	0.41	0.15	1.00

	P_2O_5	H_2O^+	FeS	Fe	Ni	Co	Cu	Zn	Pb	
A77	0.26	0.05	6.11	9.85	1.68	0.08	0.01	0.01	0.01	100.42
A78	0.36	0.04	7.38	8.09	1.15	0.06	0.01	0.01	0.01	99.54

All of the two meteorites are basically of high-Fe H-group, olivine-orthopyroxene chondrite, however, from the distinguishable chemical composition, mineral association, and spherulitic structure we suggest that each meteorite had a distinctive forming process and the equilibrium relationship between minerals did not reach when the aerolithes falled through the atmosphere and into ice and snow and when the high temperature melt crystallized at an overcooling condition.

HEATING EXPERIMENTS ON MASKELYNITE FROM THE LONAR IMPACT CRATER, INDIA

V. K. NAYAK

DEPARTMENT OF APPLIED GEOLOGY, INDIAN SCHOOL OF MINES, DHANBAD 826-004 INDIA

Since maskelynite was named and described by Tschermak (1872) for a clear, glassy pseudomorph of plagioclase in the Shergotty achondrite, it has attained a greater significance in recent years due to growing interest in shock metamorphism of terrestrial, meteoritic and lunar materials.

Lonar crater (19°58'N : 76°31'E) excavated in the Deccan basaltic rocks of the Cretaceous-Eocene age, is an authentic meteorite impact crater in India (Nayak, 1972; Fredriksson et al. 1973). It is unique in many ways because it provides the closest analog to the lunar rocks and meteorite like the Shergotty achondrite. The shock metamorphosed material used in this investigation was collected from the eastern and western sides of the Indian crater. Maskelynite occurs in a monomict breccia as clean, colourless laths of variable sizes and shows vestiges of cleavage, twin planes and planar features. It co-exists with pyroxene, basaltic glass, opaques and preserves porphyritic or micro-porphyritic textures. Its An content varies from An_{66} to An_{69} and closely corresponds to labradorite. Its average refractive index is 1.560 $\pm$ 0.002 and is optically isotropic. This refractive index value is higher than that of experimentally shocked single labradorite crystal (An_{66}; Ostertag, 1983), however, it is nearly similar to the Shergotty maskelynite (Stöffler et al. 1986).

Heating experiments on a large lath of maskelynite reveal that it reverts to a crystalline state at 800°C. At this temperature the plagioclase structure is restored perhaps by relaxation of strained bonds between the short range domains. This temperature is lower than the transformation temperature of 900°C reported for maskelynite from Clearwater West and Manicouagan craters, Quebek, Canada (Bunch et al., 1967).

The high refractive index value and lower revertion temperature of the Lonar maskelynite are discussed and compared with the recent relevant studies. In addition, the significance of shock metamorphism and shock related thermal history and their implications in relation to the Lonar maskelynite are briefly considered.

References

Bunch, T.E., Dence, M.R., and Cohen, A.J. (1967) Amer. Mineral., 52, 244-253.

Fredriksson, K., Dube, A., Milton, D.J., and Balasundaram, M.S. (1973) Science, 180, 862-864.

Nayak, V.K.(1972) Earth & Planet. Sci. Lettrs., 14 (1), 1-6.

Ostertag, R. (1983) Proc. Lunar Planet. Sci. Conf. 14th., Jour. Geophy. Res., 88, B364-B376.

Stöffler, D., Ostertag, R., Jammes, C., Pfannschmidt, G., Sengupta, P.R., Simon, S.B., Papike, J.J., and Beauchampt, R.H. (1986) Geochimica et Cosmochimica Acta, 50 (6), 889-903.

Tschermak, G. (1872) Sitzungsber. Kaiserl. Akad. Wiss. Wien, Math-Naturwiss. Kl. 65, 122-146.

THERMOANALYTICAL STUDY OF FOUR CHONDRITES FROM ANTARCTICA

Bruno Lang (1), Andrzej Grodziński (2) and Nonna Bakun-Czubarow (3)

(1) Warsaw University, Department of Chemistry, 02-089 Warsaw
(2) Institute of Electronic Materials, 02-075 Warsaw
(3) Institute of Geology, Polish Academy of Sciences, 02-089 Warsaw

Continuing our work on the thermoanalytical characterization of a number of meteorites of various type we studied four chondrites from Antarctica:

Yamato-793321	C 2
Yamato-74640	H 6
Yamato-74457	L 5
Yamato-74442	LL 4

The samples ranging in mass from 9 up to 23 mg were heated up to ~1000°C and then cooled at a rate of 10°C/min. against Al_2O_3 used as reference material. For heating in air differential thermal (DTA) and thermogravimetric (TG) curves were obtained while for heating in oxidation-suppressing atmosphere of argon only DTA-curves. They are shown in Figs.1 - 4, while in Figs.5 and 6 ESM-photomicrographs illustrating the microstructure of the analyzed samples.

Both DTA-and TG-curves are affected by many factors that influence their reproducibility and complicate both the interpretation and intercomparisons. Our experience although covering several tens of meteorites is apparently limited and insufficient to explain certain features observed on the DTA-curves. Particularly poor is our understanding the occurring oscillations of the TG-curves.

In the case of the four chondrites from Antarctica as analyzed we found in Yamato-793321 a close analog to Yamato-74662 - a carbonaceous chondrite CM 2. The ordinary chondrites Yamato--74640 (H 6) and -74457 (L 5) heated in air have shown losses in mass equal to 3.7% and 4.0%, respectively - similar but larger than those for the La Lande (L 5, -1.32%). On the other hand we found the Yamato-74442 (LL 4) increased in mass by 5%, reminding Bjurböle (L 4,+5.5%), Elenovka (L 5, +3.91%) and Nikolskoe (L 4, +5.83%).

The losses in mass of the Yamato-793321 and -74662 carbonaceous chondrites are very close: 10.9% and 11.2%, respectively. It seems reasonable to attribute them to evolved gaseous H_2O (which makes some 15% of the total mass) and volatilization of relatively abundant sulphur and carbon compounds. Both meteorites when heated in argon show on their DTA-curves a remarkable identical in shape and intensity feature at 686°C and 680°C - an exothermic peak proving formation in oxidation-suppressing atmosphere of a mineral species due to elimination of volatiles from the groundmass of the meteorites. One can hypothesize that the arising mineral species is more compact and unstable under typical terrestrial conditions.

On the DTA-curves for the remaining three chondrites is clearly seen the endothermic peak at 145°C resulting from phase transition of troilite FeS (known as peak at 139°C for pure substance). Among more or less abundant weak peaks, often pronouncedly diffuse, sometimes suspected only, remarkable are clear exothermic peaks observed on the cooling branch of the DTA-curves for the Yamato-74640 (at 470°C and 365°C) and Yamato-74442 (at 835°C and endothermic at 566°C). They are to be attributed to liquid/solid phase transition of distinct components of the molten samples including eutectic mixtures.

More detailed analysis of the obtained results is within our scope.

Acknowledgements

National Institute of Polar Research Tokyo is acknowledged for supplying the samples of the analyzed four chondrites from Antarctica.

Dr. M.Żbik assisted in taking the photomicrographs.

This work was supported by the Center for Space Research of the Polish Academy of Sciences under contract 01.20.1.5.7.

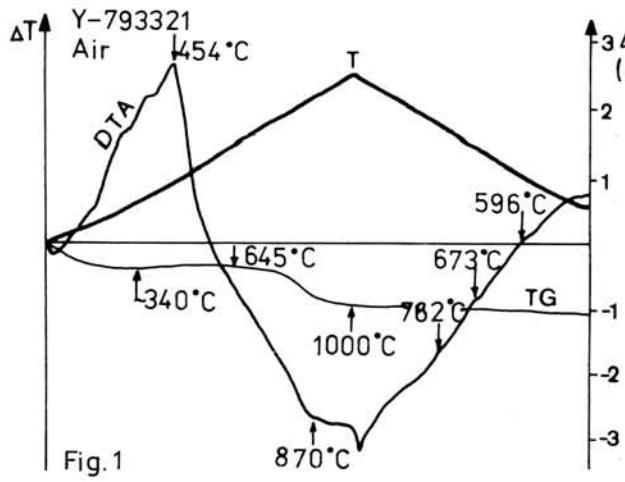

Fig.1

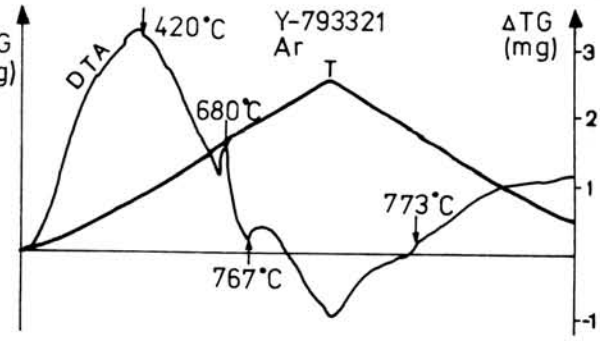

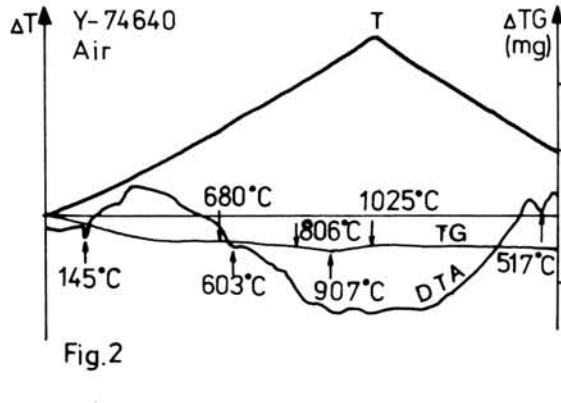

Fig.2

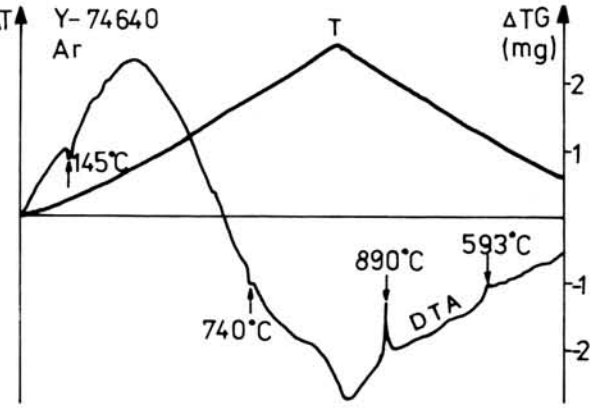

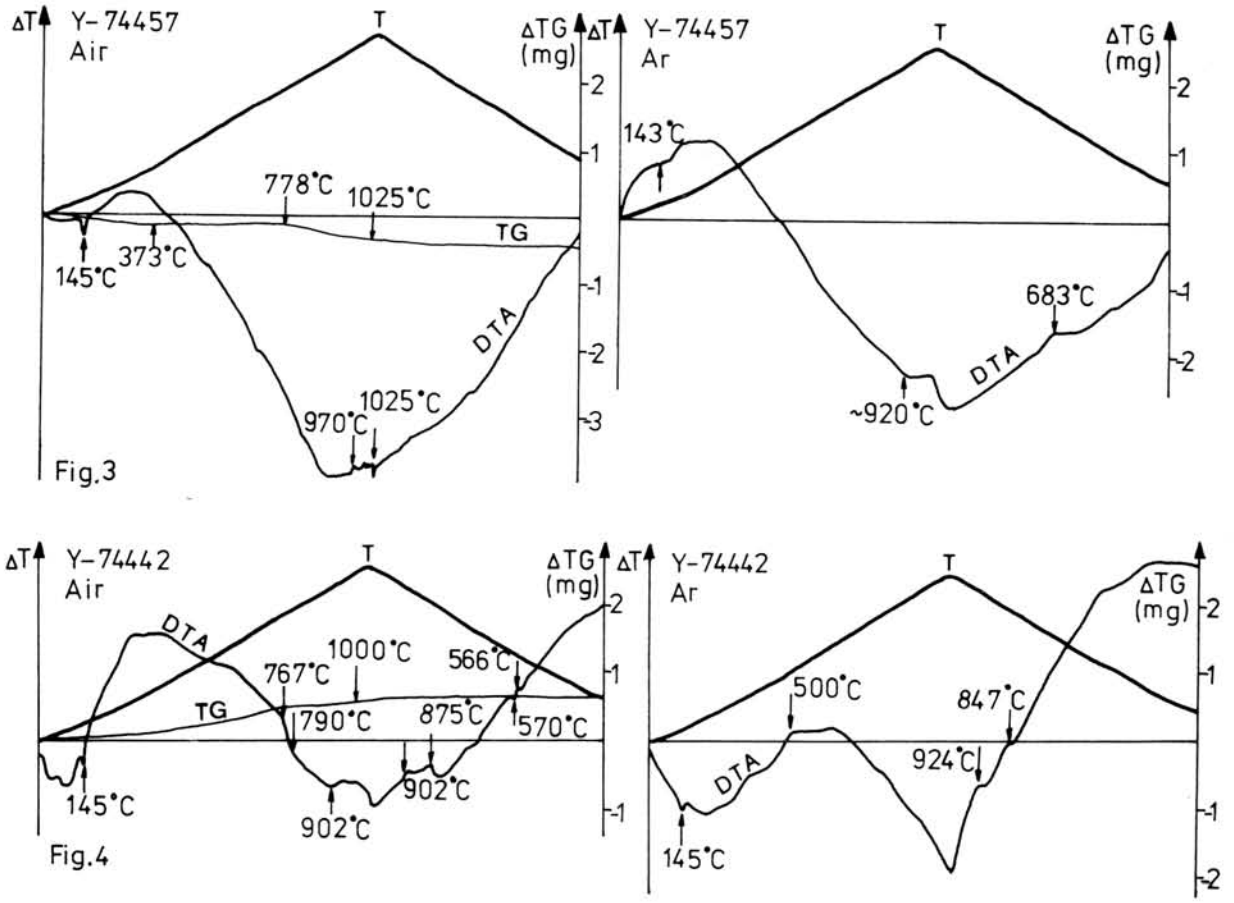

Figs 1-4 Thermoanalytical curves of the four Yamato chondrites heated and cooled in air and in the argon atmosphere.

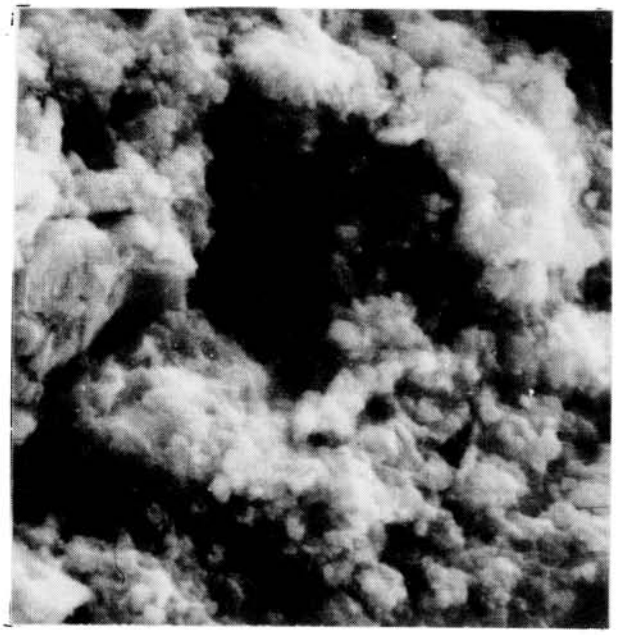

Fig.5 SEM photo of the Y-793321 chondrite, magn. 5000x

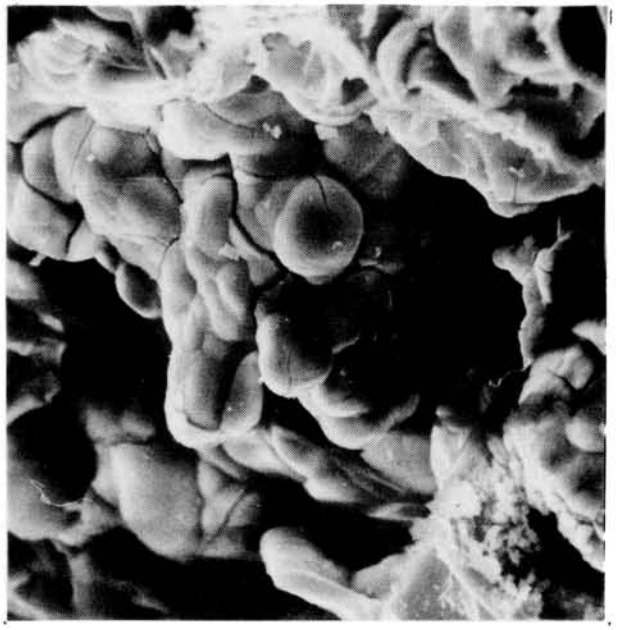

Fig.6 SEM photo of the Y-74640 chondrite, magn. 1500x

THE KEY MINERALOGICAL TAXONOMIC PARAMETERS IN EQUILIBRATED ORDINARY CHONDRITES

Wang Daode & Hou Wei

Institute of Geochemistry, Academia Sinica, Guiyang, China

Recently, we studied 26 chinese chondrites, including two new chondnites (Wuan and Laochenzhen) and other 16 chondrites. Wuan (Fa=19.60, Fs=17.85) fell as a single 50kg mass in a field in Hebei province, Wuan county at 11:00 on June 31, 1986. Laochenzhen (Fa=18.4, Fs=16.2; 115°10'E, 33°8'N) fell on February 23, 1987 in Henan province, Shenqiu county; a single 14.25 kg stone was recovered.

Olivine compositions (mol% Fa) and Co content of kamacite in 42 ordinary chondrites are listed in Table 1.Figure 1 shows median mol% Fa in olivine versus kamacite Co content for 42 equilibrated ordinary chondrites, included 26 chondrites from China. We compare olivine, low-Ca pyroxene and kamacite in the chondrites to the established compositional ranges of these minerals in H-, L- and LL- group chondrites: H: Fa 16.9-20.4, Fs 15.7-18.1, 4.0-5.2 mg/g Co in kamacite; L: Fa 22.7-25.6, Fs 18.7-22.6, 6.5-10 mg/g Co; LL: Fa 27.0-33.0, Fs 23.2-25.8, 15-110 mg/g Co (Gomes and Keil, 1980; Fodor and Keil, 1978; Afiattalab and Wasson, 1980; G. W Kallemeyn and A.E. Rubin, unpublished data). Modal analysis indicates that Qidong consists of (in wt.%): 90.2% silicates, 4.7% metallic Fe-Ni,4.3% troilite and 0.7% chromite. This abundance of metallic Fe-Ni is near the lower extreme of the L-chordrite range (4.4-11.7 wt.%) and the middle of the LL-chondrite range (3.0-6.0 wt.%). Among 150 metal grains in Qidong the vast majority are taenite; the taenite/kamacite ratio is ~60. Only four kamacite grains were found. Thus, Qidong is one of four interesting ordinary chondrites that has properties intermediate between L and LL; the other three are a Chinese chondrite Xi Ujimgin and two well-known chondrites from Europe Albareto and Bjurbale. We are not sure owe to classify these-L, LL of into a new, intermediate group. Clearly one needs to find a clustering of data other than compositional data, for example, in Cosmic-ray ages or K-Ar outgassing ages. The border between L and LL is not as well defined as most people think. We suggest that the Co content of kamacite and Fa mol% in olivine — two key mineralogical taxonomic parameters should be mesured in all new equilibrated ordinary chondrites in order to assign them to the correct group. This diagram also shows continuous chemical fractionation of Fe and Co that is recorded in these chondrites.

We thank A.E. Rubin, J. T Wasson and G.W. Kallemeyn for discussions and supports.

References: Gomes, C.B. and K. Keil, 1980. Brauilian Stone Meteorites, University of New Mexico Press, Albuquerque, 161 pp. Fodor, R.V. and K. Keil, 1978,UNM Inst. Metoritics sp. Pub. 19, 1-38.Afiattalab, F. and J.T. Wasson, 1980. Geochim. Cosmochim. Acta 44, 431-446.

Table 1. Median Fa and Co content in kamacite of the equilibrated ordinary chondrites

chondrite	Fa(mol%)	kamacite Co(mg/g)	chondrite	Fa(mol%)	kamacite Co(mg/g)
Allegan	17.7	4.60	*Jartai	24.9	9.00
*Anlong	19.2	4.40	Leedey	25.3	8.40
*Changde	19.0	4.70	*Lishui	25.4	8.20
*Changxing	18.2	4.30	Saratov	23.7	6.9
Dhajala	19.3	4.60	Tennasilm	23.1	6.50
*Enshi	17.7	4.20	*Xi Ujimgin	26.2	8.80
*Jilin	19.5	4.60	*Zhaodong	24.4	8.40
*Lunan	19.0	4.70	*Qidong	25.7	16.0
*Mianchi	19.4	4.80	*Raoyang	24.5	8.8
*Xingyang	20.0	4.50	*Sheyang	24.4	7.10
*Nanton	19.1	5.10	*Guangnan	24.9	8.90
*Laochenzhen	18.4	5.4	*Suizhou	24.6	8.30
*Wuan	19.6	5.6	*Daohe	24.6	7.80
*Zaoyang	18.3	4.90	*Bo Xian	27.7	16.2
Albareto	26.7	12.1	Dhurmsala	27.5	20.7
Bjurbole	26.1	12.3	*Dongtai	27.0	17.9
Alfianello	25.1	8.60	Guidder	28.9	25.1
Barratta	23.9	6.80	Olvenza	29.8	48.9
Barwell	25.1	7.90	Paragould	27.6	18.4
Cynthiana	25.0	10.7	*Rugao	27.6	18.1
*Guangrao	25.2	8.90	Jelica	32.30	98.30

*Chinese chondrites

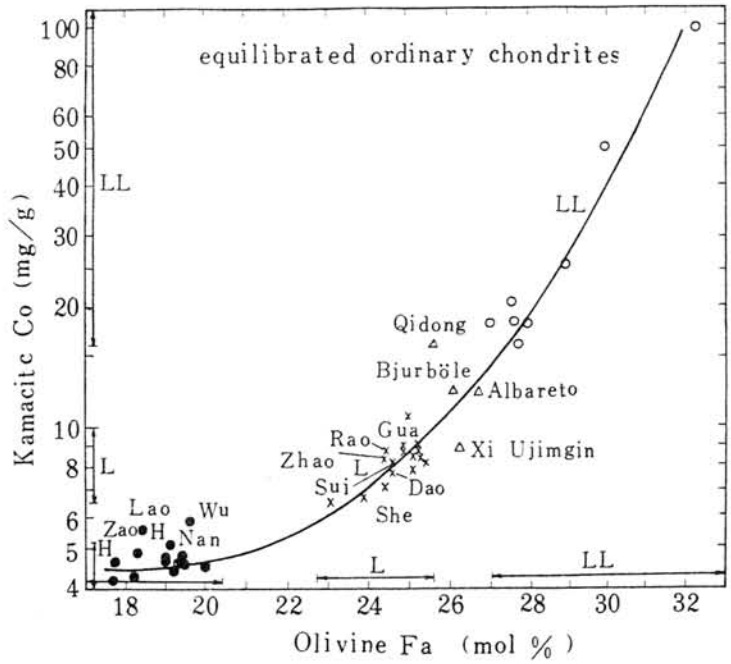

Figure 1. The median mol% Fa in olivine versus kamacite Co content for 42 ordinary chondrites

AQUEOUS ALTERATION OF CI AND CM CARBONACEOUS CHONDRITES: A REVIEW

Kazushige Tomeoka*, Harry Y. McSween# and Peter R. Buseck&, * Mineralogical Institute, Faculty of Science, University of Tokyo, Hongo, Bunkyo-ku, Tokyo 113; # Department of Geological Sciences, University of Tennessee, Knoxville, Tennessee 37916, USA; & Departments of Geology and Chemistry, Arizona State University, Tempe, Arizona 85287, USA.

The composition of carbonaceous chondrites is similar to solar abundances; thus these chondrites are commonly regarded as "primitive" solar system material. However, some chondrites, CI and CM type carbonaceous chondrites in particular, show abundant evidence of aqueous alteration (e.g. DuFresne and Anders, 1962; Bostrom and Fredriksson, 1966; Bunch and Chang, 1980; Kojima et al., 1984). Most petrographic studies suggest that the alteration probably occurred in the regolith of their parent bodies. Thus, if we are to interpret the record in these meteorites, it is obviously important that we understand the alteration correctly.

The major fraction of CI and CM carbonaceous chondrites is optically opaque matrix, consisting of extremely fine-grained minerals. Knowledge of matrix mineralogy is crucial for determing the conditions under which these meteorites formed and also the degree to which they retain their primitive character. The fine-grained and intimately intergrown nature of the matrix minerals have long hindered precise characterization and identification. However, recent transmission electron microscope (TEM) studies combined with the results from petrographic studies have greatly improved our understanding of the matrix mineralogy of the carbonaceous chondrites. We review recent mineralogical and petrological works of CI and CM chondrites and interpretations of the aqueous alteration of these meteorites.

CM matrices are complex assemblages consisting mainly of Fe-bearing serpentine, cronstedtite, and Fe-Ni-S-O phase (tochilinite), with lesser amounts of Fe-Ni sulfides, magnetite, chromite, calcite, relict olivine and organic compounds. These minerals are intimately mixed and intergrown on a submicron scale. Such heterogeneous mixtures resulted from aqueous alteration involving matrix, chondrules, and aggregates. The relative proportions, compositional heterogeneity, and crystallinity of the phyllosilicates and the Fe-Ni-S-O phase vary considerably among CM chondrites and can be correlated with degree of alteration.

TEM observations of the CM matrices enabled us to construct a plausible aqueous alteration model for the CM chondrites (Tomeoka and Buseck, 1985). Recently, based on the alteration model and bulk matrix compositions, McSween (1987) made mass balance calculations to specify the relative proportions of secondary phases in many CM matrices. His analsyes provide a more quantitative view of the aqueous alteration.

The apparent trend that matrix Fe contents of CM chondrites decrease with increacing aqueous alteration suggests that CI chondrites experienced more intense alteration than CM chondrites (McSween, 1979). However, a recent study of the Orgueil CI chondrite (Tomeoka and Buseck, 1988) reveals that its matrix mineralogy differs significantly from the CM matrices, suggesting that the CI and CM chondrites were derived from different primary materials and experienced distinct aqueous alteration. Thus, the mineralogical and petrological differences between CI and CM chondrites are probably not simply dependent on the extent of aqueous alteration.

TRACE ELEMENT GEOCHEMISTRY OF LUNAR METEORITE Y-86032 - INITIAL DATA

Christian Koeberl

Institute of Geochemistry, University of Vienna
Dr.-Karl-Lueger-Ring 1, A-1010 Vienna, Austria

Antarctica has provided a mother lode of meteorites since the discovery of meteorites at the Yamato Mountains in 1969. Amongst the most exciting discoveries was the recognition of a sample that is obviously of lunar origin. This meteorite, ALHA 81005, was discovered in 1982 by an American group at the Allan Hills in Victoria Land. Another lunar meteorite, Y-791197, was discovered among the 79 collection of Japanese Antarctic meteorites. Since then, another four lunar meteorites have been identified in the Japanese collection of Antarctic meteorites. The specimens Y-82192, Y-82193 and Y-793274 were quite small, but the most recent one, Y-86032, is a large piece, weighing 648.43 g. All lunar meteorites are anorthositic breccias, and have originated from the lunar highlands. A very important question associated with the study of the lunar meteorites concerns the question on the number of impacts that have launched the pieces from the Moon and sent them on the way to the Earth. So far the picture is not clear, although the evidence seems to favor more than one impacts. Each new lunar meteorite can help in deciding that question, and provides us with more data on different parts of the lunar surface.

We report here on the first trace element analyses of the new lunar meteorite Y-86032. Two subsamples (,84 and ,85) of Y-86032 have been available for our study, one containing normal matrix material with a fraction of a larger clast (,85), and the other one being a moderately homogeneous impact melt (,84). Y-86032 is rich in yellowish-brown impact melts, and contains numerous vesicles. Some large voids are already visible from the outside. Numerous large grey and white clasts (up to 1 cm in length) are present, some of which may be granulithic breccias. The samples have been subdivided, and so far five individual samples have been measured using INAA. The preliminary results for the bulk of the impact melt sample (,85) are given in the table below.

There are some similarities between Y-86032 and Y-82192. The REE (see Fig. 2) are much closer to Y-82192 than to Y-791197. The composition of plagioclase is more uniform in Y-86032 (An90.9-97.4) than it is in Y-82192 (An83.0-98.2) (Yanai et al., 1987). Most lithophile elements are lower in Y-86032 than in Y-82192 or Y-791197.Sc, Zr, the REE, or Th are lower than in the other lunar meteorites. There is a clear diference between Y-791197 and Y-86032, especially if the REE are concerned. In a plot of the incompatible elements Th vs.Sm the new lunar meteorite plots below all other previously known lunar meteorites (Fig. 1). The low abundance of lithophile and incompatible elements would be in better agreement with Y-82192 than with Y-791197. On the other hand, Fe, Co, and Cr are much lower in Y-86032 than in any of the other meteorites. This is infavor of the assumption that Y-86032 is different from the other known lunar meteorites. The REE point to a similarity with Y-82192, but in the case of Y-86032 the absence of a KREEP component is even more pronounced. Although there are a few points in favor of a pairing with Y-82192/Y-82193, the evidence seems to support a different source region for Y-86032, which thus comprises a new lunar sample.

Table 1. Chemical composition of the new lunar meteorite Y-86032 and comparison data for other lunar meteorites. The data are given in ppm, except as noted. The results for Y-86032 have been obtained using INAA and are preliminary. The data are for bulk matrices (impact melt for Y-86032).

	Y-86032 this work	Y-799197 Ref.1	Y-82192 Ref.1	Y-82192 Ref.2
Na (wt.%)	0.32	0.25	0.29	0.265
K	135	238	170	150
Sc	7.26	12.1	13.8	14.5
Cr	660	889	1156	1020
Mn	390	674	746	657
Fe (wt.%)	3.20	4.99	4.85	4.74
Co	13.2	24.6	18.6	19.9
Ni	150	218	159	120
Ga	4.8	3.3	10.4	3.78
As	0.27	0.3	0.028	<0.2
Se	0.3	0.56	0.3	<0.2
Br	<0.2	<0.08	0.08	<0.2
Rb	<10	8	3	<3
Sr	118	158	150	136
Zr	25	35	30	-
Sb	<0.5	<0.1	<0.1	<0.1
Cs	0.05	0.08	0.08	<0.1
Ba	30	30	20	21
La	0.95	2.45	1.11	1.13
Ce	2.6	4.53	2.77	2.98
Nd	1.73	3.58	2.1	1.97
Sm	0.52	1.17	0.627	0.631
Eu	0.722	0.717	0.779	0.754
Gd	1.1	1.60	1	-
Tb	0.21	0.23	0.21	0.17
Dy	1.1	1.67	1.08	1.13
Yb	0.595	1.11	0.71	0.76
Lu	0.089	0.142	0.10	0.115
W	0.3	-	-	-
Ir	0.0085	0.0067	0.010	0.0056
Au	0.006	0.0066	0.0031	0.0011
Hg	<0.07	<0.1	<0.05	-
Th	0.22	0.34	0.23	0.2

Ref.1: Koeberl (1988)
Ref.2: Bischoff et al. (1987)

References: Bischoff A.,Palme,H., Weber,H.W.,Stöffler, D., Braun,O., Spettel, B., Begemann,F., Wänke,H., and Ostertag,R.(1987) Proc. 11th Symp. Antarctic Meteorites, NIPR, 21-46.
Koeberl, C. (1988) Proc. NIPR Symp. Ant.Meteorites 1, 122-134.
Yanai,K.,Kojima,H.,Koeberl,C.,Graham,A.,Prinz,M., (1987) Photographic Catalog of Antarctic Meteorites, NIPR Tokyo, 298 pp.

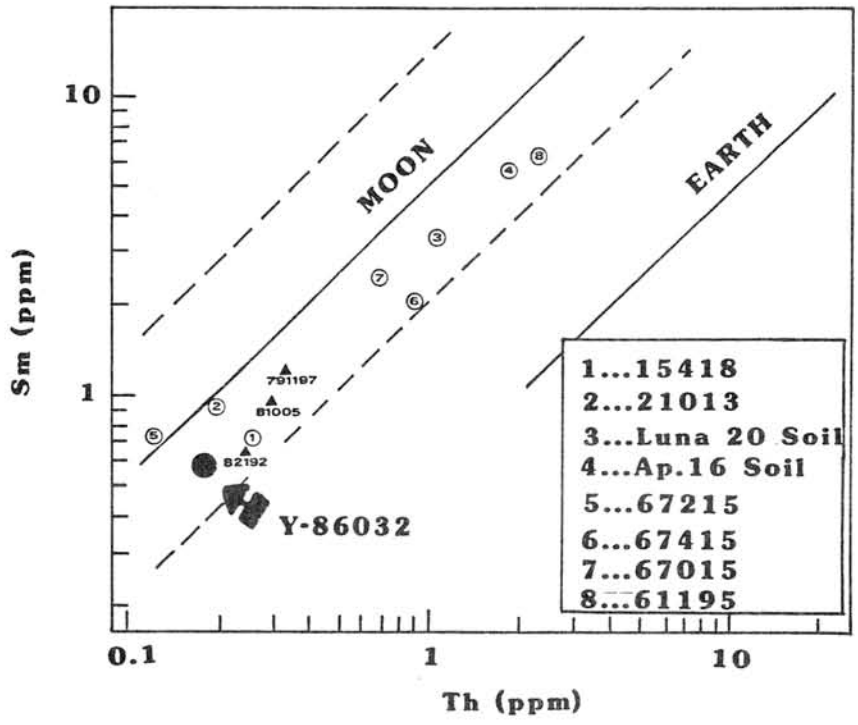

Fig. 1. Plot of Th vs. Sm. The "Moon" line is an average of lunar rocks, which is definetely different from terrestrial rocks. The new lunar meteorite Y-86032 plots below the other lunar meteorites, and lower than most lunar highland rocks.

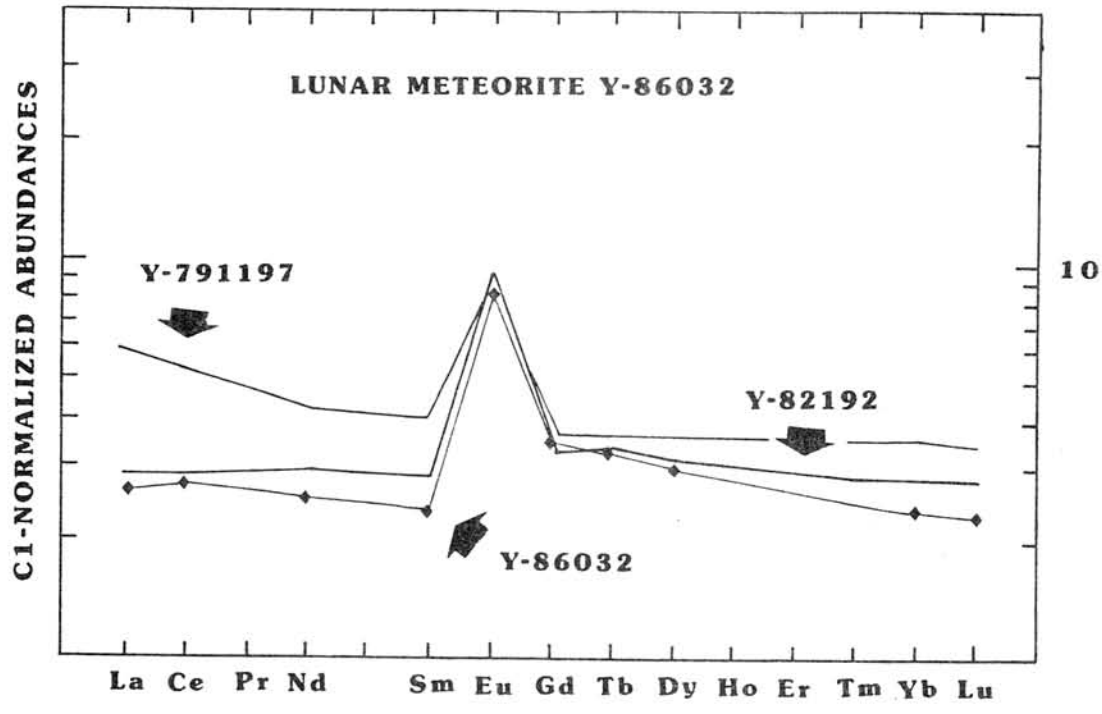

Fig. 2. Rare earth elements in the new lunar meteorite Y-86032. The similarity with Y-82192 is much closer than with Y-791197.

LUNAR METEORITE Y-86032: SAME COSMIC-RAY EXPOSURE AGE AND TRAPPED NOBLE GAS COMPONENT AS Y-82192/3.

Eugster, O.
Physikalisches Institut, University of Bern, 3012 Bern, Switzerland

Anorthositic regolith breccia Yamato-86032 was recognized by Yanai and Kojima [1] to be a lunar meteorite. This stone of 648.43 g is similar to the paired lunar meteorites Yamato-82192 and Yamato-82193 collected at the same bare ice area [1]. Sample Y-86032,86 (0.42 g) was obtained for preliminary characterization from the National Institute of Polar Research in Tokyo.

The aim of this study is the determination of the noble gas isotopic abundances, exposure age and trapped gas composition and to compare these data with those obtained from the other lunar meteorites. Split Y-86032,86 consisted of 13 fragments that were crushed to a grain size of < 700 µm. First, two bulk samples of 1 mg each were analyzed. Since trapped gas abundances turned out to be low, a third sample of 20 mg was processed. In this paper the results for the He, Ne, and Ar isotopes are reported. Kr and Xe analyses and other investigations are in progress. Table 1 gives the results obtained.

Table 1. Noble gases in lunar meteorite Y-86032,86 (preliminary data).

Sample	weight (g)	^{4}He	^{22}Ne	^{36}Ar	$\frac{^{4}He}{^{3}He}$	$\frac{^{20}Ne}{^{22}Ne}$	$\frac{^{21}Ne}{^{22}Ne}$	$\frac{^{38}Ar}{^{36}Ar}$	$\frac{^{40}Ar}{^{36}Ar}$
		10^{-8} cm^3 STP/g							
bulk (1)	0.00100	35	2.8	15.1	7.1	3.1	0.68	0.31	53
bulk (2)	0.00101	39	3.9	34.8	7.4	5.4	0.51	0.25	27
bulk (3)	0.02029	38	3.7	23.5	5.7	4.5	0.58	0.26	37

Experimental errors: Abundances ∿10%, $^{40}Ar/^{36}Ar$ ∿20%, other ratios 3-5%.

Cosmogenic, radiogenic and trapped noble gases

Inspection of the data for the different components in Table 2 indicates that Y-86032 is essentially identical to Y-82192 and Y-82193 and very different from Y-791197 [2] and A-81005 [3]. The latter two meteorites contain about 1'000-10'000 times more trapped Ne and Ar than Y-86032. Radiogenic ^{40}Ar is about 20% lower than in Y-82192/3 and less than half of that in A-81005. This difference may be due to a lower gas retention age or to lower K concentration of Y-86032.

The trapped noble gases in Y-86032 are inhomogeneously distributed. It appears that the crushed material exhibits surfaces which were not exposed to the solar wind and that the ratio of exposed to unexposed surfaces varies among the analyzed samples. However, the volume correlated cosmogenic and radiogenic components are uniformly distributed as shown in Table 2. From Fig. 1 $(^{20}Ne/^{22}Ne)_{tr}$ = 11.8 and $(^{22}Ne/^{21}Ne)_{c}$ = 1.20 is obtained adopting $(^{20}Ne/^{22}Ne)_{c}$ = 0.8 and $(^{21}Ne/^{22}Ne)_{tr}$ = 0.032. Y-82192/3 contain Ne with $(^{20}Ne/^{22}Ne)_{tr}$ = 12.02 and $(^{22}Ne/^{21}Ne)_{c}$ = 1.22 - 1.24 [4]. A ratio of $(^{20}Ne/^{22}Ne)_{tr}$ of about 12 is typical for solar wind implanted Ne in lunar highland regolith. For $(^{36}Ar/^{38}Ar)_{tr}$ a ratio of 5.08 is derived (Fig. 2), in close agreement with the value of 5.12 for Y-82192/3. For Y-86032 a Ca concentration of 10% was assumed. The ratio $(^{40}Ar/^{36}Ar)_{tr}$ is diagnostic for the origin of the sample: both sample suites, Y-82192/3 and the Y-86032 samples, yield an ordinate intercept which is typical for Ar trapped by the regolith of a moon sized object [5, 6]. For Y-86032 $(^{40}Ar/^{36}Ar)_{tr}$ = 7.4 is obtained compared to a value of 8.2 for Y-82192/3 [4].

Table 2. Cosmogenic, radiogenic, and trapped noble gases in Y-86032 (preliminary data) compared with other lunar meteorites.

Meteorite	Sample	Cosmogenic				Radiogenic	Trapped	
		^{3}He	^{21}Ne	^{38}Ar	^{22}Ne	^{40}Ar	^{20}Ne	^{36}Ar
		10^{-8} cm^3 STP/g			^{21}Ne	10^{-8} cm^3 STP/g		
Y-86032,86	bulk (1)	4.9	1.9	2.1	1.21	699	6.8	13.7
	bulk (2)	5.3	2.0	2.4	1.19	704	19.1	33.2
	bulk (3)	6.7	2.1	2.0	1.19	706	14.5	23.5
	bulk av.	5.6	2.0	2.2	1.20	703	-	-
For comparison:								
Y-82192,82 [4]	>25µm	8.05	2.20	2.26	1.24	904	10.4	8.8
Y-82193,100 [4]	>25µm	7.24	2.26	2.60	1.22	902	23.8	18.1
Y-791197 [2]	bulk	32	67.1	-	-	-	92800	33900
A-81005 [3]	bulk	22.2	41.3	64	-	1800	56000	19500

Experimental errors in this work: $^{22}Ne/^{21}Ne$ ∿3%, abundances ∿10%, except for ^{40}Ar (∿20%).

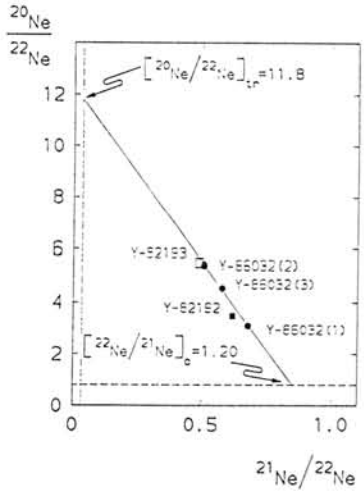

Figure 1. Neon three isotope plot. The line shown is a least squares fit for the Y-86032 data. For comparison the Y-82192 and Y-82193 data are also shown.

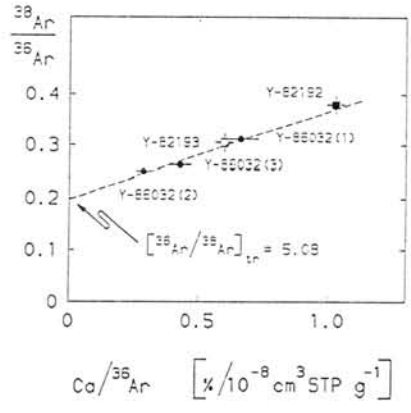

Figure 2. $^{38}Ar/^{36}Ar$ vs. $Ca/^{36}Ar$ correlation. The solid line is a least squares fit for the Y-86032 data. The Y-82192 and Y-82193 data are shown for comparison.

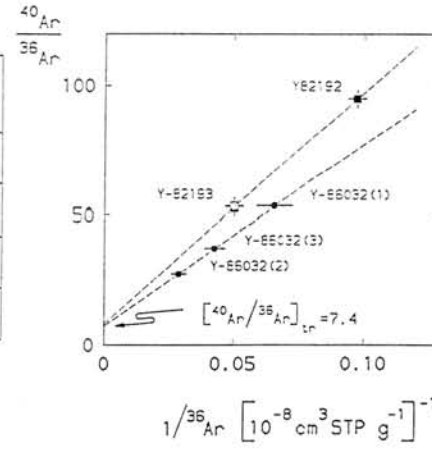

Figure 3. $^{40}Ar/^{36}Ar$ vs. $1/^{36}Ar$ correlation plot. The Y-86032 data yield essentially the same trapped ratio as the Y-82912/3 data. The different slope indicates different radiogenic ^{40}Ar content.

Cosmic-ray exposure ages

Galactic cosmic-ray ages were calculated based on the concentrations of ^{21}Ne and ^{38}Ar (bulk average, Table 2) adopting the average production rates derived for Y-82192/3 valid for a 4π exposure [4]. For Y-86032 a cosmic-ray age of 10.4 Ma is obtained (Table 3), close to the ages of 10.6 and 10.8 for Y-82192 and Y-82193, respectively. Table 3 shows that the lunar meteorites Y-791197 and Y-81005 were exposed to cosmic rays for a much longer duration.

Table 3. Cosmic-ray exposure age [Ma] of Y-86032 (preliminary data) compared with other lunar meteorites.

	Ref.	T^{21}	T^{38}	Average	Remark
Y-86032,86 (4π)		9.5 (1)	11.2 (1)	10.4 ± 2.0	
For comparison:					
Y-82192,82 (4π)	[4]	10.3	12.0	10.6 ± 0.6	(2)
Y-82192,75 (4π)	[7]	9.7	12.2	11.0	(3)
Y-82192,63C (4π)	[8]	9.7	9.9	9.8	(3)
Y-82192,64A (4π)	[8]	7.5	8.6	8.0	(3)
Y-82193,100 (4π)	[4]	10.8	12.8	10.8 ± 0.7	(2)
Y-791197 (2π)	[2]	-	-	910 ± 60	(4)
A-81005 (2π)	[3]	270	460	580 ± 180	(2)

(1) Average production rates as given for Y-82192/3 [4]; (2) from T^{21}, T^{38}, T^{83}, and T^{126}; (3) from T^{21} and T^{38}; (4) from T^{83} and T^{126}.

Conclusions

The consistency of the results obtained from the samples of Y-86032 demonstrates that reliable noble gas data can be obtained for 1 mg samples. This is important for studying meteorites with recovered weights of a few grams. From the cosmic-ray exposure age and the trapped noble gas ratios it can be concluded that Y-86032 is paired with Y-82192/3. However, the possibility that Y-86032 originates from a different meteoroid but from the same impact event on the moon can not be ruled out before the terrestrial age of Y-86032 has been determined.

Acknowledgements

The author wishes to thank K. Yanai and H. Kojima for the allocation of this valuable sample and to H. Takeda for organizing the consortium study. I thank J. Geiss and P. Eberhardt for their constant support and encouragement. The help by J. Fischer, P. Guggisberg, Iris Peter, A. Tschanz, and M. Zuber during various stages of this work is greatly acknowledged. This work was supported by the Swiss National Science Foundation.

References

[1] K. Yanai and H. Kojima, Abstr. 12th Symp. Antarctic Meteorites, Tokyo, p. 3 (1987). [2] N. Takaoka, Mem. Natl. Inst. Polar Res., Spec. Issue 41, 124-132 (1986). [3] O. Eugster, J. Geiss, and U. Krähenbühl, Planet. Sci. Lett. 78, 139-147 (1986). [4] O. Eugster and S. Niedermann, Earth Planet. Sci. Lett., in press (1988). [5] R.H. Manka and F.C. Michel, Proc. Lunar Sci. Conf. 2nd, p. 1717-1728 (1971). [6] D.D. Bogard and P. Johnson, Geophys. Res. Lett. 10, 801-803 (1983). [7] A. Bischoff, H. Palme, H.W. Weber, D. Stöffler, O. Braun, B. Spettel, F. Begemann, H. Wänke, and R. Ostertag, Mem. Natl. Inst. Polar Res., Spec. Issue 46, 21-42 (1987) [8] N. Takaoka, Mem. Natl. Inst. Polar Res., Spec. Issue 46, 96-104 (1987).